THE UNIVERSITY *of* EDINBURGH

Evolution of the Earth's mantle-crust-atmosphere system from the trace element and isotope geochemistry of the plume-mantle reservoir

Natalie Starkey

Thesis submitted as partial fulfilment of the requirement for the degree of Doctor of Philosophy (PhD)

University of Edinburgh

2009

To the Starkey family

Abstract

The 62 million year old lava flows of Baffin Island and West Greenland represent the earliest phase of magmatism in the North Atlantic Igneous Province (NAIP). These picritic lavas are characterised by high magnesium contents owing to their high proportion of olivine crystals. The parental magmas for the picrites are likely to have accumulated olivine crystals on their transit through the lithosphere and crust. Debate over the origin of accumulated crystals in the lavas results in uncertainty in the temperature and composition of the parental magmas for the early NAIP. The magnesium-rich olivine crystals (up to Fo_{93}) in the picrites of this study are shown not to have a xenocrystic origin. The samples, therefore, support the inference of high potential temperatures for the Baffin Island-West Greenland magmas, ~200^{o}C above ambient mantle.

The picrites of Baffin Island and West Greenland display the highest terrestrial magmatic $^{3}He/^{4}He$ (up to 50 R_a, where R_a is the atmospheric value 1.39 x 10^{-6}), values that are considerably higher than the highest $^{3}He/^{4}He$ in contemporary ocean island basalts, which reach a maximum of ~30 R_a. High $^{3}He/^{4}He$ in Baffin Island and West Greenland are associated with a wide range of incompatible trace element and lithophile radiogenic isotopic compositions, not dissimilar to the range of compositions displayed by lavas at mid-ocean ridges, and overlapping the range displayed by most northern hemisphere ocean island basalts. Crustal contamination modelling in which high-grade Proterozoic crustal basement rocks are mixed with depleted parents cannot account for the compositional trends displayed by the picrites.

Major and trace element compositions were determined on melt inclusions in high-$^{3}He/^{4}He$ picrites that span a wide range of whole-rock incompatible trace element and radiogenic isotopic compositions. The melt inclusions support the findings from the whole-rock study since melt inclusion compositions reflect the composition of their associated whole-rock, with no anomalous compositions present. In addition, there is no evidence for a contribution of a proportion of depleted melts to the source of the relatively enriched whole-rock samples. Therefore, since all melt inclusions

were contained within high-$^{3}He/^{4}He$ samples, it is shown that high $^{3}He/^{4}He$ is a feature of both depleted and relatively enriched melt compositions.

The wide range in whole-rock compositions of the Baffin Island and West Greenland picrites represents that of the sub-lithospheric mantle source region and is inconsistent with derivation of the picrites from residues of ancient mantle depletion. The apparent decoupling of helium from trace elements and radiogenic isotopes is hard to reconcile with simple mixing of a high-helium concentration, high-$^{3}He/^{4}He$ reservoir with various depleted and enriched helium-poor mantle reservoirs. It is possible that primordial helium has diffused into a reservoir with a composition similar to that of the convecting upper mantle. However, this must have occurred after the development of existing mantle heterogeneity. The high-$^{3}He/^{4}He$ picrites require the existence of a deep, primordial helium-rich reservoir. Whether this reservoir is present in the upper or deep mantle, or even the core, remains uncertain.

Declaration

I declare that this thesis has been composed by myself and is solely my own work unless otherwise acknowledged.

Natalie Starkey
2009

Acknowledgements

This work was funded by a PhD studentship (NER/S/A/2005/13854) from the Natural Environment Research Council (NERC).

I would like to take this opportunity to thank a few people who have helped me in different ways during my PhD. First and foremost I would like to thank my main supervisor, Godfrey Fitton, whose support gave me confidence in myself and my work during the three years I spent in Edinburgh. In addition to all his help during my write-up period, vacuuming the broken glass out of my car when it was vandalised was well beyond the call of duty of a PhD supervisor but something for which I was very grateful. My other supervisors Rob Ellam and Fin Stuart were helpful during my lab work at SUERC in East Kilbride. I also appreciate their support during my write-up. Lotte Larsen of GEUS, although not a supervisor for this project, was just as helpful. I am very grateful for her email discussions and supportive conversations at various conferences and of course, the fact that she allowed her samples to be used for the project.

All of the PhD students at Edinburgh have been great and it wouldn't have been the same without them all. Most of all I will thank Emma for all the fun times we had trying to find the right lava flow in Iceland, Gillian for her hilarious conversations, Jenny for her understanding about shopping and Rich who entertained me nearly constantly. Outside of work, Suz, my running partner, flatmate and good friend was fabulous and I can't thank her enough for being so understanding.

Finally, I cannot finish without thanking my family. Firstly, my sister for inspiring me to do a PhD, although she won't realise that herself due to her repeated warnings not to do one (apparently they are very stressful and hard work)! Secondly, the decision for me to move home for my write-up was made easy by my parents support. My main requirements at home were a desk and a bed but I was extremely happy to accept the full-board version that was supplied. I think that Chanctonbury must be the best value lodgings in the city of Bath and I'd highly recommend it! Thank you for all your help, love and encouragement.

Contents

List of figures

1 Introduction

2 Results: Petrography, whole-rock major and trace elements

3 Results: Strontium, neodymium and helium isotope compositions

4 Results: Major and trace element compositions of melt inclusions

5 Discussion

List of tables

2 Results: Petrography, whole-rock major and trace elements

Introduction

1. Introduction

1.1 Background

It has long been recognised that the composition of intraplate lavas differs from lavas produced at mid-ocean ridges (Gast et al., 1964). Ocean island basalts (OIB) and continental flood basalts (CFB) are relatively more enriched[1] in trace element and lithophile radiogenic isotope compositions than mid-ocean ridge basalts (MORB). MORB, however, display a continuum from depleted to relatively enriched compositions that overlap with some OIB (Saunders et al., 1988). With the discovery of primordial helium in the Earth's mantle in the 1960s (Clarke et al., 1969; Mamyrin et al., 1969) it was subsequently shown that intraplate basalts are characterised by a wide range of $^{3}He/^{4}He$ that can reach up to 50 R_a (where R_a is the atmospheric value 1.39 x 10^{-6}; Stuart et al., 2003; Starkey et al., 2009) compared to MORB that display a narrow range with an average of ~8 ± 1 R_a (Farley and Neroda, 1998; Hilton and Porcelli, 2003). The relatively low $^{3}He/^{4}He$ of MORB compared to OIB, coupled with their depleted trace element and radiogenic isotopic signatures relative to OIB and bulk Earth, has been used to suggest that MORB require a depleted and degassed source region in the Earth's mantle for their generation. The convecting upper mantle, depleted by removal of incompatible elements during continental crust formation and degassed near-continuously by the extraction of melts at mid-ocean ridges, is a good candidate for the source of MORB (Hofmann, 1988).

The higher $^{3}He/^{4}He$ found in some intraplate lavas is often used as evidence to indicate that the OIB source is distinct from that of MORB, requiring a reservoir with higher time-integrated $^{3}He/(U+Th)$. In addition, evidence for the existence of non-atmospheric neon in the mantle was found from the analysis of MORB that displayed enrichments in ^{20}Ne as well as nucleogenic ^{21}Ne (Craig and Lupton, 1976). Subsequently, ^{20}Ne excesses in Hawaiian basalts were shown to indicate a solar-like component and $^{3}He/^{22}Ne$ ratios were found to be similar to those measured in

[1] 'Enriched' and 'depleted' are used here as relative terms but it is noted that most OIB and all MORB are depleted relative to Bulk Earth.

implanted solar gases (Honda et al., 1991; Hiyagon et al., 1992). Therefore, a primordial gas-rich reservoir was proposed to explain the helium and neon isotopes measured in the Earth. It was suggested that the high-$^{3}He/^{4}He$ source may reside in the undegassed convectively isolated lower mantle (Craig and Lupton, 1976; Kurz et al., 1982; Allègre et al., 1983; Farley et al., 1992) or in convectively isolated domains in the lower mantle (Kellogg et al., 1999) that had preserved primordial gases since the time of Earth accretion. Mantle plumes, originating in the lower mantle, were proposed as a means of sampling this deep material and transporting it to the surface (Morgan, 1971; Dupré and Allègre, 1983; Zindler and Hart, 1986).

Helium isotopes alone cannot provide sufficient evidence with which to specifically evaluate mantle mixing processes. Consequently, other radiogenic isotopes have been investigated in relation to helium. Studies on various OIB localities have shown that data from individual islands converge on distinct compositions in incompatible trace element, Sr, Nd and Pb isotope space that are not those expected for melting of a chondritic lower mantle source (Zindler and Hart, 1986). Such observations led to the introduction of mantle components based on the most isotopically extreme compositions found in the mantle (Zindler and Hart, 1986). These are DMM (depleted MORB mantle), EM1 and EM2 (enriched mantle components), HIMU (high $^{206}Pb/^{204}Pb$ therefore high-μ ($^{238}U/^{204}Pb$)) and PREMA (a common yet relatively depleted component termed 'Prevalent Mantle'). However, none of these components displays the very high $^{3}He/^{4}He$ values expected for 'primitive' mantle. Therefore, other specific high $^{3}He/^{4}He$ components were proposed to account for the non-chondritic yet relatively undegassed nature of OIB, such as PHEM (Primitive He Mantle; Farley et al., 1992), C (Common; Hanan and Graham, 1996), FOZO (Focus Zone; Hart et al., 1992) and more recently HRDM (Helium Recharged Depleted Mantle; Ellam and Stuart, 2004). The location of these components in He-Nd isotope space is shown in Figure 1.1. These mantle components are theoretically available to mix in various proportions with each other to generate the large array of basalt compositions produced by ocean islands. The possible involvement of primitive mantle in any OIB source remains unclear since it is unknown whether unprocessed primitive mantle still exists in the Earth. The origin of many of the relatively

enriched mantle components (i.e. EM1, EM2, HIMU) are shown to be linked to the recycling of oceanic crust and lithosphere into the mantle at subduction zones (Hofmann and White, 1982). However, identifying the exact quantity and composition of components involved in mixing to produce the compositions of magmas at different ocean islands has proven difficult. This has led to much criticism of the concept of distinct mantle components by several authors (Barling and Goldstein, 1990; Morgan, 1999; Armienti and Gasperini, 2007) who conclude that they are only relevant from a Sr, Nd and Pb isotope perspective. However, Jackson and Dasgupta (2008) have recently compiled OIB data that show correlations between major elements and isotopic compositions. These correlations show that some mantle components, namely HIMU, EM1 and EM2, may display distinct major element compositions which in turn may suggest that the lithological characteristics of these mantle components can be investigated in more detail (Jackson and Dasgupta, 2008).

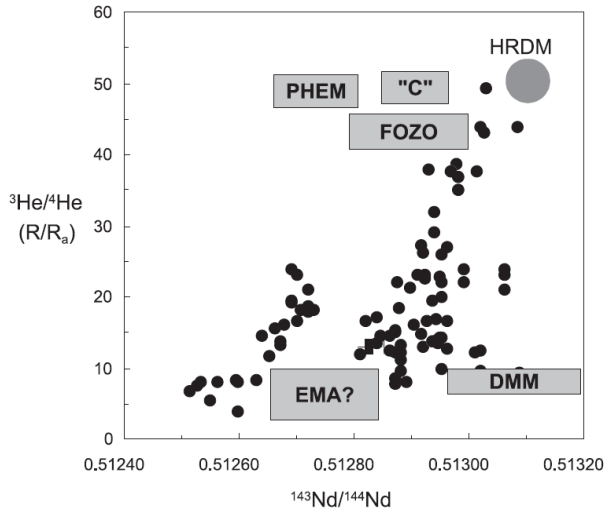

Figure 1.1. ^{3}He/^{4}He plotted against ^{143}Nd/^{144}Nd for global OIB-CFB data showing the position of various mantle components in He-Nd isotope space. EMA = Enriched Mantle Average, other acronyms defined in text. From Ellam and Stuart (2004).

1.1.1 Ocean island basalts (OIB) and their relationship to mantle plumes

OIB-like basalt is found in a variety of locations, extending from large-volume volcanic islands such as Hawaii, Galapagos and Iceland, to small-volume isolated features, such as small ocean islands and seamounts (Fitton, 2007). Many occurrences of OIB and OIB-like basalt are often used to infer the existence of a mantle plume that has risen from the lower mantle. However, the Pacific Ocean

alone is shown to host over 70,000 seamounts (Wessel and Lyons, 1997), many of which are likely to be composed of OIB, and this would require a huge number of small mantle plumes if all intraplate magmatism is plume-related. This has led some authors to question the association of all occurrences of OIB-like basalt with mantle plumes (Anderson and Schramm, 2005; Fitton, 2007). It is hard to understand how a small mantle plume could cover the vertical distance from the lower mantle to the Earth's surface without being mixed into the surrounding mantle by convection. However, volcanic islands displaying time-progressive chains and large volumes of magmatism over a long time period, such as those of Hawaii, Galapagos and Iceland, do provide better evidence for the existence of mantle plumes. A mantle plume for such occurrences would also need to be much larger than that required for a small seamount and may, therefore, be able to rise through the mantle without being destroyed by mixing during convection. In addition, some studies show 'plumes' or deep mantle upwellings associated with large ocean islands that extend all the way to the core-mantle boundary (Figure 1.2; Shen et al., 1998; Bijwaard and Sparkman, 1999; DePaolo and Manga, 2003). However, it is possible that data reduction techniques used to obtain images such as the one displayed in Figure 1.2 enhanced deep mantle anomalies. Consequently, it is unclear whether velocity anomalies can be accurately imaged in the lower mantle. It has been shown that upwelling material in Iceland cannot be imaged extending into the lower mantle (Foulger et al., 2001) but other studies have shown that it may not be possible to image below the low-velocity anomaly associated with Iceland (Keller et al., 2000; Wolfe et al., 2002). Therefore, to date, tomographic studies do not provide unequivocal evidence for deep velocity anomalies associated with OIB and new technological advances will be required to ascertain the true depth of all OIB sources.

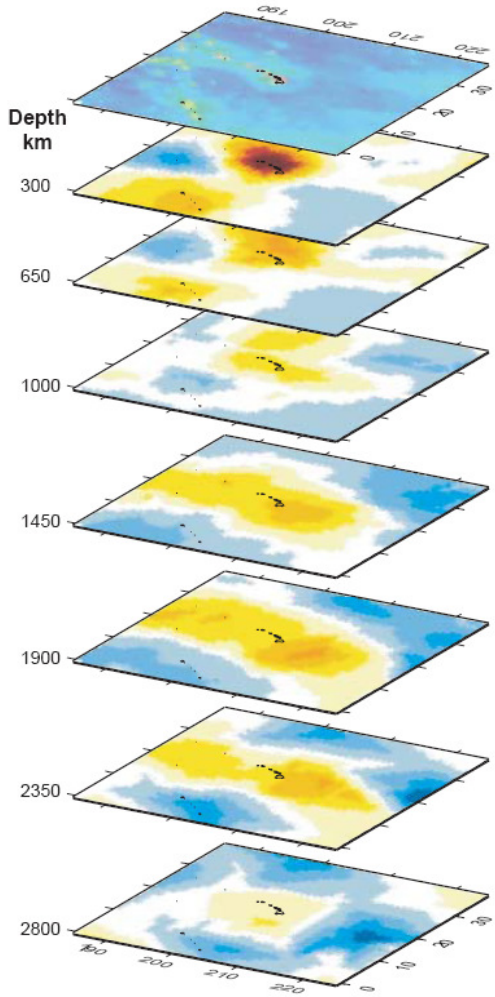

Figure 1.2. Maps of P-wave velocities under Hawaii (red = slow, blue = fast). Red and yellow regions are interpreted as anomalously hot suggesting that the high temperature anomaly associated with Hawaii continues down to the core mantle boundary. From DePaolo and Manga (2003) after Montelli et al. (2003).

Regardless of the controversy surrounding the origin of OIB, an alternative explanation is still required to account for the frequent but small-volume OIB-like basalts found throughout the ocean floor that cannot be produced by mantle plumes. OIB generation requires increased melt productivity which is caused by either the presence of fertile mantle lithologies, high mantle potential temperature and/or high upwelling rate. The concept of a mantle plume rising from the deep mantle can account for all of these requirements. However, an alternative class of model that can possibly account for the occurrence of relatively enriched basalts throughout the ocean floor without requiring mantle plumes is that of the 'plum pudding' (Batiza, 1984) or 'marble-cake' mantle (Allègre and Turcotte, 1986). In these models the

depleted mantle contains blobs or elongated streaks of enriched material that is more fusible and, therefore, sampled under low degrees of melting. At higher degrees of melting the depleted and enriched portions are homogenised to produce MORB. If these heterogeneities are present at various length-scales then they may be able to account for both small-volume OIB-like basalts and the larger melting anomalies associated with larger ocean islands (Fitton, 2007). However, it is unclear whether enriched blobs or streaks in the convecting mantle could retain high enough volatile contents over time in order to supply high-$^{3}He/^{4}He$ basalts (van Keken and Ballentine, 1999). In addition, whether heterogeneities can be sustained as discrete domains in the convecting mantle over time will depend on their exact lithology, size and shape. These features remain, as yet, poorly understood.

1.1.2 Generation of high-$^{3}He/^{4}He$ mantle

^{3}He is not produced in the Earth so that high $^{3}He/^{4}He$ represents a sample of long-lived primordial gas (Porcelli and Ballentine, 2002) that has been stored since Earth formation. When considering the preservation, storage and location of high $^{3}He/^{4}He$ in the Earth there are two main schools of thought. The first places high $^{3}He/^{4}He$ in primordial mantle and the second places high $^{3}He/^{4}He$ in incompletely degassed ancient depleted residues of mantle depletion. These models differ significantly. The former views the high-$^{3}He/^{4}He$ reservoir as a gas-rich source located in a convectively isolated lower mantle whereas the latter views the high-$^{3}He/^{4}He$ reservoir as gas-poor material dispersed in discrete domains throughout either the deep or shallow mantle, in a regime of whole-mantle convection.

A simple ‘two-reservoir’ model for the Earth separates the upper and lower mantle by a thermal boundary at 670 km. In this model, primordial gases are contained within the lower mantle, the undegassed region below the 670 km thermal boundary, such that high $^{3}He/^{4}He$ is expected to be associated with high helium concentrations. The low $^{3}He/^{4}He$ of MORB are, consequently, expected to have low helium concentrations as they are derived from the degassed upper mantle. However, early studies, originating with Fisher (1985), showed that Hawaiian and Icelandic basalts

with high $^{3}He/^{4}He$ were found to have low helium concentrations. This observation is apparently at odds with the concept of the 'two-reservoir' model for the Earth and is termed the 'helium paradox' (Hilton et al., 2000). However, how helium acts during melting and eruption processes is not fully understood and it is possible that helium concentrations measured in volcanic rocks do not represent that of their source. For example, Gonnermann and Mukhopadhyay (2007) showed that low helium concentrations in OIB magmas can result from disequilibrium open-system degassing of more volatile-rich parental magma. The higher CO_2 contents of OIB compared to MORB result in more extensive degassing of helium in OIB magmas, which according to Gonnermann and Mukhopadhyay (2007), can explain the helium paradox.

The controversy over the high $^{3}He/^{4}He$ source of some OIB is further complicated by increasing geophysical evidence to suggest that the mantle may convect as a single layer (Christensen, 1995; Forte and Mitrovica, 2001; van Keken et al., 2002). A whole-mantle that is well-mixed would certainly pose a problem for the preservation and storage of high $^{3}He/^{4}He$ during Earth history, particularly if high $^{3}He/^{4}He$ reflects high ^{3}He as opposed to low ^{4}He. However, whole-mantle convection also poses problems for models that place high $^{3}He/^{4}He$ in depleted and degassed residues of mantle depletion where high $^{3}He/^{4}He$ OIB are characterised by low ^{4}He. One way in which to preserve high $^{3}He/^{4}He$ in a well-mixed mantle is for the viscosity of the mantle to increase with depth such that it is possible for some portions of mantle to remain unmixed and thus potentially preserve high $^{3}He/^{4}He$ (van Keken and Ballentine, 1999). However, modelling of such scenarios in three-dimensions has divided opinion on whether increased viscosity of the mantle with depth would produce more or less vigorous convection (Schmalzl et al., 1995; van Keken and Ballentine, 1999). Alternatively, if the primordial source for ^{3}He is contained within a dense layer in the deep mantle then it is possible that this layer is protected from the stirring effects of mantle convection. Either way, one of the best methods available to investigate the potential location of high $^{3}He/^{4}He$ in the Earth is to focus on the compositions of lavas from locations that display high $^{3}He/^{4}He$, in conjunction

with mantle convection models and experimental studies on the partitioning of elements into the relevant mantle phases.

A compilation of isotopic data from the North Atlantic Igneous Province (NAIP) showed an association between high $^{3}He/^{4}He$ (up to 50 R_a) and relatively depleted compositions (high $^{143}Nd/^{144}Nd$, low $^{87}Sr/^{86}Sr$) (Figure 1.3; Stuart et al., 2003; Ellam and Stuart, 2004). The trend displayed by the NAIP samples, from high $^{3}He/^{4}He$ depleted compositions to low $^{3}He/^{4}He$ relatively enriched compositions, was termed the Proto-Iceland Plume (PIP) trend (Figure 1.5; Ellam and Stuart, 2004). It was shown that data arrays from other ocean islands do not cross this trend (Figure 1.4) leading Ellam and Stuart (2004) to suggest that the high $^{3}He/^{4}He$ mantle component is a discrete reservoir. This 'helium recharged depleted mantle' (HRDM) was modelled as the result of ancient mixing between primordial gas-rich mantle and depleted mantle (Figure 1.5). It was estimated that the primordial gas-rich mantle would need to be 10-100 times richer in helium than the depleted mantle end member (Ellam and Stuart, 2004). This model requires high $^{3}He/^{4}He$ to be present in a gas-rich primordial reservoir, presumably in the lower mantle while the upper mantle represents the depleted material with which high $^{3}He/^{4}He$ can mix (Ellam and Stuart, 2004).

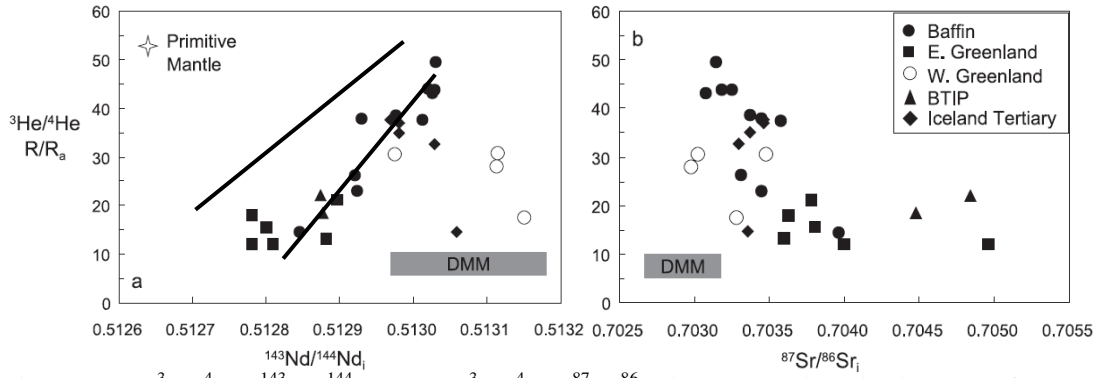

Figure 1.3. a) $^{3}He/^{4}He$ - $^{143}Nd/^{144}Nd$ and b) $^{3}He/^{4}He$ - $^{87}Sr/^{86}Sr$ isotope relationships in basalts from the North Atlantic Igneous Province. Linear trends attain high $^{3}He/^{4}He$ and high $^{143}Nd/^{144}Nd$, low $^{87}Sr/^{86}Sr$ defining the Proto-Iceland Plume (PIP) trend (indicated in black). DMM = Depleted MORB mantle. From Ellam and Stuart (2004).

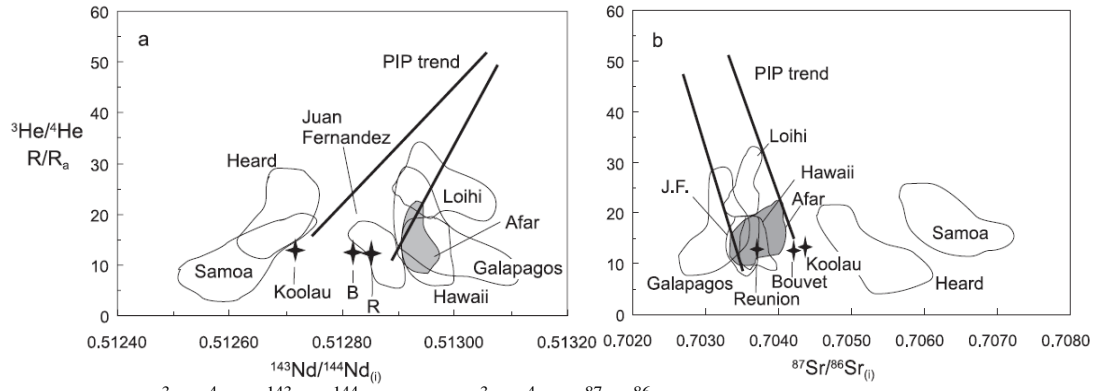

Figure 1.4. a) $^{3}He/^{4}He$ -$^{143}Nd/^{144}Nd$ and b) $^{3}He/^{4}He$ -$^{87}Sr/^{86}Sr$ isotope relationships for a global OIB compilation with black tramlines indicating Proto-Iceland Plume (PIP) trend. From Ellam and Stuart (2004).

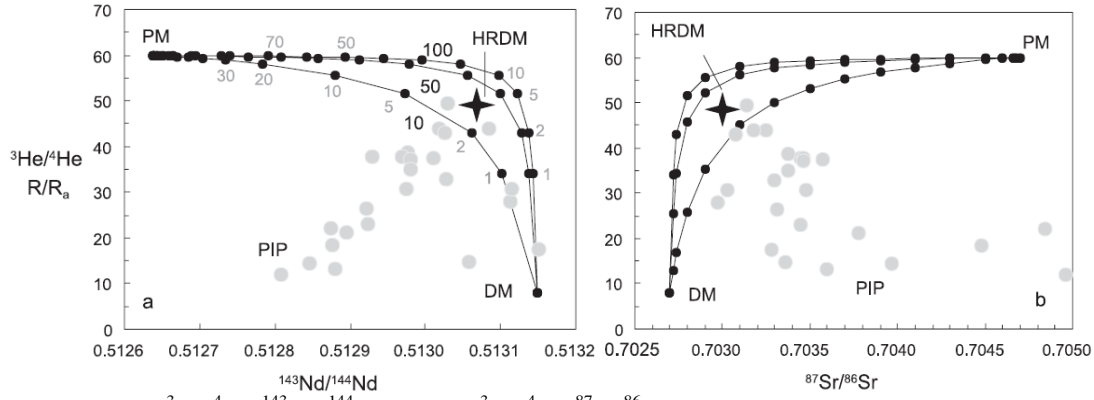

Figure 1.5. a) $^{3}He/^{4}He$-$^{143}Nd/^{144}Nd$ and b) $^{3}He/^{4}He$-$^{87}Sr/^{86}Sr$ simple binary mixing models between depleted and primordial mantle to account for the Proto-Iceland Plume (PIP) trend. PM = Primitive mantle, HRDM = Helium recharged depleted mantle, DM = Depleted mantle. Bold numbers indicate He/Nd_{PM}:He/Nd_{DM} and grey numbers indicate percentage of PM contribution to mixture. From Ellam and Stuart (2004).

Using a global high-$^{3}He/^{4}He$ OIB compilation, Class and Goldstein (2005) modelled the evolution of helium in a convecting whole mantle and showed that high-$^{3}He/^{4}He$ ocean islands were associated with depleted radiogenic isotopic compositions, in agreement with Ellam and Stuart (2004). However, their modelling suggested that high-$^{3}He/^{4}He$ OIB could instead result from the primordial helium remaining in incompletely degassed residues of ancient melting that were isolated from the convecting mantle for billions of years. Figure 1.6 illustrates the evolution of $^{3}He/^{4}He$ with time in this model and how it can apparently account for the high $^{3}He/^{4}He$ 'plume' component. However, the value for the initial $^{3}He/^{4}He$ of the Earth (230 R_a) may be overestimated in this model, being applicable only if the Earth acquired its helium by solar wind implantations on accreting materials (Porcelli and Ballentine, 2002). The Class and Goldstein (2005) model requires the high-$^{3}He/^{4}He$

helium to be contained in a gas-poor reservoir that is also depleted and present as discrete domains in a regime of whole-mantle convection. Whether these domains are present in the deep or shallow mantle is not important as long as they remain intact and not mixed into the surrounding mantle by convection. This concept is hard to reconcile with the long held view that helium is more incompatible during mantle melting than U (Marty and Lussiez, 1993) resulting in the preferential depletion of helium in the source and leading to low $^{3}He/(U+Th)$ and low $^{3}He/^{4}He$ over time.

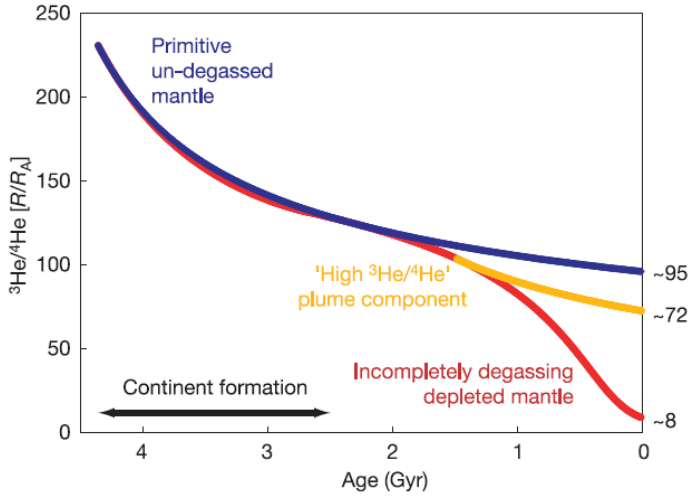

Figure 1.6. Incomplete degassing model. The curves represent the evolution of mantle with initial $^{3}He/^{4}He$ of 230 R_a. The high $^{3}He/^{4}He$ 'plume' component results from ancient, incompletely degassed residues of mantle depletion, stored in the convecting mantle. From Class and Goldstein (2005).

However, recent estimates of partition coefficients suggest that helium may actually be more compatible than U during mantle melting (Figure 1.7; Parman et al., 2005). If this is the case then helium would still be removed from the source during a depletion event, since it is still a highly incompatible element (D_{He} in olivine = 2.5 x 10^{-3} – 6 x 10^{-3} (Parman et al., 2005); 1.7 x 10^{-4} (Heber et al., 2007)), but it would not be removed as quickly as the ^{4}He-producing U and Th and therefore depleted residues could be left with high $^{3}He/(U+Th)$.

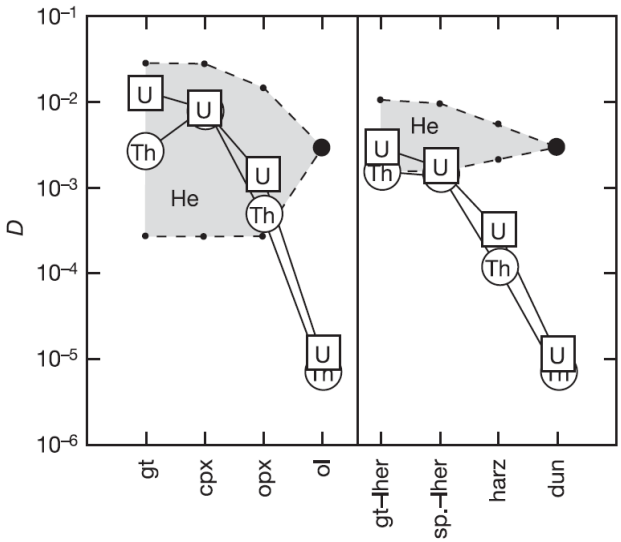

Figure 1.7. Partition coefficients during mantle melting for U, Th and He. Individual mineral-melt and bulk D values for various lithologies. From Parman et al. (2005).

Whether the helium concentration of such a residue can remain high enough to provide helium for high-$^{3}He/^{4}He$ OIB is a matter of debate. In support of the evidence for higher D values for U+Th, Parman (2007) argued that apparent frequency peaks in the high-$^{3}He/^{4}He$ global OIB dataset derive from discrete mantle domains that were depleted episodically over Earth history (Figure 1.8), showing a clear link between depleted residues and high $^{3}He/^{4}He$. However, Rudge (2008) showed that only two of the eight peaks apparent in the helium-continental crust formation correlation of Parman (2007) are likely to be statistically significant.

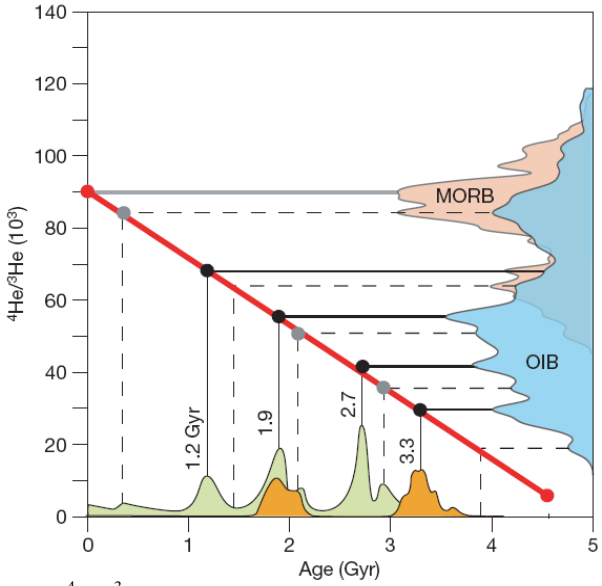

Figure 1.8. Correlation of $^{4}He/^{3}He$ peaks and zircon crustal ages from probability distribution functions for MORB and OIB. From Parman (2007).

Regardless of the recent controversy concerning the partition coefficients of He, U and Th, helium is still a light atom and a highly incompatible element. It is also a gas, although it is unknown which phase helium would take if it were present at the high temperatures and pressures expected in the deep mantle. The characteristics of helium mean that it is likely to be one of the first elements to enter a melt phase or, alternatively, it may diffuse or degas rapidly out of a source, dependent on the temperature and pressure conditions. However, whether more or less helium leaves the source in relation to U+Th during mantle melting is irrelevant since these characteristics mean that the helium concentration of the source will remain low if it has experienced any melt depletion event. Therefore, storing and preserving a high enough helium concentration in a depleted residue of mantle melting over time is difficult to achieve.

The importance of the behaviour of helium during diffusive processes has been emphasised by a study showing that the diffusion of helium from unprocessed mantle heterogeneities formed early in Earth history has the potential to enrich previously depleted mantle layers in primordial helium (Albarède, 2008). The measured diffusion rate of helium in olivine suggests that, at mantle temperatures, helium from a primordial volatile-rich reservoir could equilibrate with km-scale degassed mantle domains over the lifetime of the Earth (Shuster et al., 2004). If this is the case then the model of Albarède (2008) shows that primordial helium could diffuse into a marble-cake mantle composed, in part, of residual refractory rocks such as dunite. It is proposed that the difference in $^{3}He/^{4}He$ between MORB and OIB can be explained by the extent by which the reservoir is stretched and thinned, with the thickest refractory layers providing the highest $^{3}He/^{4}He$ by outgassing when they are stretched (Albarède, 2008). This type of model can account for the close association of high and low $^{3}He/^{4}He$ amongst a range of lava compositions, both enriched and depleted. However, there may still be problems in determining the original location of the primordial material and concerns over whether high enough $^{3}He/^{4}He$ can be preserved in such small-scale heterogeneities over time (Hart et al., 2008).

A separate suggestion for the generation of OIB magmas is that of the perisphere model of Anderson (1995). The perisphere represents a shallow trace element enriched layer lying at the base of the lithosphere. It is proposed that this layer is tapped by melts during the onset of rifting. After the perisphere is exhausted by melt extraction then the deeper depleted mantle is tapped for MORB (Figure 1.9). Where the perisphere is present, it is thought to be able to contaminate upwelling depleted material to produce OIB-like magmas (Anderson, 1995). Anderson (1998a) proposes that high $^{3}He/^{4}He$ signatures also have a shallow origin. The model of Anderson (1998a) proposes that the Earth is gas-poor with high $^{3}He/^{4}He$ representing a component of high $^{3}He/U$ rather than undegassed mantle. Therefore, high $^{3}He/^{4}He$ are derived from sources with little ingrown ^{4}He rather than excess ^{3}He (Anderson, 1998a). Anderson (1998b) proposes that the high $^{3}He/^{4}He$ shallow reservoir forms by exsolution of helium (CO_2 and other noble gases) from upwelling magmas at mid-ocean ridges (Figure 1.9). Helium becomes trapped within fluid-filled inclusions and vugs in the shallow mantle and if such helium is stored within refractory U-poor mantle then there is limited ingrowth of ^{4}He leading to high $^{3}He/^{4}He$ (Anderson, 1998b). If high $^{3}He/^{4}He$ can be formed and stored in the shallow mantle from ancient MORB-degassing events then it could be released in a mid-plate environment at a later date. This model can account for initially high $^{3}He/^{4}He$ at the start of volcanism in ocean islands and declining $^{3}He/^{4}He$ over time as the gas is exhausted from the local shallow mantle until a new pathway through the mantle and lithosphere is opened at a new ocean island (Anderson, 1998b). However, proof for the existence of such a layer remains enigmatic.

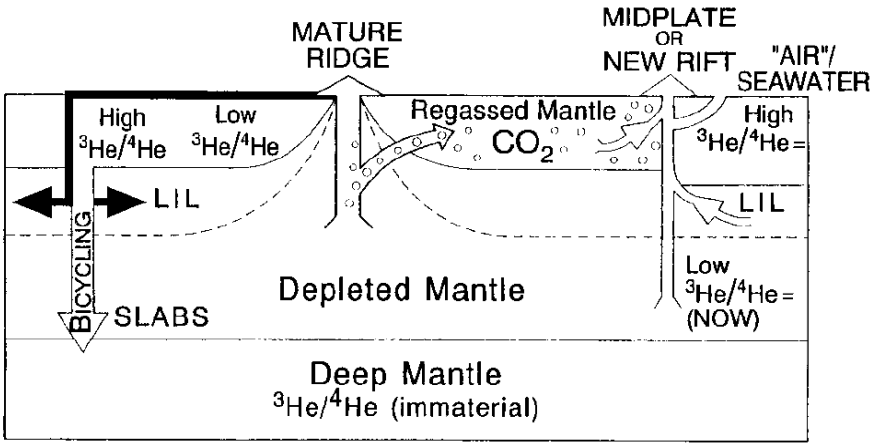

Figure 1.9. The plate model (Anderson, 1998b). Depleted mantle upwells at ridges, re-gassing the shallow mantle with ^3He. The trace element and high $^3He/^4He$ shallow reservoir 'contaminates' upwelling depleted mantle at new-rifts or in mid-plate environments to produce OIB-like magmas. From Anderson (1998b).

More recently, modelling of the helium isotope evolution of the mantle (Porcelli and Elliott, 2008) has shown that any residual mantle formed in the last few billion years would be so strongly depleted in helium that its isotopic composition is unlikely to be preserved during subsequent mixing. However, the recognition that all mantle-derived rocks have $^{142}Nd/^{144}Nd$ ratios that are 20 ppm higher than chondritic values (Boyet and Carlson, 2005) led Boyet and Carlson (2006) to argue that the Earth experienced an early differentiation event that produced a hidden 'early depleted reservoir' with high $^3He/^4He$ and super-chondritic $^{142}Nd/^{144}Nd$. The location of such a reservoir is unknown but it would need to have stayed protected from the effects of mantle convection. As suggested, the deep part of the mantle is one region that is a potential storage location for high-$^3He/^4He$ material. In addition, the deep mantle or the core mantle boundary (CMB) is thought to be the ultimate location of subducting slabs if they do pass through the 670 km transition zone and continue descending through the lower mantle as suggested by some studies (Grand, 1987; van der Hilst, et al., 1997). Seismological studies, such as that of Lay et al. (1998), provide evidence for chemically heterogeneous material in the deep mantle (~300 km above the CMB), termed the D" layer, which could apparently be represented by subducted slabs accumulating in this region to form a 'slab graveyard'. Unfortunately, this subducted material does not inherently contain high $^3He/^4He$ since any helium present in the oceanic crust would be efficiently degassed on subduction (Staudacher and Allègre, 1988). However, it is possible that subducted slabs and high $^3He/^4He$

material may mix in this region and may then be able to account for the range of trace element and radiogenic isotopic compositions observed in OIB, since subducted material is invoked to form many of the proposed key mantle components, as discussed above.

An alternative model, proposed by Samuel and Farnetani (2003), invokes the presence of a dense layer of relatively undegassed material in the D" region. This may be formed by subduction early in Earth history of meteoritic material with a high, solar implanted, helium isotope ratio (Tolstikhin and Hofmann, 2005). If the subducted slabs and dense helium-rich material are heated to the point of becoming thermally buoyant then they may rise through the mantle as plumes to supply OIB. However, some authors argue that early subducted meteoritic material cannot form the high $^{3}He/^{4}He$ required for many OIB, or even the higher-than-atmospheric $^{3}He/^{4}He$ of MORB (Hiyagon, 1994; and for a review see Porcelli and Pepin (2000)). Alternatively, the core itself, although a more controversial and unconstrained location for ^{3}He, has the advantage in that it is definitely protected from the effects of mantle convection and is a low-(U+Th) reservoir (Porcelli and Halliday, 2001). For the outer core to be a source for helium would require exceptionally high initial terrestrial helium concentrations since it is shown from metal-silicate partitioning data that the core cannot contain a significant proportion of the Earth's noble gas inventory (Sudo et al., 1994). In addition, although Os isotopes in Hawaiian lavas suggest the possibility of core involvement in their source (Brandon et al., 1999), this is not supported by W isotope anomalies (Scherston et al., 2004). Equally, Os isotope studies in the NAIP do not provide evidence for core addition to the source in this region (Brandon et al., 2007; Dale et al., 2009). If helium in OIB sources is supplied by the core then the only transport mechanism available for it to leave the core on its own is by diffusion. A better understanding of the behaviour of helium in the extreme temperature and pressure conditions expected in the core and deep mantle will be required to decide whether these regions could form a reservoir for high $^{3}He/^{4}He$.

In summary, the studies to date have failed to provide a definitive location for high $^{3}He/^{4}He$ in the Earth. The ambiguity concerns all aspects of the behaviour and partitioning of helium in different mantle phases in either the deep or shallow mantle. If helium is stored in the core then the possibility that it moves by diffusion suggests that it may be decoupled from all other lithophile elemental tracers of mantle processes. However, this could also be the case if helium is stored in the mantle. Tackley (2000) provides some schematic representations of six potential mantle dynamic situations (Figure 1.10). These are not intended to represent end-member scenarios but are provided simply to illustrate the broad range of options for the structure of the mantle. Scenarios where the high-$^{3}He/^{4}He$ source is contained in the asthenosphere are not shown here. The fact that the mantle is likely to exhibit increasing viscosity with depth leads to a strong possibility that the mantle is stratified. However, with the increasing geophysical evidence to suggest that the mantle convects as a whole presents problems in preserving high $^{3}He/^{4}He$ gas-rich primordial material over time. Whether there exists a mid-mantle boundary that inhibits flow and thus protects primordial helium in the lower mantle, or a deeper helium-rich layer near or in the core that is not involved in mantle convection, remains unknown. Either way, if helium moves by diffusion then the dynamics of the mantle are largely irrelevant. One of the best ways to investigate the potential location for the high-$^{3}He/^{4}He$ reservoir in Earth is to focus on regions on the Earth's surface where the highest, presumably most primordial $^{3}He/^{4}He$ are encountered in lavas. This way the helium isotopes can be compared to other lithophile elements whose behaviour and partitioning in the mantle are better understood.

The study presented in this thesis is based on lava samples from the highest $^{3}He/^{4}He$ magmatic province on Earth. These lavas, from the early NAIP, presumably sample some of the most primordial material available in the Earth. Therefore, the samples analysed in this study provide the best means to investigate the mantle compositions associated with high $^{3}He/^{4}He$ in the Earth in order to better constrain models for the formation, storage and preservation of the high-$^{3}He/^{4}He$ reservoir.

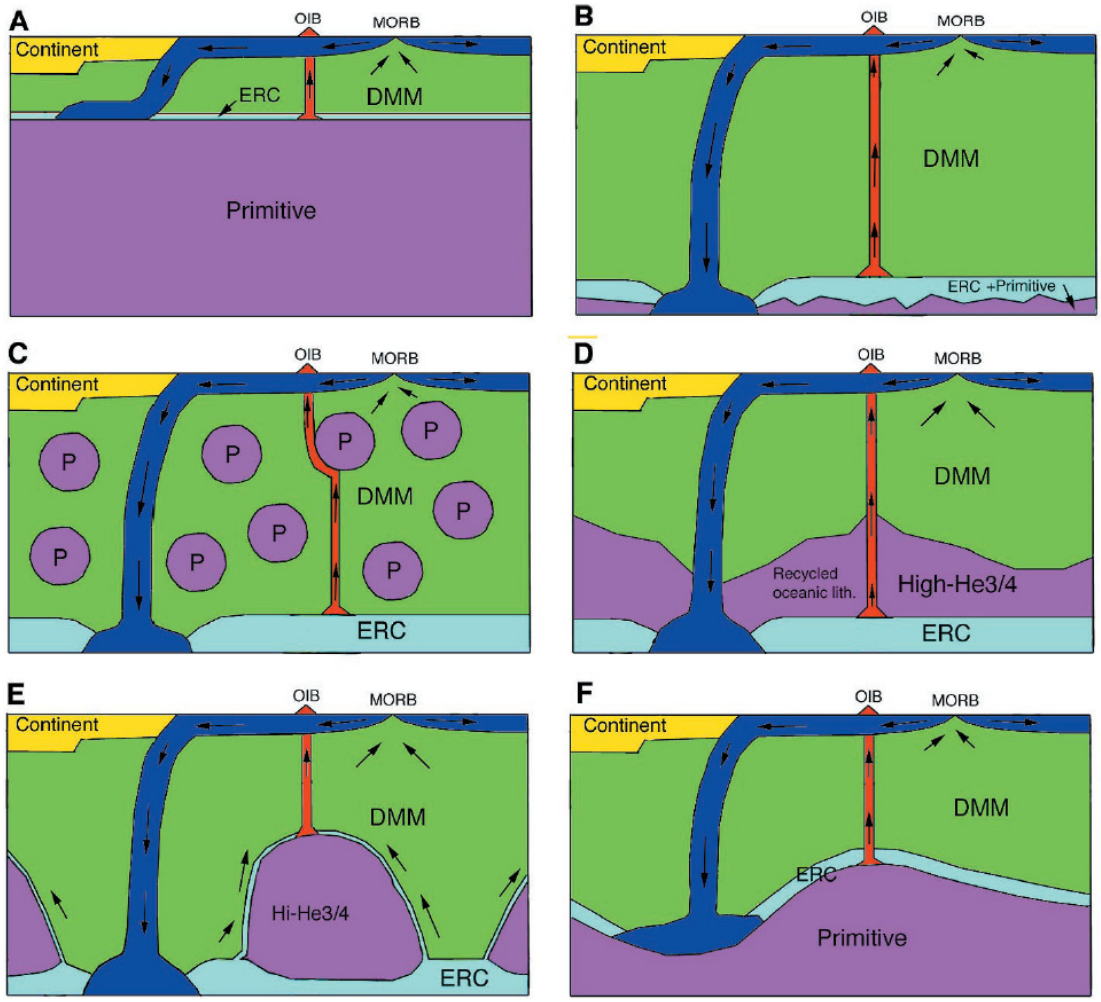

Figure 1.10. Schematic representations of mantle reservoirs and their relationship to mantle dynamics. Blue = cold slabs, Red = hot plumes, Green = DMM (Depleted MORB mantle), Purple = high $^{3}He/^{4}He$ primitive mantle, light blue = ERC (Enriched recycled crust). A) Layered convection. B) Homogenous mantle. C) Primitive blob model. D) Complete recycling model. E) Primitive piles model. F) Deep primitive layer. From Tackley (2000).

1.2 Geological history of the early North Atlantic Igneous Province

Magmatism in the NAIP has continued for the past 62 million years, from the first eruption of lavas in Baffin Island, West and East Greenland and the British Isles to present-day activity in Iceland. With lavas preserved over a pre-drift distance of more than 2000 km, and with a total volume for the Palaeocene and Eocene lavas exceeding 6 x 10^6 km^3, the NAIP remains one of the biggest 'large igneous provinces' (LIPs) on Earth (Saunders et al., 1997). Despite the evidence for crustal and lithospheric contamination of the NAIP lavas (Larsen et al., 2003; Yaxley et al., 2004; Starkey et al., 2009), many lavas appear to have transited the lithosphere rapidly and are thought to have avoided contamination (Larsen and Pedersen, 2000). In addition to the large volumes of magmatism in the NAIP, the magmas are also shown to be a few hundred degrees hotter than ambient upper mantle (Larsen and Pedersen, 2000; Herzberg et al., 2007). The NAIP lavas have high $^3He/^4He$, of up to ~20 R_a in the British Isles (Stuart et al., 2000), 30 R_a in Iceland (Macpherson et al., 2005) and 50 R_a in Baffin Island and West Greenland (Stuart et al., 2003; Starkey et al., 2009). These values exceed the $^3He/^4He$ of MORB and match or exceed OIB $^3He/^4He$. This evidence has been used to support the deep-mantle plume theory because high $^3He/^4He$ requires a reservoir with high time-integrated $^3He/(U+Th)$, potentially located in the lower mantle. The extremely high $^3He/^4He$ of the lavas in this region suggest that they sampled the most primitive mantle reservoir accessible to magma-forming processes. If this is the case then the picrites of Baffin Island and West Greenland provide the best opportunity of investigating the composition and location of these high-$^3He/^4He$ mantle sources.

1.2.1 North Atlantic Igneous Province (NAIP)

Volcanism in the NAIP occurred in two main phases (Figure 1.11; Saunders et al., 1997). The first phase consisted of continental magmatism in Baffin Island, West Greenland, Southeast Greenland, central East Greenland, the Faeroe Islands and the British Isles between 62 and 58 Ma (Figure 1.11). The second phase of volcanism was more voluminous and represented the 'break-up' phase which started ~56 Ma.

Associated with the break-up phase was the formation of thick, seaward-dipping reflector sequences (SDRS) along the East Greenland and northwest European margins and also on-shore magmatism in East Greenland (Figure 1.11 and Figure 1.12; Saunders et al., 1997; Larsen and Saunders, 1998). In general, rifting in the North Atlantic region began in the south and propagated northwards into the Labrador Sea. The early Eocene saw the main axis of rifting shift into the North East Atlantic (Figure 1.13; Vogt and Avery, 1974). The exact timing of rifting in the Labrador Sea is unknown but is not expected to have started any earlier than ~80 Ma (Roest and Srivastava, 1989), with rifting slowing down considerably by 50 Ma and ceasing by 36 Ma (Saunders et al., 1997). During this time rifting also occurred slightly farther north in the Davis Strait - Baffin Bay region, which may represent the northern limit of the Labrador Sea rifting. This led to the eruption of mafic and ultramafic volcanic rocks in West Greenland and Baffin Island. Subsidence is thought to have continued after the start of volcanism but the majority of the lavas were erupted subaerially.

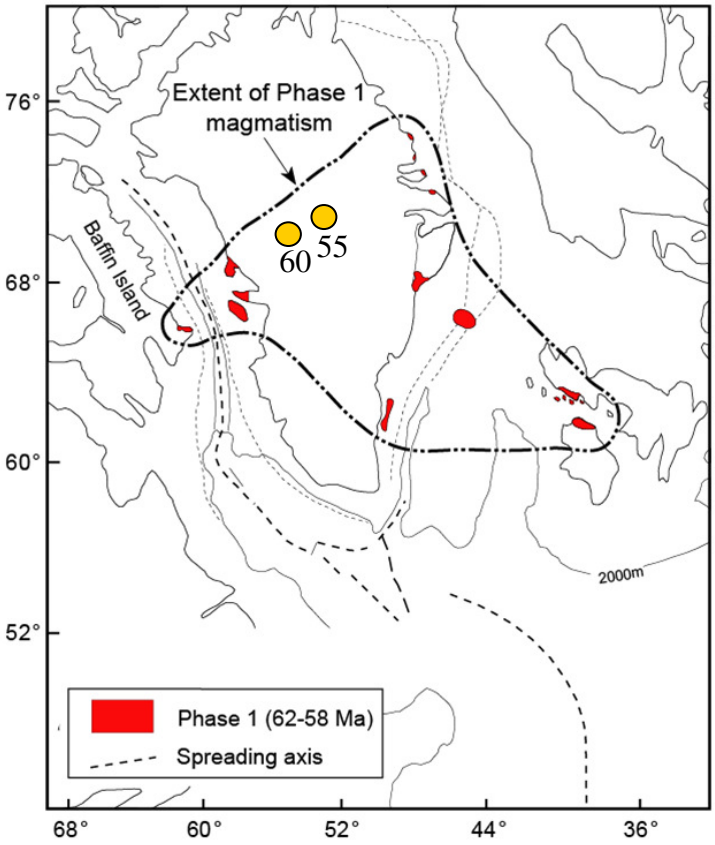

Figure 1.11. Tectonic reconstruction for the NAIP ~61 Ma with the estimated plume axis position at 60 Ma and 55 Ma and magmatic activity for Chron 26 to 24. The bold dashed line indicates the extent of Phase 1 magmatism in the NAIP. Modified from Saunders et al. (1997).

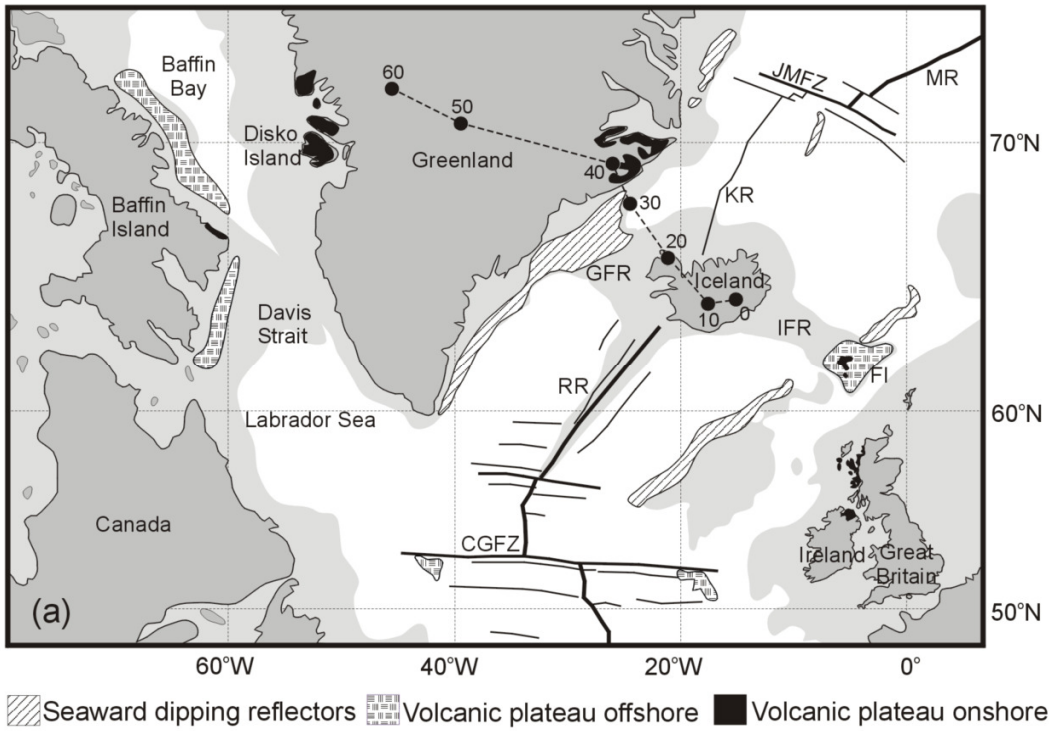

Figure 1.12. Map of the North Atlantic Igneous Province (NAIP). Location of onshore and offshore plateau basalts and seaward dipping reflectors in the NAIP. A possible plume track from 60 Ma to the present day is shown by a dashed line. CGFZ = Charlie Gibbs Fracture Zone, RR = Reykjanes Ridge, GFR = Greenland-Faeroes Ridge, IFR = Iceland-Faeroes Ridge, FI = Faeroe Islands, KR = Kolbeinsey Ridge, JMFZ = Jan Mayen Fracture Zone, MR = Mohns Ridge. From Starkey et al. (2009).

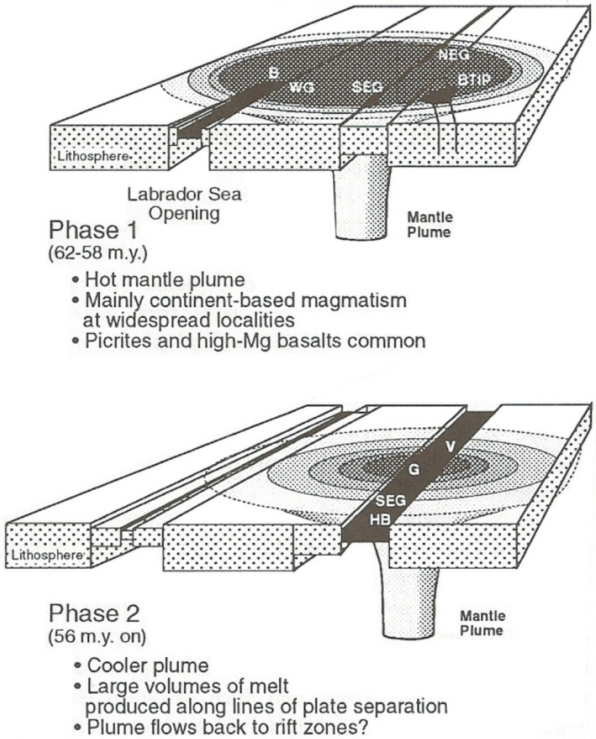

Figure 1.13. Schematic diagram to illustrate the development of the NAIP during the Palaeocene and Eocene. BTIP = British Tertiary Igneous Province, B = Baffin Island, WG = West Greenland, NEG = Northeast Greenland, SEG = Southeast Greenland, V = Voring Plateua, G = central East Greenland, HB – Hatton Bank Margin. From Saunders et al. (1997).

The Baffin Island and West Greenland lavas are considered to be stratigraphically equivalent based on age determinations (see Section 1.2.1.1 below), and the fact that the base of the Vaigat Formation and the Baffin Island lavas display a transition from sub-aqueous to sub aerial eruption (Francis, 1985; Larsen and Pedersen, 2000). The lavas were erupted through Precambrian crust and lithosphere that was thinned in response to the rifting in the Labrador Sea and Baffin Bay (Clarke and Upton, 1971). Importantly, picritic lavas are estimated to constitute 30 to 50% of the lava piles in Baffin Island and West Greenland, a much higher proportion than in other parts of the NAIP (Clarke, 1970; Clarke and Upton, 1971; Pedersen, 1985; Gill et al., 1992; Holm et al., 1993). The presence of a mantle plume in the NAIP has been suggested to account for the large volumes of lava and the rapid onset of volcanism, as well as the longevity of volcanic eruptions over a large area. At the present day the plume is thought to be present under eastern Iceland, but plate reconstructions show that it was probably located below central Greenland around 60 Ma. Figure 1.12 shows a possible hotspot track for the Iceland plume from 60 Ma to the present day.

1.2.1.1 West Greenland volcanic province

The onshore part of the Tertiary volcanic province of West Greenland comprises 68,000 km^2 of picritic and basaltic lava flows (Figure 1.14). These form an ellipse with dimensions of 430 km in a north-south direction and 200 km in an east-west direction between the Svartenhuk Peninsula and Disko (Figure 1.14; Clarke and Pedersen, 1976; Larsen and Pedersen, 2009). The succession has been divided into three lithostratigraphical units with the Vaigat Formation being the oldest, followed by the Maligât Formation then the Hareøen Formation (Hald and Pedersen, 1975). Vertical thicknesses of the exposed succession on Disko and Nuussuaq are between 2 and 3 km (Larsen and Pedersen, 2000). The picritic lavas occur only within the Vaigat Formation, covering an area of 22,000 km^2. The average thickness for the picrites is estimated at 1 km but thickness varies across the region (Dr. L.M. Larsen, personal communication 2008). From $^{40}Ar/^{39}Ar$ age determinations it appears that the West Greenland succession (Vaigat and Maligât Formations) was erupted in less than 1 million years (Storey et al., 1998). The lowermost lavas (Vaigat Formation) are

subdivided into the Anaanaa (oldest), Naujánguit and Ordlingassoq (youngest) Members (Figure 1.15; Larsen and Pedersen, 2000). The start of each phase was characterised by olivine-rich magmas, ending with either a lithospherically and/or crustally contaminated interval in the case of the Anaanaa and Naujánguit Members or an evolved interval in the case of the Ordlingassoq Member (Larsen and Pedersen, 2000). The lavas lie on Cretaceous and Tertiary sediments of the Nuussuaq Basin except for the very easternmost parts of the region where the lavas lie directly on Precambrian basement rocks.

1.2.1.2 Baffin Island volcanic province

The lavas on Baffin Island are exposed as a series of outcrops along the eastern coast between Cape Searle and Cape Dyer (Figure 1.14). They lie on Precambrian basement and Tertiary sediments and their total thickness never exceeds 750 m (Francis, 1985). The lowest few hundred metres are primarily composed of sub-aqueous flows, pillows and hyaloclastite breccias, while the upper 400 m or so comprises thin subaerial flows (Robillard et al., 1992). The Baffin Island lavas have normal magnetic polarity belonging to Chron 27n (Deutsch et al., 1971), which by correlation to the Anaanaa Member (Pedersen et al., 2002) implies an age of 61.7-62.0 Ma.

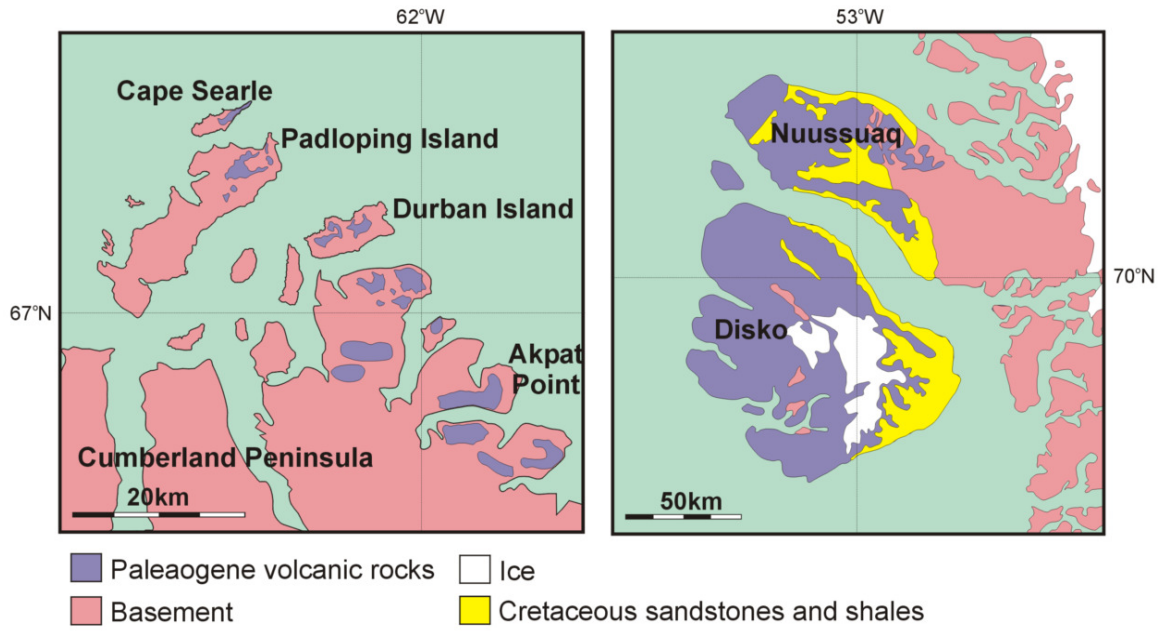

Figure 1.14. Location of onshore volcanic rocks in Baffin Island and West Greenland.

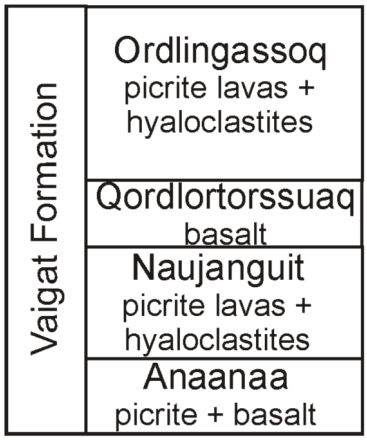

Figure 1.15. Stratigraphy for Members of the Vaigat Formation in West Greenland.

1.2.2 Crustal contamination in the early NAIP

Crustal contamination is well documented in the West Greenland lavas, occurring in episodes affecting only subordinate units of high-silica basalts and magnesian andesites (Larsen et al., 2003). Due to the thick sedimentary succession (6-8 km) in the region it is thought that magma batches may have stalled in high-level magma chambers, during the emplacement of the Vaigat Formation, where contamination occurred (Dr. L.M. Larsen personal communication). However, the magnesian basalts and picrites were thought to have erupted rapidly, passing through the thick lithosphere over a short timescale and are, consequently, thought to have avoided contamination (Gill et al., 1992; Holm et al., 1993; Lightfoot et al., 1997; Larsen and Pedersen, 2000). However, ascent velocities of magmas can vary greatly and magmas with lower ascent velocities are more susceptible to contamination.

The upper crust on Padloping Island is composed of amphibolite or granulite facies orthogneisses with the most common phase assemblage being quartz, plagioclase, K-feldspar and biotite (Clarke and Upton, 1971; Jackson and Taylor, 1972). Partial melts produced experimentally from these compositions are shown to produce broadly granitic compositions (Yaxley et al., 2004). Modelling suggests that the bulk lavas of Baffin Island were affected by <1% crustal contamination of evolving picritic liquids with granitic partial melts (Yaxley et al., 2004). However, melt inclusions in the same samples record an order of magnitude more contamination which may suggest that contamination occurred during precipitation of liquidus

olivine in wall-rock reactions (Yaxley et al., 2004). This is investigated in detail with the whole-rock and melt inclusion studies presented in Chapters 2, 3 and 4.

1.2.3 Characterising the composition of the NAIP lavas

The lavas of the NAIP varied in composition both spatially and temporally. The onset of magmatism was characterised by stratigraphically inter bedded sequences of depleted and relatively enriched lavas whereas only more enriched lavas are present in the more recent NAIP magmatism in Iceland (Fitton et al., 1997). The Baffin Island and West Greenland lavas are commonly compared to the products of melting at mid-ocean ridges (N- (normal) and E- (enriched) MORB) since they are very similar in their trace element and radiogenic isotope compositions (Francis, 1985; Robillard et al., 1992; Fitton et al., 1997; Kent et al., 2004; Starkey et al., 2009). The main compositional difference is that $^{3}He/^{4}He$ is considerably higher for the lavas of Baffin Island and West Greenland (up to 50 R_a) than lavas produced at mid-ocean ridges (8 ± 1 R_a). Similarly, the relatively enriched trace element signatures that characterise the lavas of Iceland have been compared to E-MORB (Fitton, 2007). The main difference again being the higher $^{3}He/^{4}He$ of Icelandic lavas (up to 30 R_a) compared to MORB. Whether the enriched component in the early NAIP lavas is derived from the same source as the Icelandic lavas is discussed further in Chapter 5. However, if they are derived from the same relatively enriched source then it must be a very long-lived component in the NAIP. It is also interesting to note that the more depleted component in the NAIP, comparable to N-MORB, seems only to have been available at the onset of magmatism in Baffin Island, West Greenland, Hatton Bank and the British Isles and is apparently no longer available or not sampled at the present day (Fitton et al., 1997).

Various models have been suggested to account for the compositional changes in the NAIP involving mixtures of relatively enriched, high $^{3}He/^{4}He$ plume material from the lower mantle with depleted upper mantle 'MORB-source'. Kempton et al. (2000) focus on one model for the Iceland plume involving a mix of enriched and depleted portions from the lower mantle forming the core of the plume, surrounded by a

sheath of depleted mantle entrained at the 670 km thermal boundary layer (Figure 1.16). Some end-member plume models are summarised by Fitton et al. (1997), and shown in Figure 1.17, illustrating the possibility that plumes may originate in the lower mantle or at 670 km and entrain material from a thermal boundary layer as they rise (as in Kempton et al., 2000). A hot enough plume may, however, be able to reach the Earth's surface with little or no entrainment of upper mantle material. These models rely on high $^{3}He/^{4}He$ residing in the deep mantle but also diffusing from the upwelling lower mantle into the entrained upper mantle along with the heat. However, as shown above, debate in the literature centres around the location of high $^{3}He/^{4}He$ in Earth and how it might have been preserved through Earth history. Therefore, other models may be able to account for the NAIP magmatism. These are investigated in Chapter 5.

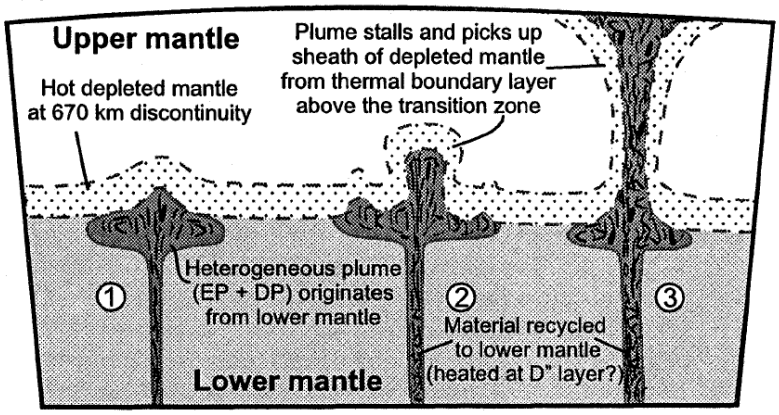

Figure 1.16. Schematic representation of Iceland plume structure showing potential location of enriched and depleted domains. From Kempton et al. (2004).

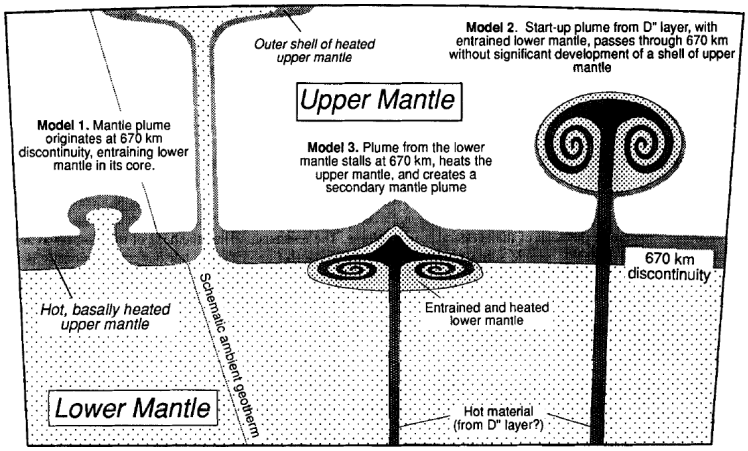

Figure 1.17. Schematic representation of various plume models. From Fitton et al. (1997).

1.3 Sampling of the lavas for this study

The Baffin Island samples for this study were collected by Dr. F. M. Stuart during an expedition in 2004 which concentrated on the sampling of olivine-rich lavas suitable for helium isotope analyses. The Baffin Island collection consists of nineteen picrite samples with high olivine contents.

The West Greenland samples were collected by the Geological Survey of Denmark and Greenland (GEUS) and belong to a much larger collection held at GEUS in Copenhagen, Denmark. The West Greenland collection consists of fourteen picrite samples that were selected by Dr. L.M. Larsen (GEUS) as suitable for helium-isotope analysis based on their high olivine content.

Analytical details for the whole-rock and microbeam geochemical techniques undertaken on the samples in these two collections are given in Appendix A. Petrological information on the samples in these two collections is available in Appendix B1 and Chapter 2. The geochemical data are presented in Appendices E-M and discussed in Chapters 2, 3, 4 and 5.

1.4 Aims of this study

The aim of this study is to present a detailed geochemical investigation of the Baffin Island and West Greenland lavas of the early NAIP using petrology, whole-rock geochemistry and microbeam geochemical techniques. The lavas from the early NAIP in Baffin Island are shown to display the highest terrestrial $^{3}He/^{4}He$ (up to 50 R_a; Stuart et al., 2003) and therefore they are thought to sample the most undiluted, high-$^{3}He/^{4}He$ reservoir in the Earth. The new collections of samples are investigated to determine whether extremely high $^{3}He/^{4}He$ is a widespread feature of the stratigraphically equivalent lavas of Baffin Island and West Greenland. In addition, it has been shown that high $^{3}He/^{4}He$ in the NAIP (Ellam and Stuart, 2004) and in global OIB (Class and Goldstein, 2005), is associated with depleted mantle

compositions. This observation is in disagreement with the prevailing orthodoxy that high $^{3}He/^{4}He$ is contained in primordial, undegassed and therefore unprocessed mantle. The samples from the Baffin Island and West Greenland collections of this study can be used to better characterise the apparently depleted yet high-$^{3}He/^{4}He$ reservoir in the Earth. Although this thesis provides primarily a local study of the Baffin Island-West Greenland lavas, it also includes a much broader study investigating the evolution of the mantle and the location, storage and preservation of high $^{3}He/^{4}He$ since the time of Earth formation.

A summary of the content of the chapters in this thesis is presented below:

Chapters 2 and 3 present the major and trace element data on the whole rocks along with the Sr, Nd and He isotope results. In these two chapters the whole-rock data are assessed in detail along with a discussion on crustal contamination. Where crustal contamination is ruled out it is then possible to ascribe the variation in whole-rock compositions to that of their mantle source.

Chapter 4 presents the olivine major element and melt inclusion major and trace element compositions of the samples that were analysed by electron and ion microprobe. Melt inclusion compositions were investigated in order to understand in better detail the small-scale melt compositions that contributed to the whole-rocks. In Chapter 4, the presence of xenocryst olivine populations are discussed along with an assessment on crustal contamination at small melt scales in order to support the findings from the whole-rock study of Chapters 2 and 3.

The aim of Chapter 5 is to collate all of the discussions from the previous results chapters in order to fully interpret the data from the whole-rock compositions, olivine crystal compositions and melt inclusion compositions. Models for the evolution of helium in the Earth and its storage and preservation since Earth formation are discussed in a global context. Finally, Chapter 6 presents the broad conclusions that result from this study.

Two peer-reviewed papers have been published in Earth and Planetary Science Letters on some of the work that is presented in this thesis. Copies of these papers are included at the end of the thesis. Starkey et al. (2009) presented all of the whole-rock data from the samples of this study along with data from a previous PhD thesis of Lass-Evans (2004). The study of Dale et al. (2009) uses some of the Baffin Island and West Greenland samples of this study for osmium isotope analyses. Both of these papers place the early NAIP samples into a more global context by comparing them to global ocean-island basalts. These papers also discuss and review the current theories for the location of high $^{3}He/^{4}He$ in the Earth.

Results

2 Results: Petrography, whole-rock major and trace elements

2.1 Introduction

This chapter focuses in detail on the petrology and major and trace element chemistry of the Baffin Island and West Greenland lavas. Lavas sampled from the Iceland plume, and particularly the products of its earliest magmatism at 62 Ma, have been the focus of continued debate in the literature concerning the highly magnesian composition of the parental magmas and in turn the source of the highly magnesian olivine crystals the rocks contain (Clarke and Pedersen, 1976; Francis, 1985; Gill et al., 1992; Larsen and Pedersen, 2000; Herzberg and O'Hara, 2002). In particular, the composition and temperature of primary magmas for these lavas is frequently discussed (Gill et al., 1992; Larsen and Pedersen, 2000; Herzberg and O'Hara, 2002; Herzberg et al., 2007). Primarily, this study is concerned with the source for high $^{3}He/^{4}He$ in the Earth. This requires a detailed understanding of the petrology and geochemistry of the rocks hosting the high-helium isotope ratios. Major and trace element data coupled with detailed petrographic work allow the lavas to be characterised and compared to mid-ocean ridge and ocean island basalts. Whole-rock Sr and Nd isotope compositions, along with the helium isotope data are presented and discussed in Chapter 3. These data further constrain the composition of the source for high $^{3}He/^{4}He$ and provide a means of testing the conclusions resulting from the major and trace element data. Helium is contained within melt inclusions hosted by olivine phenocrysts. Consequently, in-situ major element analyses of the olivine crystals along with major and trace element analyses of the melt inclusions were carried out to provide a more detailed view of the magmatic system. Olivine crystals and their compositions are discussed in this chapter and the detailed melt inclusion study is presented in Chapter 4.

2.2 Samples

The nineteen picrite samples from Baffin Island were collected from Padloping Island (8 samples), Durban Island (6 samples) and Akpat Point (5 samples) during an expedition in 2004. The 14 West Greenland samples form part of an existing collection (Larsen and Pedersen, 2000) and were selected as suitable for He isotope determinations because of their high olivine phenocryst content. These samples are from the Vaigat Formation on Disko Island and the Nuussuaq Peninsula (Figure 2.1): from the lowermost Anaanaa Member (4 samples), the Naujánguit Member (5 samples) and the Ordlingassoq Member (5 samples). In both the Baffin Island and West Greenland collections, samples were chosen for their high olivine phenocryst content and large size of olivine crystals for noble gas isotope analyses. Consequently, the samples of this study are biased through having unrepresentatively high phenocryst contents compared to other lavas from the region.

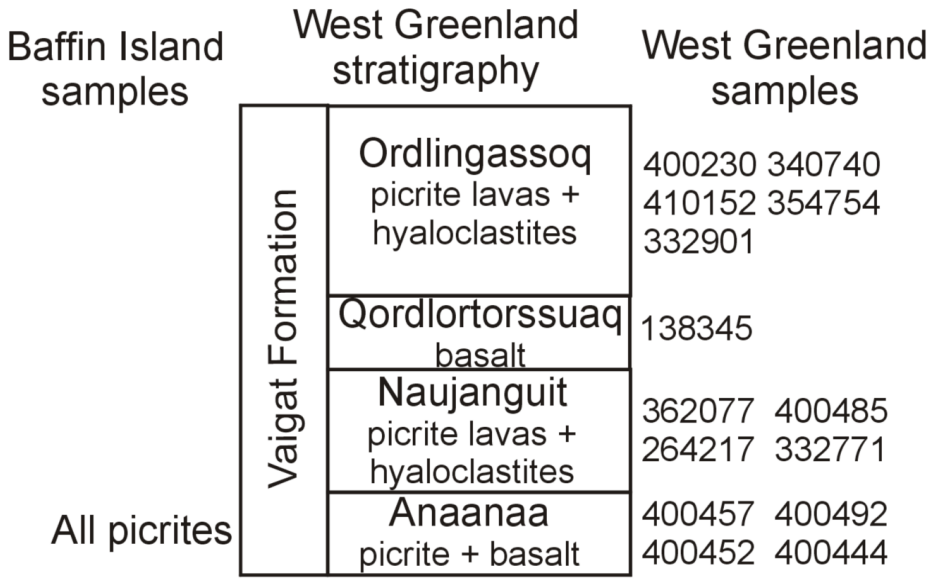

Figure 2.1. Stratigraphic location of Baffin Island and West Greenland samples of this study.

2.3 Results

2.3.1 Petrography

Nearly all the samples in this study are highly porphyritic or glomeroporphyritic and are thought to be lava flows. Olivine is the main phenocryst phase, occurring as

single crystals and glomerocrysts and composing between 21 and 45 modal percent of the rock across all samples (except for DUR1 which has 2.5 modal percent olivine, by far the lowest value observed; Appendix B). In most cases the groundmass is composed of an intergrowth of olivine, clinopyroxene and plagioclase microlaths, in a glassy matrix in which Fe-Ti oxides and sub-ophitic clinopyroxene enclosing plagioclase laths may be present. Fe-Ti oxide minerals are present in some samples. Rare plagioclase phenocrysts and glomerocrysts can occur (e.g. 400230) that, when present, are large but not common. Clinopyroxene was not observed as a phenocryst phase in these samples, in agreement with other Baffin Island (Clarke and Upton, 1971; Francis, 1985) and West Greenland (Larsen and Pedersen, 2000) picrite studies.

In general, the West Greenland samples were chosen at GEUS carefully to avoid altered samples. Despite this, alteration appears to have affected the West Greenland picrites more than those of Baffin Island. Occasional zeolites are observed in the West Greenland thin sections which are never observed in the Baffin Island samples. It has been suggested by Neuhoff et al., (2006) that low-grade zeolite metamorphism has affected the West Greenland lava pile. As already shown in Section 1.2, the lava pile in West Greenland is much thicker than that in Baffin Island. This suggests that the Baffin Island samples may never have been under the correct conditions for alteration/metamorphism to occur. Alteration is expected to be obvious in the major and trace element compositions of the samples, particularly due to increased K and Rb contents. These features are presented and discussed in Section 2.4.

Olivine morphologies can be complex with some lavas containing up to five different crystal shapes (Figure 2.2). The most common olivine crystals are euhedral and equant in shape and it is these that can form glomerocrysts. Subhedral, rounded and embayed crystals occur commonly and can often appear skeletal when they partially or completely enclose groundmass. Donaldson (1976) ascribes this feature to rapid growth rather than resorption. Long hopper-type crystals are present that are likely to have grown rapidly. Euhedral-subhedral olivine phenocrysts are typically ~0.1 mm to ~1.5 mm. Olivine crystals can host chromite and glass inclusions. Chromite

crystals may occur as single crystals within olivine and can also be encapsulated within rounded melt inclusions in olivine phenocrysts. Chromites display an array of growth shapes from feathery textures to well-developed square-sectioned crystals. When trapped within melt inclusions the chromites are unlikely to have grown directly from the trapped melt due to their large size in comparison to the volume of melt within which they are located. Melt inclusions can be partially or completely re-crystallised but many pristine clean glassy inclusions occur. These were chosen for the electron microprobe and ion microprobe studies (Chapter 4) to investigate the individual melt compositions of the Baffin Island-West Greenland source region.

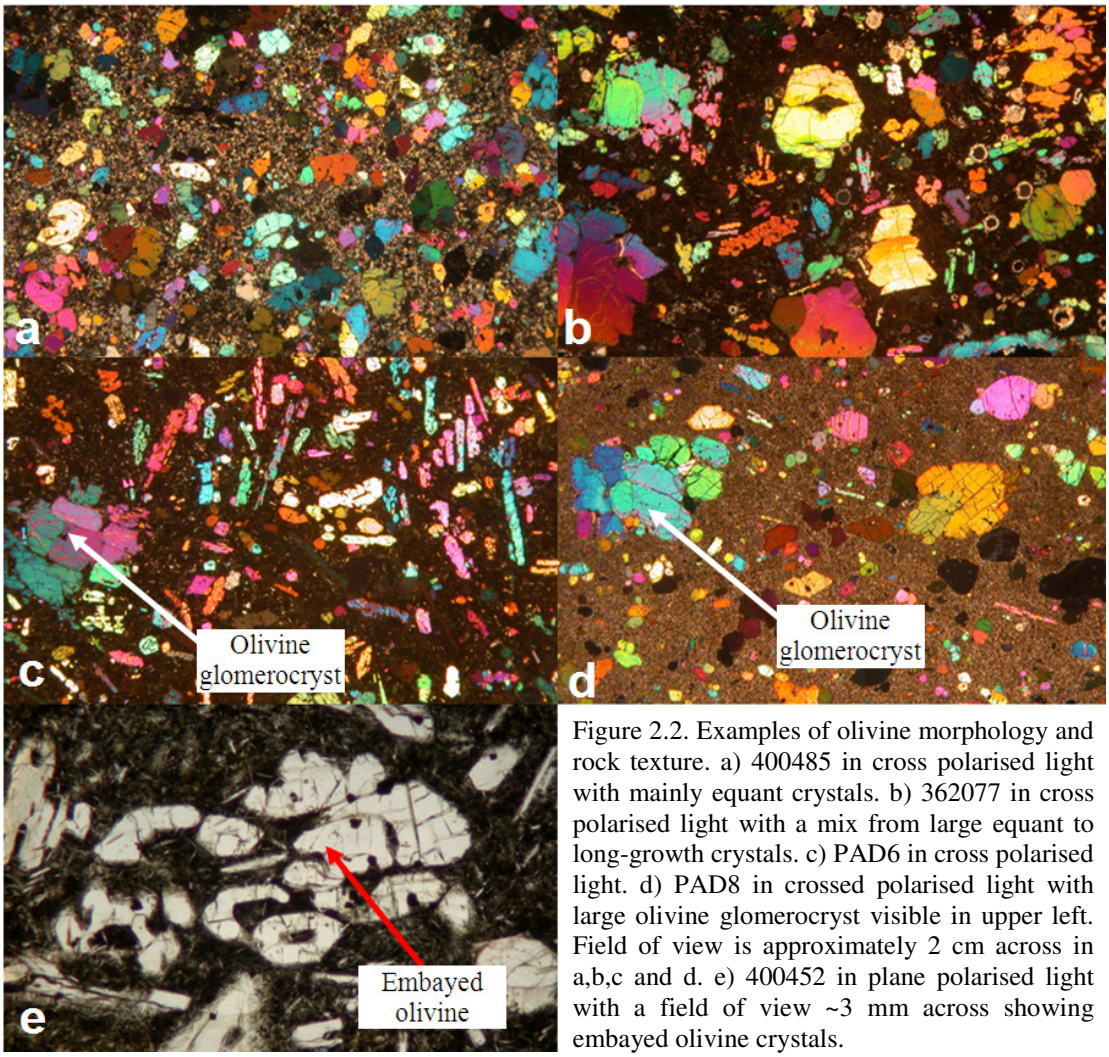

Figure 2.2. Examples of olivine morphology and rock texture. a) 400485 in cross polarised light with mainly equant crystals. b) 362077 in cross polarised light with a mix from large equant to long-growth crystals. c) PAD6 in cross polarised light. d) PAD8 in crossed polarised light with large olivine glomerocryst visible in upper left. Field of view is approximately 2 cm across in a,b,c and d. e) 400452 in plane polarised light with a field of view ~3 mm across showing embayed olivine crystals.

2.3.2 Olivine compositions

Olivine phenocryst core and rim compositions were measured on a Cameca SX100 electron microprobe at the University of Edinburgh (analytical details can be found in Appendix A6) in order to investigate the variation in compositions. The compositions of olivine phenocrysts are used to determine the parental melt compositions and temperatures (this chapter Section 2.4.2). Olivine compositions are also used for determination of the forsterite content of the olivine crystals that host melt inclusions (Chapter 4).

The compositions of 549 olivine crystals (477 core compositions and 72 rim compositions) from 22 samples (11 from Baffin Island and 11 from West Greenland) were measured. Histograms of olivine forsterite contents (forsterite mole percentage is equal to magnesium number = atomic 100Mg/(Mg+Fe); Figure 2.3) indicate that olivine core compositions are unimodal with a range from Fo_{78-93} for Baffin Island (average of $Fo_{87.6}$) and Fo_{77-93} for West Greenland (average of Fo_{86}). The olivine phenocrysts fall into three categories: 1) large, near-equant crystals (~1.5 mm) with wide, highly magnesian cores (Fo_{90-93}) and thinner, normally zoned rims (Fo_{78}-Fo_{85}). 2) Medium-sized crystals (~0.5 mm) of varied morphology (equant, tabular, skeletal) with normal zoning from Fo_{88} in the core to Fo_{77-85} at the rim. 3) Small, normally zoned and unzoned skeletal and tabular crystals (<0.2 mm) with core compositions Fo_{87-88} and, if zoned, with rims down to Fo_{74-84}. There is substantial overlap between the composition of small crystals and the rims of large crystals. This suggests that small crystals nucleated and grew at the same time as the rims on the larger crystals whose high forsterite cores had grown from more primitive magma. Large crystals were more likely to have been growing gradually and continuously during the entire phase of magma evolution to achieve normal zoning from high forsterite cores to low forsterite rims.

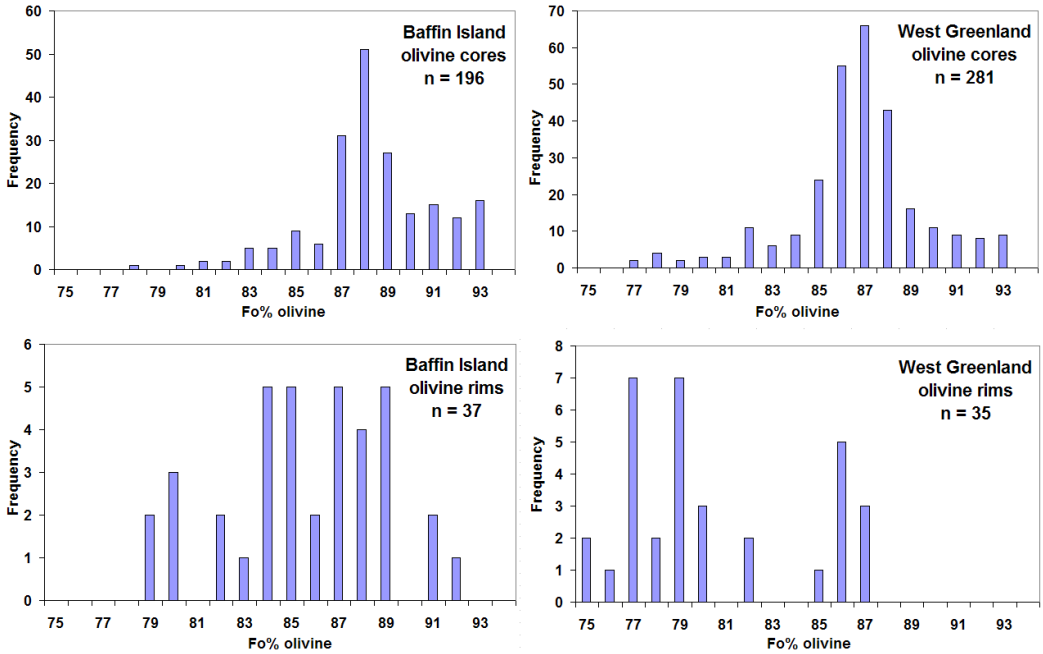

Figure 2.3. Frequency histograms of Baffin Island and West Greenland olivine core and rim compositions (% mole forsterite) determined by electron microprobe.

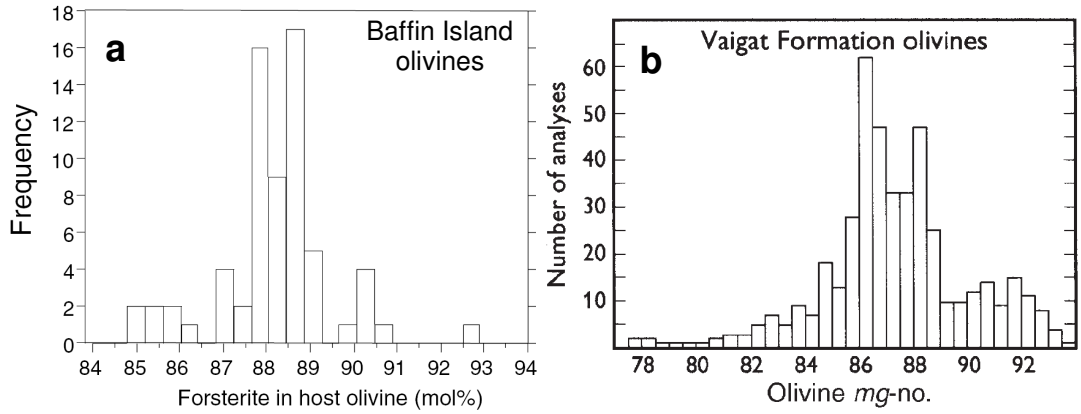

Figure 2.4. Frequency histograms for a) 67 olivine analyses from Baffin Island. From Yaxley et al. (2004). b) 418 olivine analyse from Vaigat Formation, West Greenland. From Larsen and Pedersen (2000).

Olivine phenocryst compositions determined in other studies from Baffin Island and West Greenland lavas typically range from Fo_{78-93} (Francis, 1985; Larsen and Pedersen, 2000; Figure 2.4) which is in broad agreement with this study. The majority of olivine analyses in the Baffin Island study of Yaxley et al. (2004) fall between Fo_{88-90}. Larsen and Pedersen (2000) conclude that the majority of olivine phenocrysts in the West Greenland lavas have compositions of Fo_{86-89} but a relatively small proportion of olivine compositions extend up to Fo_{93} (these form <1% of a thin section).

There is no significant difference between the olivine compositions measured in picrites from Baffin Island and West Greenland. There is, however, considerable debate as to the nature of the highly magnesian crystals (Francis, 1985; Larsen and Pedersen, 2000). Oxide variation plots for minor elements in Baffin Island and West Greenland olivines of this study show smooth continuous trends in Cr_2O_3, NiO and CaO from Fo_{74-93} (Figure 2.5). These data suggest that all the crystals, including the highly magnesian olivines, belong to the same magmatic system, evolving from magmas that were related, as suggested by Larsen and Pedersen (2000) for the West Greenland picrites.

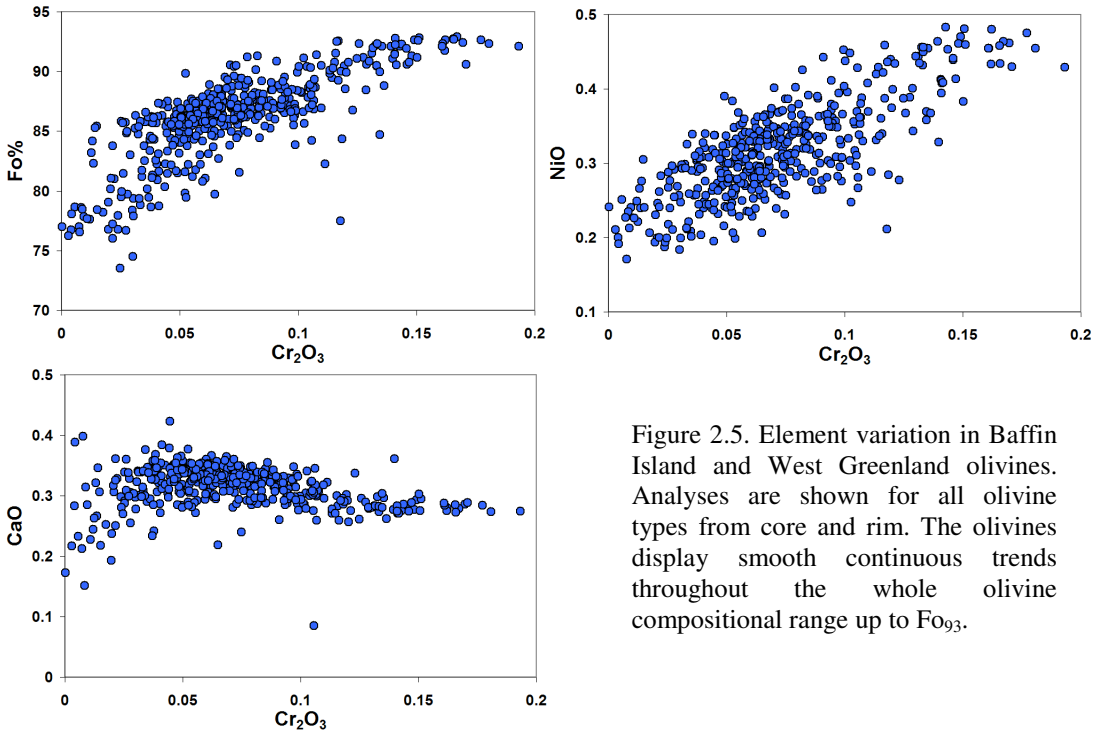

Figure 2.5. Element variation in Baffin Island and West Greenland olivines. Analyses are shown for all olivine types from core and rim. The olivines display smooth continuous trends throughout the whole olivine compositional range up to Fo_{93}.

Francis (1985) suggests that the highly forsteritic olivine crystals (Fo_{93}) in the Baffin Island picrites could be xenocrysts as they display kink-banding and the olivine glomerocrysts have polygonal 120º grain boundaries suggesting that the crystals were deformed as a solid assemblage. However, the Ca contents of the olivines are much higher than that of olivines in mantle-derived xenocrysts and Francis (1985) suggested that the xenocrysts represent early-formed dunite cumulates from the floor of the magma chamber. Such crystals cannot be classed as true xenocrysts since they represent the products of the earliest crystallisation from the most primitive liquids in

the magmatic system rather than from some exotic melt composition.

The olivine crystals in this study do not display kink-banding but occasionally the crystals composing the olivine glomerocrysts have 120º grain boundaries. The olivines also have high Ca and Cr contents (Figure 2.5), in agreement with Larsen and Pedersen's (2000) study of highly magnesian olivines in West Greenland picrites. The West Greenland olivine crystals are considered to be integral to the cognate mineral assemblage for the same reasons proposed for the Baffin Island crystals in this study (high Ca and Cr contents, continuous compositional arrays). Herzberg and O'Hara (2002), on the other hand, report the potential for the Fo-rich crystals to be wall-rock xenocrysts with the fractional melts that produced them having been lost through mixing of the magmas prior to eruption. Alternatively, the Fo-rich crystals may be phenocrysts crystallised from fractional melts that exited the melting regime or were never sampled due, once again, to mixing of melts during eruption (Herzberg and O'Hara, 2002). Either of these options is possible but it would also be hard to detect such crystals petrographically or chemically.

The presence of melt inclusions within all types of crystals observed within Baffin Island and West Greenland picrites, including even large, highly magnesian crystals, indicates that the crystals must have grown from melts, ruling out an origin as mantle xenocrysts (Francis, 1985; Larsen and Pedersen, 2000). The primary question is whether all of the phenocrysts in any one sample are genetically related or whether a proportion are sourced from exotic magmas. Dale et al., (2009) rule out a varied origin for the different populations of olivine crystals in Baffin Island and West Greenland picrites due to their chondritic to suprachondritic osmium isotope compositions. Unfortunately, apart from ruling out the possibility that the highly magnesian olivines are mantle xenocrysts, their origin and relationship to the erupted magma compositions remains unknown. Davidson et al. (2007) have described such crystals as 'antecrysts', a term to account for the fact that the crystals did not grow directly from the melts in which they are hosted and therefore are not true phenocrysts. The 'antecrysts' may have grown from an earlier parental melt that shared a common history in the magmatic system but that is not directly sampled by

the magmas, possibly due to small melt volumes. It is likely that the complex magmatic plumbing system that existed at Baffin Island-West Greenland allowed for crystals that grew from melts that were originally from a common source, but that experienced varied crystallisation histories, to be mixed together during eruption. Although the small-volume melts that produced the highly forsteritic olivines are not directly sampled during eruption it is possible that they were sampled by melt inclusions that were trapped in olivine crystals prior to mixing of melts. In this case, comparison of the compositions of melt inclusions in low- and high-forsterite olivine crystals will test whether the parental melts for these highly forsteritic crystals are of an exotic composition (i.e. true xenocrysts).

High ascent velocities have been assumed for the lavas of West Greenland which helps to account for the large volumes of lava erupted in a short timescale (Storey et al., 1998) and also provides a means for accumulating olivine in the lavas, thus increasing their bulk MgO content. Lass-Evans (2004) found that dykes from Baffin Island (which presumably were emplaced at higher velocity than the associated lavas) contained a much higher proportion of highly magnesian olivines and no olivine crystals with $<Fo_{89}$. Eruptions with particularly high ascent velocities may be able to scavenge crystals from conduit walls and from deep in the plumbing system and carry more crystals in suspension than eruptions with lower ascent velocities (Larsen and Pedersen, 2000). It has been suggested that lavas erupted at lower ascent velocities could not transport all the olivine crystals, especially those from greater depth that settled out prior to eruption (Larsen and Pedersen, 2000). Therefore, most commonly, erupted lavas are mixtures of liquids, recycled antecrysts and true phenocrysts (Davidson et al., 2007). It is not a surprise then that olivine phenocrysts are often not in equilibrium with the liquids within which they are found. However, since it is likely that the erupted liquid is itself a mixture of many liquid compositions, it does not rule out the possibility that crystals were once in equilibrium with liquids related to the system as a whole, whose compositions has been obscured through mixing. The plumbing system for Baffin Island and West Greenland has been described as similar to the crystal-rich narrow magma chambers that are envisaged for mid-ocean ridges (Sinton and Detrick, 1992) except that the

vertical extent is much greater (Larsen and Pedersen, 2000). This type of system can allow for mixing of magmas that have differentiated to various degrees at different levels and that may have lost or accumulated olivine. The potentially large and complicated magmatic system makes it very hard to assess the ultimate source composition of high $^{3}He/^{4}He$. Helium isotope ratios are measured on gas exsolved from melt inclusions in olivine crystals and ideally these ratios need to be correlated to the olivine compositions and populations of crystals in the relevant sample. The helium isotope ratios are measured in 1-2g of olivine, which are a mix of all crystals present in the sample. Consequently, it is difficult to connect $^{3}He/^{4}He$ to a particular olivine composition and melt inclusion major and trace element composition. However, understanding the various potential locations for high $^{3}He/^{4}He$ is important and future studies will focus on this problem more directly. Without the requirement for extreme exotic melt compositions to produce the crystal compositions observed, the $^{3}He/^{4}He$ can at least be linked directly to the whole-rock and melt inclusion compositions.

2.4 Whole-rock chemistry

2.4.1 Whole-rock major element compositions

Major elements were determined on whole-rock powders by X-ray fluorescence (XRF) at the University of Edinburgh (analytical details are included in Appendix A2). Major element data were corrected to 100% totals on a volatile free basis with all Fe expressed as FeO.

The Baffin Island and West Greenland samples are classified as picrites according to the IUGS classification due to their high MgO content (>12 wt%; Le Bas, 2000). In this classification the samples extend compositionally into the field of komatiites due to their MgO content reaching 24 wt% (Figure 2.6). However, the absence of spinifex texture in the Baffin Island and West Greenland lavas means that, petrographically, the samples cannot be classed as komatiites.

Oxide variation diagrams demonstrate strong similarities between the Baffin Island and West Greenland picrites. The samples of this dataset extend up to particularly high bulk MgO with a range from 9.66 to 28.28 wt%. The samples define negative linear trends (Figure 2.6) in SiO_2 (44.2–49.1 wt%), Al_2O_3 (4.8–15.8 wt%), Na_2O (0.7–1.8 wt%) and CaO (7.1–12.6 wt%) versus MgO. These trends are the same as the general trends shown by published Baffin Island and West Greenland samples (Francis, 1985; Robillard et al., 1992; Holm et al., 1993; Lightfoot et al., 1997; Graham et al., 1998; Larsen and Pedersen, 2000; Yaxley et al., 2004; Figure 2.6). FeO increases with increasing MgO from 9.6 to 12.0 wt% but in general the trend is fairly flat over the full range. TiO_2 (0.44–1.26 wt%), P_2O_5 (0.04–0.14 wt%), K_2O (0.02–0.41 wt%) and MnO (0.16–0.19 wt%) all display some degree of scatter (Figure 2.6). Sample DUR1 has very low MgO (9.6 wt%) compared to other samples in this dataset. DUR1 is unusual in this study in that it is particularly phenocryst-poor. The whole-rock linear trends between major elements with MgO (Figure 2.6) resemble a liquid line of descent because the concentration of olivine phenocrysts drives the bulk composition along a trend that runs close to an olivine-control line. If the lavas accumulated olivine, and if the linear correlations represent olivine addition lines, then they should project back to the cumulus olivine composition (Krishnamurthy and Cox, 1977). However, it is probably meaningless to find a cumulus olivine composition for the dataset as a whole since lavas from different locations are likely to originate from local plumbing systems that may have subtly different compositions. Separating the data by locality leaves too few samples in each group to provide a trend reliable enough for an accurate estimate of cumulus olivine composition. Either way, the expected olivine cumulus composition will be highly forsteritic for most regions as highly magnesian crystals are commonly found.

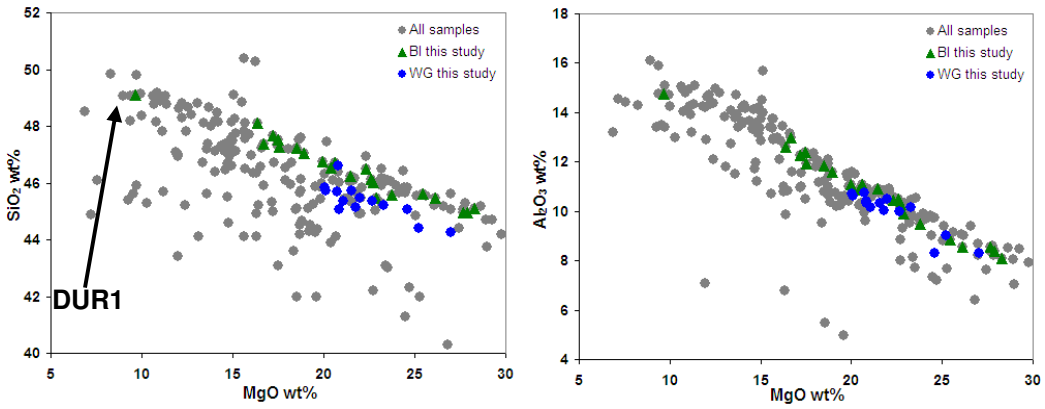

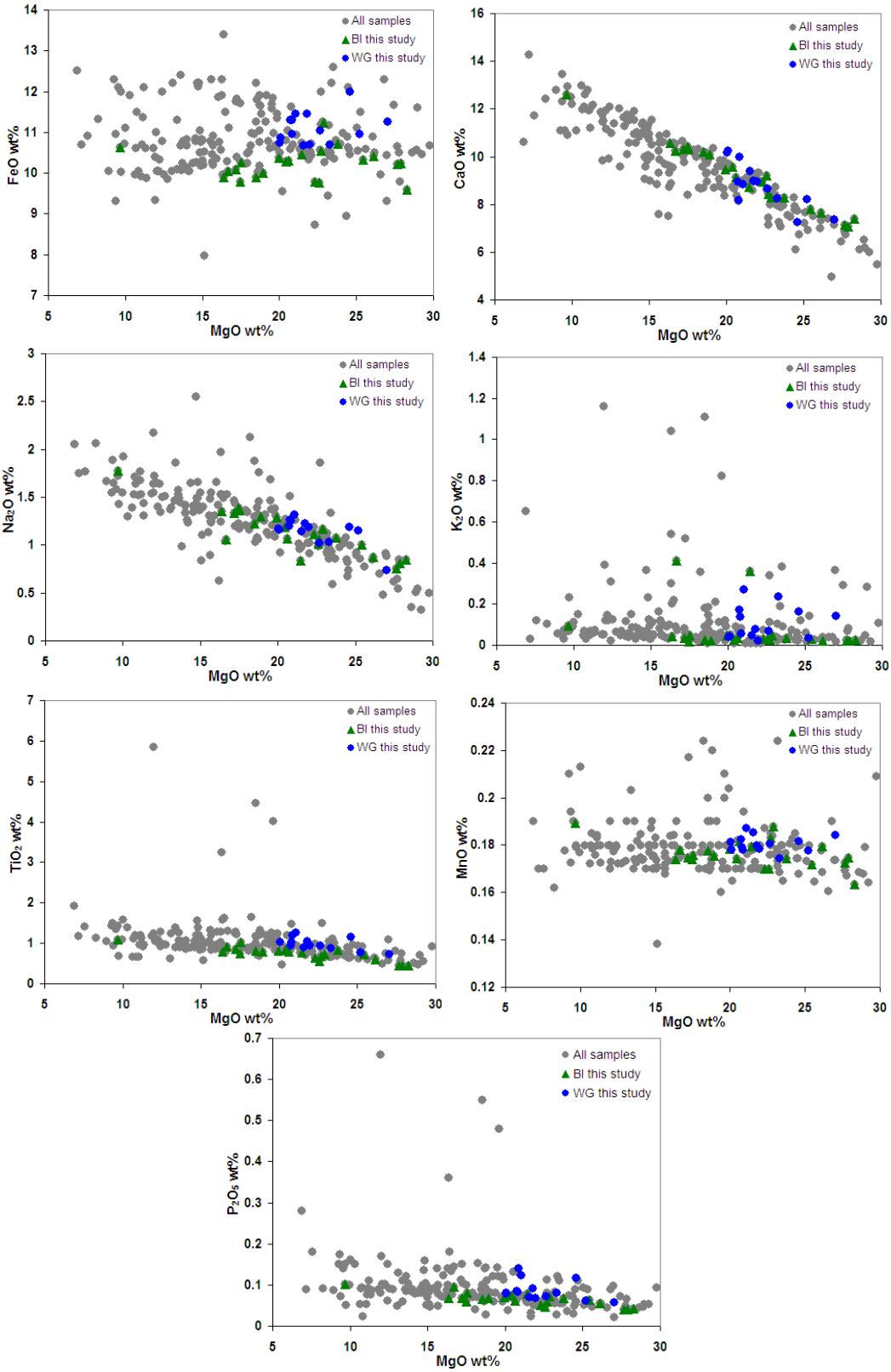

Figure 2.6. Major element plots versus MgO for Baffin Island and West Greenland samples of this study and other datasets (Francis, 1985; Robillard et al., 1992; Holm et al., 1993; Lightfoot et al., 1997; Graham et al., 1998; Larsen and Pedersen, 2000; Lass-Evans, 2004; Yaxley et al., 2004;). SiO_2, Al_2O_3, Na_2O and CaO all display negative correlations with MgO. FeO, TiO_2, P_2O_5, K_2O and MnO display some degree of scatter.

The Baffin Island and West Greenland samples of this study are classed as basalts or picro-basalts on a Total Alkali Silica (TAS) diagram (Le Maitre et al., 1989; Figure 2.7). The picrites in this study are tholeiitic although some alkalic lavas are found inter bedded within the sequences in West Greenland (Larsen et al., 2003).

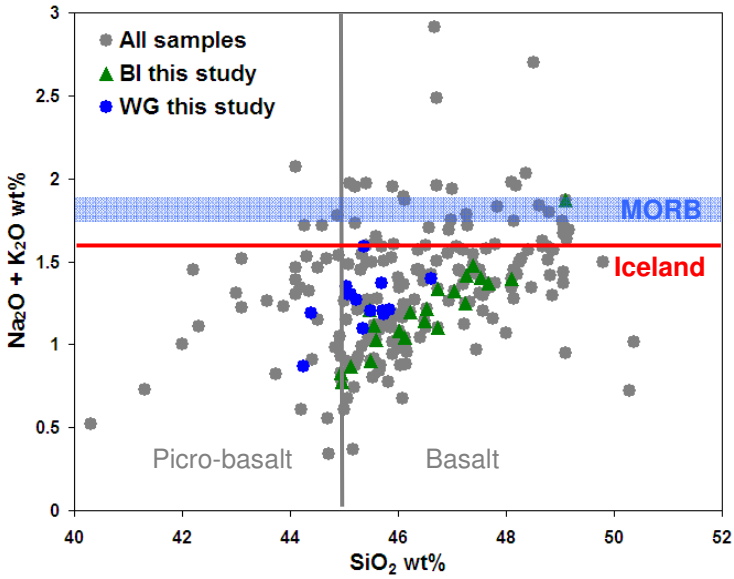

Figure 2.7. Total Alkali versus Silica (TAS) diagram after Le Maitre et al. (1989) for Baffin Island and West Greenland samples (this study and all other available analyses (Francis, 1985; Robillard et al., 1992; Holm et al., 1993; Lightfoot et al., 1997; Graham et al., 1998; Larsen and Pedersen, 2000; Yaxley et al., 2004; Lass-Evans, 2005). Samples overlap the picro-basalt to basalt transition (indicated by grey vertical line at 45 wt% SiO_2). Samples define a linear trend scattering to high Na_2O + K_2O with increasing SiO_2.

Na_2O/TiO_2 ratios are used by Jackson and Dasgupta (2008) to indicate the relative pressure of melting for magmas from different tectonic settings. MORB ranges from ~1.82 to 1.87 (Su, 2003) representing low pressure melting. Iceland and Galapagos also exhibit fairly high Na_2O/TiO_2 averages of ~1.56 and ~1.68 respectively and Hawaii has a lower average of ~0.96 suggesting the highest pressure melting under thick lithosphere (Jackson and Dasgupta, 2008). Average Na_2O/TiO_2 for the Baffin Island and West Greenland samples in this study are ~1.55 (σ = 0.22) and ~1.17 (σ = 0.14) respectively (taking all published analyses into account gives average Na_2O/TiO_2 of ~1.45 (σ = 0.33) for Baffin Island and ~1.17 (σ = 0.22) for West Greenland). These values suggest higher average pressures of melting for both Baffin Island and West Greenland compared to Iceland (and MORB). This is consistent with the magmas having been erupted through thick lithosphere. In addition, the lower Na_2O/TiO_2 of the West Greenland samples suggests a higher pressure of melting than for the Baffin Island samples, probably reflecting a local variation in lithospheric thickness.

Herzberg and O'Hara (1998) show that ancestral Iceland plume picrites are very similar to liquids produced by melting of a garnet lherzolite source at 3.8 GPa and that if a harzburgitic source is required then pressures extend to slightly higher values (3.8-4.5 GPa). These pressures of segregation suggest that the melts were produced around 100 km depth, therefore below a thick lithospheric lid (Larsen and Pedersen, 2000). The magmas were unlikely to have ponded at this depth because they would have fractionated to basaltic compositions, which implies that they probably entered steep conduits through the lithosphere and crust prior to eruption.

2.4.2 Picrites, parental magma composition and temperature

Many picrites may obtain a high MgO content due to olivine accumulation, maybe as a result of crystal settling or scavenging of crystals during magma ascent through crystal-rich conduits. Such olivine crystals have the potential to be in textural but not compositional equilibrium with their groundmass. It is possible to ascertain whether olivine crystals are in compositional equilibrium with their host rock by comparing a calculated equilibrium olivine composition of a particular bulk rock composition (Fo_{calc}) to the highest olivine forsterite value measured by electron microprobe in the same rock (Fo_{max}). If Fo_{max} is higher than Fo_{calc} then it is possible that the high-forsterite olivines crystallised from a more magnesian melt. The bulk rock composition probably represents liquid plus accumulated crystals, so we should expect $Fo_{calc} > Fo_{max}$. The following modelling relies on the assumption that the bulk rock directly represents the magma composition. However, liquids have accumulated olivine phenocrysts that are likely to have crystallised from liquids with other compositions. In this case, the bulk rock composition would not actually be equal to a liquid composition that represented the system.

Sample	Fo_{max}	Fo_{calc}	Sample	Fo_{max}	Fo_{calc}
PAD4	92.6	92.7	138345	92.8	93.2
PAD5	92.2	92.4	264217	90.5	92.9
PAD6	92.3	91.7	332901	90.5	92.8
PAD8	91.3	92.5	340740	91.1	92.4
PAD9	92.1	94.8	354754	88.6	92.1
APO1	89.9	94.4	362077	92.3	93.5
APO4	88.9	93.5	400230	91.9	92.3
APO7	92.9	93.9	400452	88.0	92.8
DUR3	91.5	92.1	400457	86.0	92.9
DUR6	92.4	91.5	400485	87.7	93.7
DUR8	91.1	92.8	410152	87.1	92.1

Table 2.1. Fo_{max} (most magnesian olivine measured by electron microprobe) and Fo_{calc} (calculated olivine composition in equilibrium with whole-rock compositions) for Baffin Island and West Greenland samples whose olivine compositions have been determined.

Table 2.1 shows that, as expected, the majority of whole-rock compositions are in equilibrium with olivine that is slightly more magnesian than the most forsterite-rich olivine in each sample. There are however some exceptions, notably PAD6 and DUR6. In general, the West Greenland picrites contain less-magnesian olivine crystals than the calculated equilibrium olivine composition. Larsen and Pedersen (2000) suggest that highly magnesian olivine crystals in the West Greenland picrites were commonly left behind in the conduit system so that the more Fe-rich olivine crystals were erupted. If, on the other hand, the olivine in equilibrium with the erupted lava is more magnesian than the most forsteritic olivine in the rock then it suggests that the lava acquired olivine crystals from the conduit walls where they had been left by more slowly ascending lavas, as demonstrated by Lass-Evans (2004) with Baffin Island dykes.

For samples where whole-rock and olivine compositions are available it is possible to estimate a parental melt composition for each of the individual lavas (Table 2.2). Firstly K_D (the partition coefficient of Fe/Mg between liquid and olivine) is calculated for each sample using $K_D^{Ol/L}{}_{FeO/MgO} = 0.381 - 0.790/MgO + 1.039/MgO^2$ (where MgO is the wt% concentration in the liquid; Herzberg and O'Hara, 2002). The K_D value is used to calculate the liquidus equilibrium olivine forsterite using $Fo_{calc} = 100/(1 + (0.56098 \times K_D \times (FeO/MgO))$ where FeO and MgO are the wt% concentration in the liquid. Fo_{calc} is compared to the most magnesian olivine

measured in the real rock (Fo_{max}) by electron microprobe. Olivine addition or subtraction is undertaken depending on whether Fo_{calc} is lower or higher than Fo_{max}. This is achieved by incrementally adding or subtracting the relevant analysed olivine composition in small increments (0.1 wt% is chosen here) until a melt composition is reached that is in equilibrium with the observed olivine composition (similar to method used by Green et al., 2001). The new melt composition is inferred to be the composition of the parental melt since this is 'the most primitive magma that can be inferred from direct observation of a rock suite and the observation that retains the earliest evidence of differentiation is the most magnesian olivine phenocryst composition' (Herzberg et al., 2007). One of the main areas of uncertainty and disagreement in parental melt calculations lies in the measurement of the olivine with the highest forsterite in the real rock (Herzberg et al., 2007). It is possible that the olivine with highest forsterite in any particular sample is not measured because it was not sampled (either left behind at depth or simply it did not appear in the particular thin sections chosen for analysis). A further possible explanation is that, as previously discussed, highly magnesian olivines (>Fo_{93}) may be the consequence of extreme fractional melts or wall-rock xenocrysts (Francis, 1985; Herzberg and O'Hara, 2002; Yaxley et al., 2004). This is investigated in more detail in Chapter 4.

Despite the problems discussed above, the maximum calculated parental melt MgO are similar to those found in more extensive studies in the literature. The parental melt composition of the Baffin Island-West Greenland samples studied vary from 9.2 wt% to 22.0 wt% MgO. The upper limit is similar to that found by Yaxley et al. (2004) of 21.5 wt% MgO for Baffin Island picrites. Parental melt compositions can be compared to estimates of primary melts (O'Hara, 1968). Herzberg and O'Hara (1998) show that the composition of picrites (and komatiites) can be matched to experimentally-produced primary magma compositions. Herzberg and O'Hara (2002) use inverse and forward models to calculate primary magma compositions along with eruption and potential temperatures for Baffin Island and West Greenland. When considering calculations from depleted and fertile peridotite sources, the primary magmas for Baffin Island and West Greenland are found to contain 18–20 wt% MgO with eruption temperatures of 1400–1440°C and potential

mantle temperatures of 1520–1570°C. Herzberg and O'Hara (2002) note that Fe-rich sources yield lower MgO contents (14 wt%) for primary magmas which may explain some of the low MgO estimates from this study. Larsen and Pedersen (2000) suggest that Fo_{93} crystals in West Greenland picrites can be used to determine parental melt compositions of 20–21 wt% MgO and liquidus temperatures of 1515–1560ºC. This requires high degrees of melting (~25%) at depths of 60-120 km (Scarrow and Cox, 1995; Lightfoot et al., 1997; Graham et al., 1998). Disregarding high forsterite crystals and assuming that Fo_{86-89} olivines are the most primitive phenocrysts requires parental melts with only 11–13 wt% MgO (Francis, 1985).

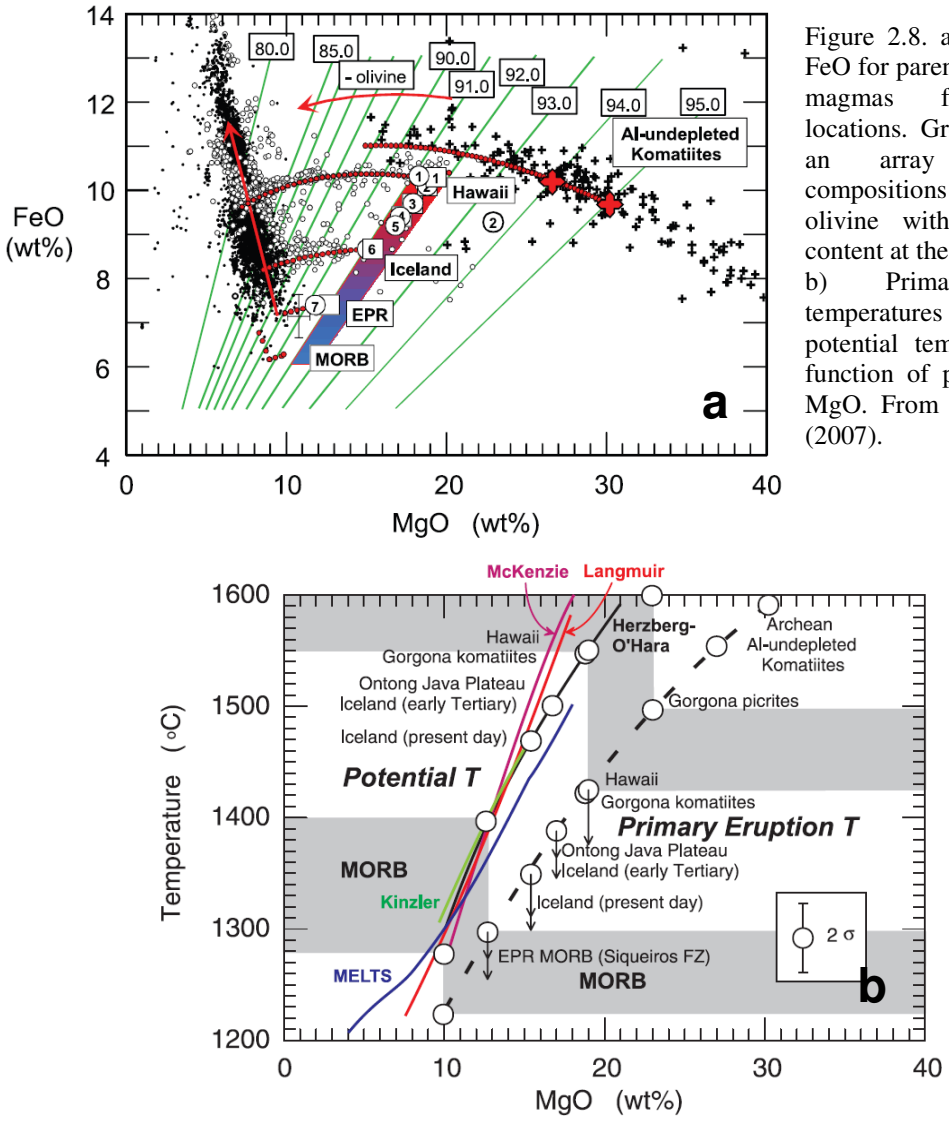

Figure 2.8. a) MgO against FeO for parental and primary magmas from various locations. Green lines show an array of liquid compositions that precipitate olivine with a given Fo content at the surface. b) Primary eruption temperatures and mantle potential temperatures as a function of primary magma MgO. From Herzberg et al. (2007).

The wide range of parental melt compositions obtained in this study most likely reflects the heterogeneous nature of the source for the Baffin Island and West Greenland magmas. In addition, the wide range of maximum forsterite olivine compositions also suggests that the olivine crystals were not in equilibrium with one magma but were instead part of a complex heterogeneous source. In general, the various studies available agree on high parental and primary melt MgO contents in the region of 18–21 wt%, and by inference, high mantle potential temperatures. Estimated potential temperatures range up to ~1570^{O}C, approximately 200°C above those estimated for ambient mantle (1280–1400°C; Herzberg and O'Hara, 2002; Herzberg et al., 2007; Figure 2.8), supporting the hypothesis of a thermal anomaly associated with the early Iceland plume.

Table 2.2. Calculated parental melt compositions.

Sample	PAD4	PAD5	PAD6	PAD8	PAD9	APO1
SiO_2	46.79	47.33	47.33	47.39	46.81	47.78
Al_2O_3	11.18	11.99	11.64	12.22	11.35	14.06
FeO	10.31	9.90	10.06	10.45	10.41	10.98
MgO	20.35	18.12	18.81	16.82	18.90	13.08
CaO	9.22	10.34	9.81	10.47	10.38	11.76
Na_2O	1.08	1.24	1.27	1.42	1.18	1.24
K_2O	0.03	0.03	0.03	0.05	0.04	0.03
TiO_2	0.79	0.81	0.82	0.90	0.64	0.72
MnO	0.18	0.18	0.17	0.20	0.23	0.28
P_2O_5	0.06	0.07	0.06	0.08	0.06	0.06
wt% olivine added	-0.9	-1.2	5.1	-9.3	-28.4	-38.5
Fo_{max}	92.64	92.20	92.33	91.30	92.12	89.93
Fo_{calc}	92.73	92.35	91.72	92.49	94.82	94.39

Sample	APO4	APO7	DUR3	DUR6	DUR8
SiO_2	48.94	46.23	47.85	47.57	46.33
Al_2O_3	14.66	10.05	12.96	11.73	11.63
FeO	9.75	10.64	9.78	9.87	11.52
MgO	11.32	21.98	16.01	18.73	18.20
CaO	12.53	8.84	10.90	9.84	9.74
Na_2O	1.56	1.13	1.45	1.26	1.37
K_2O	0.04	0.04	0.02	0.04	0.06
TiO_2	0.89	0.82	0.79	0.73	0.86
MnO	0.24	0.19	0.18	0.16	0.22
P_2O_5	0.07	0.07	0.06	0.06	0.08
wt% olivine added	-28.1	-11.6	-4.3	7.4	-14.5
Fo_{max}	88.91	92.90	91.48	92.43	91.08
Fo_{calc}	93.53	93.91	92.06	91.54	92.80

Sample	138345	264217	332901	340740	354754	362077
SiO_2	45.42	46.10	46.06	45.57	47.08	44.88
Al_2O_3	10.63	11.92	10.30	11.55	13.63	10.36
FeO	10.84	11.01	12.74	11.18	11.62	11.44
MgO	21.93	18.10	18.45	17.35	13.04	21.39
CaO	8.66	10.17	8.98	11.18	11.36	9.42
Na_2O	1.08	1.35	1.47	1.40	1.52	1.32
K_2O	0.25	0.02	0.20	0.06	0.22	0.04
TiO_2	0.92	1.05	1.44	1.35	1.19	0.88
MnO	0.18	0.20	0.23	0.20	0.23	0.20
P_2O_5	0.08	0.08	0.14	0.16	0.11	0.07
wt% olivine added	-4.6	-11.8	-19.15	-10.5	-21.0	-12.7
Fo_{max}	92.80	90.49	90.50	91.06	88.60	92.32
Fo_{calc}	93.22	92.87	92.79	92.38	92.13	93.51

Sample	400230	400452	400457	400485	410152
SiO_2	45.30	47.64	47.80	46.42	47.13
Al_2O_3	10.47	14.15	15.10	13.51	13.80
FeO	11.58	10.97	11.37	12.58	11.74
MgO	20.55	11.17	9.20	12.48	11.02
CaO	9.37	12.85	13.07	12.00	12.02
Na_2O	1.28	1.56	1.55	1.19	1.79
K_2O	0.08	0.06	0.10	0.23	0.37
TiO_2	1.10	1.24	1.42	1.19	1.71
MnO	0.19	0.25	0.27	0.30	0.25
P_2O_5	0.09	0.10	0.11	0.09	0.17
wt% olivine added	-4.05	-26.8	-33.35	-38.3	-26.2
Fo_{max}	91.91	87.97	85.95	87.67	87.08
Fo_{calc}	92.34	92.77	92.85	93.74	92.13

2.4.3 Whole-rock trace element abundances

Selected trace element (Nb, Zr, Y, Ni, Cr, V, Sc, Cu, Sr, Zn, Rb, Ba) abundances were determined on whole-rock powders by XRF spectrometry at the University of Edinburgh (analytical details are available in Appendix A2). Results show that incompatible trace element concentrations for West Greenland picrites are generally slightly higher than those of Baffin Island for a given MgO (Figure 2.9). Across the region, Ni (147–1409 ppm) and Cr (420–2679 ppm) increase with increasing MgO. V (150–286 ppm), Sc (25–45 ppm) and Y (9–23 ppm) decrease with increasing MgO and Cu (54–132 ppm), Sr (46–265 ppm), Nb (0.5–6 ppm) and Zr (21–70 ppm)

show poor negative correlations with MgO whilst Zn (65–93 ppm), Rb (0–33 ppm) and Ba (0–89 ppm) are scattered with increasing MgO (Figure 2.9).

Log(Nb/Y) against log(Zr/Y) is used here to compare Baffin Island and West Greenland picrites to Icelandic basalts and N-MORB (Figure 2.10). On this diagram, Icelandic basalts and N-MORB form parallel arrays separated by ΔNb=0 (where ΔNb = 1.74 + (log (Nb/Y) – 1.92 log (Zr/Y)); Fitton et al., 1997). Positive values of ΔNb characterise Icelandic basalts whereas N-MORB have negative values. The Baffin Island and West Greenland picrites represent some of the very earliest magmas produced by the proto-Iceland plume so it is logical to compare them to the more recent products of the plume in Iceland using ΔNb. The picrites of this study span ΔNb=0 (the transition from N-MORB to Icelandic-type basalts). ΔNb is insensitive to the effects of variable degrees of mantle melting, source depletion through melt extraction, crustal contamination and subsequent alteration (Fitton et al,. 1997). Therefore, both relatively enriched (Icelandic-type) and relatively depleted (N-MORB) material was available in the source of the proto-Iceland plume lavas.

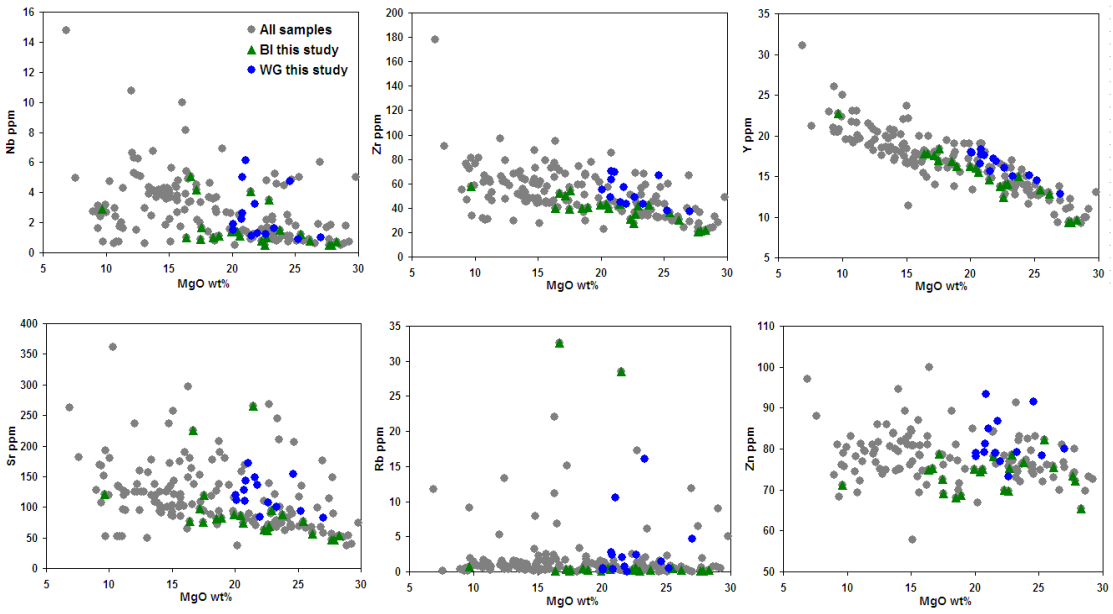

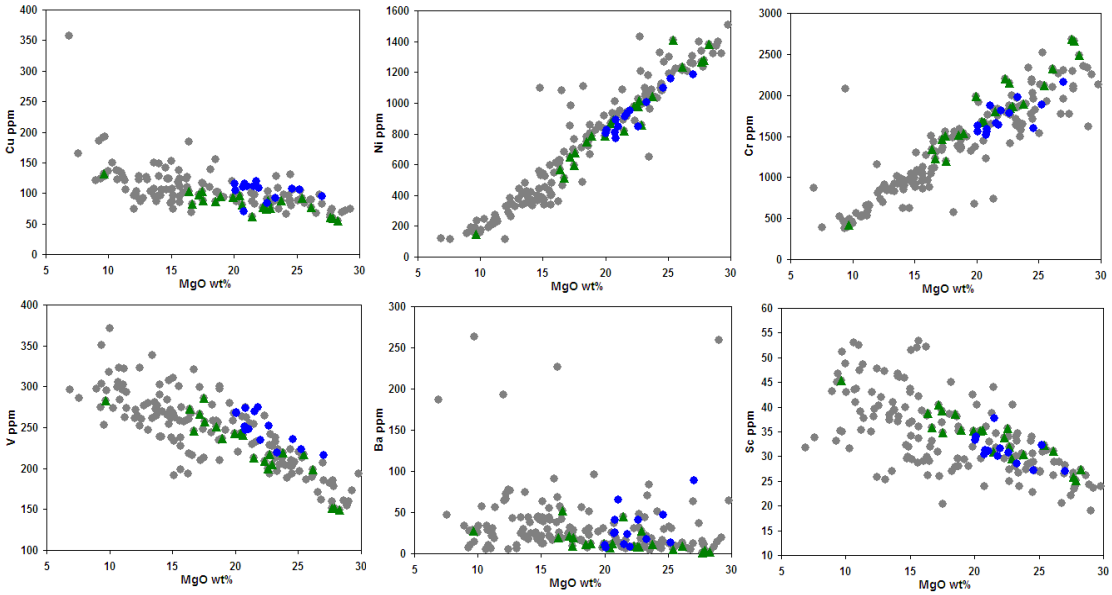

Figure 2.9. Trace element variation diagrams for Baffin Island and West Greenland samples of this study and all other published analyses (Holm et al., 1993; Lightfoot et al., 1997; Graham et al., 1998; Lass-Evans, 2004; Yaxley et al., 2004) for comparison.

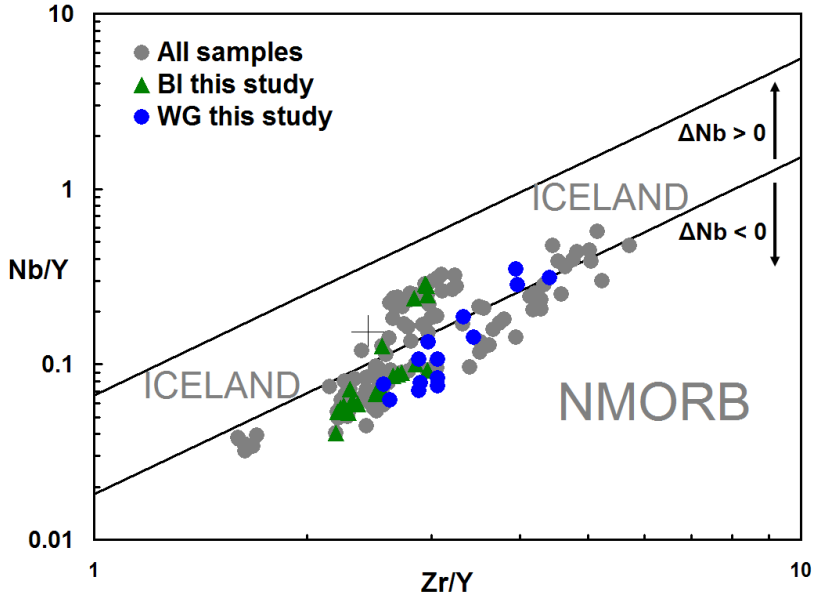

Figure 2.10. Nb/Y versus Zr/Y for Baffin Island and West Greenland samples used in this study and all other available analyses (Holm et al., 1993; Lightfoot et al., 1997; Graham et al., 1998; Lass-Evans, 2004; Yaxley et al., 2004;). Samples with ΔNb > 0 lie in the Iceland (E-MORB) field (between the tramlines) and samples with ΔNb < 0 lie in the N-MORB field. Grey cross between tramlines represents composition of primitive mantle. The Baffin Island and West Greenland samples span the transition from negative to positive values.

2.4.4 Rare earth element (REE) abundances

REE abundances were determined on whole-rock powders by ICP-MS at the Scottish Universities Environmental Research Centre (SUERC). Details of the analytical procedure are included in Appendix A3.

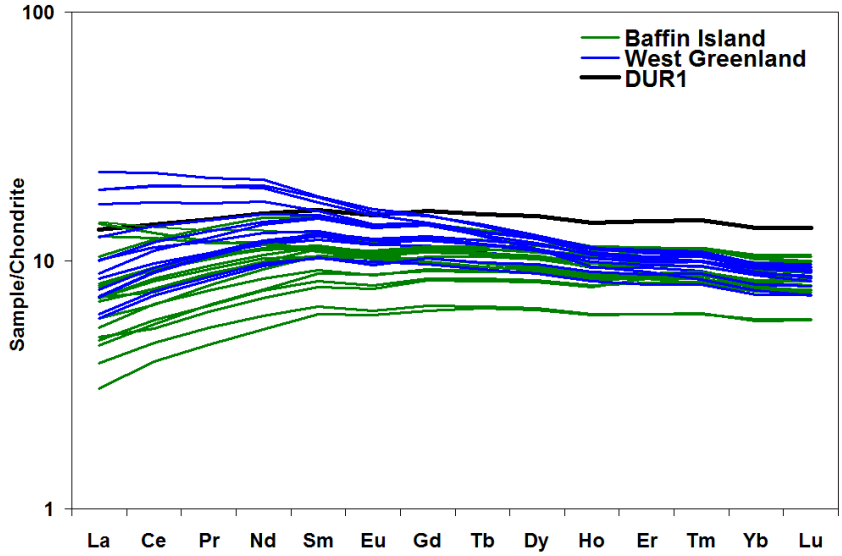

Figure 2.11. Chondrite-normalised REE diagram for Baffin Island and West Greenland samples of this study. DUR1 is shown in black to indicate its higher abundance of HREE.

Chondrite-normalised REE plots highlight the relationship already observed in the incompatible element plots, the higher abundances of incompatible elements in West Greenland than in Baffin Island lavas (Figure 2.11; Figure 2.12). Chondrite-normalised REE patterns of Baffin Island rocks are flatter than those of West Greenland which tend to be slightly HREE-depleted relative to Baffin Island samples. Sample DUR1 from Baffin Island is anomalous in that it has higher abundances of HREE than the other samples from West Greenland or Baffin Island (Figure 2.11). This may be related to the virtually aphyric nature of this sample. Comparison of the Baffin Island and West Greenland samples to MORB highlights the relative depletion in the HREEs of all the Baffin Island and West Greenland samples but with similar LREE abundances.

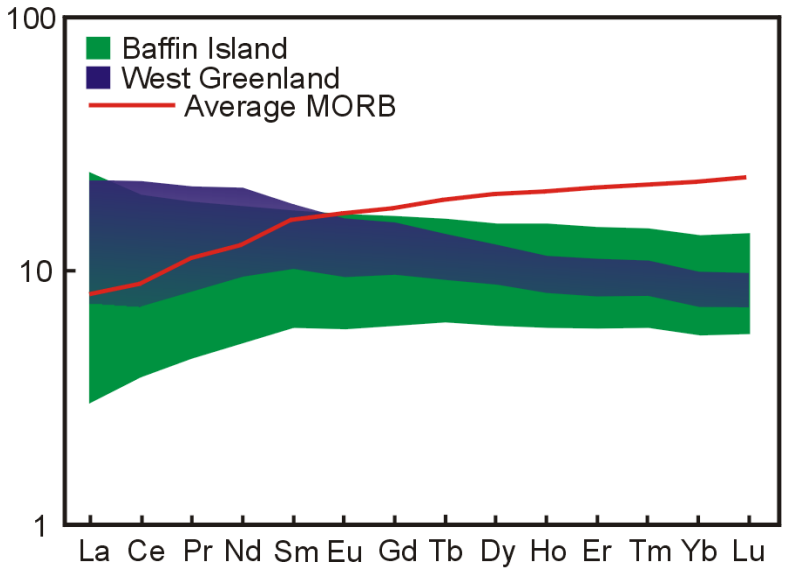

Figure 2.12. Chondrite-normalised REE diagrams for Baffin Island and West Greenland samples from Starkey et al. (2009) which includes more Baffin Island samples in comparison to this study. Average MORB from Workman and Hart (2005) is shown for comparison.

Samples from the Vaigat Formation of West Greenland are separated into Members (Anaanaa, Naujánguit, Qordlortorssuaq, Ordlingassoq) in a chondrite-normalised REE diagram (Figure 2.13) to highlight the variation in compositions throughout the sequence. The Naujánguit Member lavas are the most depleted and the Ordlingassoq Member samples are the most enriched. This is in agreement with Holm et al. (1993) who found, from Sr and Nd isotopes, that Naujánguit Member lavas are related to a depleted MORB-type component and Ordlingassoq Member lavas to more of an enriched Iceland-plume-type component. The Anaanaa Member samples (n = 4) scatter throughout most of the range in compositions displayed by the other Members. The Anaanaa lavas should be most similar in composition to the lavas of Baffin Island since they are believed to correlate stratigraphically. The Baffin Island lavas show a wider range in compositions, extending to much more depleted LREE abundances and with a wider range in HREEs, suggesting that the magmas erupted in Baffin Island were more varied in composition than those erupted in West Greenland.

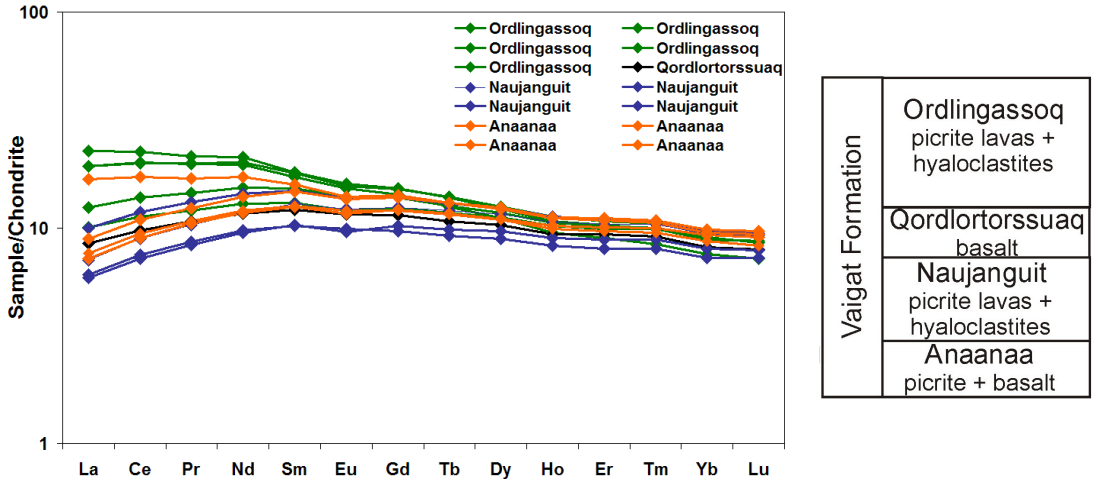

Figure 2.13. Chondrite-normalised REE diagram for West Greenland with the samples separated into the various Members of the Vaigat Formation to highlight the variation in compositions throughout the sequence. The box (right) indicates the stratigraphic position of Vaigat Formation Members.

Another diagram that can be used to compare the Baffin Island and West Greenland lavas to MORB is presented in Figure 2.14. Nb/Zr and $(La/Sm)_n$ are element ratios that can indicate the relative enrichment or depletion of a source. $(La/Sm)_n = 0.8$ has been suggested by Mahoney et al. (2002) as a division between N-MORB (< 0.8) and E-MORB (> 0.8). The Baffin Island and West Greenland lavas fall comfortably within the field defined by basalts from all mid-ocean ridges (from PetDB database; www.petdb.org; Appendix D) and they span the transition from N-MORB to E-MORB, in agreement with ΔNb.

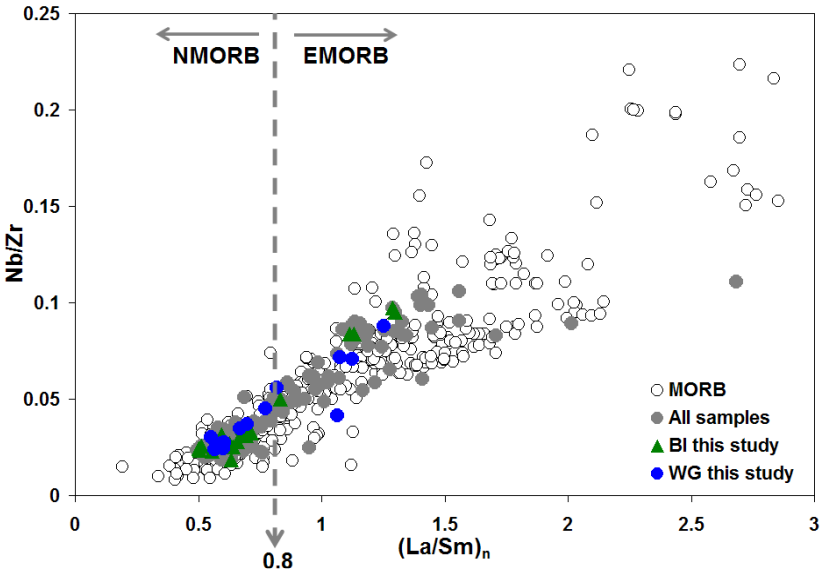

Figure 2.14. Nb/Zr against $(La/Sm)_n$ for Baffin Island and West Greenland of this study and all other published data (Holm et al., 1993; Lightfoot et al., 1997; Graham et al., 1998; Lass-Evans, 2004; Yaxley et al., 2004).

Several authors have already noted that the Baffin Island lavas can be subdivided into N-type and E-type based on their trace element chemistry (Robillard et al., 1992; Kent et al., 2004). N-type magmas are dominated by higher MgO and have LREE depleted patterns typical of N-MORB. E-type lavas have flat to slightly enriched LREE patterns similar to E-MORB. However, the N- and E-type groups are not distinguishable by their major element compositions. Holm et al. (1993) also noted that the West Greenland picrites fall into broadly similar N- and E-type groups.

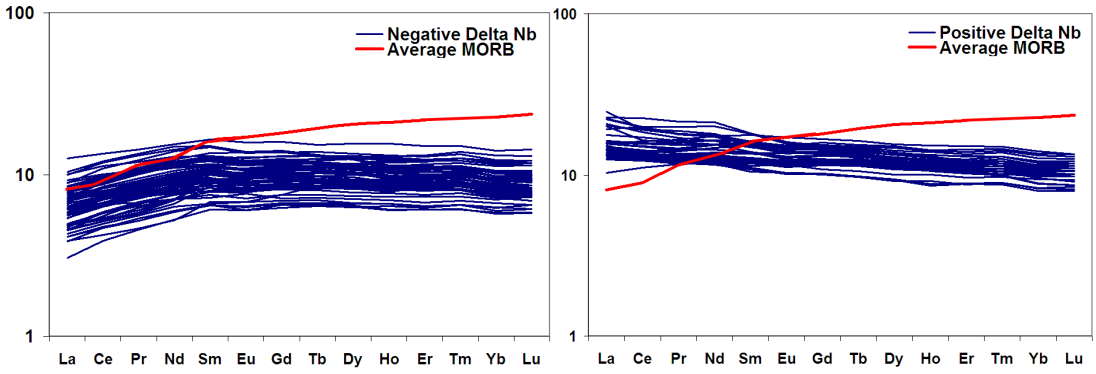

Figure 2.15. Chondrite-normalised REE diagrams for all Baffin Island and West Greenland samples (samples from Starkey et al. (2009)) separated by ΔNb = 0 into N- and E-type. Average MORB from Workman and Hart (2005) is shown for comparison.

This division by REE into depleted and relatively enriched groups is apparent in the samples of this study. In Figure 2.15 the samples are divided by ΔNb into N- (negative ΔNb) and E- (positive ΔNb) type. E-type samples show relative LREE enrichment compared to the N-type samples and fall to the upper end of overall concentrations of HREE. This is in correspondence with the higher La/Sm of E-type samples ($(La/Sm)_n > 0.8$). It is clear that the N-type samples have REE profiles that are more similar to the REE profile for DMM (Workman and Hart, 2005) except for the lower concentrations of HREE.

Whether the N- and E-type lavas have distinct mantle sources or not has been the subject of debate. Robillard et al. (1992) comment on the N- and E-type nature of Baffin Island picrites that are intermixed throughout the volcanic sequence. It is noted that crustal contamination involving a lower crustal component cannot account for the compositional differences between the N- and E-type lavas (lower La/Sm and K/Ti in N-type). Although the degree of partial melting can account for differences

in La/Sm and Zr/Y, it cannot account for the difference in REE abundances, Sr, Y and Zr (Robillard et al., 1992). Instead, two distinct mantle sources are required to account for the differences between N- and E-type lavas.

Incompatible trace elements can be used to assess the extent of crustal contamination in the Baffin Island and West Greenland samples (Figure 2.16). High Ba/Nb indicates contamination since Ba is abundant in crustal rocks. The Baffin Island and West Greenland samples have a wide range of Ba/Nb but with fairly restricted $(La/Sm)_n$. The samples can be divided into two groups at $(La/Sm)_n = 0.8$, as already highlighted in Figure 2.14. Each group has fairly constant $(La/Sm)_n$ with variable Ba/Nb such that $(La/Sm)_n$ variations within each group reflect source variations. The relatively enriched group ($(La/Sm)_n > 0.8$) has a more restricted range but with very similar average Ba/Nb to the more depleted group. Proterozoic crustal basement rocks for the region (Theriault et al., 2001) have high Ba/Nb and slightly higher $(La/Sm)_n$ than the Baffin Island and West Greenland lavas. Mixing trajectories between a depleted parent magma and any of the crustal rocks (Figure 2.16) fails to explain the relative enrichment of the group of lavas with $(La/Sm)_n > 0.8$. Therefore, the difference in relative enrichment between the two groups is most likely to be related to variations in source composition. Despite this, increasing Ba/Nb within each group of lavas can be explained by crustal contamination but only if it is assumed that this contamination overprinted the existing depleted and relatively enriched sources (i.e. the two groups require different parental melt compositions regardless of crustal contamination). If crustal contamination has occurred then only around 1-2% contamination is required to produce the entire range in Ba/Nb of the lavas. The potential for crustal contamination, especially of the high $^3He/^4He$ lavas, is further discussed in Chapter 3 using isotopic data in conjunction with trace elements and, importantly, is related to the helium isotope ratios.

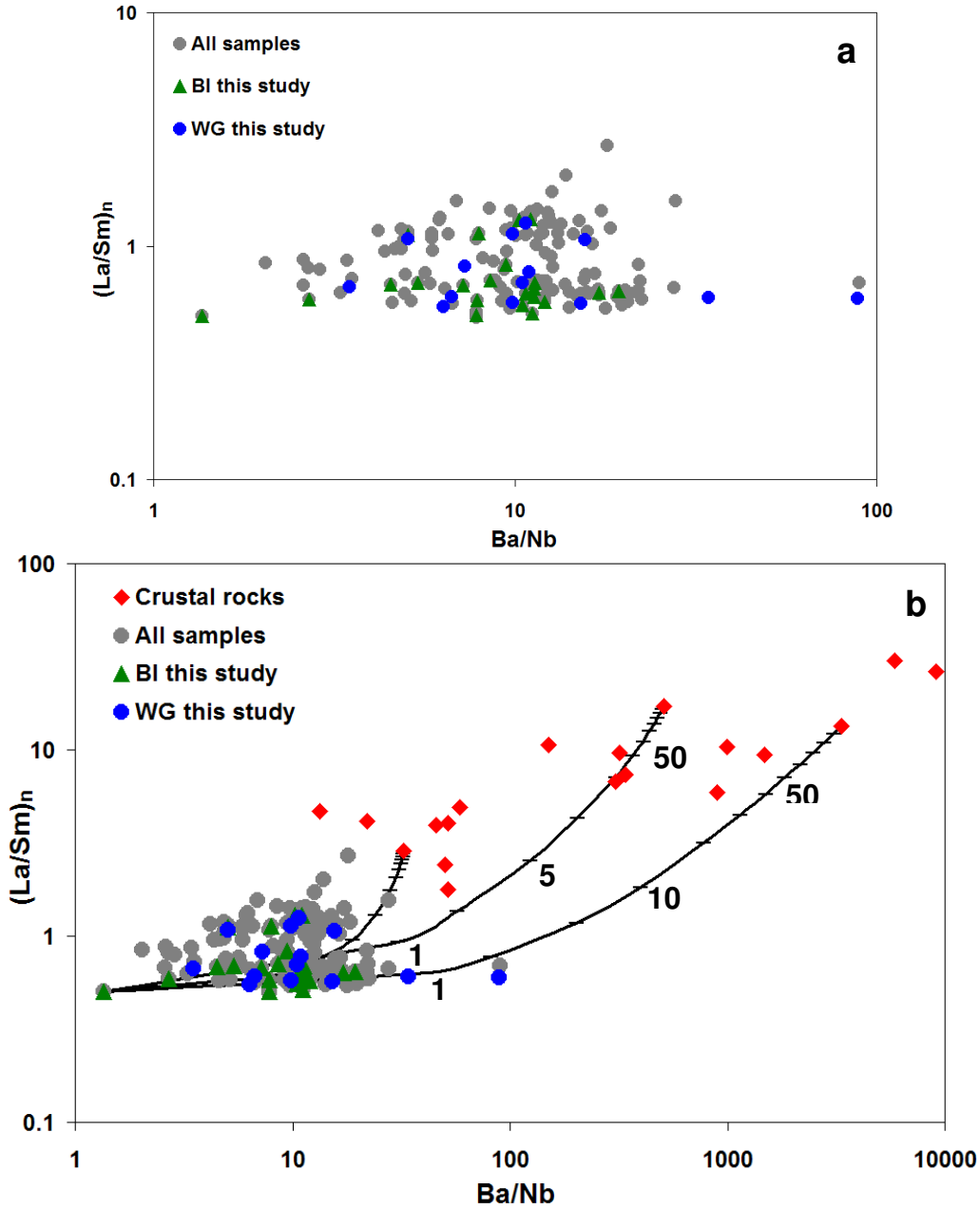

Figure 2.16. $(La/Sm)_n$ against Ba/Nb for Baffin Island and West Greenland samples of this study and all other available data for comparison (Holm et al., 1993; Lightfoot et al., 1997; Graham et al., 1998; Lass-Evans, 2004; Yaxley et al., 2004). a) The samples fall into two groups separated by $(La/Sm)_n$ = 0.8. Both the depleted and relatively enriched groups span a wide range in Ba/Nb. b) Crustal contamination trajectories for mixing between a depleted parent and various Proterozoic crustal basement rocks (Theriault et al., 2001) fail to account for the difference in $(La/Sm)_n$ between the two groups. Bold numbers adjacent to small tick marks on the mixing curves indicate the percentage of crust added to the mixture.

2.5 Summary

This chapter presents the petrography, major and trace element data for the Baffin Island and West Greenland picrite samples used in this study. These new data are compared to all other available data for these regions showing that these new samples are very similar in their petrography and composition except that they tend to fall to the high-MgO-end of the compositional array. Highly magnesian olivine crystals, up to Fo_{93}, are a common feature of both the Baffin Island and West Greenland picrites. An origin as mantle xenocrysts is ruled out as an explanation for the highly magnesian olivine crystals. The term 'antecryst' (Section 2.3.2) is probably the most appropriate description for many of the crystals within these lavas. Importantly, although this may suggest that few of the crystals are true phenocrysts, it does, at the same time, rule out an origin of the forsterite-rich crystals from an exotic melt. A simple model for the formation of the final erupted magmas most likely involves the mixing together of crystals and liquids from various levels within the magmatic conduit. The crystal content, and therefore the bulk composition of the final product, is dependent on magma ascent velocities and the particular route taken by the magma through the plumbing system.

Crustal contamination of the Baffin Island and West Greenland lavas was investigated. Trace element ratios indicate that the magmas may have experienced up to ~2% crustal contamination, in agreement with the conclusions of other studies. Radiogenic isotope ratios provide the best method to assess this issue and are investigated further in Chapter 3.

This study highlights the similarity of the Baffin Island and West Greenland lavas to global MORB. The incompatible trace element compositions measured in this study can be matched to the global MORB dataset and the lavas can thus be divided into N- (normal) and E- (enriched) type based on their trace element composition. It has previously been suggested that the more enriched lavas were produced by crustal contamination of a more depleted parent. This study shows that this cannot be the case and that the depleted and relatively enriched groups require different sources

that may have been subject to varying degrees of contamination. Taking this information into consideration suggests that both depleted and relatively enriched sources were available for the magmas of the earliest Iceland plume in Baffin Island and West Greenland. Interestingly, lavas from the British Tertiary Igneous Province, erupted contemporaneously ~2000 km away (Saunders et al., 1997), also display N-MORB and E-MORB type compositions (Fitton et al., 1997). Icelandic lavas, erupted more recently, have only E-MORB mantle sources (Fitton et al., 2007). These observations aid in the understanding of the temporal and spatial evolution of the NAIP magma sources. The interplay of depleted and relatively enriched sources has been discussed by others (Francis, 1985; Fitton et al., 1997; Saunders et al., 1997; Kempton et al., 2000; Larsen and Pedersen, 2000; Ellam and Stuart, 2000) and various models have been suggested to account for the compositional changes. These models are discussed in detail in Chapter 5 taking all the other chemical data into account.

When considering the various petrogenetic models available for the NAIP, it is important to focus on the very earliest Iceland plume magmatism sampled in Baffin Island and West Greenland. Despite the similarity of these lavas to global MORB there are some key characteristics displayed by the lavas that set them apart. The Baffin Island and West Greenland lavas have particularly high magnesium contents, similar to values found in komatiites. These high magnesium contents are commonly used to show that the mantle source for these lavas was particularly hot compared to ambient upper mantle.

3 Results: Strontium, neodymium and helium isotope compositions

3.1 Introduction

This chapter presents the strontium, neodymium and helium isotope data for the Baffin Island and West Greenland samples, following on from Chapter 2 in which the petrology, major and trace element data were presented and discussed. One of the principal aims of this study, as set out in the introduction, is to investigate the nature of the high $^{3}He/^{4}He$ reservoir in the Earth. An important first step is to determine whether crustal contamination has affected any of the samples in order to ensure that this has not overprinted any geochemical signal from the mantle source of the lavas. Measurement of helium isotopes on a new set of Baffin Island and West Greenland picrites was a basic requirement in order to determine whether high $^{3}He/^{4}He$ is a common feature of the region after especially high $^{3}He/^{4}He$ were found in Baffin Island samples (Stuart et al., 2003). Secondly, after characterising the samples for major and trace element abundances (Chapter 2), it was important to determine strontium and neodymium isotope ratios in support of this work. Coupled with trace element ratios, isotopes are very useful for modelling the effects of crustal contamination on the magmas. The results and modelling are presented in this Chapter along with a discussion on the possible source of high $^{3}He/^{4}He$ in the Earth which is continued in more detail in Chapter 5.

3.2 Strontium and neodymium isotope results

Strontium and neodymium isotopes were measured on separate splits of whole-rock powders by thermal ionisation mass spectrometry (TIMS) at the Scottish Universities Environmental Research Centre (SUERC). Analytical details and the full dataset are available in Appendix A4, H and I.

Baffin Island and West Greenland $^{87}Sr/^{86}Sr$ vary from 0.702883 to 0.711773 and $^{143}Nd/^{144}Nd$ from 0.512712 to 0.513075. Isotopic values are age corrected for decay

of ^{87}Rb and ^{147}Sm respectively, to the isotopic value at ~60 Ma (Figure 3.1). $^{87}Sr/^{86}Sr$ was determined in nineteen Baffin Island lavas and these vary from 0.702883 to 0.711773. This range includes two particularly high values, which may suggest that some samples are crustally contaminated (namely DUR6 and DUR7). Crustal contamination is investigated further in Section 3.4.2. The range in $^{87}Sr/^{86}Sr$ for the fourteen West Greenland samples varies from 0.703042 to 0.704628. The $^{143}Nd/^{144}Nd$ for the twelve Baffin Island samples varies from 0.512876 to 0.513058 and a similar range for the thirteen West Greenland samples of 0.512712 to 0.513075. Figure 3.1b shows the similarity of Sr and Nd isotope values of this study to others reported for the region (shown in grey), from the Vaigat Formation picrites of West Greenland (Holm et al., 1993; Lightfoot et al., 1997; Graham et al., 1998) and Baffin Island picrites (Stuart et al., 2003; Kent et al., 2004; Lass-Evans, 2004). Figure 3.1b shows that the Baffin Island and West Greenland lavas extend well beyond the enriched end of the Iceland field (delineated in red) but that they do not reach such depleted Sr and Nd isotopic values.

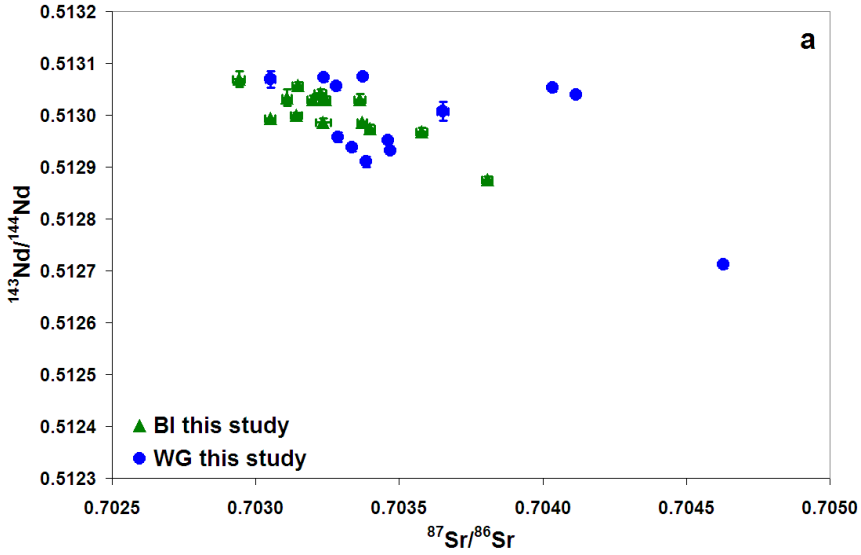

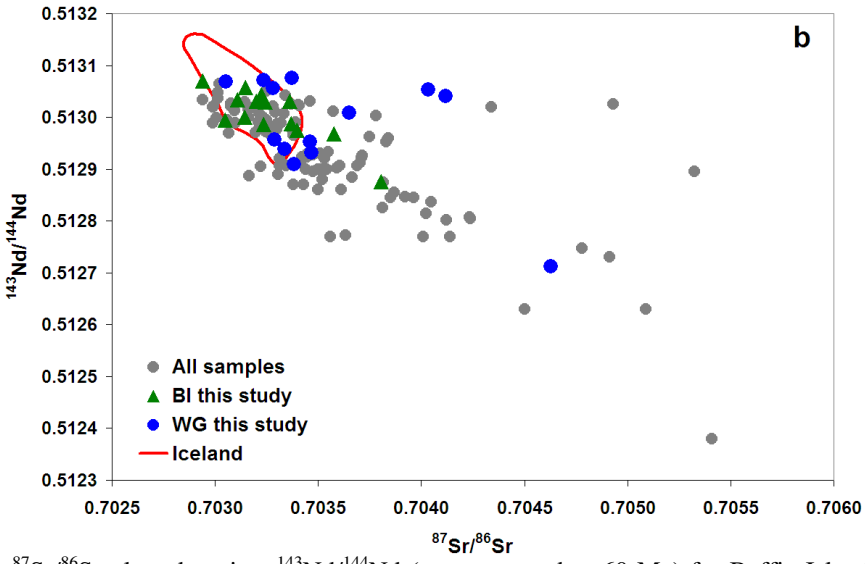

Figure 3.1. $^{87}Sr/^{86}Sr$ plotted against $^{143}Nd/^{144}Nd$ (age corrected to 60 Ma) for Baffin Island and West Greenland samples. a) Samples of this study with error bars for ±2sd. b) Samples of this study compared with all published data and with a field indicating the Icelandic range (red line).

Holm et al. (1993) carried out a detailed geochemical study on the West Greenland picrites which revealed a compositional difference between the earlier erupted picrites of the Naujanguit Member and the later erupted picrites of the Ordlingassoq Member. Naujanguit picrites are reported to extend to higher $^{143}Nd/^{144}Nd$ and lower $^{87}Sr/^{86}Sr$, suggesting a depleted MORB-type component in the source of these magmas (Holm et al., 1993). The Ordlingassoq picrites are reported to be slightly less depleted in composition, resembling Icelandic picrites (Holm et al., 1993). Figure 3.2 shows the progression in composition up-sequence in ε_{Nd}^{60} and ε_{Sr}^{60} for the Vaigat Formation. Included in Figure 3.2 are the West Greenland data for the samples of this study, encompassing the lowermost Vaigat Member (the Anaanaa) and the Qordlortorssuaq Member that lies between the Naujanguit and Ordlingassoq Members. Although there is some overlap in compositions, and despite the fact that the data are fairly limited for some Members, it is clear that the samples show temporal variation from high ε_{Nd}^{60}, low ε_{Sr}^{60} to lower ε_{Nd}^{60} and higher ε_{Sr}^{60} up-sequence. These findings are paralleled by the REE compositions as discussed in Chapter 2. Baffin Island samples span the entire compositional range displayed by the Vaigat Formation picrites. This is surprising since the Baffin Island lavas are thought to correlate with the lowermost Anaanaa Member suggesting that more depleted compositions might be expected, as are found in the Anaanaa Member.

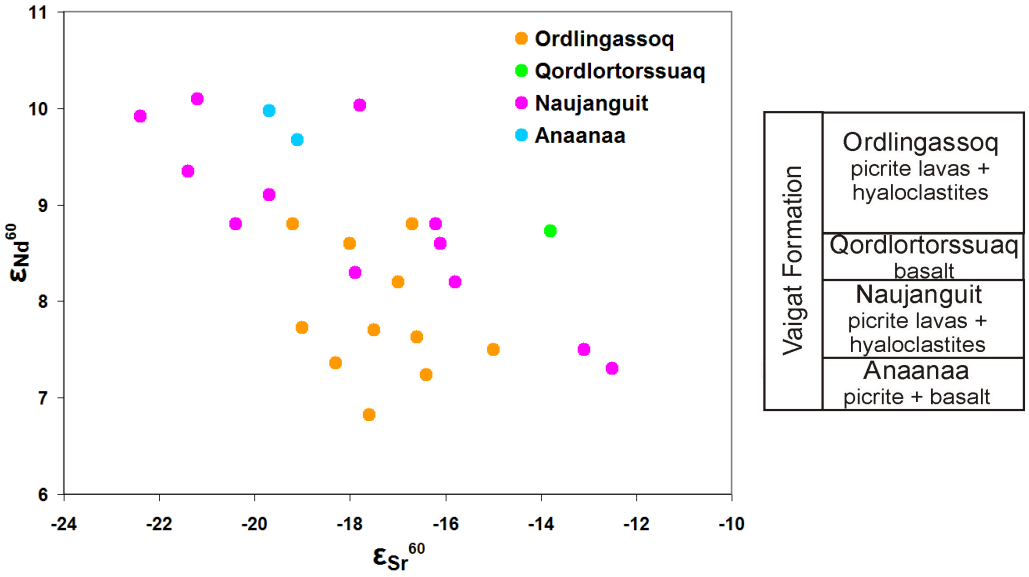

Figure 3.2. ε_{Nd}^{60} plotted against ε_{Sr}^{60} for Vaigat Formation picrites. The box (right) indicates the stratigraphic position of Vaigat Formation Members. Data sources: Anaanaa and Qordlortorssuaq are this study only. Naujanguit and Ordlingassoq are this study and Holm et al. (1993). Samples show a progression from more depleted to more enriched compositions up-sequence.

3.3 Helium isotope data

Helium isotopes were determined at the Noble Gas Laboratory at SUERC, East Kilbride, in gases released by *in vacuo* crushing of separated olivine phenocrysts. The magmatic helium is present within CO_2-rich shrinkage bubbles that form in many olivine-hosted melt inclusions on cooling. $^3He/^4He$ for the Baffin Island samples were determined by Dr Sudeshna Basu (SUERC, East Kilbride) using the same procedure as for the West Greenland samples. Full analytical details are available in Appendix A along with the $^3He/^4He$ dataset in Appendix J.

$^3He/^4He$ were determined in 28 samples (seventeen from Baffin Island and eleven from West Greenland) that display a range from 16.4 to 49.8 R_a. These ratios overlap the high values previously obtained for Baffin Island (Stuart et al., 2003) and are significantly higher than the highest value determined previously for West Greenland picrites (30 R_a; Graham et al., 1998). Sample 400457 reported by Graham et al. (1998) was re-analysed in this study and yielded $^3He/^4He$ of 16.4 ± 2 R_a, within analytical uncertainty of the value (17.55 R_a) published by Graham et al. (1998). High $^3He/^4He$ occur in all Members of the Vaigat Formation of West Greenland

(Figure 3.3; red font for sample numbers indicates high $^3He/^4He$ >35 R_a). Baffin Island picrites are thought to correlate stratigraphically with the lowest part of the Vaigat Formation (Anaanaa Member) suggesting that the very earliest lavas of the Iceland plume had high $^3He/^4He$. The high ratios in all parts of the West Greenland formation, from the Anaanaa through to the Ordlingassoq Member, show that the high $^3He/^4He$ signature persisted during eruption of the entire formation, which is thought to have taken ~1 million years (Storey et al., 1998).

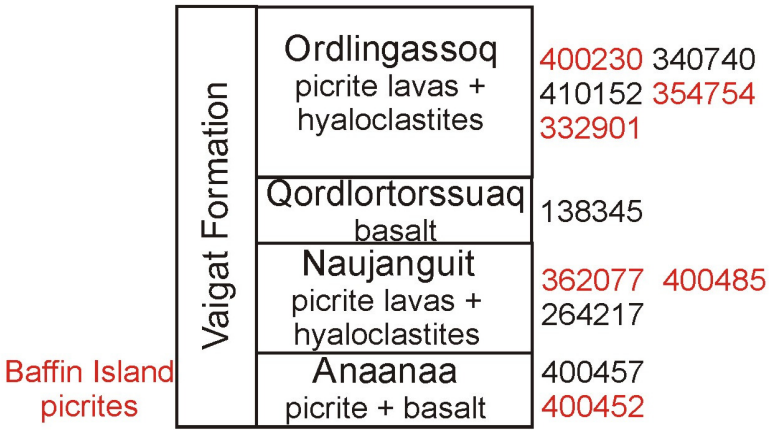

Figure 3.3. Stratigraphy Members of the Vaigat Formation of West Greenland. Samples with high $^3He/^4He$ (>35 R_a), that occur in all Members of the Vaigat Formation, are highlighted in red.

3.3.1 Integrity of helium isotope data

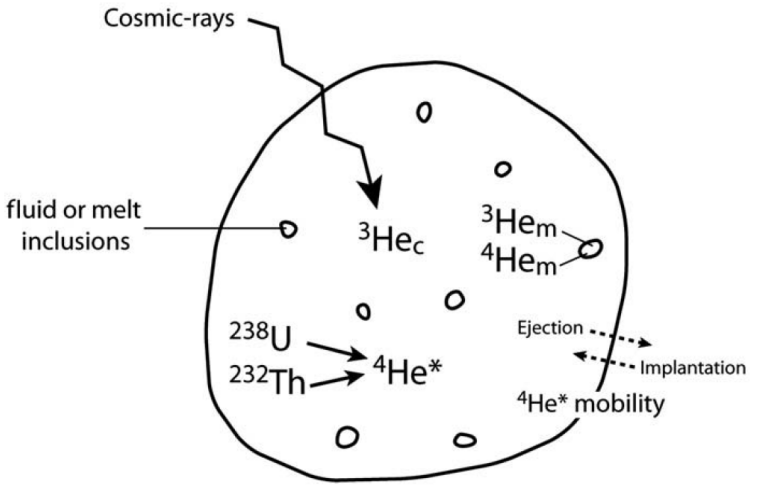

Figure 3.4. Schematic diagram illustrating the different sources of helium in a phenocryst exposed to cosmic-rays. $^4He^*$ = radiogenic ^4He, ^3He_c = cosmogenic ^3He, ^3He_m or ^4He_m = magmatic ^3He or ^4He. From Blard and Farley (2008).

The new $^{3}He/^{4}He$ data in this study add to the high $^{3}He/^{4}He$ values already established for this region (Stuart et al., 2003), confirming this part of the North Atlantic Igneous Province as having the highest magmatic terrestrial $^{3}He/^{4}He$. However, before a mantle origin can be assigned to the high $^{3}He/^{4}He$ values, the possibility that high $^{3}He/^{4}He$ is due to nucleogenic or cosmogenic ^{3}He production must first be ruled out. The schematic diagram in Figure 3.4 illustrates potential sources of ^{3}He within a ferromagnesian phenocryst. Nucleogenic ^{3}He, which is produced by thermal neutron capture by ^{6}Li in crystals has been shown not to be a significant process in Palaeocene basalts (Graham et al., 1998; Marty et al., 1998; Stuart et al., 2000), so is ruled out as an explanation for the high $^{3}He/^{4}He$. Cosmogenic ^{3}He can be produced through spallation reactions involving cosmic ray secondary particles interacting with target nuclei of Si, O and Mg (Kurz, 1986). Rocks exposed at the Earth's surface for a long period of time have a higher chance of accumulating a significant cosmogenic helium component. However, the Baffin Island and West Greenland samples were collected from freshly exposed cliff sections which minimises the time for this process to take effect. Foeken et al. (2009) show that when olivine crystals are crushed *in vacuo* it is magmatic gases trapped within melt inclusions that are released rather than the gases trapped within the olivine crystal lattice. The crystal lattice is the most likely location for both the nucleogenic and cosmogenic ^{3}He and radiogenic ^{4}He (Foeken et al., 2009). However, one possibility is that the measured $^{3}He/^{4}He$ was increased by diffusion of cosmogenic ^{3}He, produced within the glass of the melt inclusion, into the bubble. The positive correlation of $^{3}He/^{4}He$ against ^{4}He in Figure 3.5 for the samples of this study suggests that cosmogenic ^{3}He has not diffused into the bubble hosting the helium. In order to assess whether nucleogenic, cosmogenic or radiogenic helium is present within the olivine crystal lattice, crystals that are crushed *in vacuo* can be transferred to a high temperature vacuum furnace where they are melted to provide a $^{3}He/^{4}He$ for helium trapped in the olivine lattice. Stuart et al. (2003) show that this process yields low $^{3}He/^{4}He$ for Baffin Island picrites, suggesting that cosmogenic helium is not present in significant amounts. The lower $^{3}He/^{4}He$ obtained by this method indicate that radiogenic ^{4}He is present in the crystal lattice so $^{3}He/^{4}He$ determined by crushing should be considered as a minimum for the magmatic helium

isotope ratio.

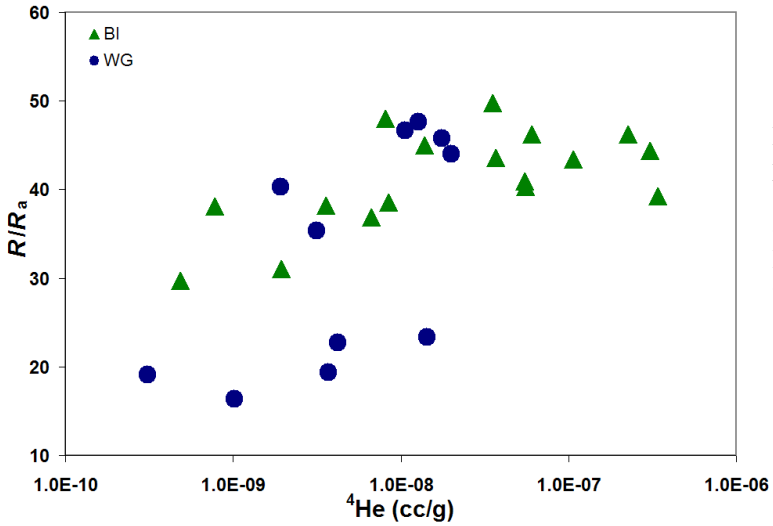

Figure 3.5. $^{3}He/^{4}He$ plotted against ^{4}He for *in vacuo* crushing of olivine from Baffin Island and West Greenland samples.

It is possible for $^{3}He/^{4}He$ to be lowered by crustal contamination since crustal rocks have low $^{3}He/^{4}He$ due to radiogenic production of ^{4}He from the decay of U and Th. However, previous studies of early Tertiary proto-Iceland plume samples show that crustal contamination does not affect the $^{3}He/^{4}He$ in the olivine-hosted melt inclusions because these may have been trapped during the early stages of crystallisation prior to contamination in lithospheric or crustal reservoirs (Ellam and Stuart, 2004). Such early-trapped melt inclusions, along with their $^{3}He/^{4}He$, could be protected from the effects of crustal contamination within their olivine host. However, helium in melt inclusions trapped during late-stage olivine crystallisation may register the effects of crustal contamination in the same way that the bulk composition of rocks can be affected since the latent heat of crystallisation can induce melting of crustal rocks. Such a process could produce a picrite whose olivine crystallised from uncontaminated magma but whose groundmass is substantially contaminated. The possible effects of crustal contamination on bulk-rock compositions is discussed in detail in Section 3.4.1.

3.3.2 Where is the helium?

It is sensible to link the helium isotope ratios to petrographic information on the samples since the helium is held in melt inclusions hosted within olivine crystals.

Full details of the analytical procedure for helium isotope determination are included in Appendix A5 but it is important to note that each individual helium isotope ratio is measured by crushing approximately 1-2g of a mixture of all olivine crystals available in the sample. This means that it is impossible to assign $^{3}He/^{4}He$ values to a particular olivine crystal and associated melt inclusion of a specific composition. Future analytical developments in the measurement of helium isotope ratios may mean that it will be possible to make *in-situ* helium isotope measurements. Consequently, for the time being, it is only possible to compare the helium isotope ratios to their associated whole-rock composition. However, melt inclusions provide detailed information on the various melt compositions in the mantle source region and analysis of a large number can help to characterise the possible melt compositions associated with the helium.

It is possible that high $^{3}He/^{4}He$ is present within melt inclusions hosted only in high-forsterite olivine crystals, which, as discussed in Chapter 2, some authors (Francis, 1985) consider as xenocrysts. If this is the case then it would suggest that the melt composition with which helium is associated may not be related to the other melt compositions sampled in this study. The possibly 'exotic' xenocrystic melt compositions, carrying the high $^{3}He/^{4}He$, may only be available in small melt volumes sampled by very few melt inclusions (since olivine with $>Fo_{90}$ constitute <1% of a thin-section (Larsen and Pedersen, 2000)). However, this would require extremely high helium concentrations in the few melt inclusions in high forsterite olivine. A very simple way to investigate this idea is to link olivine compositions in individual samples to the helium isotope ratio (Figure 3.6) of the sample. It is apparent from Figure 3.6 that there is no correlation between either maximum or average forsterite content with $^{3}He/^{4}He$. This suggests that helium isotopes are not associated with a particular olivine composition, or therefore melt and source composition. However, care should be taken with these plots due to the olivine compositional data being fairly limited in some samples. Nevertheless, the data presented in Chapter 2 rule out the possibility that the high-forsterite olivine crystals in this study were mantle xenocrysts and, therefore, that high $^{3}He/^{4}He$ is not hosted by an 'exotic' melt composition unrelated to the overall magmatic system.

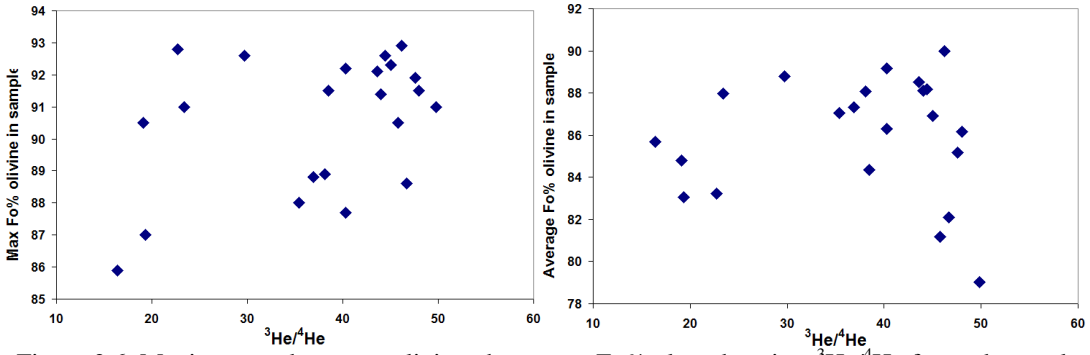

Figure 3.6. Maximum and average olivine phenocryst Fo% plotted against $^{3}He/^{4}He$ for each sample. No correlation between olivine composition and helium isotope ratio is apparent.

3.4 Investigating the composition of high-$^{3}He/^{4}He$ mantle

3.4.1 Ruling out crustal contamination of the high-$^{3}He/^{4}He$ Baffin Island and West Greenland magmas

There is the potential for crustal contamination to have affected the early NAIP magmas since they were erupted through continental crust and have low concentrations of incompatible elements making them more susceptible to small additions of crust. It is, therefore, critical to assess the extent to which crustal contamination may have influenced the Baffin Island and West Greenland picrites before trace element and isotopic variations can be ascribed to heterogeneity within the mantle source.

High volumes of magma were erupted in the early NAIP over a short time interval (<1 my; Storey et al., 1998). The large volumes of primitive magma presumably ascended rapidly through the lithosphere and crust since they avoided fractional crystallisation. In addition, the high olivine crystal content of the picrite magmas increased the density so that the magmas probably required fast ascent velocities to keep the olivine crystals in suspension. These two factors mean that the magmas were unlikely to have ponded in the crust resulting in a low potential for crustal contamination. High $^{3}He/^{4}He$ is unlikely to be attributable to a crustal source since crustal rocks have extremely low $^{3}He/^{4}He$ due to radiogenic production of ^{4}He from decay of U and Th. However, the latent heat of crystallisation may have induced crustal contamination so producing a lava whose olivine phenocrysts crystallised

from an uncontaminated magma but with a groundmass that is significantly contaminated. If this were the case then we would expect whole-rock $^{143}Nd/^{144}Nd$ to be lowered, $^{87}Sr/^{86}Sr$ to be raised and incompatible element abundances to increase whilst $^{3}He/^{4}He$ remains largely unaffected (Stuart et al., 2000). Therefore, it is sensible to be suspicious of the high-$^{3}He/^{4}He$ samples that are less depleted since they may represent originally depleted magmas that incorporated LREE-enriched crustal material.

Before any detailed crustal contamination modelling is undertaken, it should be noted that when the West Greenland samples of this study were selected by Dr. L.M. Larsen (GEUS), they were also screened for crustal contamination based on their stratigraphic level in the Vaigat Formation. No samples collected from a horizon that had previously been identified as crustally or lithospherically contaminated were included. Where available, whole-rock compositions were used and incompatible trace element ratios such as Th/Nb were useful for detecting crustal interaction. A number of the Baffin Island and West Greenland samples have high Th/Nb that exceeds the 0.09 threshold set by Dr. L.M. Larsen (personal communication, 2008) for detecting contaminated samples (Figure 3.7). It is therefore important to compare the Sr and Nd isotope composition of these samples to investigate the potential for crustal interaction. Only DUR7, DUR6, PAD6, 400452 and 400444 have slightly high Th/Nb (~0.1 for all except 400444 which has Th/Nb = 0.28). All of these samples have fairly high $^{87}Sr/^{86}Sr$ which is outside the Iceland range. This is expected for crustally contaminated samples since crustal rocks have radiogenic $^{87}Sr/^{86}Sr$. However, the $^{143}Nd/^{144}Nd$ of these samples are not as low as would be expected for crustal contamination of depleted magmas. Sample 400452 is one of the most radiogenic (high $^{143}Nd/^{144}Nd$) samples with $^{143}Nd/^{144}Nd = 0.513053$ so is very unlikely to have incorporated significant amounts of crustal rocks (with low $^{143}Nd/^{144}Nd$). Probably the most important sample in this set is PAD6, as it has high $^{3}He/^{4}He$ along with the lowest $^{143}Nd/^{144}Nd$ of all the high-$^{3}He/^{4}He$ samples. PAD6 could therefore represent an originally radiogenic (high $^{143}Nd/^{144}Nd$) magma that was enriched through incorporation of crustal rocks. If it can be shown that it is not contaminated then this sample holds important information on the source

composition for high $^{3}He/^{4}He$ in the Earth. PAD6 is therefore considered in detail in subsequent crustal contamination modelling (Section 3.4.2).

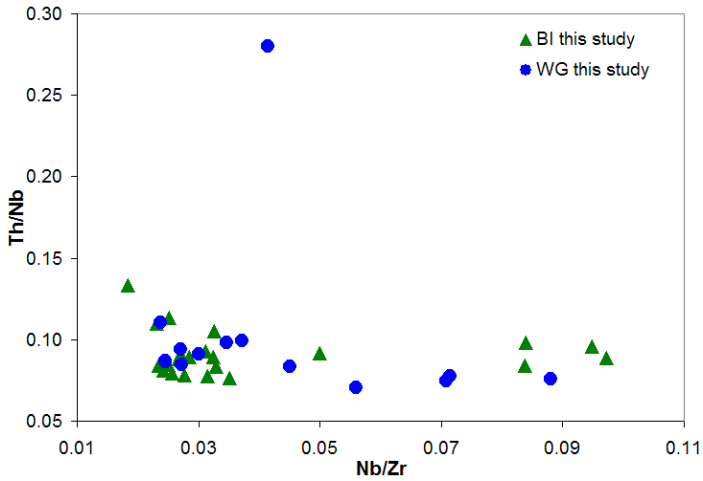

Figure 3.7. Th/Nb against Nb/Zr for Baffin Island and West Greenland samples. Samples with Th/Nb > 0.09 may have been affected by crustal contamination.

The previous Baffin Island dataset (Stuart et al., 2003; Lass-Evans, 2004) will briefly be considered here along with the samples of this study. Based on the Th/Nb > 0.09 criterion, several samples of the previous dataset are potentially contaminated (BI/DI/20-23, BI/PI/18-22, BI/CS/4). Only one of these samples has a measured $^{3}He/^{4}He$ and it happens to be relatively low (~14.5 R_a). It is important to note that although these lavas may be contaminated they do not play an important role in the conclusions drawn from this research project since they have low or unknown $^{3}He/^{4}He$. It is interesting to note that the potentially contaminated lavas occur in flow groups with the flows surrounding them not being affected. It would appear that crustal contamination was selective. In addition to these flows, dyke samples BI/CS/-7, -8. -11, -12, -13 and BI/PI/16 have high Th/Nb. This characteristic is associated with high $^{87}Sr/^{86}Sr$ and low $^{143}Nd/^{144}Nd$, along with low Ti, Nb, Zr, Nb/Zr and Zr/Y (despite no correspondingly high Rb or La/Sm), strongly suggesting they are contaminated by crust (as noted previously by Stuart et al. (2003) and Lass-Evans (2004)). These dykes are discussed further in Section 3.4.4.

3.4.2 Modelling crustal contamination of depleted parent magmas

The Baffin Island-West Greenland samples define a negative trend in a plot of Nb/Zr against $^{143}Nd/^{144}Nd$. This follows the trend defined by Icelandic basalts (Fitton et al., 2003; grey field in Figure 3.8) suggesting that the compositional variation of the Baffin Island-West Greenland picrites reflects variations in the mantle source. However, the Baffin Island-West Greenland samples scatter to slightly lower $^{143}Nd/^{144}Nd$, beyond the Iceland range. This might be due to the addition of small amounts of crust. It should be established whether or not the relatively enriched (high Nb/Zr; low $^{143}Nd/^{144}Nd$; positive ΔNb; high $(La/Sm)_n$) high $^{3}He/^{4}He$ melts could have been produced by crustal contamination of high $^{3}He/^{4}He$, more depleted melts. Figure 3.8 shows curves for simple binary mixing between a typical depleted Baffin Island-West Greenland magma composition and various high-grade Proterozoic crustal basement rocks for the region (Theriault et al., 2001). The range in Nb/Zr of crustal rocks is similar to that of the Baffin Island-West Greenland samples but Nb/Zr is higher in the enriched samples than in any of the crustal rocks. The plot in Figure 3.8 is therefore useful in distinguishing between the effects of source variation, crustal contamination and partial melting. Crustal contamination trajectories are nearly horizontal and therefore too shallow to model the steep trend defined by the picrites. It is possible that some of the scatter in $^{143}Nd/^{144}Nd$ at a given Nb/Zr might be due to crustal contamination but in most cases the amount of crust involved would have to be less than 2%. Furthermore, the $^{143}Nd/^{144}Nd$ of sub-sets of samples with narrow ranges of Nb/Zr does not co-vary with any other index of contamination (e.g. Sr/Nd, K/Nb, Rb/Ba. Rb/Sr, U/Nb or Ba/Th) suggesting that the range in $^{143}Nd/^{144}Nd$ at any given Nb/Zr reflects the natural range in the mantle source (as in Iceland). This plot does, however, support the earlier suggestion (Stuart et al., 2003) that sample BI/CS/7, a high-$^{3}He/^{4}He$ dyke from Cape Searle, is crustally contaminated. The modelling suggests that a mix of ~3% of locally available crustal rocks with a depleted parent magma could account for the very low $^{143}Nd/^{144}Nd$ of this sample. The original mantle source $^{143}Nd/^{144}Nd$ of BI/CS/7 cannot be reconstructed because the degree of contamination is unknown, so it will not be considered in further discussions. In addition, it seems that another dyke (BI/CS/8)

and a West Greenland sample (400444) experienced similar levels of contamination, as implied by their high Th/Nb.

The main features displayed by the picrites in Figure 3.8 are supported by a plot of K/Nb versus $^{143}Nd/^{144}Nd$ (Figure 3.9). The main trend, of decreasing K/Nb with decreasing $^{143}Nd/^{144}Nd$, defined by the Baffin Island-West Greenland picrites in Figure 3.9 is, again, most likely due to source variation. Crustal rocks have high K/Nb and correspondingly low $^{143}Nd/^{144}Nd$ so crustal contamination can account for the displacement of BI/CS/7, BI/CS/8 and 400444 from the main trend, in agreement with Figure 3.8. Also shown is a vector for the effects of alteration which is expected to increase K/Nb whilst leaving $^{143}Nd/^{144}Nd$ unaffected. Low-grade metamorphism of the West Greenland lavas, associated with precipitation of zeolites, has occurred (Neuhoff et al., 2006). Metamorphic fluids could precipitate minerals such as phillipsite which could easily increase the K contents of originally low-K rocks. Alteration may explain the displacement of five samples to high K/Nb (Figure 3.9). The overall trend displayed by the samples in Figure 3.9 supports the earlier findings that the samples with high $^{3}He/^{4}He$ and low $^{143}Nd/^{144}Nd$ (e.g. PAD6, BI/CS/6, 400230 and 332901) have not been affected by crustal contamination, and certainly not to a large enough degree to alter the Nd isotope ratios by a discernable amount. Crustal contamination would act by shifting the most radiogenic (high $^{143}Nd/^{144}Nd$) samples from the main trend on a crustal contamination vector similar to the one shown in Figure 3.9. The fact that the important high $^{3}He/^{4}He$, low $^{143}Nd/^{144}Nd$ samples also display low K/Nb indicates that their source $^{143}Nd/^{144}Nd$ has not been affected by crustal contamination.

In summary, crustal contamination cannot account for both the low $^{143}Nd/^{144}Nd$ and the relative enrichment in incompatible elements (e.g. Nb) that characterise the less depleted picrites, suggesting that the range of compositions of the high $^{3}He/^{4}He$ picrites reflects their mantle source. It can, therefore, be concluded that high $^{3}He/^{4}He$ is a feature of a range of mantle compositions, irrespective of the possible effects of small amounts of crustal contamination.

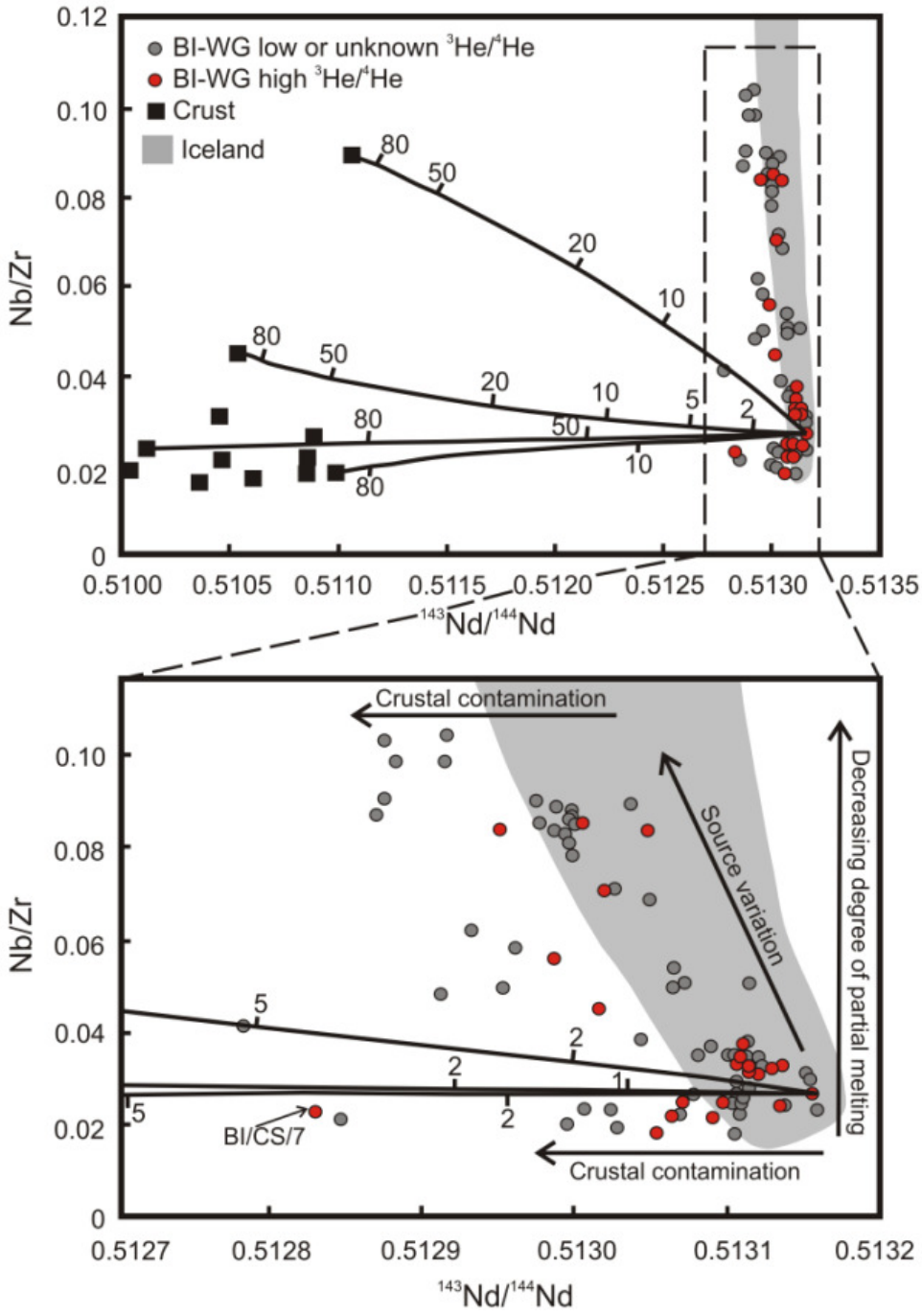

Figure 3.8. Nb/Zr plotted against $^{143}Nd/^{144}Nd$ for all Baffin Island and West Greenland samples with high $^{3}He/^{4}He$ (>35 R_a; red circles) and low or unknown $^{3}He/^{4}He$ (grey circles) from this and previous studies (Graham et al., 1998; Stuart et al., 2003). $^{143}Nd/^{144}Nd$ is the measured values to allow for comparison to Icelandic basalts. Grey field represents Icelandic basalts (from Fitton et al., 2003). Simple binary mixing lines between a depleted parent and various crustal end members (black squares; Baffin Island Proterozoic and Archaean basement rocks (Theriault et al., 2001)) are shown by solid lines with tick marks indicating percentage of crust in the mixture. Baffin Island-West Greenland samples define a negative trend similar to that for Iceland. The near horizontal crustal contamination mixing lines cannot produce the high $^{3}He/^{4}He$, relatively enriched (high Nb/Zr, low $^{143}Nd/^{144}Nd$) samples from more depleted magma compositions. The trend in Baffin Island-West Greenland is more likely to be due to source variations although small variations in $^{143}Nd/^{144}Nd$ within each group may be due to small amounts (<2%) of crustal contamination. Modified from Starkey et al. (2009).

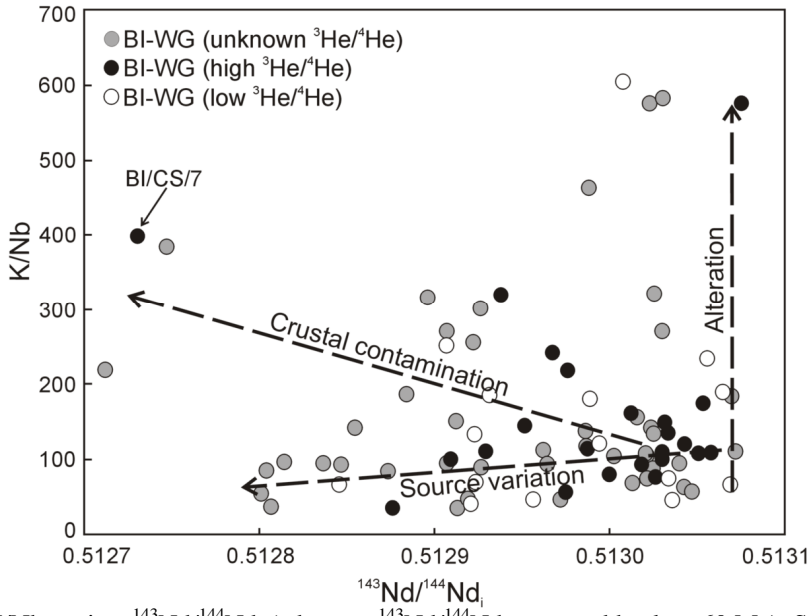

Figure 3.9. K/Nb against $^{143}Nd/^{144}Nd_i$ ($_i$ denotes $^{143}Nd/^{144}Nd$ corrected back to 60 Ma). Samples define a positive trend of increasing K/Nb with increasing $^{143}Nd/^{144}Nd$ which is thought to reflect that of the source. Scatter of some samples to higher K/Nb is either due to alteration or small amounts of crustal contamination (when accompanied by low $^{143}Nd/^{144}Nd$). High $^{3}He/^{4}He$, low $^{143}Nd/^{144}Nd$ picrites fall within the main Baffin Island-West Greenland trend and are apparently unaffected by crustal contamination. From Starkey et al. (2009).

3.4.3 Helium-strontium-neodymium isotope and trace element relationships

An important motivation of this study was to test the hypothesis of Stuart et al. (2003) that high $^{3}He/^{4}He$ resides in depleted mantle. The earlier study of Baffin Island picrites demonstrated that high $^{3}He/^{4}He$ was associated with depleted compositions (high $^{143}Nd/^{144}Nd$, low $^{87}Sr/^{86}Sr$ and low La/Sm; Stuart et al., 2003; Ellam and Stuart, 2004; Figure 3.10; Figure 3.11).

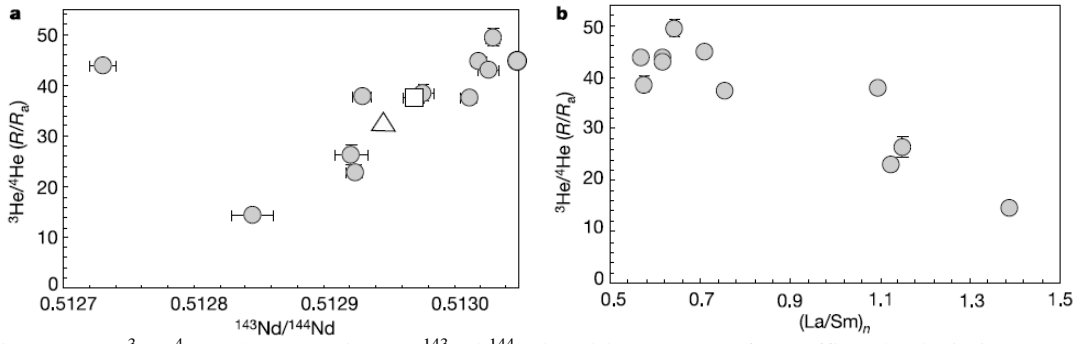

Figure 3.10. $^{3}He/^{4}He$ plotted against a) $^{143}Nd/^{144}Nd$ and b) $(La/Sm)_n$ for Baffin Island picrites (grey circles), Palaeogene ankaramite from NW Iceland (white square) and basaltic glass from Loihi seamount (white triangle). From Stuart et al. (2003).

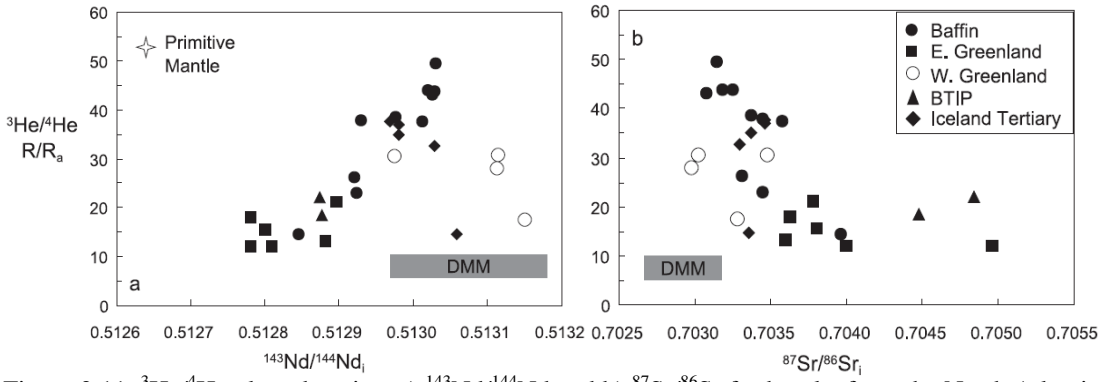

Figure 3.11. $^{3}He/^{4}He$ plotted against a) $^{143}Nd/^{144}Nd$ and b) $^{87}Sr/^{86}Sr$ for basalts from the North Atlantic Igneous Province. Linear trends attain high $^{3}He/^{4}He$ at high $^{143}Nd/^{144}Nd$ and low $^{87}Sr/^{86}Sr$. From Ellam and Stuart (2004).

More recently, Class and Goldstein (2005) showed that a compilation of global OIB indicated the same feature (Figure 3.12). OIB are separated by $^{3}He/^{4}He$, with the highest $^{3}He/^{4}He$ islands (Iceland, Hawaii, Galapagos, Juan Fernandez and Samoa) displaying the most depleted $^{143}Nd/^{144}Nd$, $^{208}Pb/^{204}Pb$ and $^{206}Pb/^{204}Pb$ (Figure 3.12).

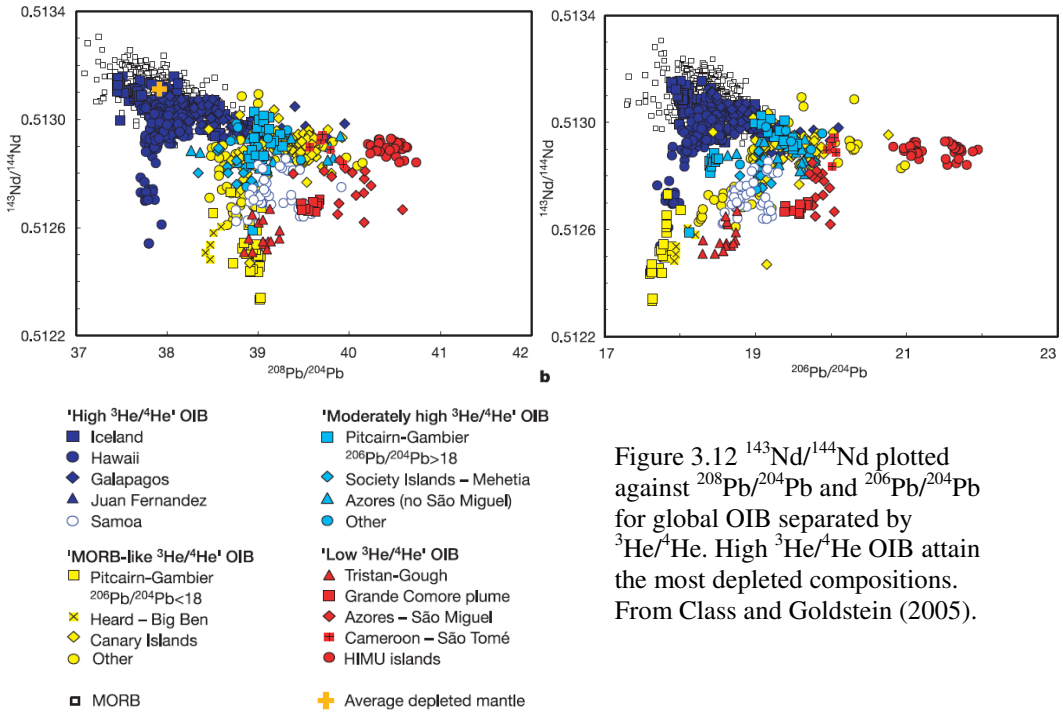

Figure 3.12 $^{143}Nd/^{144}Nd$ plotted against $^{208}Pb/^{204}Pb$ and $^{206}Pb/^{204}Pb$ for global OIB separated by $^{3}He/^{4}He$. High $^{3}He/^{4}He$ OIB attain the most depleted compositions. From Class and Goldstein (2005).

The findings of these studies (Stuart et al., 2003; Ellam and Stuart, 2004; Class and Goldstein, 2005) are inconsistent with any Earth evolution model that places high $^{3}He/^{4}He$ in a primitive reservoir. Two main explanations have been put forward to

account for the discrepancy. Either a substantial portion of depleted mantle has mixed with primitive, gas-rich high-$^{3}He/^{4}He$ mantle (Stuart et al., 2003; Ellam and Stuart, 2004), or high $^{3}He/^{4}He$ resides in depleted residues of ancient mantle depletion (Class and Goldstein, 2005; Boyet and Carlson, 2006). The data presented in this and the previous chapter can help to characterise the nature of the high-$^{3}He/^{4}He$ material in more detail and can further relate helium isotopes to other lithophile radiogenic isotopic tracers and trace element ratios.

The Nd and Sr isotope ratios of the new suite of Baffin Island and West Greenland picrites span a wide range of compositions. The $^{3}He/^{4}He$ data, from these samples and previous studies (Graham et al., 1998; Stuart et al., 2003), are plotted against Sr and Nd isotopes in Figure 3.13.

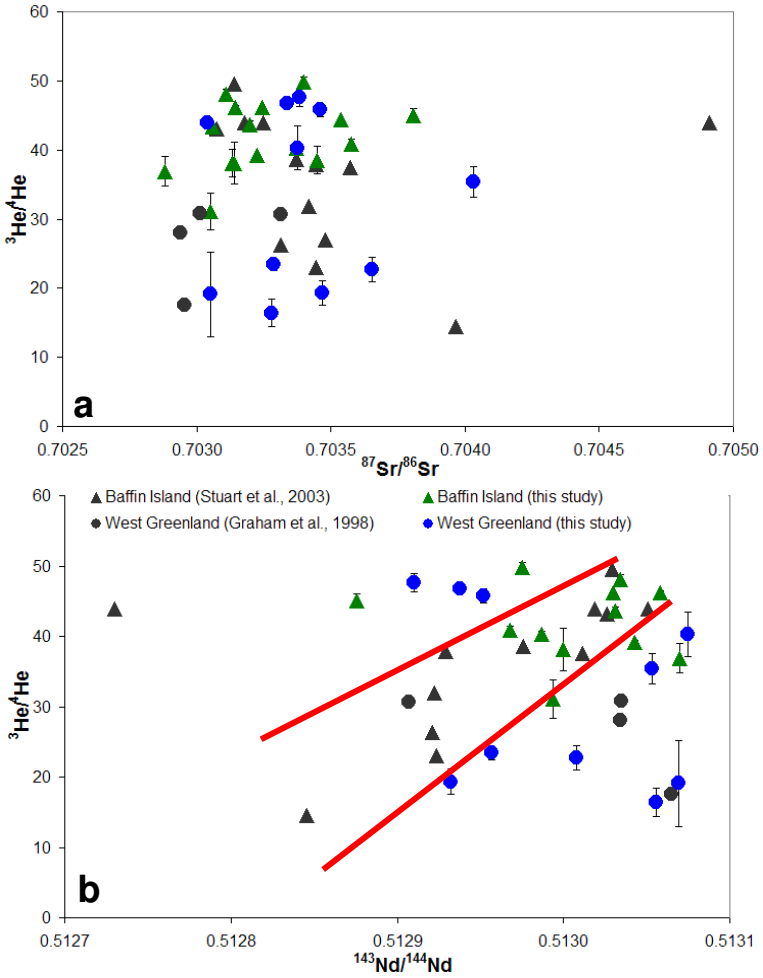

Figure 3.13. $^{3}He/^{4}He$ plotted against a) $^{87}Sr/^{86}Sr$ and b) $^{143}Nd/^{144}Nd$ for Baffin Island and West Greenland samples. Error bars for $^{3}He/^{4}He$ analyses of this study are shown. PIP trend (Ellam and Stuart, 2004) indicated by red lines.

Picrites with $^{3}He/^{4}He$ higher than ~35 R_a, the likely upper limit of contemporary OIB (maximum $^{3}He/^{4}He$; ~34 R_a from Iceland (Macpherson et al., 2005), ~32 R_a from Loihi (Kurz et al., 1982), 27.4 R_a from Galapagos (Kurz and Geist, 1999) and ~33.8 R_a from Samoa (Jackson et al., 2007)), display a wide range in $^{87}Sr/^{86}Sr$ (0.70288-0.70388) and $^{143}Nd/^{144}Nd$ (0.51288-0.51308). These values are comparable with those of picrites with $^{3}He/^{4}He$ lower than 35 R_a. Although the association of high $^{3}He/^{4}He$ with high $^{143}Nd/^{144}Nd$ and low $^{87}Sr/^{86}Sr$ typical of depleted mantle is still strong, several high $^{3}He/^{4}He$ samples have lower $^{143}Nd/^{144}Nd$ and higher $^{87}Sr/^{86}Sr$ than the range previously identified for Baffin Island picrites by Stuart et al. (2003). The linear array previously recognised in $^{3}He/^{4}He$-$^{143}Nd/^{144}Nd$ space (PIP trend; Figure 3.11; Ellam and Stuart, 2004) is no longer apparent.

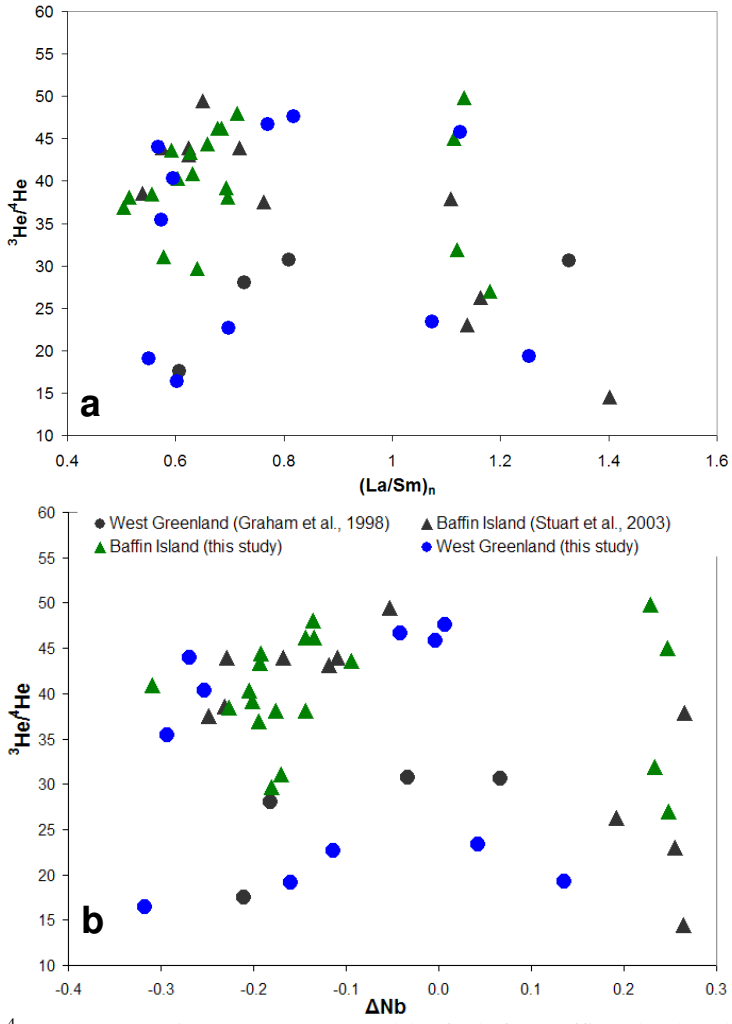

Figure 3.14. $^{3}He/^{4}He$ plotted against a) $(La/Sm)_n$ and b) ΔNb for Baffin Island and West Greenland samples from this and previous studies (Graham et al., 1998; Stuart et al., 2003). The new data show that high $^{3}He/^{4}He$ is a feature of both depleted ($(La/Sm)_n < 1$; negative ΔNb) and relatively enriched ($(La/Sm)_n > 1$; positive ΔNb) compositions.

The same is true when comparing trace element ratios with helium isotope ratios (Figure 3.14). In the previous dataset (Stuart et al., 2003), high $^{3}He/^{4}He$ samples all had $\Delta Nb < 0$ and $(La/Sm)_n < 1$ which supported the conclusion that high $^{3}He/^{4}He$ is only associated with depleted compositions. However, the new data show that both the depleted ($\Delta Nb < 0$ and $(La/Sm)_n < 1$) and relatively enriched ($\Delta Nb > 0$ and $(La/Sm)_n > 1$) groups also have $^{3}He/^{4}He$ up to 50 R_a. The new high $^{3}He/^{4}He$ samples are still predominantly depleted but, as observed in the Nd and Sr isotopic data, several samples have relatively enriched compositions ($(La/Sm)_n > 1$ and $\Delta Nb > 0$).

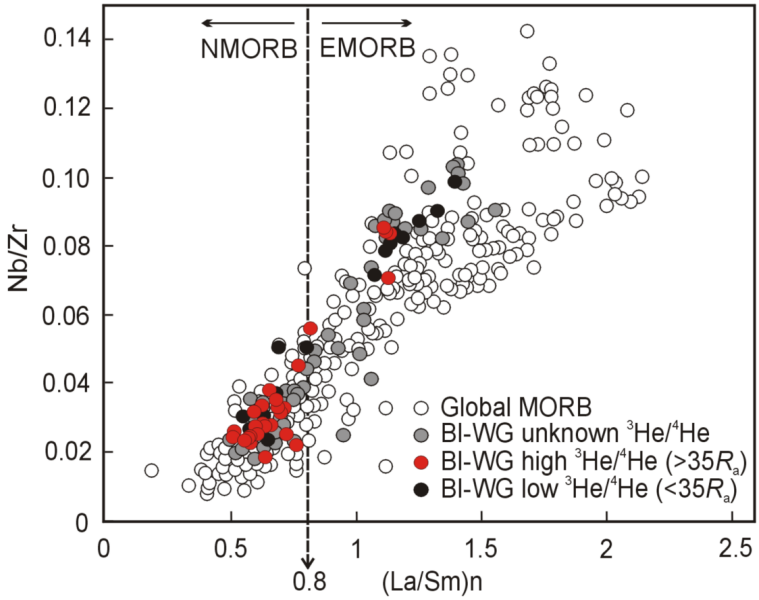

Figure 3.15. Nb/Zr plotted against $(La/Sm)_n$ for global MORB (www.petdb.org) and Baffin Island and West Greenland picrites showing the relatively enriched nature of some of the high-$^{3}He/^{4}He$ picrites in Baffin Island and West Greenland. Adapted from Starkey et al. (2009).

A plot of Nb/Zr against $(La/Sm)_n$ was used previously (Chapter 2) to demonstrate the similarity of the trace element concentrations of Baffin Island and West Greenland picrites to MORB. In this chapter the helium isotope data are included and displayed in Figure 3.15. As expected from the data presented above, although most of the high $^{3}He/^{4}He$ samples fall within the N-MORB field, several high-$^{3}He/^{4}He$ samples have E-MORB-type compositions. The REE data (Figure 3.16) support these observations. REE profiles for the high-$^{3}He/^{4}He$ samples are separated into depleted ($^{143}Nd/^{144}Nd > 0.513$) and relatively enriched groups ($^{143}Nd/^{144}Nd < 0.513$; Figure 3.16) and show that although there is some overlap between the two groups, the high-$^{3}He/^{4}He$ relatively enriched samples (with $^{143}Nd/^{144}Nd < 0.513$) have flatter

REE profiles than the more depleted ($^{143}Nd/^{144}Nd > 0.513$) high-$^{3}He/^{4}He$ samples which have LREE-depleted patterns (Starkey et al., 2009).

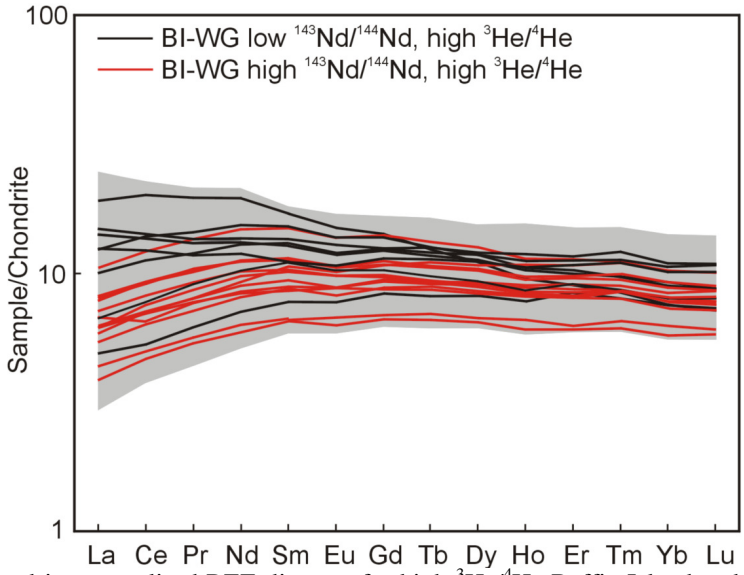

Figure 3.16. Chondrite-normalised REE diagram for high-$^{3}He/^{4}He$ Baffin Island and West Greenland picrites separated by $^{143}Nd/^{144}Nd = 0.5130$ into depleted and relatively enriched groups. Adapted from Starkey et al. (2009).

3.4.4 When did the depleted and relatively enriched NAIP mantle sources form?

Various authors have commented on the nature of the N- and E-type division of the Baffin Island and West Greenland magmas (Robillard et al., 1992; Kent et al., 2004). This and the previous chapter demonstrated that the lavas are indistinguishable from MORB in their trace element compositions, spanning the range from N-MORB to E-MORB. It has also been shown that it is not possible to produce the more enriched lavas by crustal contamination of initially depleted parent magma (in agreement with the conclusion of Robillard et al. (1992) and Kent et al. (2004)). Although crustal contamination may have affected some lavas, the Baffin Island and West Greenland lavas require at least two different mantle source components to begin with; a depleted and a relatively enriched source.

Sm-Nd isochrons can be used to estimate the age of possible mantle sources for the Baffin Island-West Greenland lavas. On a plot of $^{143}Nd/^{144}Nd$ against $^{147}Sm/^{144}Nd$

(Figure 3.17) Baffin Island-West Greenland samples fall into a depleted and a more enriched group with a separation at $^{147}Sm/^{144}Nd$ = 0.19-0.20 and $^{143}Nd/^{144}Nd$ = 0.51295-0.51300. Some samples scatter to higher $^{147}Sm/^{144}Nd$ than expected for their $^{143}Nd/^{144}Nd$. These samples are the dykes that were discussed earlier and include the high-$^{3}He/^{4}He$ sample BI/CS/7 which has always been considered to be crustally contaminated due to its low $^{143}Nd/^{144}Nd$ (Stuart et al., 2003). Baffin Island and West Greenland samples with high-$^{3}He/^{4}He$ fall into both the relatively enriched and depleted groups (orange diamonds), although they are more common in the depleted group.

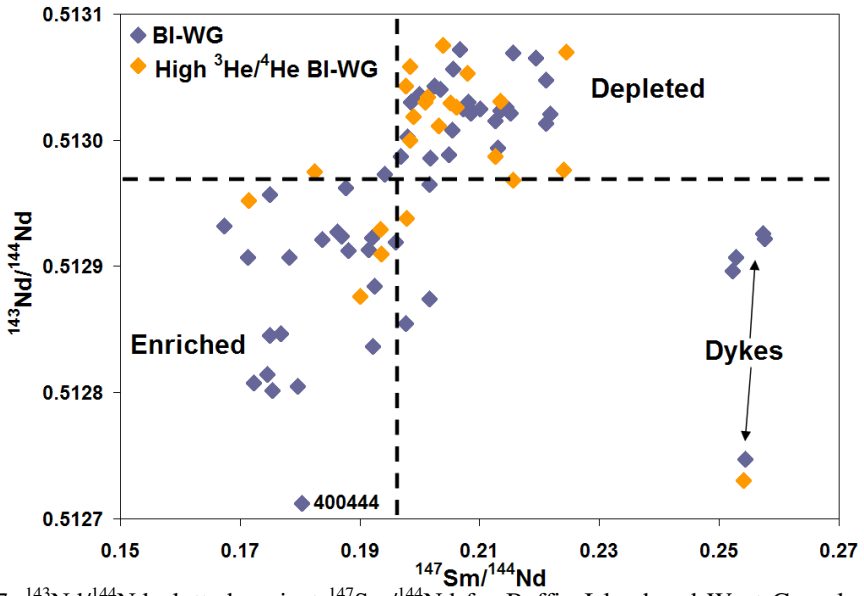

Figure 3.17. $^{143}Nd/^{144}Nd$ plotted against $^{147}Sm/^{144}Nd$ for Baffin Island and West Greenland samples (this study and Starkey et al. (2009)). Samples with high $^{3}He/^{4}He$ are found throughout the full range of compositions. In general the Baffin Island and West Greenland samples fall into two groups; a relatively enriched group (low $^{143}Nd/^{144}Nd$ and $^{147}Sm/^{144}Nd$) and a depleted group (high $^{143}Nd/^{144}Nd$ and $^{147}Sm/^{144}Nd$).

Figure 3.18 shows Sm-Nd isochrons that would be produced by variable enrichment of a depleted mantle source at 400, 600, 800 and 1000 Ma. $^{143}Nd/^{144}Nd$ = 0.5131 and $^{147}Sm/^{144}Nd$ = 0.2290 (Sm = 0.270 ppm, Nd = 0.713 ppm; Salters and Stracke, 2004) were used for the present day depleted mantle. The Sm-Nd isochrons radiate from the present day depleted mantle composition showing the effects of variable enrichment at the times indicated. The slope of the isochrons suggests that the depleted and relatively enriched groups in Baffin Island and West Greenland could be generated from depleted mantle that was variably enriched at some point between

400-800 Ma. This probably also applies to the six samples (BI/CS/-7, -8, -9, -11, -12, -13 and BI/PI/16) at very high $^{147}Sm/^{144}Nd$ (0.25-0.26) and 400444 at low $^{143}Nd/^{144}Nd$ but 'normal' $^{147}Sm/^{144}Nd$ (indicated on Figure 3.17) except that they have recently undergone some crustal interaction to shift their compositions from the main trend. The contaminant for the dykes appears to differ from that for 400444. The particularly high (depleted) Sm/Nd coupled with low (enriched) $^{143}Nd/^{144}Nd$ of the dykes is hard to explain by addition of continental crust, nor is it obvious why the dykes should be so different from the lava flows in their Sm/Nd and $^{143}Nd/^{144}Nd$.

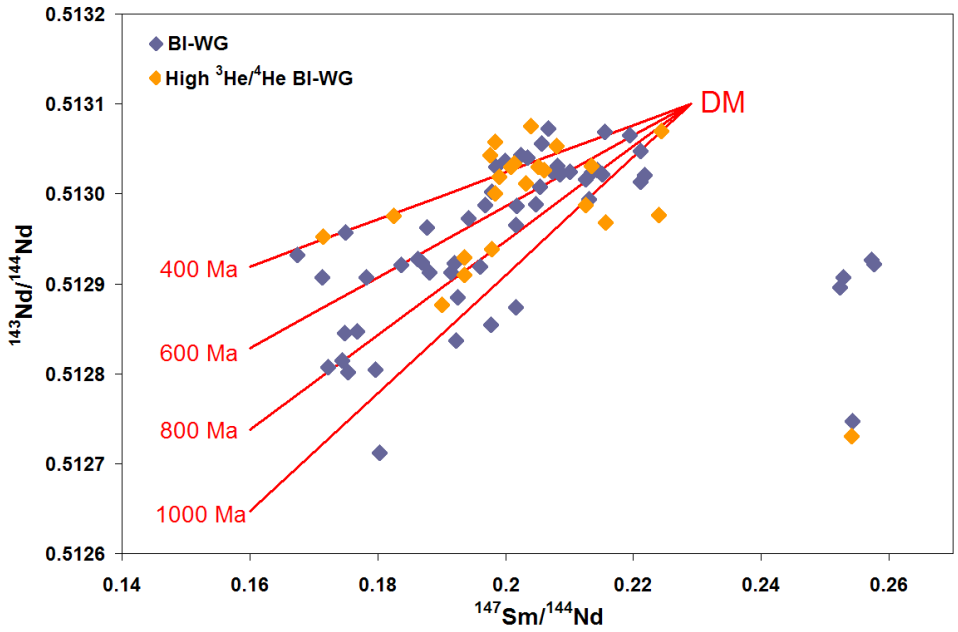

Figure 3.18. $^{143}Nd/^{144}Nd$ plotted against $^{147}Sm/^{144}Nd$ showing Sm-Nd isochrons for the age of enrichment of a depleted mantle source. The slope of the Baffin Island-West Greenland data array suggests that enrichment of the mantle source occurred between 400-800 Ma.

A plausible source for the enrichment between 400-800 Ma in the Baffin Island-West Greenland mantle source could be subducted oceanic lithosphere and crust. Mixing of subducted material into depleted upper mantle has been suggested to account for the relative enrichment of Icelandic basalts compared to MORB (Chauvel and Hemond, 2000; Skovgaard et al., 2001; Fitton et al., 2003; Thirlwall et al., 2004; Foulger et al., 2005). If enrichment in the Icelandic source is a long-lived feature then subducted material may also be able to account for the composition of the relatively enriched E-type samples in the early NAIP, with the more depleted upper mantle N-MORB source accounting for the N-type lavas. However, an important

question is concerned with the extent and scale of mixing between depleted and enriched components in the NAIP source. The early NAIP lavas are characterised by inter bedded sequences of depleted and relatively enriched lavas whereas only E-type lavas are erupted in Iceland suggesting that a larger proportion of subducted material is required in more recent NAIP magmatism, if it is subducted material that produced the enrichment. It is also important to consider how the introduction of subducted material relates to the helium isotope anomaly in the NAIP. High $^{3}He/^{4}He$ may already have been a feature of the depleted NAIP source prior to the phase of enrichment but it could have been introduced at the same time as the subducted material or even after the heterogeneity in the NAIP source was already established. These issues are discussed in more detail in Chapter 5 along with a review of the other studies that focus on the potential for subducted material in the NAIP source.

3.5 Summary

The Baffin Island and West Greenland picrites reach $^{3}He/^{4}He$ values up to ~50 R_a. These new data confirm that the earliest NAIP magma had the highest terrestrial magmatic $^{3}He/^{4}He$. The high $^{3}He/^{4}He$ samples display a wide range in Sr and Nd isotopic compositions, similar to the range observed among samples with lower $^{3}He/^{4}He$. The lack of correlation between helium isotopes and lithophile radiogenic isotopes and trace elements is a feature not previously found in other datasets. The lavas show a similar level of depletion to MORB in Sr and Nd isotopes and can be divided into N- and E-type lavas based on their isotopic composition and their trace elements and REE concentrations. The picrites of the Vaigat Formation show a progression from depleted MORB-like compositions to more enriched 'Icelandic' or E-type compositions up-sequence, as has previously been noted by Holm et al. (1993). Since the Baffin Island picrites span the entire range of West Greenland compositions it is not possible to use the data to correlate them stratigraphically with the West Greenland lavas. Either the Baffin Island lavas erupted over the same time interval as the entire Vaigat Formation in West Greenland or the Baffin Island lavas only erupted during the Anaanaa phase, as suggested by Larsen and Pedersen (2000), but they tapped a source that was more diverse compositionally. Crustal

contamination of originally depleted parent magma cannot account for the range in compositions from N- to E-type in Baffin Island and West Greenland (as shown by Robillard et al. (1992) and Kent et al. (2004)). Crustal contamination may have affected some lavas but by such a small degree that $^{143}Nd/^{144}Nd$ cannot have been altered significantly. In addition, crustal contamination is ruled out for all of the high $^{3}He/^{4}He$ picrites of this study. Subsequently, the range in $^{143}Nd/^{144}Nd$ at high $^{3}He/^{4}He$ displayed by the picrites reflects that of their mantle source. At 60 Ma the depleted and relatively enriched components must have been present as discrete domains in the mantle source, possibly having separated from a common depleted source at ~400-800 Ma. The depleted and relatively enriched components may have been variably contaminated by a small degree after separation from their depleted mantle source. However, these components were likely to have been closely associated spatially over time since depleted and relatively enriched lavas were erupted simultaneously at the same location or within a very short time of each other, forming inter bedded lava sequences. Whatever the scale of heterogeneity within the source of the Baffin Island and West Greenland lavas, it was probably present over a large distance to account for the huge volumes of associated magmatism across the North Atlantic Igneous Province (Saunders et al., 1997).

4 Results: Major and trace element compositions of melt inclusions

4.1 Introduction

This chapter focuses on the major and trace element compositions of melt inclusions hosted within olivine phenocrysts in the Baffin Island and West Greenland picrite samples. The samples in this study have been well characterised for their whole-rock major and trace elements, Sr, Nd and He isotopes (Chapters 2 and 3; Starkey et al., 2009). The major element compositions of olivine phenocrysts and melt inclusions were measured by electron microprobe and samples were then chosen for ion microprobe analysis of melt inclusion trace element concentrations. These samples display extremely high $^{3}He/^{4}He$ (>40 R_a) with a range in whole-rock incompatible trace element ratios and Sr and Nd isotope ratios (Chapter 2 and 3; Starkey et al., 2009). This is the first study to focus specifically on linking both major and trace element compositions of melt inclusions with helium isotope variations. The melt inclusion data complement the whole-rock analyses by providing a more focused study of the magmatic system and the melt compositions that contributed to the erupted lavas. These melt compositions can help test the conclusions drawn from the whole-rock data regarding the source composition for high $^{3}He/^{4}He$ in the Earth.

4.2 Melt inclusions

4.2.1 Background

Melt inclusions represent tiny samples of individual melt fractions trapped inside growing crystals during an interruption in crystallisation. In ideal circumstances, melt within an inclusion is quenched rapidly resulting in a glass that remains unaffected by any subsequent groundmass crystallisation. The trapped glass may then preserve information on the conditions in the magmatic system at a particular time. Analyses of a number of melt inclusions for a range of elemental abundances can be used to investigate the individual melts that contributed to the erupted lava and hence provide information about their source.

Many studies have shown that the compositional variation of melt inclusions in mafic volcanic rocks is much greater than that of the lavas that host them (Sobolev and Shimizu, 1993; Gurenko et al., 1996; Sobolev, 1996; Kamenetsky et al., 1995, 1997; Kent et al., 2002; Saal et al., 1998; Maclennan et al., 2003). Variations have been variously attributed to a number of processes that occur in any basaltic system such as variations in source composition (Sinton et al., 1993; Sobolev and Chaussidon, 1996; Saal et al., 1998), variations in the degree and style of melting and mineralogy of mantle source (Sobolev and Shimizu, 1993; Nielsen et al., 1995; Sobolev 1996; Shimizu, 1998; Maclennan et al., 2003) and crystal fractionation and crustal assimilation (Kent et al., 1999, 2002; Danyushevsky et al., 2004; Yaxley et al., 2004; Kamenetsky and Gurenko, 2007). Correspondence of average melt inclusion composition with that of the host lava is a widely recognised feature (Nielsen et al., 1995; Kent et al., 1999, 2002; Slater et al., 2001; Norman et al., 2002; Maclennan et al., 2003). It has been suggested that melt inclusions sample the melt compositions that are available prior to mixing and aggregation of melts that produce the erupted lava (Sobolev and Shimizu, 1993; Kent et al., 1999). In this way, melt inclusions have the potential to preserve compositions that are not represented by the bulk rock, such as volumetrically small melt fractions, depleted melts, and those melts that are only available in the initial stages of melt evolution. If melt inclusions can trap pure unmixed melts then they also have the potential to record primary magma compositions. However, more recently it has been shown that it is possible for melt inclusions to be trapped after mixing of melts has occurred (Maclennan, 2008). Unfortunately, there are also a few processes that are thought to affect the composition of melt inclusions post-trapping, so that the measured melt inclusion composition may not directly reflect that of the trapped melt. These include post-entrapment crystallisation (Roedder, 1979; Danyushevsky et al., 2000; Kress and Ghiorso, 2004), diffusive re-equilibration (Danyushevsky et al, 2000; Gaetani and Watson, 2000; Cottrell et al., 2002; Spandler et al., 2007), breaching and alteration. Many of these factors can be overcome with careful petrographical selection of inclusions prior to analysis. For example, melt inclusions that appear to have crystallised or those that are situated near to a crack in the olivine can be avoided.

4.2.2 Whole-rock versus in-situ measurements

The whole-rock composition of samples is very useful for characterising and comparing rocks by providing what is effectively an average composition of the individual melts that contributed to the erupted lava. However, the source for most igneous rocks is likely to be heterogeneous on both small and large scales. Any melts that separate from the homogeneous or heterogeneous source will also be expected to fractionate to varying degrees as they are trapped in the lithosphere or crust on the way to the surface for eruption (Cox et al., 1979). Melt batches in various stages of fractionation may collect and partly or wholly mix in a magma chamber or in magma conduits. In order to get a more precise view of the magmatic system it is possible to make in-situ measurements of individual crystal or melt compositions using, in this study, electron and ion microprobes. In Baffin Island and West Greenland, as in many other igneous systems, tiny portions of melt are frequently trapped as inclusions in olivine crystals during crystallisation. Melt inclusions therefore sample melt compositions present during the period that olivine crystals were forming and therefore may trace processes that happened over this time, such as melt evolution and crustal contamination. Importantly, it is the melt inclusions that trap volatiles (CO_2 and noble gases) and so they provide another reason to investigate melt inclusion compositions in more detail to link to the helium isotope data obtained in this study. The potential effects of post-entrapment processes on the major element composition of melt inclusions means that measured melt inclusion compositions should be carefully assessed (Sobolev, 1996; Danyushevsky, 2002a,b). Post-entrapment processes are discussed further in Sections 4.3 and 4.4.1.2.

4.2.3 Aims of melt inclusion study

The aim of the study reported in this chapter was to investigate the composition of melt inclusions in high-$^3He/^4He$ samples that span a range of whole-rock compositions. Melt inclusions sample the individual melt compositions that contributed to the erupted lava. In particular, melt inclusion incompatible trace element concentrations and REE profiles can be used to characterise these individual

melts and test the conclusions drawn from the whole-rock study (Chapter 2 and 3; Starkey et al., 2009) that crustal contamination has not affected the high $^{3}He/^{4}He$ whole-rock relatively enriched samples and, therefore, that high $^{3}He/^{4}He$ is a feature of both depleted and relatively enriched mantle sources. Since all the samples chosen for the melt inclusion study have high $^{3}He/^{4}He$, then the range of melt inclusion compositions in depleted and relatively enriched whole-rock samples will be assessed to investigate the mantle composition(s) with which high $^{3}He/^{4}He$ is associated. If crustal contamination of depleted melts to produce relatively enriched melts can be ruled out, then the range in melt inclusion compositions reflects that of the source. In addition, if all the melt inclusions in a whole-rock relatively enriched sample (low $^{143}Nd/^{144}Nd$, positive ΔNb and high $(La/Sm)_n$) display the same level of enrichment, then high $^{3}He/^{4}He$ cannot be associated with depleted melt compositions. However, if whole-rock relatively enriched samples contain a range of depleted and relatively enriched melt inclusions then mantle evolution models that place high $^{3}He/^{4}He$ in a discrete depleted mantle composition, as suggested by some studies (Ellam and Stuart, 2004; Class and Goldstein, 2005), cannot be ruled out.

4.2.4 Previous studies

There have been five melt inclusion studies using Baffin Island and West Greenland samples. In one study (Smit et al., 2004) melt inclusions in a sample with high $^{3}He/^{4}He$ from Baffin Island were analysed, but this study did not include trace element analyses that the authors noted would be required to understand better the source composition of the lava. Of the other melt inclusion studies the most extensive has been that of Yaxley et al. (2004) who focussed on melt inclusions in six previously unreported Baffin Island picrites. Experimental reheating was used to homogenise the melt inclusions with 68 melt inclusions analysed by electron microprobe for major elements and 28 by LA-ICP-MS for trace elements. Yaxley et al. (2004) found that the melt inclusion compositions were more heterogeneous than that of their host lavas, a feature the authors thought reflected the effects of crustal contamination. Yaxley et al. (2004) concluded that crustal contamination of evolving picritic liquids with about 15% of broadly granitic crust could account for the trends in the melt inclusion data. Interestingly, the whole-rock compositions of the lavas in

the Yaxley et al. (2004) study showed the effects of only 1-2% crustal contamination, suggesting that the melts may have incorporated crustal rocks during olivine crystallisation (Yaxley et al., 2004). The study of Harlou et al. (2006) also recorded the effects of crustal contamination on Baffin Island melt inclusions. These authors analysed Sr isotopes and trace element concentrations in 30 melt inclusions in five Baffin Island picrites from the collection of Stuart et al. (2003). However, the conference abstract of Harlou et al. (2006) provides no data so it is unclear whether the high $^{3}He/^{4}He$ picrites from the Stuart et al. (2003) collection were selected. Nevertheless, melt inclusion Sr isotope ratios indicated that there were three main groups of melt inclusion compositions in any one sample; 1) depleted, low $^{87}Sr/^{86}Sr$, 2) slightly elevated $^{87}Sr/^{86}Sr$ and 3) very high $^{87}Sr/^{86}Sr$, falling on mixing trajectories between depleted parents and crustal rocks. REE patterns of the melt inclusions were said to be similar to that in the whole-rocks. However, it is unclear how the $^{87}Sr/^{86}Sr$ relate to the whole-rock compositions and therefore whether crustal contamination is more apparent in the melt inclusion compositions as suggested by Yaxley et al. (2004).

For the West Greenland picrites, there have been two melt inclusion studies that both focussed on major element analyses. Larsen and Pedersen (2000) presented major element data for melt inclusions in four picrite samples from the Vaigat Formation of West Greenland. They showed that melt inclusions in different volcanic members evolved along individual liquid lines of descent and that compositional differences in melt inclusions are inherited from the primary melts. However, Larsen and Pedersen (2000) concluded that the melt inclusions have undergone Fe-loss meaning that caution should be applied to any petrogenetic conclusions based on the melt inclusion data. Peate et al. (2007) analysed major elements in melt inclusions in five West Greenland samples from a previous dataset that had been analysed for He isotopes (Graham et al., 1998) but showed a maximum of only 30 R_a. The results indicate the potential for crustal contamination in one of the samples due to raised K/Ti but the authors noted that a better evaluation would only be possible with trace element data.

The studies that are briefly summarised above provide only an overview of the work that has been completed. It would seem that there is little consensus from these studies as to whether crustal contamination plays an important role in producing the compositional variation of Baffin Island and West Greenland melt inclusions. The lack of agreement may be related to the fact that not all inclusions are affected by the same degree of crustal contamination or by the same contaminant, if affected at all. Most studies conclude that melt inclusion incompatible trace element concentrations are required in order to make firm conclusions on the petrogenetic history of samples.

Crustal contamination has clearly affected the whole-rock composition of some samples in Baffin Island and West Greenland (Larsen and Pedersen, 2000; Yaxley et al., 2004; Starkey et al., 2009) and may also be recorded by melt inclusions (Yaxley et al., 2004; Harlou et al., 2006). However, the aim here is to determine whether crustal contamination has affected the compositions of melt inclusions in high $^{3}He/^{4}He$ samples. The samples chosen for this study do not appear to have undergone detectable crustal contamination in their whole-rock compositions. However, the Yaxley et al. (2004) data suggest that melt inclusions may record up to an order of magnitude more intense contamination than the whole-rocks. This suggests that melt inclusions should represent a better method to investigate the intricacies of melt composition variations, especially if incompatible trace element concentrations are obtained.

4.2.5 Linking helium isotopes to melt inclusions

Commonly, melt inclusions contain a bubble that is thought to form when the melt inclusion is cooling. Crystallisation causes the pressure inside the inclusion to decrease, since olivine is denser than melt, which in many cases causes the nucleation of a bubble (Figure 4.1; Danyushevsky et al., 2000). The size of a bubble is controlled by the relative size of the inclusion and its cooling history (fast cooling rates and/or small inclusions may not nucleate bubbles (Tait, 1992; Lowenstern, 1994). The bubble is the likely repository for CO_2 and other volatiles, including the noble gases (Kent, 2008).

Helium isotope ratios are measured by crushing ~1-2g of olivine phenocrysts to release the gases contained within the bubbles in the melt inclusions. Therefore, any study investigating the major, trace element and radiogenic isotope composition of high $^{3}He/^{4}He$ mantle is hindered by the question of whether helium isotope ratios can be linked directly to the whole-rock composition of the sample. It is not known if all of the melt inclusions in any one sample contain helium and, if they do, whether they all have the same helium isotope ratio. It is possible that the individual melts, sampled by crystallising olivines at different stages of melt evolution, have different helium isotope ratios associated with them. If this is the case then there is the potential for large variations in melt inclusion $^{3}He/^{4}He$ in any one sample. This study focuses on the major and trace element composition of individual melt inclusions in high $^{3}He/^{4}He$ samples in order to determine whether high $^{3}He/^{4}He$ can be linked to a specific melt composition. Ideally, Sr, Nd and He isotope measurements would be made directly from melt inclusions which would allow direct comparison of the isotope ratios in each melt inclusion to provide more detailed information on the source of high $^{3}He/^{4}He$. Although measurement of in-situ melt inclusion Sr isotopes is now technically possible (Harlou et al., 2006; Jackson and Hart, 2006), unfortunately both in-situ melt inclusion Nd and He isotope measurements are beyond current capabilities, particularly in terms of gaining the required precision. Since major and trace element compositions of melt inclusions can be obtained relatively easily, these compositions will be compared to $^{3}He/^{4}He$ measured by crushing, since more advanced techniques are not available.

4.3 Post-entrapment modification processes affecting melt inclusion compositions

4.3.1 Post-entrapment crystallisation (PEC) of melt inclusions

One of the main post-entrapment modification processes affecting all inclusions is crystallisation of the trapped melt onto the inner walls of the inclusion during cooling (Roedder, 1984; Sobolev, 1996; Kress and Ghiorso, 2004). The trapped melt is saturated in the host mineral, which in this case is olivine, so olivine crystallises at the inclusion-crystal interface (Figure 4.1c,g). Olivine crystallisation on the inner wall of the melt inclusion is recognisable in thin section and particularly in back-

scattered electron (BSE) images as a thin rim of Fe-rich olivine (Figure 4.1c,g). The inclusion margin provides a site of lower nucleation energy (Roedder, 1979) so that the olivine crystallises in concentric rings that become progressively Fe-rich with each increment of olivine that crystallises (Kent, 2008). Post-entrapment crystallisation (PEC) alters the composition of the melt so that the measured composition does not necessarily reflect that of the original trapped melt. When melt inclusions are cooled rapidly to form glasses, it is possible to reconstruct the original trapped composition of the melt inclusion. This involves returning the melt inclusion to a composition that is in equilibrium with the host olivine.

There are two main methods suggested for correcting the compositions of olivine-hosted inclusions. In the first, the melt inclusion is heated to the temperature at trapping, prior to analysis, so that any olivine that crystallised on the inclusion wall is melted back in (Nielsen et al., 1995; Danyushevsky et al., 2002a). The melt is then rapidly quenched to glass (Nielsen et al., 1995; Nielsen et al., 1998; Danyushevsky et al., 2002a). However, it is possible to overheat inclusions causing more olivine to be melted into the inclusion than that which originally crystallised out, resulting in incorrect major element compositions. Overheating is thought to occur if the inclusion was trapped at a higher pressure than it was possible to obtain in heating experiments or if the melt inclusion is over saturated in volatiles. Experimental re-heating of melt inclusions can have a detrimental effect on the concentrations of volatile elements (Kent, 2008). The second procedure to obtain the initial composition of trapped melts is carried out after analysis and involves numerical corrections to the compositions of unheated inclusions. These corrections involve the addition of olivine, of a composition in equilibrium with the melt, in small increments until a new composition is reached that is in equilibrium with the observed host olivine (similar to the methods used by Sobolev (1996) and Green et al. (2001)). This correction is only applied to the major elements that are compatible in olivine. Incompatible major and trace elements will not be taken into the lattice of the olivine crystallising on the inclusion wall. Therefore, the only effect on incompatible elements during PEC is that their concentrations are increased relative to the initial trapped melt due to the reduction in the volume of the melt inclusion.

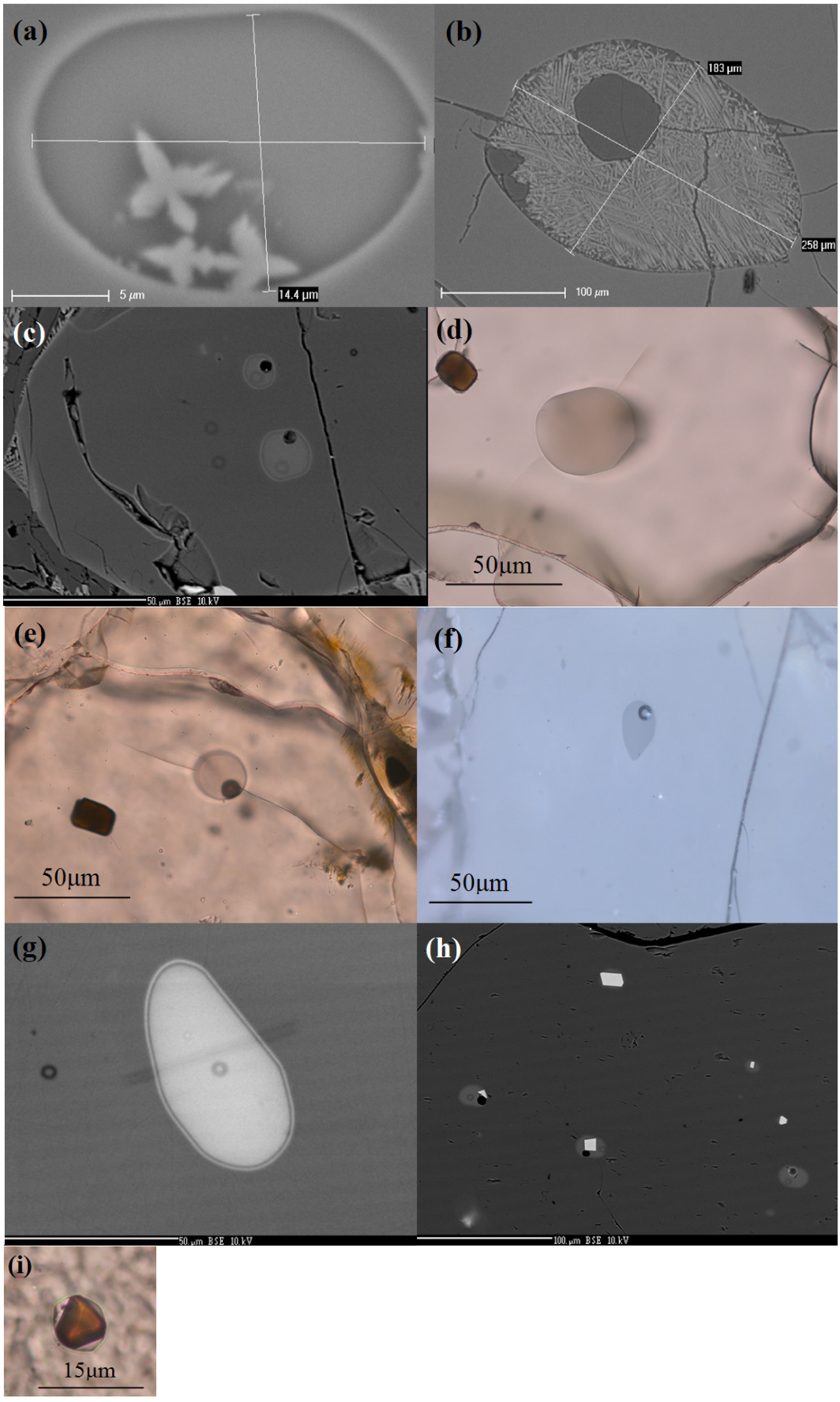
(a)
5 µm
14.4 µm
(b)
183 µm
258 µm
100 µm
(c)
50 µm BSE 10.kV
(d)
50µm
(e)
50µm
(f)
50µm
(g)
50 µm BSE 10.kV
(h)
100 µm BSE 10.kV
(i)
15µm

Figure 4.1. a) 362077. Scanning electron microscope (SEM) image of a partially re-crystallised melt inclusion with a newly grown chromite crystal. b) SEM image of completely re-crystallised melt inclusion. c) PAD6. BSE image of two olivine-hosted melt inclusions with bubbles. Small shadow dots are electron microprobe spots. d) 362077. Transmitted light image of melt inclusion and spinel (upper left) in olivine. e) DUR8. Transmitted light image of melt inclusions with brown bubble and square spinel in olivine. f) PAD6. Transmitted light image of melt inclusion which is only partially at the surface of the crystal. g) 400452. BSE image of melt inclusion with electron microprobe profile line. Electron microprobe spots in melt inclusion and adjacent olivine can be seen. A clearly defined rim (post-entrapment crystallisation of olivine) at the melt inclusion-host olivine interface can be seen. h) PAD6. BSE image of melt inclusions with associated square chromite spinels (white) within olivine. i) PAD6. Transmitted light image of an octahedral chromite crystal captured within a melt inclusion.

Complete PEC of melt inclusions is possible where other daughter minerals, such as feldspar and pyroxene, in addition to olivine may crystallise (Figure 4.1a,b). If this is the case then the changes to the melt composition are too complex to correct for the extent of crystallisation of each phase numerically. Crystallised inclusions, whether partly or wholly crystallised, can usually be recognised using standard light microscopy and avoided during analyses. Within any one sample it is possible that only some of the inclusions are affected by complete crystallisation while others remain pristine. In this study, crystallised melt inclusions and any inclusions displaying unusual features, such as irregular margins, were avoided during analysis. Analyses were only made on pristine glassy inclusions which avoided the complications of re-homogenising inclusions in heating experiments.

4.3.2 Post-entrapment diffusive re-equilibration of melt inclusions

Diffusive re-equilibration between the melt inclusion and its host is thought to occur during PEC when the inclusion is cooling (Qin et al., 1992; Danyushevsky et al., 2000, 2002b; Gaetani and Watson, 2000; Cottrell et al., 2002; Spandler et al., 2007). There is potential for the inclusion to exchange diffusively partially or completely with its host crystal and the melt surrounding the host crystal. If diffusive re-equilibration occurs then the melt inclusion does not record the composition of the original trapped melt. The primary question is exactly how much this process can significantly alter the composition of melt inclusions and whether it can be corrected numerically. In addition, some elements may be affected more than others resulting in fractionation of elements from one another (Qin et al., 1992; Cottrell et al., 2002).

Theoretical, observational and experimental studies (Danyushevsky et al., 2000, 2002a,b; Gaetani and Watson, 2000; Cottrell et al., 2002; Spandler et al., 2007) show that small inclusions with a large ratio of inclusion radius to host-crystal radius that cool slowly are found to equilibrate more rapidly. In addition, elements compatible in the host phase and elements with higher diffusivities will obviously equilibrate more rapidly (Kent, 2008).

Diffusive re-equilibration is sometimes known as 'Fe-loss'. This describes the potential diffusion of Fe^{2+} cations from, and Mg^{2+} cations into the inclusion (Danyushevsky et al., 2002b). This process is thought to occur until partial or complete re-equilibration of the olivine rim into the host olivine and/or external melt at temperatures below trapping (Yaxley et al., 2004). When melt inclusions are cooled slowly, the progressively Fe-rich olivine that grows during PEC within the inclusion is thought to equilibrate with the more magnesian olivine in the remainder of the host mineral. The inclusion itself then also seeks to equilibrate with the rim of olivine by adding Fe to maintain Fe/Mg equilibrium (Danyushevsky et al., 2000). The melt inclusion itself is expected to be affected more by diffusive re-equilibration than the host olivine since diffusion rates in melts are faster and the host olivine has a larger volume that can more easily accommodate the diffusive changes without detection. Figure 4.2 illustrates the effects on the FeO and MgO content of melt inclusions in different cooling scenarios and the complications of reconstructing the trapped melt compositions.

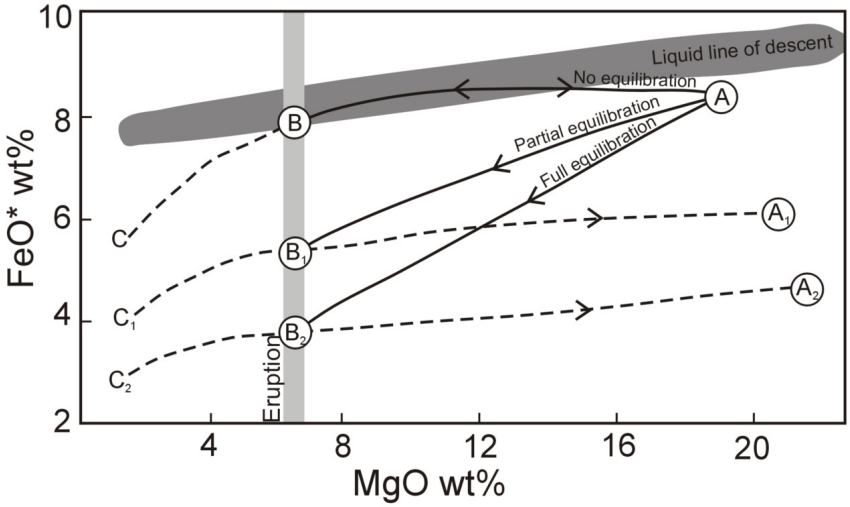

Figure 4.2. Schematic diagram illustrating the effects of melt inclusion re-equilibration within host olivine (modified from Danyushevsky et al. (2000) and Kent (2008)). A-B = path of cooling melt inclusion with starting composition 'A' which crystallises olivine with no re-equilibration between newly grown olivine and host olivine. This path can be reversed by either homogenisation experiments or numerical correction. A-B_2 = path of cooling melt inclusion with starting composition 'A' which crystallises olivine with full re-equilibration between newly grown olivine and host crystal. B-C, B_1-C_1 and B_2-C_2 = paths followed by melt inclusions during rapid cooling after eruption with near-fractional olivine growth. C, C_1 and C_2 can be corrected numerically to B, B_1 and B_2 but if corrections on B_1 and B_2 are continued then the inclusions take path B_1-A_1 or B_2-A_2 resulting in lower Fe and higher Mg number than the original trapped liquids.

There are a several methods available in the literature that make corrections for Fe-loss, should it be detected, from either naturally quenched glassy inclusions or from those that have been experimentally re-heated (Danyushevsky et al., 2000). Figure 4.3 shows the effects of numerical Fe-loss corrections to the re-heated Baffin Island melt inclusions from Yaxley et al. (2004). Inclusions are corrected to an assumed FeOt content similar to that defined by the whole-rocks and glasses. If inclusions have lost Fe during diffusive re-equilibration then they are expected to display a negative correlation in a plot of FeO of the melt inclusion against Fo% of the host olivine since inclusions hosted by high forsterite olivine crystals are subject to a greater degree of Fe-loss (Danyushevsky et al., 2000, 2002b; Yaxley et al., 2004). In addition, Danyushevsky et al. (2000, 2002b) show that if melt inclusions fall below the trend defined by the liquid line of descent of the whole-rocks on a plot of FeO against MgO (i.e. at lower FeO) then they are also said to have experienced Fe-loss. One of the main problems involved with correcting melt inclusion compositions is identifying how much PEC and Fe-loss have occurred. If both processes occurred together then it may be impossible to estimate how much each process has affected

the melt inclusion compositions, meaning that it may be impossible to reconstruct the trapped melt composition.

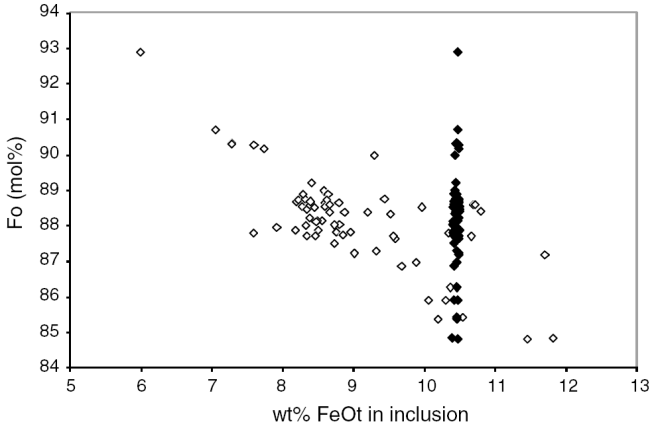

Figure 4.3. Baffin Island re-heated melt inclusions (white diamonds) and re-heated inclusions corrected for Fe-loss (black diamonds). From Yaxley et al. (2004).

4.3.2.1 Diffusive re-equilibration of incompatible trace elements

Modelling of diffusive re-equilibration for REE between olivine and melt by Cottrell et al. (2002) shows that, over time, the slightly higher partition coefficients of the HREE in olivine result in a higher potential for the HREE to be modified by post-entrapment diffusion than those of the LREE (Figure 4.4; Cottrell et al., 2002). Further experimental work by Spandler et al. (2007) also shows fast diffusivities for REE in olivine. The rates indicated suggest that REE can diffusively re-equilibrate on a timescale of years and therefore the preservation of trapped melt compositions in olivine-hosted melt inclusions may be compromised. Despite the experimental evidence, observations based on the compositions of natural olivine-hosted inclusions show REE profiles that do not match those expected from modelled equilibrated inclusions, showing little evidence for diffusion of the HREE (Figure 4.4; Cottrell et al., 2002). This is in agreement with the experimental work of Cherniak (2007) who found diffusion rates for the REE in olivine that were 3-4 times slower than those found in the Spandler et al. (2007) study. Such rates would be more in keeping with the compositions of natural melt inclusion suites (Cottrell et al., 2002). Furthermore, if the composition of inclusions closely matches that of the associated whole-rocks then substantial re-equilibration of inclusions is unlikely to have occurred. If this is the case then melt inclusions should have preserved a record of magmatic diversity. The limited experimental data and numerical modelling

available in the literature is inconclusive but the compositions of natural olivine-hosted melt inclusion suites do not suggest that re-equilibration is very extensive. For the purposes of this study the effects of diffusive re-equilibration of REE in melt inclusions are assumed to be negligible.

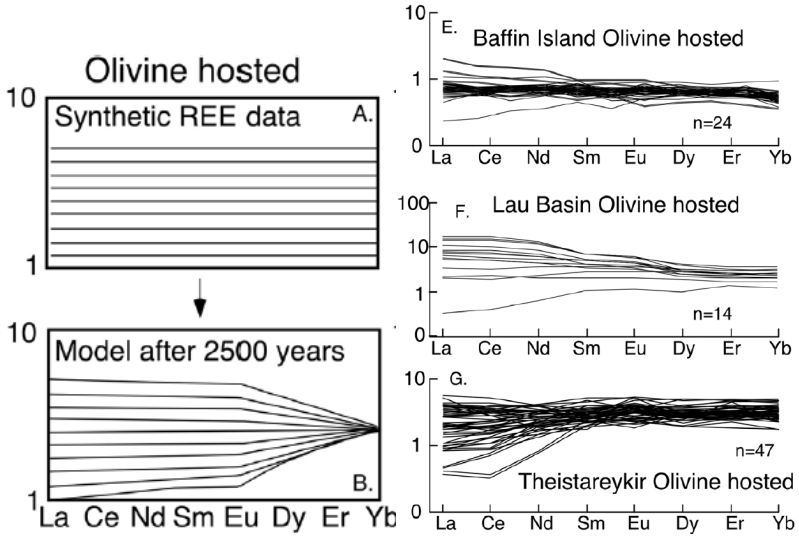

Figure 4.4. Left panel (A,B): Model results illustrating evolution of REE in synthetic host olivine over 2500 years. HREE equilibrate with their host more rapidly than LREE despite unknown diffusivities of REE in olivine. Right panel (E,F,G): Observations in natural olivine-hosted melt inclusion data sets do not support the model results. Baffin Island melt inclusion patterns are for unpublished data of A.J.R. Kent. From Kent (2008).

4.4. Results

Detailed light microscopy was carried out on all samples to identify melt inclusions suitable for the electron and ion microprobe analyses. It was important to assess the quality of the melt inclusions prior to analyses to check that only clean, glassy inclusions were analysed. Any inclusions that had partially or completely recrystallised were avoided (see Figure 4.1a,b) and also any melt inclusions close to cracks in the olivine. Often melt inclusions contain a spinel crystal which, due to its large size in comparison to the glass inclusion, will have been present before melt entrapment (Figure 4.1h,i). It has been shown that a spinel crystal can attach itself to a crystallising olivine resulting in irregular growth and subsequent entrapment of the spinel and silicate melt in an inclusion (Roedder, 1984).

4.4.1 Melt inclusion major elements

The major element compositions of 182 olivine hosted melt inclusions were measured by electron microprobe at the University of Edinburgh in 9 picrite samples (3 from Baffin Island and 6 from West Greenland). These analyses were complemented by measurement of the host olivine composition adjacent to the melt inclusion. The data and full analytical details can be found in Appendix L and A6 respectively. Despite the fact that more analyses would have been possible if individual olivine crystals had been picked from crushed rock and mounted, polished thin sections were used in order to retain textural information that may otherwise have been destroyed during crushing. Multiple copies of polished thin sections of the same sample were made to increase the number of melt inclusions available for analysis.

Major element variation diagrams for the melt inclusions in the Baffin Island and West Greenland picrites are shown in Figure 4.5. Major element melt inclusion compositions from the two regions cover a similar range. Negative linear correlations are observed with SiO_2 (47.3–56.9 wt%) and Al_2O_3 (14.5–24.7 wt%) versus MgO (0.7–8.6 wt%). FeO (1.7–10.4 wt%) versus MgO displays a positive correlation. CaO (8.9–17.7 wt%), Na_2O (1.7–4.9 wt%), K_2O (0.1–1.2 wt%), TiO_2 (0.7–2.6 wt%), MnO (0–0.4 wt%) and P_2O_5 (0.1–0.7 wt%) versus MgO all show some degree of scatter. Figure 4.5 also indicates that there does not seem to be a relationship between host olivine forsterite and the MgO content of the melt inclusions.

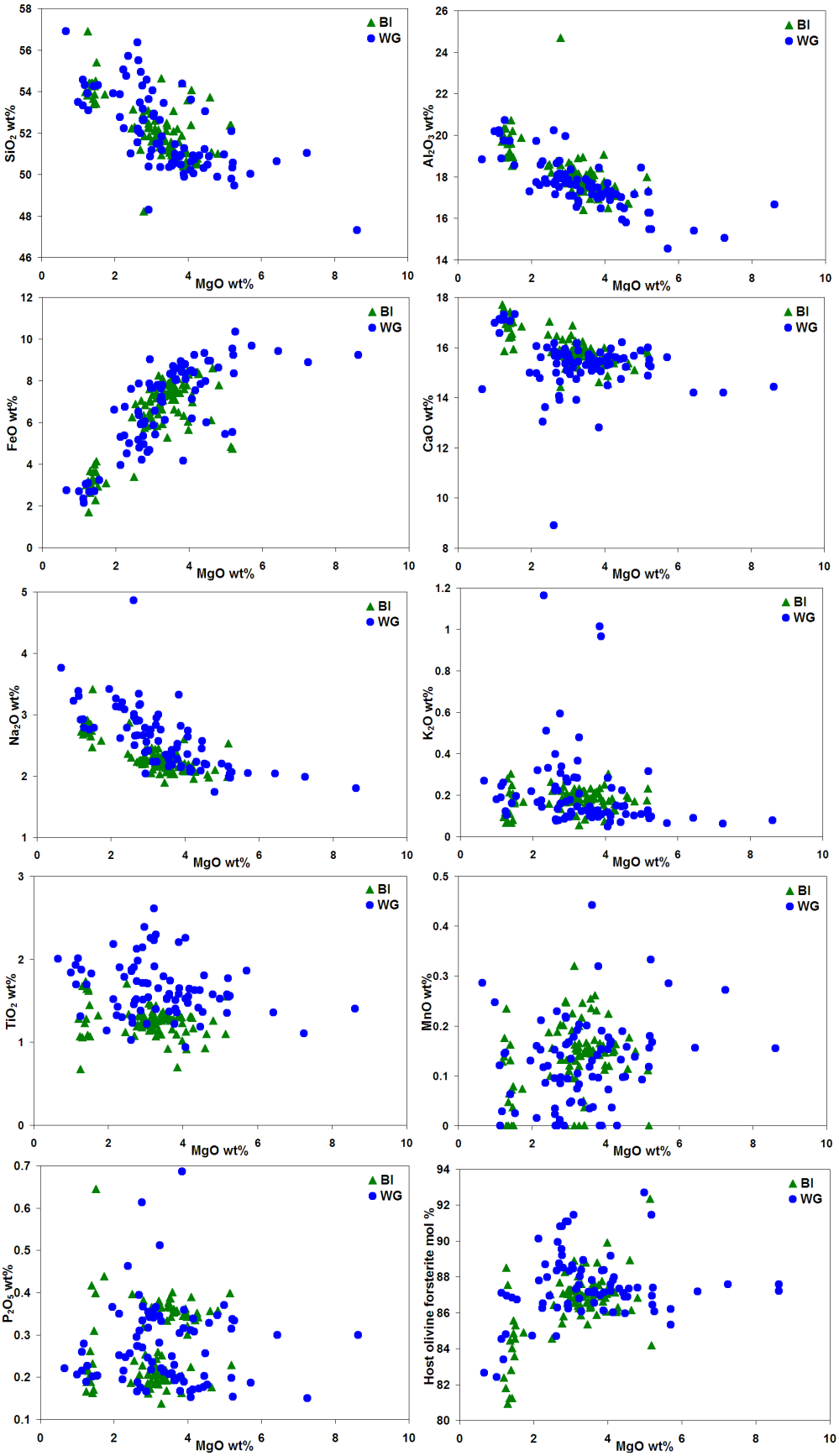

Figure 4.5. Major element variation diagrams for melt inclusions in Baffin Island and West Greenland picrites.

4.4.1.2 Post-entrapment effects on Baffin Island and West Greenland melt inclusion compositions

If PEC and diffusive re-equilibration have affected the melt inclusions in this study then it is highly unlikely that the major element compositions measured in the melt inclusions reflect that of the trapped melt. In order to investigate the potential for the operation of these processes, the measured major element composition of the Baffin Island and West Greenland melt inclusions are compared to the Baffin Island and West Greenland whole-rock compositions. As already shown, the melt inclusions show a positive correlation in a plot of FeO against MgO (Figure 4.5). When the whole-rock compositions are included they are observed to fall to the high end of melt inclusion FeO contents (Figure 4.6), scattering around FeO = 10.5 wt%, with higher MgO contents from ~7-30 wt% MgO. The linear array displayed by the whole-rocks is not a surprising feature since the magmas were likely to have accumulated olivine (as discussed in Chapter 2). Therefore, the whole-rock trend can be shown to resemble a liquid line of descent (LLD) because the concentration of olivine phenocrysts in the lavas drives the bulk composition along a trend that runs close to an olivine-control line. The fact that the majority of melt inclusions scatter to values well below the whole-rock trend is often cited as evidence that the inclusions have experienced Fe-loss. A plot of host olivine Fo% against FeO wt% of the associated melt inclusion (Figure 4.7) is commonly used to assess Fe-loss.

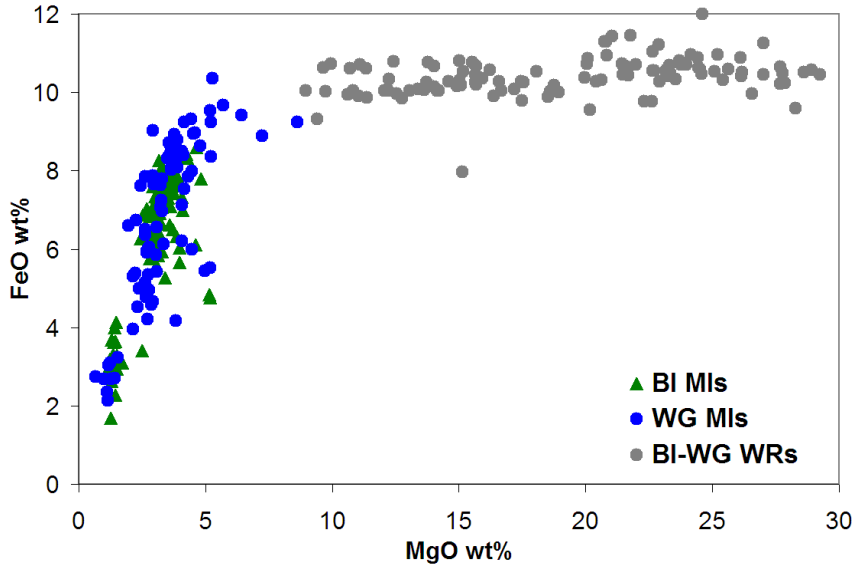

Figure 4.6. FeO wt% plotted against MgO wt% for the Baffin Island and West Greenland whole-rocks and melt inclusions.

The Baffin Island and West Greenland melt inclusions as a whole do not produce the negative trend that would suggest Fe-loss has occurred. However, in Figure 4.7, the melt inclusions define two groups which, if considered separately, each define weak negative correlations. Sets of melt inclusions from any one sample do not themselves define separate negatively correlated trends but this would only be expected if all the melt inclusions in the samples experienced the same amount of Fe-loss. If Fe-loss has affected the inclusions of this study then it has been by variable amounts.

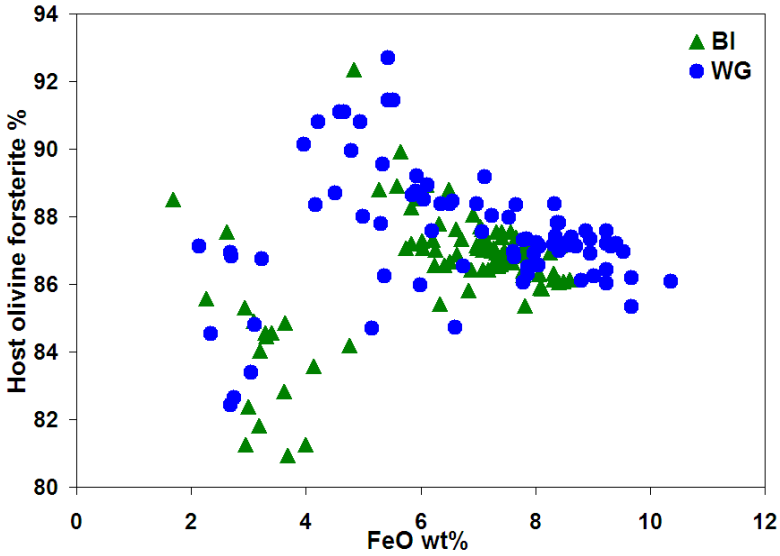

Figure 4.7. Fo mol% of host olivine plotted against FeO wt% of the associated melt inclusion. The data fall into two groups. The weak negative correlation within each group of melt inclusions is commonly cited as evidence of Fe-loss from the inclusion during diffusive re-equilibration of the melt inclusion with the host olivine.

Fe-loss can be investigated further by extending the LLD of the Baffin Island-West Greenland whole-rock compositions down to compositions represented by the melt inclusions (lower MgO and FeO). The LLD for the melt inclusions is calculated by subtracting equilibrium olivine in 0.1 wt% increments from an estimated groundmass composition using a constant value of K_D = 0.3 (Roedder and Emslie, 1970). The groundmass composition for calculations was estimated from a Baffin Island sample of this study (DUR1; indicated in Figure 4.8) which is particularly crystal-poor compared to all other samples in the study. DUR1 falls at the evolved end of the olivine control line for the whole-rocks, with low FeO and MgO, and has a melt composition in equilibrium with olivine of ~Fo_{86}. DUR1 was also used in the calculations to obtain the whole-rock LLD except that olivine was instead added in

0.1 wt% increments to DUR1 until melt compositions were obtained that were in equilibrium with olivine up to ~Fo_{94}.

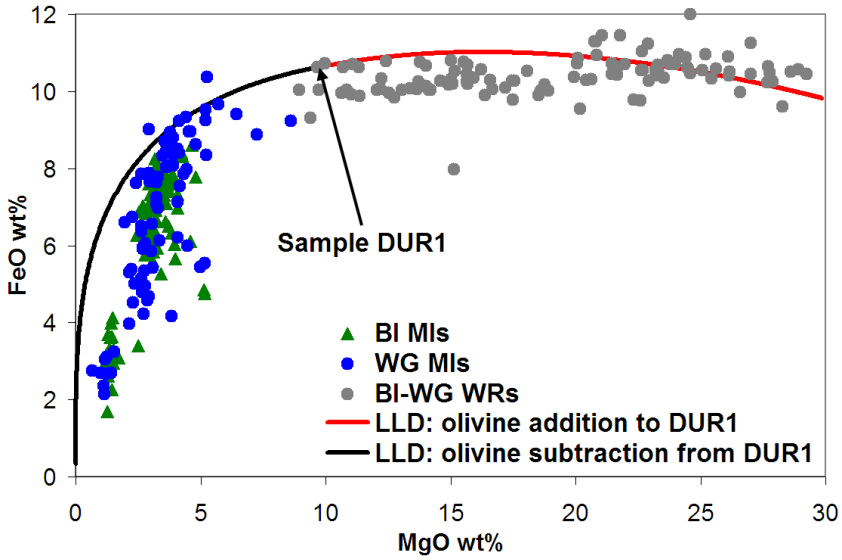

Figure 4.8. FeO wt% plotted against MgO wt% for Baffin Island and West Greenland whole-rocks and melt inclusion. A LLD is shown which was calculated from the sample representing the least magnesian liquid (DUR1) that can account for both the whole-rock data trend and the melt inclusion data.

The LLD (Figure 4.8) for the melt inclusions therefore represents perfect fractional crystallisation of olivine from a melt composition in equilibrium with olivine of ~Fo_{86} down to melt compositions in equilibrium with olivine of $Fo_{0.}$ This curve provides a reasonable fit for the melt inclusion data trend except that the LLD appears to be shifted to lower MgO as crystallisation proceeds. Alternatively, at a given MgO, the melt inclusions fall to low FeO, which may indicate the potential for Fe-loss. In the case of perfect fractional crystallisation, and without any Fe-loss, the melt inclusion compositions would follow the LLD perfectly, and the final layer of olivine deposited on the melt inclusion wall would be in equilibrium with the measured melt composition. Each preceding olivine layer would have been in equilibrium with the melt that it grew from such that the melt inclusion would have evolved to lower MgO and FeO with falling temperature as each successive olivine layer became less magnesian. If this were the case then the measured melt inclusion compositions could be returned to their composition at trapping, prior to olivine crystallisation on the inclusion wall, by incrementally adding olivine of a composition in equilibrium with the measured melt back into the melt until a

composition was reached that was in equilibrium with the host olivine (i.e. reversing the LLD).

The fact that the melt inclusions do not fall directly on the curve defined by perfect fractional crystallisation, regardless of Fe-loss, is unsurprising since perfect fractional crystallisation will be an unattainable process in the natural system. In addition, if Fe-loss has occurred, even without the effects of PEC, then the melt inclusions would not be expected to fall on the fractional crystallisation curve. Fe-loss would be expected to move the melt inclusion compositions to lower FeO and higher MgO, away from the theoretical curve, due to the diffusion of Fe^{2+} out of, and Mg^{2+} into the melt inclusion (Danyushevsky et al., 2000). This process does not result in the inclusion attaining equilibrium with the Fe and Mg content of the host olivine but rather the Fe/Mg ratio. In the model used here the host olivine has ~Fo_{86} and the dashed line shown in Figure 4.9 has constant Fe/Mg to indicate the position of melts in equilibrium with olivine of ~Fo_{86}. If the melt inclusions maintained perfect equilibrium with the host olivine as they cooled and crystallised then their Fe/Mg ratio would remain unchanged but their MgO and FeO contents would change. The line of constant Fe/Mg in Figure 4.9 illustrates the direction along which inclusions would equilibrate during Fe-loss. Thus, the trend of the melt inclusions in FeO against MgO (Figure 4.6 and Figure 4.8) can be adequately explained by imperfect fractional crystallisation of olivine on the inclusion walls coupled with variable Fe-loss.

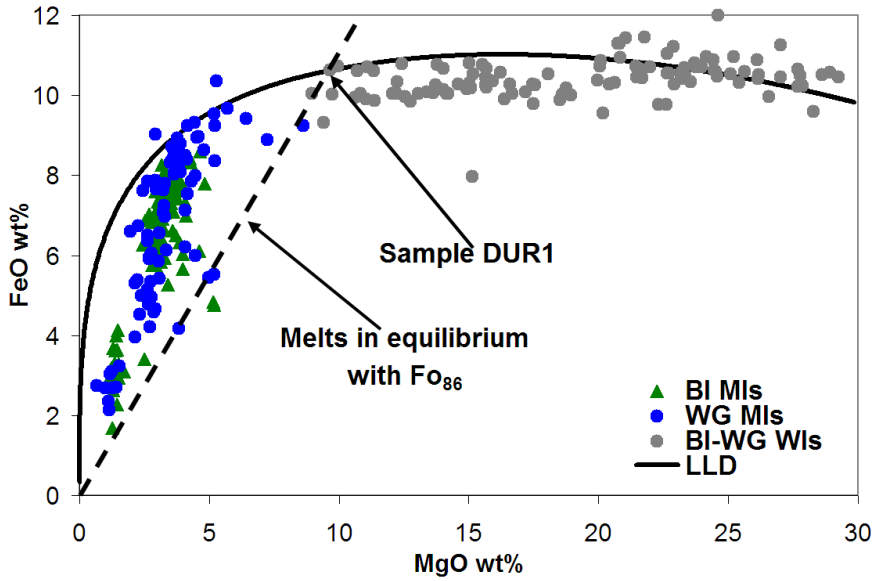

Figure 4.9. FeO wt% plotted against MgO wt% of Baffin Island and West Greenland whole-rocks and melt inclusions. The dashed line is the position of melts in equilibrium with an olivine of a fixed composition of Fo_{86} and therefore goes through sample DUR1.

The results of this simple modelling indicate that it is impossible to estimate both the amount of fractional crystallisation and the extent of re-equilibration for any given melt inclusion. Unfortunately, this also means that elements compatible in olivine measured in the melt inclusions cannot be restored to their exact concentrations at trapping. Fortunately, it is still possible to use incompatible trace elements to investigate melt inclusions. As opposed to the major elements, incompatible trace elements are not directly involved in PEC since they all have low and similar D values meaning they are not compatible in the crystallising olivine lattice. However, the volume of a melt inclusion must decrease during PEC as the newly crystallised olivine reduces the volume of the inclusion. Therefore, it can be assumed that concentrations of incompatible trace elements will increase relative to their concentration in the trapped melt, in line with the reduced volume of the inclusion. As described above, it is not possible to make an accurate estimate of the amount of crystallisation that has taken place in an inclusion. Therefore, corrections for the relative increase in incompatible trace element concentrations cannot be made. However, the concentration of all incompatible trace elements will be affected by a similar amount during PEC, due to their similar D values, so that the use of trace element ratios avoids the problem of unknown absolute abundances. The incompatible trace element data therefore provide a useful way to characterise the

various melt compositions that contributed to the erupted lavas. The melt inclusions can be compared to the whole-rock compositions to investigate the conclusions drawn from the whole-rock dataset.

4.4.2 Melt inclusion incompatible trace elements

Melt inclusion incompatible trace elements were analysed on the ion microprobe at the University of Edinburgh on four of the samples (PAD6 and DUR8 from Baffin Island; 362077 and 400452 from West Greenland) analysed in the melt inclusion major element study. In total, the incompatible trace element compositions of 85 melt inclusions were determined. The data and full analytical details can be found in Appendix M and A7 respectively. The four samples chosen all have high $^{3}He/^{4}He$ and cover a range from whole-rock depleted to relatively enriched compositions.

The following features that are discussed can be observed in Figure 4.10, 4.11 and 4.14. The melt inclusions in any one sample display a wide range of incompatible trace element concentrations. Melt inclusion incompatible trace element ratios for the four samples in this study cover the entire range displayed by all of the 112 whole-rock compositions from the Baffin Island and West Greenland picrites reported by Starkey et al. (2009). Melt inclusions in the Baffin Island samples of this study are more enriched than those in the West Greenland samples. This is likely to be a function of sampling as the whole-rock compositions of the Baffin Island samples chosen (PAD6 and DUR8) are more enriched (with low $^{143}Nd/^{144}Nd$, positive ΔNb and high $(La/Sm)_n$) than the whole-rock compositions of the West Greenland samples (400452 has very high $^{143}Nd/^{144}Nd$ but $^{143}Nd/^{144}Nd$ for 362077 has not been determined. Both of the West Greenland samples have negative ΔNb and low $(La/Sm)_n$). Therefore, it is highly unlikely that melt inclusions in all West Greenland samples are depleted since West Greenland whole-rocks can be as enriched as the relatively enriched Baffin Island whole-rock samples. These data show that the relatively enriched whole-rock samples contain only relatively enriched melt inclusions and that the depleted whole-rock samples contain only depleted melt inclusions. PAD6 and DUR8 are important as they are two of the few relatively enriched high-$^{3}He/^{4}He$ samples available. Figure 4.10 uses a plot of (log)Nb/Y

against (log)Zr/Y to show that the melt inclusions in PAD6 and DUR8 are characterised by positive ΔNb (Fitton et al., 1997), in agreement with the PAD6 and DUR8 whole-rock compositions. It is noted that, based on ΔNb alone, PAD6 contains one depleted melt inclusion (sample number PAD6 MI26), with ΔNb slightly less than zero (-0.094; Figure 4.10). However, this melt inclusion has $(La/Sm)_n$ = 1.04, as expected for relatively enriched melts since it is shown that $(La/Sm)_n$ > 0.8 characterises E-MORB (Mahoney et al., 2002). Therefore, it would appear, for some reason, that the ΔNb of this one inclusion in PAD6 is anomalously low but this is not a characteristic reflected in all incompatible trace element ratios. Therefore, these data rule out the possibility that a proportion of depleted melts contributed to the enriched whole-rock samples.

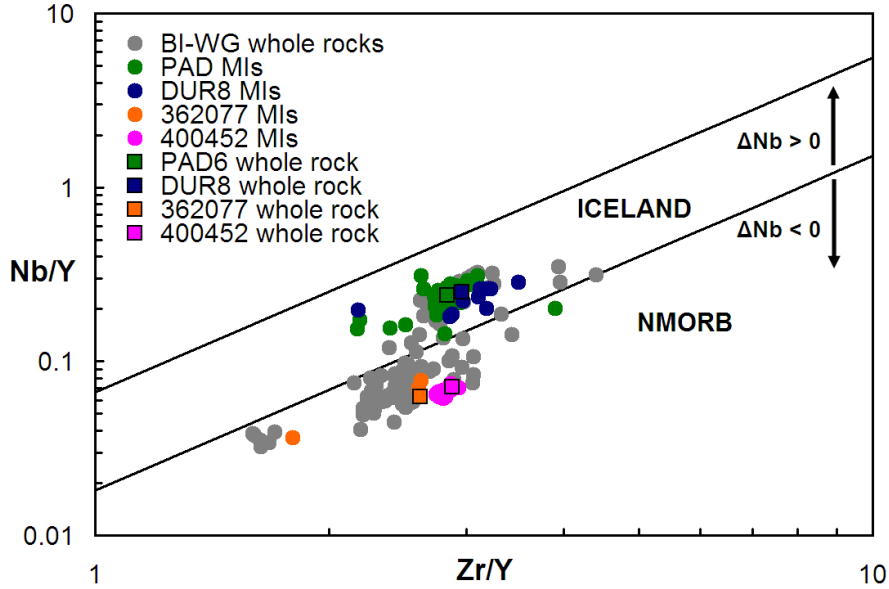

Figure 4.10. Nb/Y plotted against Zr/Y for Baffin Island and West Greenland melt inclusions compared to their whole-rock compositions. Samples with whole-rock positive ΔNb do not, on the whole, contain melt inclusions with negative ΔNb.

It is very important to be able to rule out the existence of depleted melts in relatively enriched whole-rock samples in terms of determining the composition with which $^3He/^4He$ is associated. In Chapters 2 and 3 and Starkey et al. (2009), it was not possible to completely rule out the contribution of a proportion of depleted melts to the relatively enriched whole-rock samples. Depleted melts could have been sampled in very small melt volumes whose effects were lost through mixing with relatively enriched melts in the erupted lava. If these depleted melts were associated with high

$^{3}He/^{4}He$, as some authors suggest (Ellam and Stuart, 2004; Class and Goldstein, 2005), then the fact that relatively enriched whole-rock samples display high $^{3}He/^{4}He$ does not necessarily mean that high $^{3}He/^{4}He$ is associated with relatively enriched melt compositions at all. However, only one inclusion in both the whole-rock relatively enriched samples is found to be depleted and, as shown above, other incompatible element ratios of this melt inclusion do not support the depleted signature suggested by its ΔNb. Furthermore, if high $^{3}He/^{4}He$ is present in depleted melts only, then any depleted melt inclusion would have to contain exceptionally high [He] with high $^{3}He/^{4}He$ such that their small population dominates the overall measured $^{3}He/^{4}He$ in high $^{3}He/^{4}He$ relatively enriched whole-rock samples. Such a situation seems unlikely. Since all the samples chosen for this melt inclusion study have high $^{3}He/^{4}He$, and helium isotopes are contained within melt inclusions, a simple conclusion can be drawn concerning the composition with which high $^{3}He/^{4}He$ is associated. High $^{3}He/^{4}He$ is clearly a feature of both depleted and relatively enriched melt compositions, as suggested by the whole-rock study (Chapter 3; Starkey et al., 2009).

It is therefore not surprising that the Baffin Island melt inclusions also plot to higher La/Yb and Nb/Zr in Figure 4.11, where the Baffin Island whole-rock and melt inclusion compositions of this study are compared to the Baffin Island melt inclusions of Yaxley et al. (2004). The range in La/Yb and Nb/Zr is very similar in both studies. The trend displayed by the melt inclusions in Baffin Island in Figure 4.11 represents that of source variation, as indicated by the arrow, and cannot be explained by crustal contamination which would shift compositions towards high La/Yb and K/Nb, as shown by some of the Yaxley et al. (2004) melt inclusions (Figure 4.11). Therefore, there is no evidence for crustal contamination in either the whole-rock compositions or the melt inclusion compositions for the four samples investigated in the melt inclusion study.

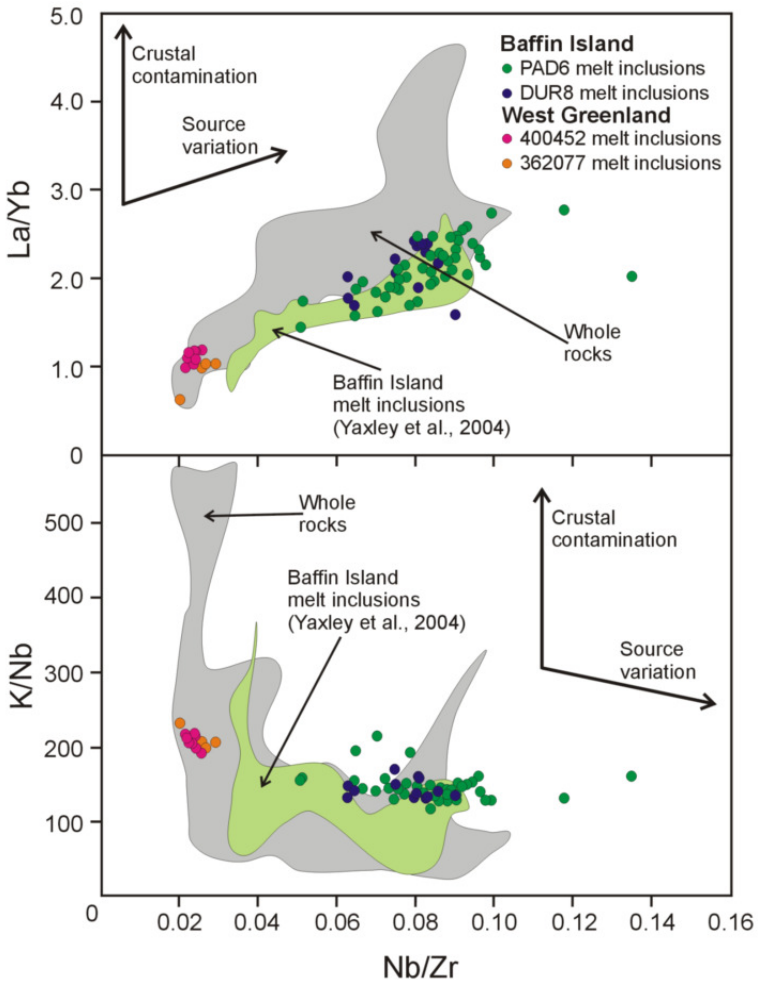

Figure 4.11. La/Yb and K/Nb plotted against Nb/Zr for Baffin Island and West Greenland melt inclusions (this study and Baffin Island melt inclusions of Yaxley et al. (2004)) compared to the Baffin Island-West Greenland picrite whole-rock compositions.

By considering all the REEs it can be seen that chondrite-normalised REE profiles for Baffin Island melt inclusions are flatter than those for West Greenland, which are slightly more LREE depleted (Figure 4.12), in keeping with their whole-rock REE profiles. The broad conformity of melt inclusion and whole-rock profiles (Figure 4.12) is an important observation as it rules out the existence of anomalous melt compositions, exotic to the magmatic system, in the source of these lavas. The rare highly forsteritic olivine crystals present in the Baffin Island and West Greenland picrites have been suggested to represent xenocrysts (Francis, 1985). Since mantle xenocrysts cannot have trapped melt inclusions then the only other possible source of these forsteritic olivines is as crystals precipitated from extreme fractional melts in

wall-rock reactions (Herzberg and O'Hara, 2002). If this was the case then melt inclusions trapped in these crystals would be expected to be very depleted.

Crustal contamination may have occurred after olivine crystallisation had ceased and all the melt inclusions had been trapped, with the latent heat of crystallisation having induced melting of crustal rocks. If crustal contamination occurred after the trapping of all melt inclusions then the bulk-rock REE profile would be expected to show LREE enrichment compared to the melt inclusions. Therefore, it should be possible to identify crustally contaminated melts in REE profiles unless all melt inclusions and the whole-rock were affected by exactly the same amount of contamination. The fact that whole-rock and melt inclusion profiles are parallel suggests that crustal contamination has not affected samples PAD6, DUR8, 362077 or 400452, either during or subsequent to olivine crystallisation. This observation supports previous findings from the whole-rock study (Chapter 2 and 3; Starkey et al., 2009).

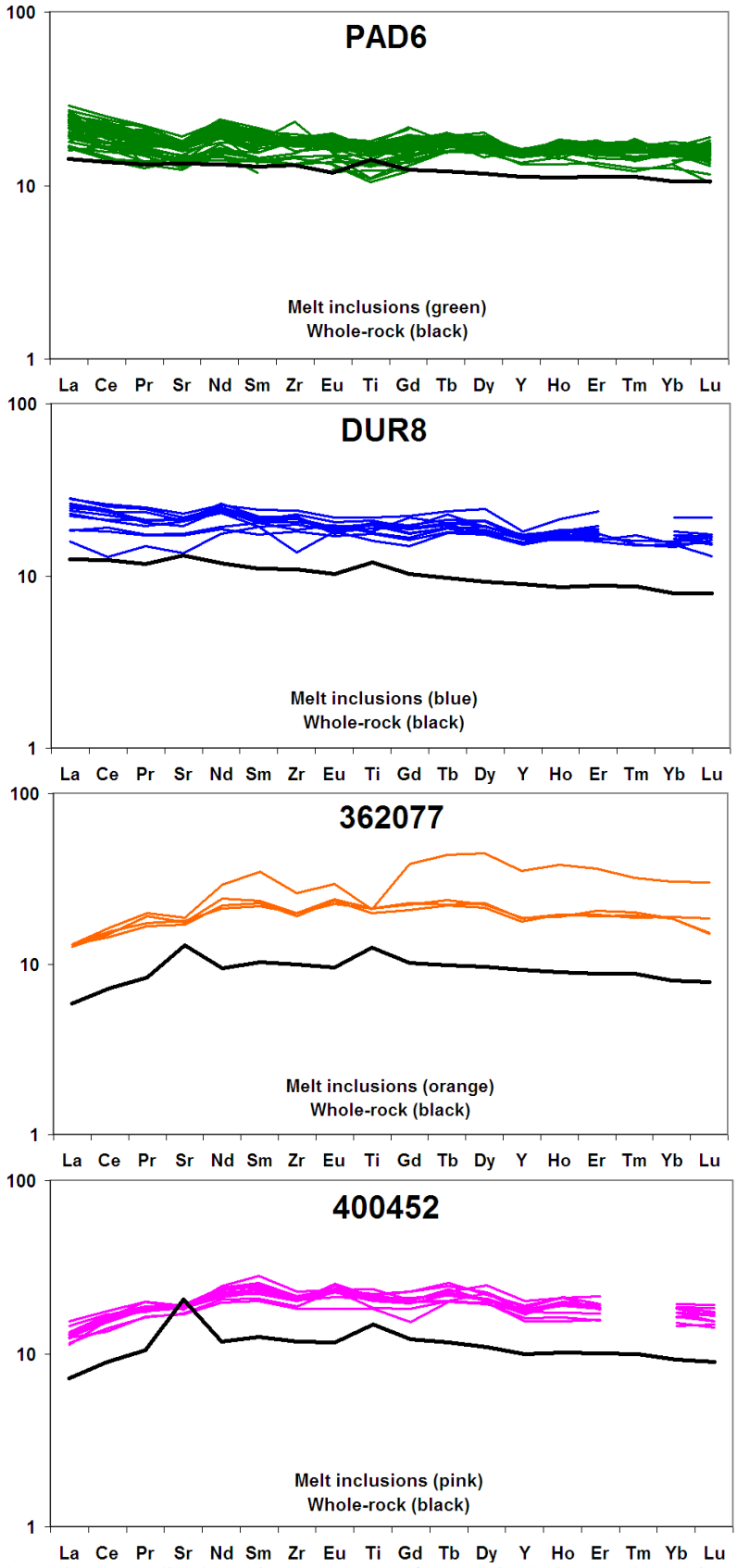

Figure 4.12. Chondrite-normalised multi-element plots for melt inclusions and associated whole-rocks of Baffin Island and West Greenland samples.

4.4.2.1 Effect of post-entrapment crystallisation on melt inclusion incompatible trace element concentrations in Baffin Island and West Greenland

An obvious feature of the REE profiles is the lower concentrations of the whole-rock profiles compared to the melt inclusion profiles. This is likely to be because the whole-rock compositions reflect those of the groundmass plus the accumulated olivine crystals. Olivine crystals will dilute the incompatible element concentrations because olivine contains virtually no incompatible elements. It follows that the melt inclusion compositions should be equivalent to the whole-rock composition minus the accumulated olivine crystals (i.e. the groundmass composition). However, as shown in Section 4.4.1.2 using melt inclusion major element concentrations, it is likely that PEC has affected the melt inclusions. It was predicted that the volume decrease due to PEC of olivine onto the internal walls of the inclusion will increase the incompatible element concentrations through reduction of the melt inclusion volume. Therefore, a simple way to test the extent of PEC in each sample is to compare the melt inclusion compositions to that of their associated host-rock groundmass composition. Groundmass compositions were calculated by subtracting the bulk composition of olivine phenocrysts, determined by electron microprobe analysis and point counting (Appendix B2), from each whole-rock composition. Since the groundmass composition should theoretically represent an average of all the melt inclusion compositions then it follows that no PEC has occurred if the estimated groundmass composition is similar to that of the average of the melt inclusions in the same sample. However, PEC is likely to have occurred if the average melt inclusion composition has a higher concentration of incompatible elements than the estimated groundmass of the associated sample. Figure 4.13 shows REE profiles for the whole-rock, estimated groundmass and average of the melt inclusions for each sample. It would appear that PAD6 is the least affected by PEC since the REE profile for the estimated groundmass is very close to that of the average profile of the melt inclusions (Figure 4.13). REE profiles for the other three samples (DUR8, 362077 and 400452) show that the average profiles of the melt inclusion compositions have higher concentrations than the groundmasses, suggesting that PEC has occurred (Figure 4.13).

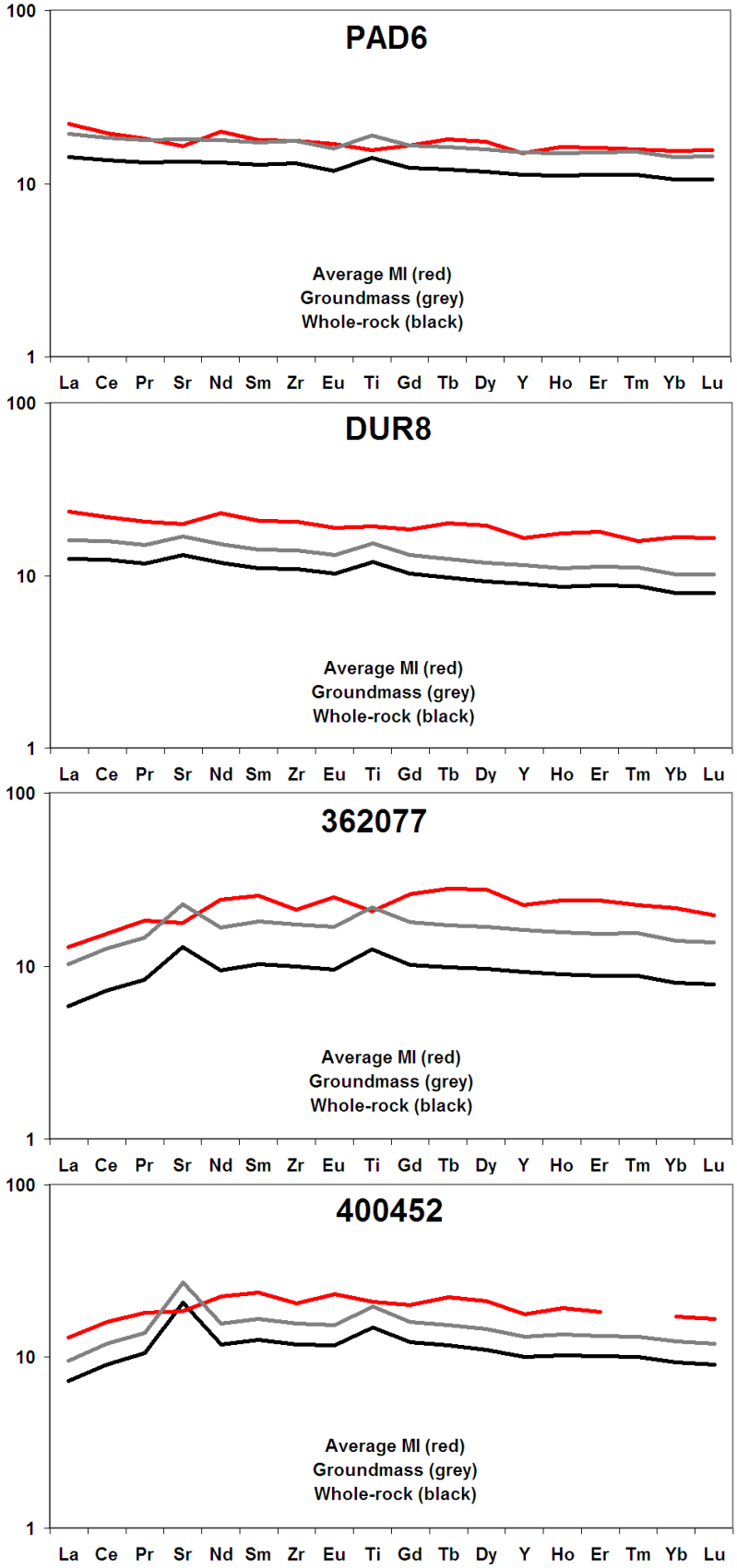

Figure 4.13. Chondrite-normalised multi-element plots comparing whole-rock, estimated groundmass and average melt inclusion compositions for Baffin Island and West Greenland samples.

This information may indicate that PAD6 cooled rapidly, resulting in the melt in the inclusions being quenched to glass such that they avoided olivine crystallisation. The other three samples may have cooled more slowly allowing for varying amounts of olivine crystallisation on their inclusion walls. Despite the high potential for PEC in the majority of melt inclusions, the fact that the melt inclusion REE profiles are parallel to that of their whole-rock suggests that the REE concentrations have all been increased by the same proportion, as predicted, since D values are low and similar for all the REE. Therefore, the incompatible trace elements, and in particular incompatible trace element ratios can still provide important information on the source of the melts in the Baffin Island and West Greenland picrites and the melt inclusions can be compared to whole-rock compositions.

In Chapters 2 and 3 and Starkey et al. (2009), the Baffin Island and West Greenland picrite whole-rock compositions were compared to MORB to show their similarity in incompatible trace element and radiogenic isotope compositions. Despite the broader range in compositions displayed by the Baffin Island and West Greenland picrite melt inclusions compared to their host rock, the majority of these melt inclusions fall within the MORB range in a plot of Nb/Zr against $(La/Sm)_n$ (Figure 4.14). The MORB range extends to more enriched values (higher Nb/Zr and $(La/Sm)_n$) reflecting the diversity of compositions produced at mid-ocean ridges. Once again, the Baffin Island and West Greenland picrite melt inclusions appear to be distinct from one another with the West Greenland melt inclusions being more depleted. However, as already discussed, this is related to the generally more depleted nature of the whole-rocks chosen from West Greenland for this study. Crustal contamination of these high-$^3He/^4He$ picrites is ruled out in both the whole-rocks (Chapter 2 and 3; Starkey et al. 2009) and the melt inclusions. That the melt inclusion compositions reflect the compositions of their whole-rocks supports the conclusions of Chapter 3. High $^3He/^4He$ is associated with a wide range of $^{143}Nd/^{144}Nd$, and therefore high $^3He/^4He$ is a feature of a wide range of mantle compositions similar to those observed at mid-ocean ridges.

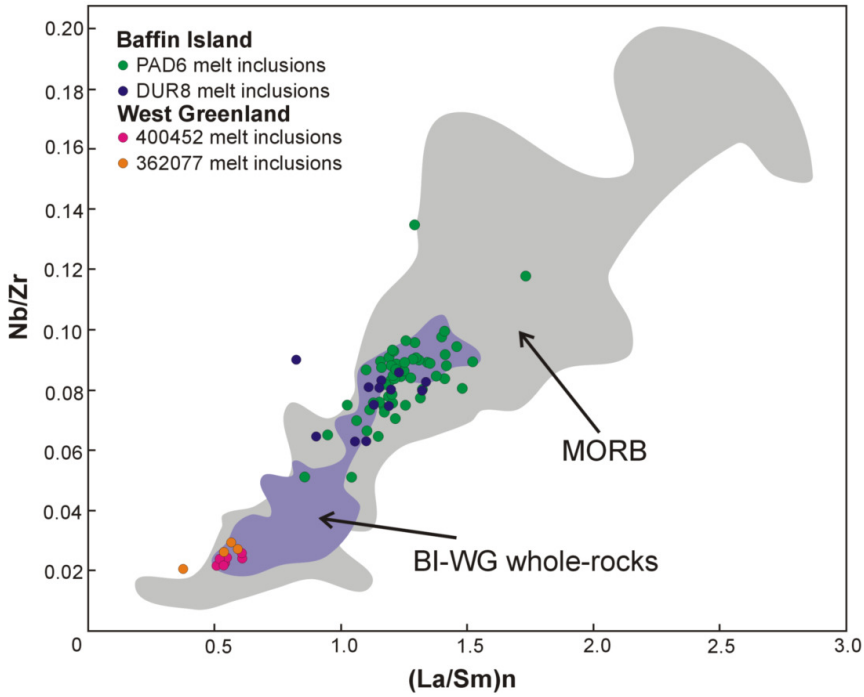

Figure 4.14. Nb/Zr plotted against $(La/Sm)_n$ for Baffin Island and West Greenland picrite melt inclusions and their respective whole-rocks. The grey field indicates the range in MORB.

4.5 Summary

Melt inclusions are an important component of lavas as they are derived directly from discrete compositions present in the host magmatic system. Whole-rock compositions provide an average composition of all the individual melts that contributed and were mixed together to form the erupted lava. Whole-rock analyses are the quickest and easiest way to examine a suite of rock samples and provide a useful overview of the magmatic system. Melt inclusions, on the other hand, are more likely to represent the individual melt compositions prior to mixing (Sobolev and Shimizu, 1993; Kent et al., 1999), although some authors propose that, in some cases, melt mixing may occur prior to trapping of melts (Maclennan, 2008). Despite this, analysis of a number of melt inclusions in any one sample allows for the composition of melts that contributed to the lavas to be better characterised, even if the melt inclusions themselves have not sampled pristine unmixed melts. Whole-rock analyses on the Baffin Island and West Greenland picrites could not rule out the existence of a proportion of depleted melts within relatively enriched whole-rock

samples. Such depleted melts may be present in small proportions in relatively enriched samples but are 'averaged out' by magma mixing.

For the Baffin Island and West Greenland samples, their helium isotope ratios were compared to their whole-rock major and trace element and radiogenic isotope compositions. The helium isotope ratios measured in Baffin Island and West Greenland are effectively a measure of the average composition of helium isotopes in many melt inclusions in one sample, since the ratio is obtained by crushing of many crystals together. As shown, high $^{3}He/^{4}He$ in Baffin Island and West Greenland are associated with a wide range of whole-rock compositions, depleted and relatively enriched. However, some authors argue that high $^{3}He/^{4}He$ is only associated with depleted mantle compositions (Ellam and Stuart, 2004; Class and Goldstein, 2005). Therefore, because helium isotopes are trapped within melt inclusions, measurement of the major and trace element composition of melt inclusions present in these high-$^{3}He/^{4}He$ picrite samples is an obvious way to evaluate the precise melt compositions with which high $^{3}He/^{4}He$ is associated.

In this study it is shown that the major element compositions of the melt inclusions cannot be corrected to their composition at trapping because of the effects of variable amounts of PEC and diffusive re-equilibration. Post-entrapment processes do not directly involve incompatible elements, especially in melt inclusions hosted in olivine (Cottrell et al., 2002). However, it is noted that PEC can cause an increase in the concentration of incompatible elements due to a reduction in melt inclusion volume. Since such a process affects all incompatible elements in a melt inclusion by the same proportion, the slope of REE profiles and incompatible element ratios remains a useful way to characterise the melt inclusion compositions of samples.

Melt inclusions in Baffin Island and West Greenland high-$^{3}He/^{4}He$ picrites exhibit a greater compositional variability than their host lavas, a feature commonly recognised in many datasets (Sobolev and Shimizu, 1993; Gurenko et al., 1996; Sobolev, 1996; Kamenetsky et al., 1995, 1997; Saal et al., 1998; Kent et al., 2002; Maclennan et al., 2003). It would appear from these data that the whole-rock

composition of samples provides an average of the individual melt compositions sampled by the melt inclusions since average melt inclusion REE patterns in any one sample are very similar to that of their whole-rock. Importantly, it was shown that the two samples analysed in this study with relatively enriched whole-rock compositions (PAD6 and DUR8) contained only relatively enriched melt inclusion compositions. Since all the samples measured in the trace element melt inclusion study have high $^{3}He/^{4}He$ then the similarity of the melt inclusion compositions to their host lavas supports the conclusion from the whole-rock study that high $^{3}He/^{4}He$ is present in both depleted and, more importantly, relatively enriched melt compositions.

Discussion

5 Discussion

5.1 Introduction

The purpose of this chapter is to collate and review all of the data and discussions from the results presented in Chapters 2, 3 and 4. The primary aim, set out in the introduction, is to establish a coherent understanding of the nature of the mantle source of the Baffin Island and West Greenland picrites through detailed petrographic and geochemical studies. The source composition of the early NAIP magmas is not as well characterised as that of the more recent magmatism in Iceland, where the various components that contribute to the magmas have been discussed in detail (e.g. Hards et al., 1995; Kerr et al., 1995; Thirlwall, 1995; Fitton et al., 1997; Hanan and Schilling, 1997; Chauvel and Hémond, 2000; Kempton et al., 2000; Skovgaard et al., 2001). In this chapter, the Baffin Island and West Greenland lavas are compared to the products of Icelandic magmatism to assess whether the whole of the NAIP has sampled the same source components over the 60 million years of magmatic activity. The early NAIP lavas sample the highest-$^{3}He/^{4}He$ reservoir available in the Earth suggesting that the Baffin Island and West Greenland samples can provide a means of assessing the source composition for the high-$^{3}He/^{4}He$ reservoir not only in the NAIP but globally. In turn, an evaluation can be made of the various models proposed for the location, storage and preservation of the high-$^{3}He/^{4}He$ reservoir in the Earth.

5.2 Olivine crystals; phenocrysts, xenocrysts, antecrysts

The Baffin Island and West Greenland lavas in this study are highly magnesian, with associated high olivine phenocryst contents. The whole-rock major element compositions define linear arrays in oxide variation diagrams, falling on olivine-control lines which are used to show that magmas initially with lower magnesium contents were likely to have accumulated olivine crystals prior to eruption. Crystal accumulation is a common process in many igneous systems but the origin of accumulated crystals in lavas is often not clear. All accumulated crystals may be

genetically related to the magmatic system and represent crystals from earlier batches of magma that were left behind in conduit systems and picked up by subsequent magmas. Alternatively, a proportion of accumulated crystals could be foreign to the magmatic system, representing xenocrysts incorporated into magmas from the mantle, or from other lithologies available in the lithosphere or crust.

Olivine crystals with extremely high forsterite (up to Fo_{93}) compose a minor but ubiquitous part of the Baffin Island and West Greenland crystal assemblages. Some authors cite the presence of metamorphic textures and kink-banding of high-forsterite olivine crystals as evidence of their xenocrystic origin (Francis, 1985). These features have not been recognised in the high-forsterite olivine crystals of this study. In agreement with the West Greenland study of Larsen and Pedersen (2000), the continuous major element compositional trends displayed by the olivine crystals (Fo_{75-93}) of this study suggest that all crystals are genetically linked to each other, having precipitated from liquids that were related to the same source. In addition, the melt inclusion data presented in Chapter 4 showed no evidence for anomalous melt inclusion compositions that might have indicated the existence of exotic melts sampled by olivine xenocrysts. The compositions of melt inclusions in high-forsterite olivine (Fo_{93}) crystals are similar to the compositions of melt inclusions hosted in less forsteritic olivine crystals. Since high-forsterite crystals (~Fo_{93}) are relatively scarce in the samples used in this study there are only a few melt inclusions available that are hosted within such crystals. Figure 5.1 shows that the La/Yb of melt inclusions in the few ~Fo_{93} crystals available fall within the La/Yb range of melt inclusions in the same sample but hosted by lower-forsterite olivine. It is apparent that there is a compositional gap between Fo_{89}-Fo_{92} in the olivine crystals containing melt inclusions (Figure 5.1), for which there is not an obvious explanation. Such evidence could be used to suggest that the high-forsterite crystals are xenocrysts. However, as shown in Chapter 2, the olivine crystals themselves display continuous compositional trends from low to high forsterite without any gaps. Additionally, it is unlikely that xenocrysts were able to trap 'xenocrystic' melts that were, coincidentally, the same composition as those trapped by the other, lower-forsterite olivine crystals. Therefore, it is possible that olivine crystals within the Fo_{89}-Fo_{92}

range did not, for some reason, trap melt inclusions or that none were sampled in this study.

It can be concluded that all the olivine crystals analysed in this study, particularly those for which it was possible to analyse melt inclusions, do at least represent magmatic phenocrysts. Despite this, it was pointed out in Chapter 2 that high-forsterite olivine crystals are unlikely to have precipitated from the liquid represented by the rock in which they are now present and therefore cannot be classed as true 'phenocrysts'. Equally, the high-forsterite crystals are not 'foreign' to the magmatic system as they do not show anomalous olivine or melt inclusion compositions, so they cannot be classed as true xenocrysts either. It is possible that the crystals represent early-formed cumulates of earlier magmas from the same magmatic system, as suggested for forsterite-rich and deformed olivine crystals from Hawaiian lavas (Helz, 1987). Therefore, the term 'antecrysts', as suggested in Chapter 2, is a more appropriate name for the crystals since they are related to the magmatic system but not necessarily to the particular liquid within which they were eventually brought to the surface. Such 'antecrysts' may have been stored in crystal-rich zones either on conduit walls or in magma chambers after being dropped by earlier magmas overloaded with crystals.

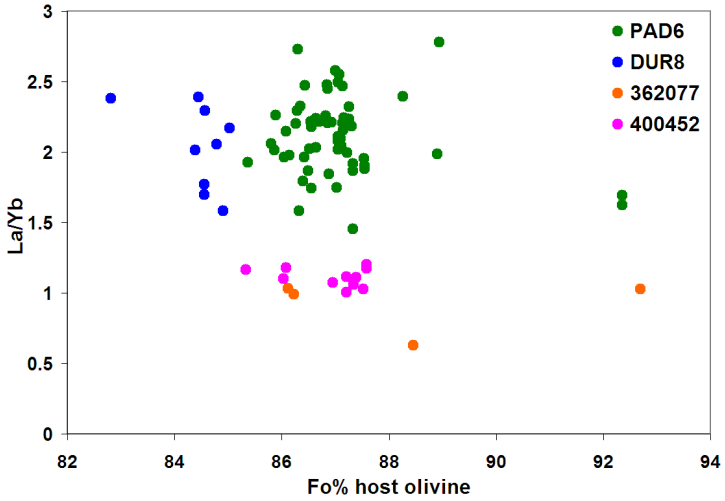

Figure 5.1. Melt inclusion La/Yb plotted against Fo mol% of host olivine for Baffin Island and West Greenland picrites. The range in La/Yb of melt inclusions hosted in high-forsterite olivine is in the same range as the La/Yb of melt inclusions hosted in lower-forsterite olivine.

Knowledge of olivine and whole-rock compositions allowed for an estimation of the MgO content of the parental magmas for the Baffin Island and West Greenland lavas. Estimated parental melt MgO contents for the lavas of this study are between 9 and 22 wt% MgO, reaching a maximum MgO similar to estimates from other Baffin Island and West Greenland studies (18-21 wt% MgO; Larsen and Pedersen, 2000; Herzberg et al., 2007). It has been shown that the Baffin Island and West Greenland primary magmas therefore require a mantle potential temperature of 1600^{o}C (Larsen and Pedersen, 2000; Herzberg and O'Hara, 2002), at least 200^{o}C higher than ambient mantle (Herzberg et al., 2007). However, it is estimated that the temperature anomaly in Iceland at the present day is less, with a mantle potential temperature of only ~1460^{o}C (Slater et al., 2001; Herzberg et al., 2007). This suggests that, if Iceland and the early NAIP lavas are related to the same melting anomaly that it has cooled over time.

5.3 Investigating the source composition for the Baffin Island-West Greenland picrites

5.3.1 Relationship between N- and E- type compositions

The Baffin Island and West Greenland picrites span a wide range of incompatible trace element and radiogenic isotopic compositions from depleted to relatively enriched. It was shown in Chapters 2 and 3 that the generally depleted nature of the early NAIP lavas is not dissimilar to the level of depletion displayed by MORB. Chondrite-normalised REE patterns for the Baffin Island and West Greenland picrites show a wide range in LREE concentrations and generally flat profiles (Figure 5.2). The samples are compared to an estimated composition for average MORB (Workman and Hart, 2005) in Figure 5.2, which shows the comparatively lower concentrations of the HREE in the Baffin Island and West Greenland picrites. Such a feature may be related to the deep melting of the Baffin Island and West Greenland picrites under thick lithosphere where garnet, which fractionates the HREE from the LREE, is expected to be present as a residual phase in the melting zone.

Incompatible trace element ratios for the Baffin Island and West Greenland picrites also show the compositional similarity of the lavas to those commonly erupted at mid-ocean ridges (Figure 5.3). As already shown in Chapter 2, the Baffin Island-West Greenland lavas fall into the 'normal' and 'enriched' divisions suggested for MORB ($\Delta Nb < 0$; $(La/Sm)_n < 0.8$ for N-MORB and $\Delta Nb > 0$; $(La/Sm)_n > 0.8$ for E-MORB; Mahoney et al., 2002; Fitton, 2007), a feature previously recognised by others (Robillard et al., 1992; Holm et al., 1993; Kent et al., 2004). It was shown in Chapter 3 that the depleted samples, with negative ΔNb, have REE profiles with lower concentrations of LREE than the E-type lavas, and they are therefore most similar to average MORB albeit still with overall lower HREE concentrations (Figure 5.2).

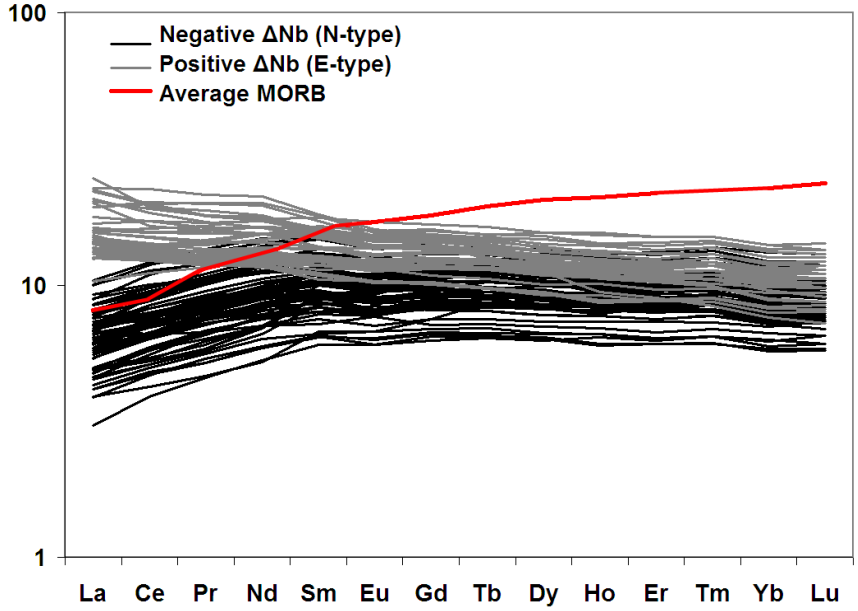

Figure 5.2. Chondrite-normalised REE diagram for Baffin Island and West Greenland samples (grey = $\Delta Nb > 0$ and black = $\Delta Nb < 0$; Starkey et al., 2009) and average MORB (red) from Workman and Hart (2005).

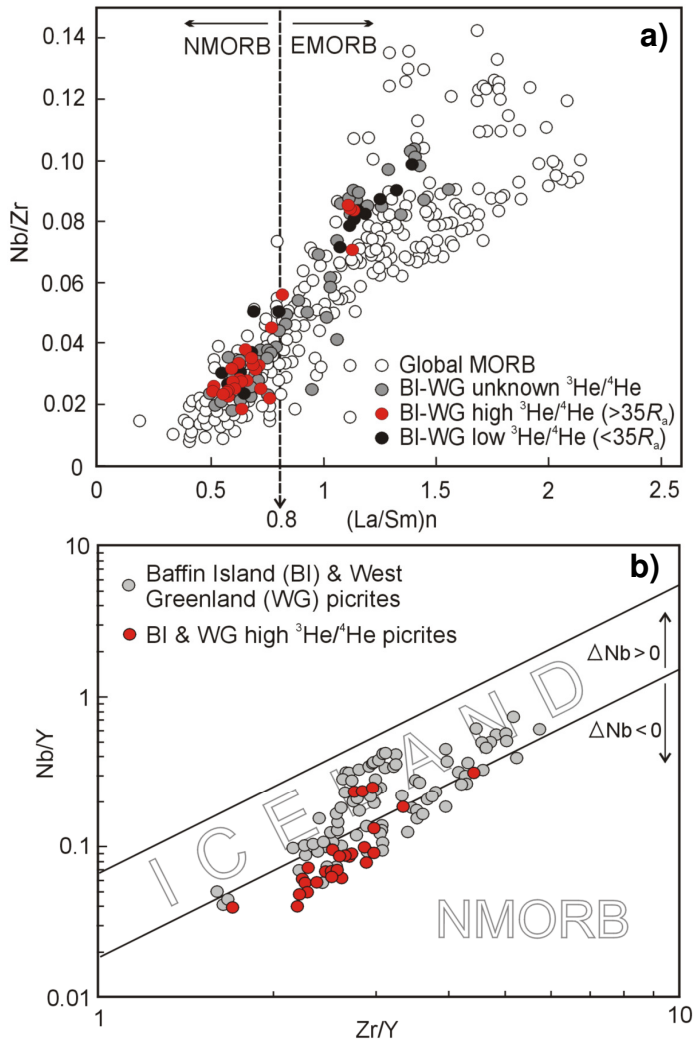

Figure 5.3. a) Nb/Zr plotted against $(La/Sm)_n$ and b) Nb/Y plotted against Zr/Y for Baffin Island and West Greenland picrites. High ^{3}He/^{4}He samples (up to 50 R_a) are shown in red.

The Sr and Nd isotope ratios of the Baffin Island-West Greenland lavas extend to higher $^{87}Sr/^{86}Sr$ and lower $^{143}Nd/^{144}Nd$ than that estimated for present day 'plume-free' Mid-Atlantic Ridge MORB (Figure 5.4; 'plume free' Mid-Atlantic Ridge MORB has $^{87}Sr/^{86}Sr = 0.70231$ and $^{143}Nd/^{144}Nd = 0.51328$; Taylor et al., 1997) and for MORB corrected to 62 Ma (Figure 5.4; Kent et al., 2004). Approximately one half of the Baffin Island-West Greenland samples fall outside a field for global N-type MORB (Figure 5.4; MORB with depths of >2000 m and with $\Delta Nb < 0$ and $(La/Sm)_n < 0.8$ (www.petdb.org)). The Baffin Island-West Greenland samples that do not fall into the N-MORB field are either E-type in composition or N-type

samples that have experienced some crustal contamination. This is discussed in more detail in the next section.

Despite the strong similarity of most of the Baffin Island-West Greenland samples to MORB in incompatible trace element and radiogenic isotope ratios, the Baffin Island-West Greenland magmas have much higher helium isotope ratios, up to 50 R_a (Stuart et al., 2003; Starkey et al., 2009) compared to an average of ~8 R_a for MORB. They have been shown to have had a mantle source that was 100-200°C hotter than ambient upper mantle (Larsen and Pedersen, 2000; Herzberg et al., 2007). Importantly this study shows that high $^3He/^4He$, up to 50 R_a, in Baffin Island and West Greenland lavas are associated with both normal (N-type) and relatively enriched (E-type) (Figure 5.3) lavas, a feature that has not previously been recognised in either region.

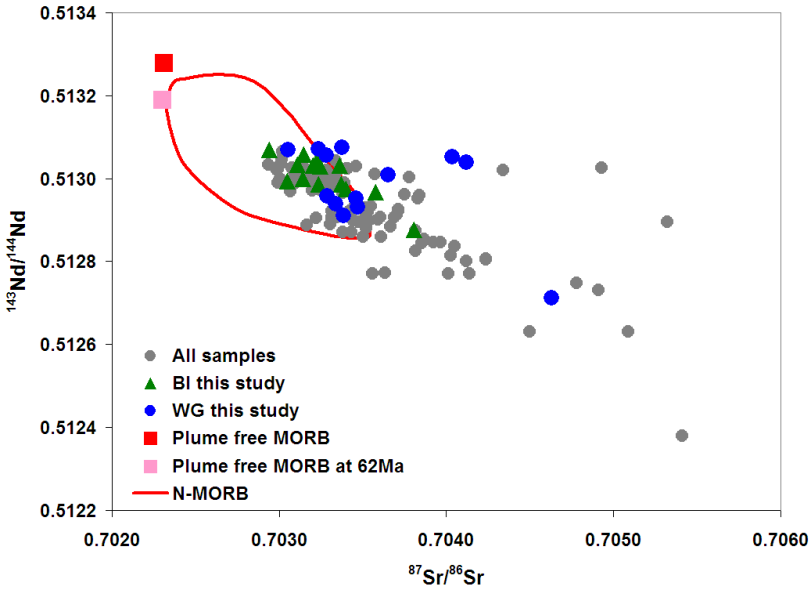

Figure 5.4. $^{143}Nd/^{144}Nd$ plotted against $^{87}Sr/^{86}Sr$ for Baffin Island and West Greenland picrites, 'plume-free' Mid Atlantic Ridge MORB (Taylor et al., 1997), 'plume-free' Mid-Atlantic Ridge MORB at 62 Ma (Kent et al., 2004) and N-MORB (from www.petdb.org; samples with $\Delta Nb < 0$ and $(La/Sm)_n < 0.8$).

5.3.2 Can crustal contamination of N-type magmas produce the E-type Baffin Island and West Greenland magmas?

It was noted in previous chapters that the early NAIP magmas were erupted through thick continental lithospheric mantle and crust and therefore an important part of this study was to investigate whether crustal or lithospheric mantle contamination may have affected the composition of the magmas. Furthermore, for discussions concerning the source composition of high $^{3}He/^{4}He$ in the Earth it is important to rule out the possibility that the high-$^{3}He/^{4}He$ relatively enriched samples ($\Delta Nb > 0$, $(La/Sm)_n > 0.8$, $^{143}Nd/^{144}Nd < 0.5130$) were produced through crustal or lithospheric mantle contamination of depleted parental magmas. The depleted nature of the Baffin Island-West Greenland lavas makes them highly susceptible to small amounts of contamination. Contamination of depleted melts to produce the relatively enriched high-$^{3}He/^{4}He$ lavas must be ruled out before the compositional variability of the lavas can be attributed to that of the mantle source.

The results of modelling the effects of contamination on a typical depleted parental melt for Baffin Island-West Greenland were reported in Chapters 2 and 3 using binary mixing calculations. It is shown that E-type lavas of Baffin Island and West Greenland cannot be produced by crustal contamination of N-type lavas, in agreement with other studies on Baffin Island picrites (Robillard et al., 1992; Kent et al., 2004). Importantly, this modelling also applies to the high $^{3}He/^{4}He$ (>35 R_a), relatively enriched samples (E-type; low $^{143}Nd/^{144}Nd$; high $(La/Sm)_n$, positive ΔNb) PAD6, DUR8, 332901, 354754 and 400230. However, despite the fact that crustal contamination of the whole-rock compositions of these samples was ruled out, Yaxley et al. (2004) showed that the whole-rock composition of Baffin Island picrites may not be as sensitive to crustal contamination as their melt inclusions. Consequently, part of the reason for investigating melt inclusion compositions in PAD6 and DUR8 (high $^{3}He/^{4}He$, relatively enriched samples; Chapter 4) in particular was to examine the potential for crustal contamination at smaller melt scales. If crustal contamination occurred during olivine crystallisation (when the melt inclusions were being trapped), or after olivine crystallisation had ceased, then anomalous compositions (displaying LREE enrichment indicating the incorporation

of crustal material into the melts) should be apparent in either the melt inclusions or the whole-rock. When discussing the possibility for xenocryst olivine populations in the Baffin Island-West Greenland lavas, neither PAD6 nor DUR8, both high-$^{3}He/^{4}He$ E-type lavas containing highly forsteritic olivine, were shown to contain any melt inclusions with anomalous compositions. The melt inclusion REE profiles in each sample individually are parallel to each other and to their associated whole-rock REE profile suggesting that the erupted lavas are composed of melts that were no different to the melt compositions sampled by the inclusions.

However, the fact that crustal contamination is ruled out in the whole-rock and melt inclusion compositions of these important E-type high-$^{3}He/^{4}He$ samples does not mean that it is necessarily ruled out in all of the Baffin Island and West Greenland lavas. As shown in Chapter 3, the whole-rock composition of some of the lavas, with especially low $^{143}Nd/^{144}Nd$ (<0.51285), can be modelled by a few percent of crustal contamination of a depleted parent. This applies to the high-$^{3}He/^{4}He$ sample BI/CS/7 ($^{143}Nd/^{144}Nd$ = 0.51273; Starkey et al., 2009) and this sample was consequently excluded from future discussions concerning of the nature of the high-$^{3}He/^{4}He$ reservoir in the Earth. Another sample, 400444, should be treated with suspicion but as $^{3}He/^{4}He$ has not been determined on this sample it does not form an important part of the conclusions in this study.

It was shown by Robillard et al. (1992) that the difference between the N- and E-type lavas in Baffin Island cannot be due to variations in the conditions of partial melting of a single homogeneous mantle source. Kent et al. (2004) agree that the Baffin Island lavas were produced through mixing of at least two components to explain the variations in the isotopic and chemical compositions of the lavas. The $\delta^{18}O$ of Baffin Island olivine phenocrysts are also found to lie within the narrow range expected for olivine in equilibrium with melts derived from MORB-source mantle peridotite (Kent et al., 2004). Any crustal contamination of the magmas during olivine crystallisation, even by only a few percent, would be expected to shift the $\delta^{18}O$ of the olivine phenocrysts out of the narrow MORB range. In addition, Kent et al. (2004) show that the $\delta^{18}O$ of olivine phenocrysts in E-type lavas are lower than those in N-type lavas which is inconsistent with crustal contamination. The potential

incorporation of sub-continental lithospheric mantle (SCLM) is a particularly important process to consider in the early NAIP magmas since it was shown that the alkalic lavas of the Manîtdlat Member of the Vaigat Formation in West Greenland could be modelled as melts of SCLM (Larsen and Pedersen, 2003). The depleted compositions of the Baffin Island-West Greenland picrites mean that they are not expected to have incorporated a significant amount of SCLM. In addition, osmium isotopes show that the Baffin Island and West Greenland picrites from this study are unlikely to have incorporated any crustal material or SCLM (Dale et al., 2009). The samples do not display a co-variation of $^{187}Os/^{188}Os$ with Os concentration and they do not fall on mixing trajectories from parental melts to ancient Os-poor extremely radiogenic crustal material or Os-rich, ^{187}Os-depleted SCLM (Dale et al., 2009). In agreement, Kent et al. (2004) show that the Os-Sr-Nd relationships for the Baffin Island N-type and E-type picrites preclude SCLM mixing with a depleted source if the Manîtdlat Member is used as an end-member composition in calculations.

The whole-rock and melt inclusion study presented in this thesis, along with the other Baffin Island and West Greenland studies discussed above, rule out the possibility that E-type lavas in Baffin Island and West Greenland were produced by crustal or lithospheric contamination of depleted melts. In fact, crustally contaminated sample BI/CS/7 from the study of Stuart et al. (2003) that was discussed earlier is an N-type lava (with negative ΔNb and low $(La/Sm)_n$). The very low $^{143}Nd/^{144}Nd$ in this sample requires up to 5% crustal contamination showing that even high percentages of crustal contamination did not shift this sample to an E-type composition. Therefore, as concluded in Chapter 3 and Starkey et al. (2009), high $^{3}He/^{4}He$ is associated with a wide range of whole-rock incompatible trace element and radiogenic isotopic compositions. Based on the whole-rocks, the composition of the high-$^{3}He/^{4}He$ mantle extends down to $^{143}Nd/^{144}Nd = 0.51876$ and $^{87}Sr/^{86}Sr = 0.70381$ (Nd and Sr isotopes age corrected to 60 Ma; based on sample PAD6 with $^{3}He/^{4}He = 45\ R_a$).

5.3.3 High-$^3He/^4He$ N- *and E-type* melts

It is important to note that the main conclusion discussed above, that high $^3He/^4He$ is a feature of both depleted and relatively enriched incompatible trace element and radiogenic isotope compositions, is based only on the whole-rocks. One drawback with this is that it is not possible to completely rule out the possibility that adding a proportion of depleted melts with high-$^3He/^4He$, was responsible for high $^3He/^4He$ in relatively enriched whole-rock samples.

It was shown in Chapter 4 that mixing and aggregation of melts to produce erupted lavas could effectively destroy the evidence for the former existence of a small proportion of depleted melts within a predominantly enriched melt. Fortunately, melt inclusions have the potential to sample the melts that contributed to the magma prior to melt mixing and eruption. Since the helium isotopes are contained within melt inclusions, it is sensible to compare helium isotope ratios directly to the composition of the glasses in the melt inclusions. Measurement of melt inclusion compositions (presented in Chapter 4) allowed for the individual melts, and therefore the erupted lavas, to be characterised in detail along with the associated investigation into the effects of crustal contamination at small melt scales. The melt inclusion compositions rule out the possibility that a small proportion of depleted melts contributed to the relatively enriched whole-rock samples since the relatively enriched whole-rock samples, PAD6 and DUR8, do not contain any depleted melt inclusions. This is a particularly important observation and supports the earlier conclusions from the whole-rock study. These new data remove the requirement for the high-$^3He/^4He$ mantle to have a unique depleted composition, as proposed by some authors (Stuart et al. 2003; Ellam and Stuart, 2004; Class and Goldstein, 2005). Melt inclusion compositions in the samples investigated in this study reflect the composition of their whole-rocks and neither whole-rock nor melt inclusion compositions were produced through crustal contamination. This suggests that incompatible trace element and isotopic variations within the Baffin Island and West Greenland picrites are related to variations in the mantle source.

5.3.4 High $^{3}He/^{4}He$ in Baffin Island and West Greenland in relation to OIB

The association of high $^{3}He/^{4}He$ with a wide range of depleted and relatively enriched compositions in one location is not a feature that has been recognised in the OIB database. This is partly because the highest $^{3}He/^{4}He$ recorded by contemporary ocean island volcanism (Iceland, Loihi, Galapagos and Samoa) appear to be quite similar to each other, converging on $^{3}He/^{4}He$ slightly higher than 30 R_a (Figure 5.5; Kurz et al., 1982; Kurz and Geist, 1999; Macpherson et al., 2005; Jackson et al., 2007). This is considerably lower than the highest $^{3}He/^{4}He$ (~50 R_a) recorded for Baffin Island-West Greenland. Clear correlations between $^{3}He/^{4}He$ and other isotope systems are observed for moderately high-$^{3}He/^{4}He$ OIB (e.g. Hawaii (Kurz and Kammer, 1991), Iceland (Brandon et al., 2007) and Samoa (Jackson et al., 2007)). However, extrapolation of these trends to the high $^{3}He/^{4}He$ values in the early Iceland plume lavas does not produce reasonable mantle compositions (e.g. Brandon et al. 2007).

Although the $^{143}Nd/^{144}Nd$ and $^{87}Sr/^{86}Sr$ range of the Baffin Island-West Greenland picrites overlaps the range recorded by the high-$^{3}He/^{4}He$ northern hemisphere ocean islands (Iceland, Hawaii, Galapagos), they are distinct from the isotopic composition of basalts from Samoa, Heard Island and Kerguelen (Figure 5.5). It has been proposed that the compositional difference between high-$^{3}He/^{4}He$ basalts from the southern and northern hemisphere islands reflects distinct high-$^{3}He/^{4}He$ reservoirs (Jackson et al., 2007). However, to explain this, the existence of distinct reservoirs may not be necessary. Due to the broad range of compositions with which high $^{3}He/^{4}He$ is associated, this study suggests that helium is decoupled from other lithophile trace elements and radiogenic isotope tracers (Starkey et al., 2009). Therefore, the difference in composition between northern and southern hemisphere ocean island $^{3}He/^{4}He$ may simply be due to the addition only of helium with high $^{3}He/^{4}He$ to normal northern hemisphere mantle and to isotopically distinct 'DUPAL-type' mantle prevalent in the southern hemisphere (Starkey et al., 2009). The various models for the production of high-$^{3}He/^{4}He$ mantle were introduced in Chapter 1 and the discussion is expanded in Sections 5.4.1 and 5.4.2 of this chapter.

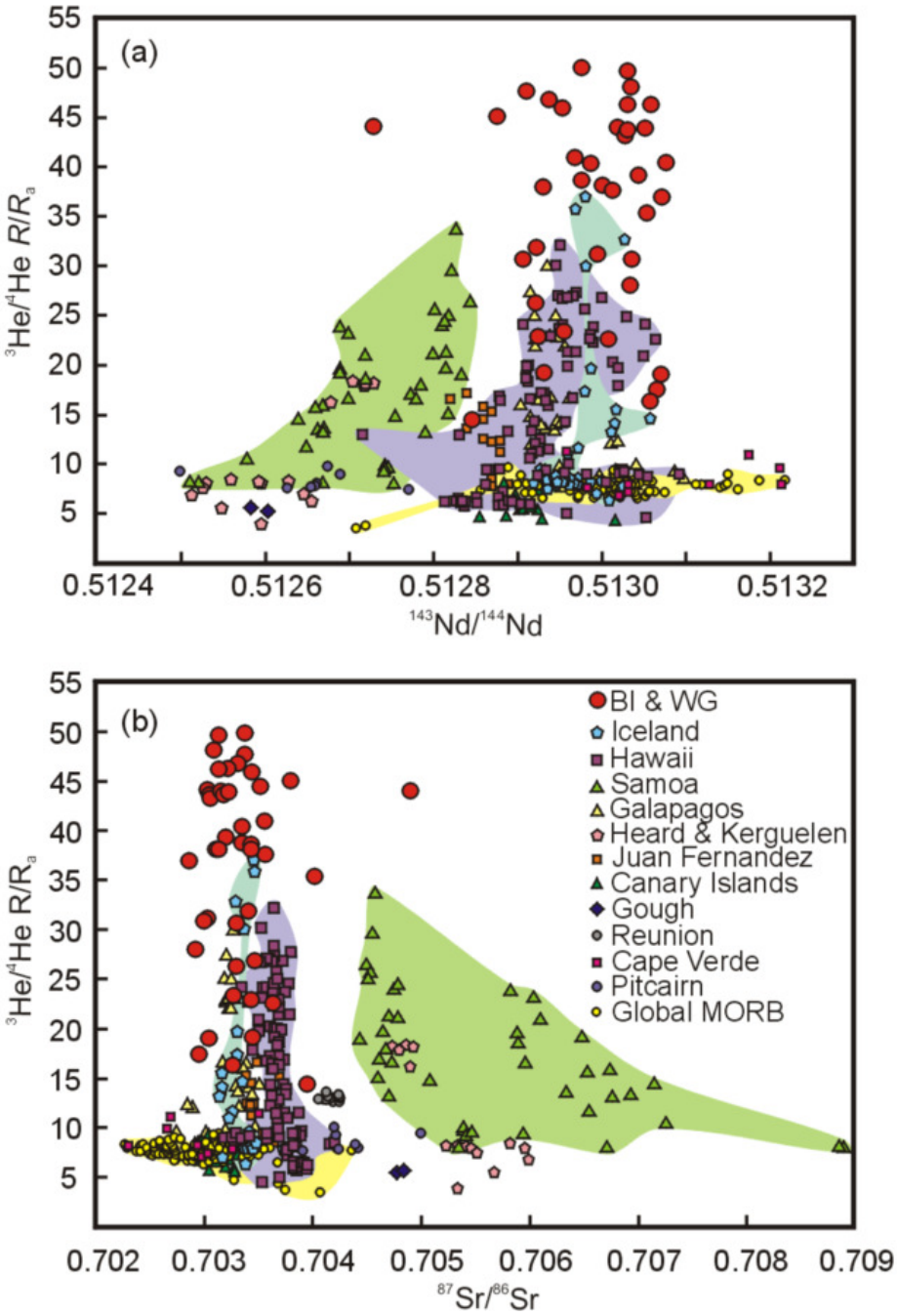

Figure 5.5. ^{3}He/^{4}He plotted against (a) ^{143}Nd/^{144}Nd and (b) ^{87}Sr/^{86}Sr for global OIB (Abedini et al., 2006), MORB (www.petdb.org), Baffin Island (this study; Stuart et al., 2003) and West Greenland (this study; Graham et al., 1998). ^{3}He/^{4}He of OIB reach a maximum of ~30-35 R_a with each island displaying a fairly narrow range in ^{143}Nd/^{144}Nd and ^{87}Sr/^{86}Sr at high ^{3}He/^{4}He. Fields are shown for Samoa (pale green), Hawaii (lilac), Iceland (pale blue) and MORB (pale yellow) to highlight the data amongst the other islands. ^{3}He/^{4}He of Baffin Island and West Greenland (red circles) reach a maximum of ~50 R_a but display the same range in ^{143}Nd/^{144}Nd and ^{87}Sr/^{86}Sr at both high and low ^{3}He/^{4}He. The Baffin Island and West Greenland ^{143}Nd/^{144}Nd range spans most of the MORB range (yellow circles). From Starkey et al. (2009).

5.3.5 The spatial and temporal association of N- and E-type lavas in the NAIP

The Iceland plume today produces only E-type (or 'Icelandic') magma compositions ($\Delta Nb > 0$; Fitton et al., 1997) which are associated with a maximum $^{3}He/^{4}He$ of around 30 R_a (Macpherson et al., 2005). Lavas of the British Tertiary Igneous Province (BTIP), erupting at approximately the same time as the Baffin Island-West Greenland lavas though 2000 km away, produced N- and E-type magma compositions with a maximum $^{3}He/^{4}He$ of around 22 R_a (Fitton et al., 1997; Stuart et al., 2000). The samples of the Vaigat Formation of West Greenland, documented in more detail stratigraphically than those of Baffin Island (Larsen and Pedersen, 2000), show a compositional progression up-sequence. The lava flows in the lowest part of the Vaigat Formation, the Anaanaa Member, are more depleted than lavas of the proceeding members, which become progressively more enriched up-sequence (Figure 5.6). The Baffin Island lavas are thought to be stratigraphically equivalent to the lowermost Anaanaa Member of West Greenland. They would therefore be expected to show a restricted and depleted compositional range in line with the Anaanaa samples. The Baffin Island lavas instead scatter throughout the entire range of compositions present in the Vaigat Formation (Figure 5.6). Either the Baffin Island lavas actually relate stratigraphically to the entire time interval associated with the Vaigat, rather than just the lowermost member, or the mantle source region for Baffin Island differed to that of West Greenland.

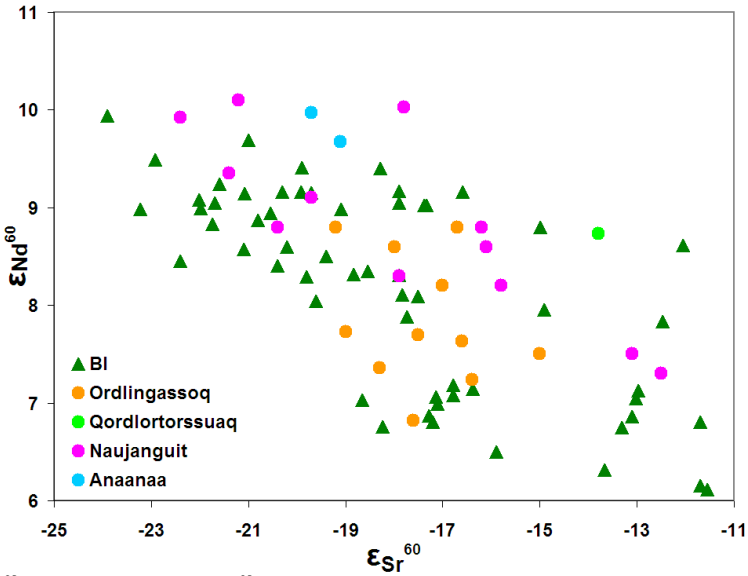

Figure 5.6. εNd^{60} plotted against εSr^{60} for Baffin Island and West Greenland picrites. The Vaigat Formation is separated into its respective members to show that Baffin Island picrites span the entire range of compositions and do not display the more restricted compositions of the stratigraphically equivalent Anaanaa Member.

This study shows that high $^3He/^4He$, up to 50 R_a, are found throughout the entire Vaigat Formation. Although $^3He/^4He$ values are lower in more recent magmatism (i.e. Iceland), the earliest phase of magmatism in the western NAIP, lasting for ~1 my (Storey et al., 1998), was characterised by extremely high $^3He/^4He$. The division of the Baffin Island-West Greenland lavas into N- and E-type is fairly arbitrary since they show a continuous compositional range across any boundary previously defined for N- and E-MORB (e.g. $\Delta Nb = 0$ (Fitton, 2007); $(La/Sm)_n = 0.8$ (Mahoney et al., 2002)). This suggests that depleted and relatively enriched material is closely associated within the source both temporally and spatially. The switch from depleted to enriched material over space and time does not seem to show a simple progression. This suggests that both depleted and relatively enriched components were available in the NAIP source but that the more depleted component is, for some reason, not sampled by Iceland. However, it should be noted that depleted lavas do occur in Iceland but they are derived from an enriched 'E-type' mantle source (and display positive ΔNb) but are depleted because of melt extraction. Depleted Icelandic lavas are discussed further in the following sections.

5.3.6 Investigating the origin of the depleted and enriched components in the NAIP

Numerous studies have focused on the ultimate source of the depleted and enriched lavas in Iceland and the NAIP in general (Hards et al., 1995; Kerr et al., 1995; Thirlwall, 1995; Fitton et al., 1997; Hanan and Schilling, 1997; Chauvel and Hémond, 2000; Kempton et al., 2000; Skovgaard et al., 2001; Kent et al., 2004). As shown in Chapter 1, a mantle plume is often proposed to account for the magmatism across the NAIP region. A mantle plume in the NAIP would suggest that the components thought to be available in the present-day Icelandic mantle source should have been available in the Baffin Island-West Greenland mantle source. Saunders et al. (1997) proposed that the Iceland plume structure is composed of three main components: a depleted plume component, a relatively enriched plume component and depleted upper mantle (MORB-source). Within the classic plume model the 'plume' component is expected to be hot 'primitive' lower mantle material, carrying with it the primordial noble gas signature, located in the axial region of the plume (Fitton et al., 1997; Kempton et al., 2000). A plume model can account for the close association of depleted and enriched components in the NAIP, the higher temperature and high $^{3}He/^{4}He$ of the lavas, and the longevity of magmatism. However, such plume models are now hard to reconcile with more recent geophysical data suggesting that the upper and lower mantle are not convectively isolated and 'enriched' components in OIB are too depleted to result from melting of an inferred primitive mantle composition.

Iceland can be classed as either an ocean island or as an anomalous segment of mid-ocean ridge (E-MORB; Fitton, 2007), with neither of these classifications necessarily requiring a mantle plume. The structure of the convecting upper mantle, the most likely location of the MORB-source, may be best represented by a model similar to that of the 'plum-pudding' or 'marble-cake' mantle (Allègre and Turcotte, 1986; Batiza, 1984), as outlined in Chapter 1. If this is the case then the depleted upper mantle (N-MORB) is expected to contain a proportion of relatively enriched blobs or streaks (E-MORB). An upper mantle with small-scale heterogeneities has been

suggested to explain the close association of N- and E-type lavas along mid-ocean ridge segments (e.g. Fitton, 2007; Mahoney et al., 2002). Perhaps such an explanation could account for the E-type lavas of Iceland (Foulger et al., 2005; Fitton, 2007). However, if Icelandic lavas are sourced from the depleted upper mantle, streaked with relatively enriched material, then it is surprising that N-type lavas are not erupted at all in Iceland. It has been suggested that this may be related to the generally lower degrees of melting of OIB compared to MORB that result in only the more enriched and fusible portions of the upper mantle source being melted (Elliott et al., 1991). Additionally, if Iceland is classed simply as an anomalous segment of mid-ocean ridge then an explanation must be provided for the much greater production of E-MORB lavas compared to other mid-ocean ridge segments. The greater extent of melt production in the Iceland region is often ascribed to a thermal anomaly, possibly related to a mantle plume originating in the deep mantle. Alternatively, some authors believe that there is no temperature anomaly associated with Iceland and instead propose that increased mantle fertility, due to the presence of subducted ocean crust in the Icelandic source, can account for the increased melt production (Foulger et al., 2005).

Despite the presence of E-type lavas that are similar to Icelandic lavas in the Baffin Island and West Greenland lava piles, N-type lavas also occur and therefore the early NAIP differs from Iceland. Nevertheless, this feature alone does not necessarily mean that the source of magmatism in the two regions of the NAIP is completely different. The early NAIP lavas, in Baffin Island, West Greenland and the BTIP, were erupted through thick lithosphere and crust. The magmas may have tapped a deeper source region than the present day Icelandic lavas. Additionally, different degrees of melting in the two regions will produce magmas with different compositions, even if their source is identical. The depleted and relatively enriched components in the Baffin Island-West Greenland lavas are discussed in the following sections in relation to MORB and more recent NAIP magmatism in order to better refine the source(s) for the NAIP.

5.3.6.1 Depleted (N-MORB) component

The depleted N-type component in Baffin Island and West Greenland cannot be compared to any Icelandic components since N-type magma is not available, or is not sampled, in the NAIP at the present day. It is shown in this thesis that the incompatible trace element and Sr and Nd isotopic composition of the more depleted Baffin Island-West Greenland lavas show a striking similarity to N-MORB (Section 5.3.1). This strongly suggests that the source of at least some of the early NAIP lavas could be represented by depleted upper mantle that is similar, or identical, to the MORB-source. Within a simple plume model, depleted lavas erupted at the surface could originate from the depleted upper mantle entrained by the rising plume (Fitton et al., 1997; Saunders et al., 1997; Kempton et al., 2000). In support of this hypothesis it has been shown that N-type lavas were only erupted on the periphery of the NAIP (in Baffin Island, West Greenland and the BTIP) in line with entrainment of N-MORB, as predicted by the simple plume model (Saunders et al., 1997). However, the observation that depleted and relatively enriched lava flows are inter-bedded throughout the Baffin Island and West Greenland succession suggests that E-type components must be closely associated with N-type components in the source. It is certainly possible that turbulent flow near the edge of a plume could mix relatively enriched 'plume' material into the entrained MORB-source. However, uncertainty in whether mantle convection extends through the whole Earth or is confined to layers complicates the prediction of the composition of lavas expected from a plume originating in the deep mantle.

The very simple model described in the previous section, of depleted upper mantle streaked with portions of relatively enriched material, could account for the incompatible trace element and radiogenic isotope compositions of the Baffin Island-West Greenland lavas. However, the upper mantle alone cannot account for the higher temperature and high $^{3}He/^{4}He$ of the NAIP lavas in relation to MORB or the larger volumes of magma generated in the NAIP. The possibility that heat and helium could be added to the depleted upper mantle on their own, by diffusion, is discussed in Section 5.4.2 of this chapter. Such a process would avoid the

requirement for a mantle plume in order to explain the thermal and helium isotope anomalies. However, the ultimate source for the depleted lavas in Baffin Island and West Greenland cannot be fully evaluated without first considering the more enriched lavas.

5.3.6.2 Relatively enriched (E-type) component

Icelandic lavas (E-type component in the NAIP) span a wide range of compositions and are themselves shown to be composed of depleted and relatively enriched components. Some authors believe that the more depleted lavas in Iceland are sourced in N-MORB mantle (Hanan and Schilling, 1997; Hanan et al., 2000), while other authors strongly disagree and believe they are produced in a separate depleted Iceland plume (DIP) component, distinct from N-MORB (Fitton et al., 1997; Kempton et al., 2000; Fitton et al., 2003). The enriched components in many OIB sources are commonly thought to be the result of contributions from recycled ocean crust (Hofmann and White, 1982; Zindler and Hart, 1986; Hauri and Hart, 1993; Hofmann, 1988, 1997), forming mantle components such as HIMU and EM (Zindler and Hart, 1986; Hauri and Hart, 1993; Hofmann, 1997). Baffin Island and West Greenland E-type lavas are isotopically distinct from the N-type lavas, extending to higher $^{87}Sr/^{86}Sr$ and lower $^{143}Nd/^{144}Nd$. However, these compositions are not as extreme as the OIB that are believed to contain HIMU and EM in their source. This does not, however, rule out the possibility that recycled ocean crust is involved to some degree in the source of the Icelandic lavas (Fitton, 2007), and in turn, the Baffin Island-West Greenland lavas. Figure 5.7 shows that the E-type component in the early NAIP lavas does not reach such enriched trace element compositions (lower Nb/Zr) as the modern Icelandic lavas but instead extends to more enriched isotopic signatures (lower $^{143}Nd/^{144}Nd$). However, very low $^{143}Nd/^{144}Nd$ in Baffin Island and West Greenland picrites is shown to be due to crustal contamination with the uncontaminated picrites extending only slightly lower in $^{143}Nd/^{144}Nd$ than Icelandic lavas (Chapter 2 and 3; Starkey et al., 2009). Although the type of enrichment in the two regions is not identical, it is clear that they both sample some form of enriched component in their source. Therefore, for the purposes of evaluating the possible

source of the E-type lavas in the early NAIP, and in turn the N-type lavas, the Baffin Island-West Greenland lavas will be compared to the depleted and enriched components thought to be present in the Icelandic source.

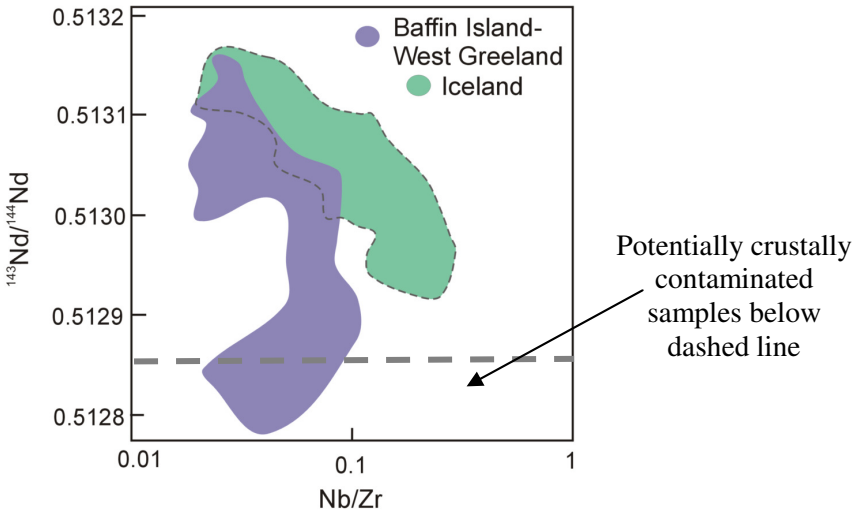

Figure 5.7. $^{143}Nd/^{144}Nd$ plotted against Nb/Zr for Baffin Island-West Greenland samples and Iceland. Baffin Island-West Greenland lavas extend to much lower $^{143}Nd/^{144}Nd$ (relatively more enriched) than the Icelandic lavas despite showing a more restricted range in Nb/Zr. Part of the range to low $^{143}Nd/^{144}Nd$ of the Baffin Island-West Greenland picrites is most likely due to crustal contamination.

Fitton et al. (2003) argue for the involvement of ancient recycled oceanic lithospheric mantle as the source of the DIP component, as do Skovgaard et al. (2001) and Chauvel and Hémond (2000). These authors show that the most depleted Icelandic basalts may be sourced from melting of the lower parts of the subducted ocean crust, such as the gabbroic section (Chauvel and Hémond, 2000). This was contrary to Hanan and Schilling (1997) who proposed that N-MORB source mantle could account for the most depleted Icelandic lavas and that they did not therefore require a separate depleted source. However, Fitton et al. (1997) had shown that Icelandic basalts and N-MORB define separate and parallel arrays on a logarithmic plot of Nb/Y versus Zr/Y, with Icelandic basalts displaying higher Nb/Y at any given Zr/Y (Figure 5.8). This evidence strongly suggests that N-MORB and Icelandic basalts, even extremely depleted Icelandic basalts, cannot share the same source.

Several authors have used various lines of evidence in support of a DIP component that is distinct from N-MORB (e.g. Hards et al., 1995; Kerr et al., 1995; Thirlwall,

1995; Fitton et al., 1997; Chauvel and Hémond, 2000; Kempton et al., 2000). Thirlwall (1995) uses Pb isotopes to show that Icelandic basalts and N-MORB define separate sub-parallel arrays on a plot of $^{207}Pb/^{204}Pb$ versus $^{206}Pb/^{204}Pb$, thereby ruling out significant mixing of N-MORB-source mantle with the Iceland plume. Kempton et al. (2000) use NAIP hafnium and trace element data (Figure 5.9) to indicate the distinction between the depleted and enriched Iceland plume components and their distinction from N-MORB. Figure 5.9 shows that N-MORB has negative ΔεHf (the vertical deviation of a given sample from the mantle array regression line in Hf-Nd isotope space) and negative ΔNb. The depleted and enriched Icelandic plume components conversely have positive ΔNb with positive and negative ΔεHf respectively (Kempton et al., 2000).

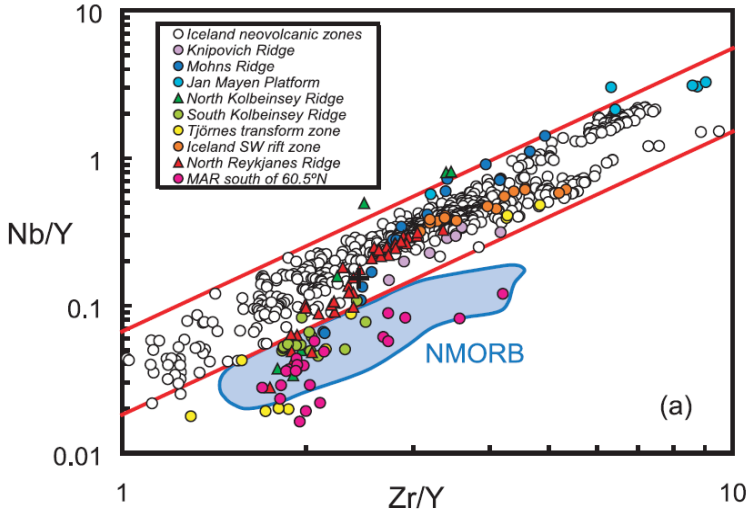

Figure 5.8. Nb/Y plotted against Zr/Y for basalts from Iceland and the Mid-Atlantic Ridge to illustrate the Iceland array. ΔNb = 0 is defined by the lower red line separating Iceland and N-MORB samples. From Fitton et al. (2003).

Hf isotope data are not available on the Baffin Island-West Greenland samples in this study but fortunately there are some Hf isotope data available for the Baffin Island picrites of the Lass-Evans (2004) study. ΔεHf is positive for all Baffin Island samples that were analysed (n=15; Figure 5.10; Lass-Evans, 2004). This is an interesting result since these samples span a range from N- to E-type (negative to positive ΔNb) but show no overlap with N-MORB in their Hf isotopes. This suggests, surprisingly, that N-MORB may not have played a role in the genesis of any of the Baffin Island lavas. However, subsequent Hf isotope data for North

Atlantic MORB showed a much wider range in Hf isotope ratios (Chauvel and Blichert-Toft, 2001) than the samples used by Kempton et al. (2000) shown in Figure 5.9, meaning that at least some of the Baffin Island samples overlap the North Atlantic MORB range (Figure 5.10). The conclusion is that over half of the Baffin Island samples, where Hf isotope ratios are available, fall outside of the North Atlantic MORB range. Four of these samples have positive ΔNb and plot within the DIP field so would appear to require a separate depleted component to N-MORB within their source, as with Icelandic basalts.

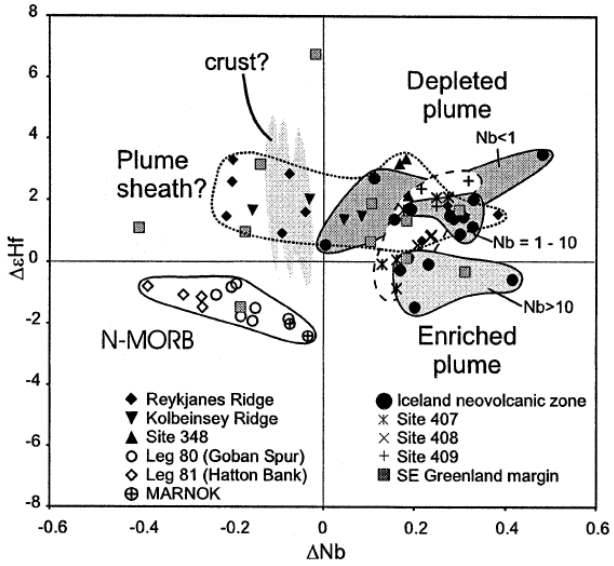

Figure 5.9. ΔεHf plotted against ΔNb for NAIP basalts. Iceland depleted plume components that are not in the plume sheath are clearly distinct from N-MORB. From Kempton et al. (2000).

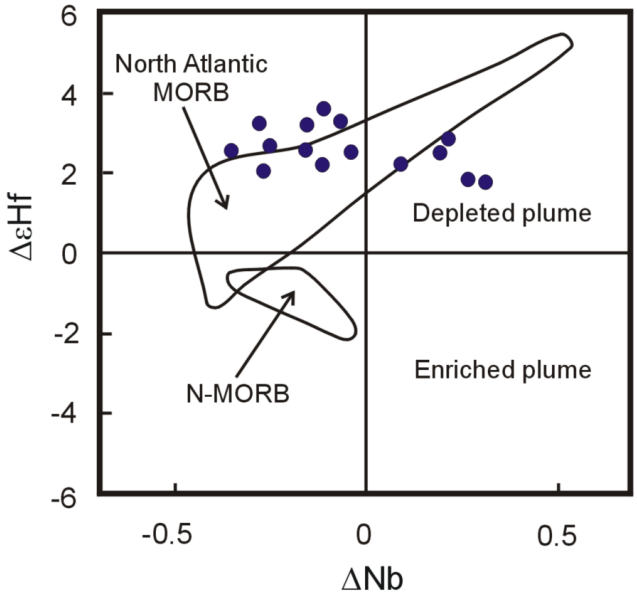

Figure 5.10. ΔεHf plotted against ΔNb for Baffin Island picrites (blue circles; Lass-Evans, 2004), North Atlantic MORB (Chauvel and Blichert-Toft, 2001) and N-MORB (Kempton et al., 2000).

The possibility of a depleted component, distinct from N-MORB, in the Baffin Island and West Greenland magma source can also be tested with incompatible trace elements. Depleted Icelandic lavas are defined as having Nb/Zr < 0.06 by Fitton et al. (2003), while obviously displaying positive ΔNb. Only seven of the Baffin Island-West Greenland samples of this study with positive ΔNb extend below Nb/Zr = 0.06 (Figure 5.11) and none of these extend into the depleted end of the array. These few samples may share the same history as that suggested for the DIP component in Icelandic samples; being sourced from melted ancient subducted oceanic lithospheric mantle. Some authors propose that the DIP component is sampled in Iceland due to fortuitous conditions that allow for high degrees of melting at a rift (Chauvel and Hémond, 2000). It is possible that the greater depth of melting at Baffin Island and West Greenland, under ~100 km thick lithosphere, affected the sampling of this component, i.e. it was simply not possible to melt the depleted component at that depth. Therefore, the seven Baffin Island-West Greenland samples that share some similarities with the DIP component on a plot of Nb/Y against Zr/Y may, alternatively, have experienced a completely different origin. Other characteristics of the depleted Icelandic lavas are: positive Sr and Eu anomalies, low Ce/Pb and Zr/Sm, and high Sm/Nd and Sr/Nd. The more depleted of the E-type Baffin Island-West Greenland samples (positive ΔNb with Nb/Zr < 0.06) display higher Sm/Nd and lower Zr/Sm (Figure 5.12) but do not share the other features of the DIP component. Nevertheless, the number of Baffin Island-West Greenland samples that fall into the DIP group (Nb/Zr < 0.06) is fairly limited, as shown, despite the large dataset for the region. This suggests that if the DIP component was present in the early NAIP, it was not easily sampled. However, there is not enough evidence here to conclude whether the small number of relatively depleted E-type lavas of Baffin Island and West Greenland share the same source as the depleted Icelandic lavas.

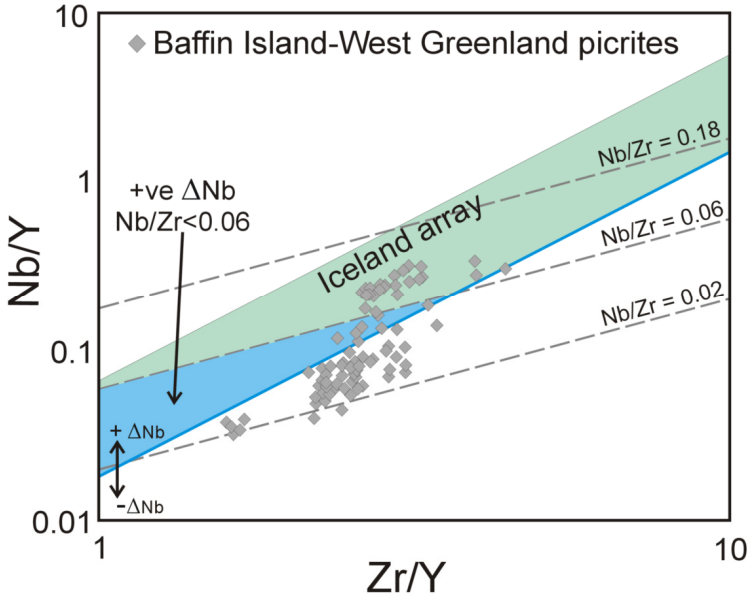

Figure 5.11. Nb/Y plotted against Zr/Y for Baffin Island-West Greenland samples. Very few samples fall below Nb/Zr < 0.06 at positive ΔNb suggesting that the DIP component may not have been a significant component in the earliest NAIP magmatism. Modified from Fitton et al. (2003).

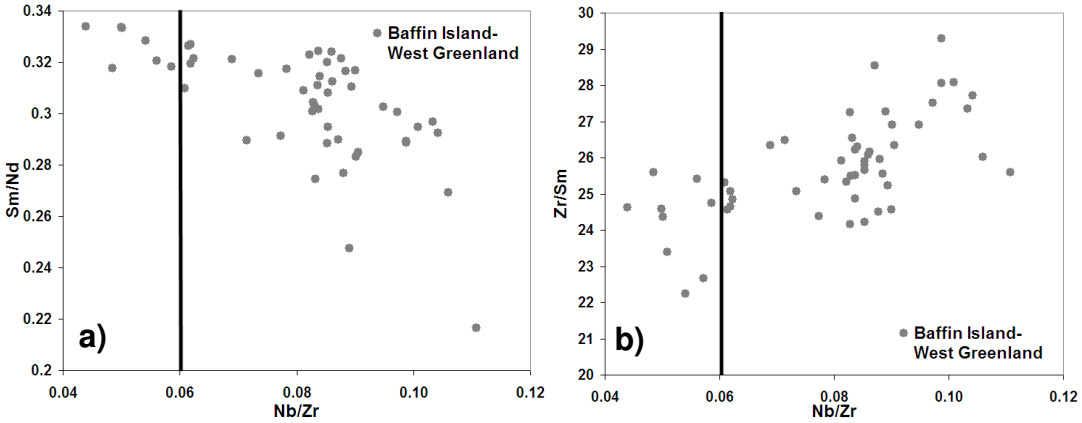

Figure 5.12. a) Sm/Nd plotted against Nb/Zr and b) Zr/Sm plotted against Nb/Zr for the E-type (positive Nb) Baffin Island-West Greenland samples. Nb/Zr = 0.06 separates 'Depleted Iceland Plume' (DIP) lavas from relatively enriched Icelandic lavas (Fitton et al., 2003).

The remainder of the E-type Baffin Island-West Greenland lavas (with Nb/Zr > 0.06) fall into the relatively more enriched region of the Iceland array on a plot of Nb/Y against Zr/Y (ΔNb > 0) (Figure 5.11). However, as shown in Figure 5.11, the early NAIP samples in Baffin Island and West Greenland have a more restricted range in compositions (Nb/Y and Zr/Y) than Iceland lavas. It has been shown above that ancient subducted oceanic lithospheric mantle is the most likely source for the more depleted E-type component (DIP), particularly in Icelandic lavas, even if it was not sampled or was not available at the onset of magmatism in the early NAIP. It

therefore seems logical to investigate whether the more enriched parts of subducted lithosphere could have been incorporated into the early NAIP source (as suggested for Iceland by Fitton et al. (2003)) to account for the E-type Baffin Island-West Greenland lavas with Nb/Zr > 0.06.

Modelling by Chauvel and Hémond (2000) showed that the relatively more enriched lavas in Iceland (with Nb/Zr > 0.06) could result from melting of the basaltic part of ocean crust that was incorporated into magmas along with the more depleted gabbroic section that formed the Icelandic picrites (with Nb/Zr < 0.06). It is therefore possible that a similar origin applies to the enriched E-type Baffin Island-West Greenland samples despite the fact they do not reach such high Nb/Zr as the Icelandic lavas. Kent et al. (2004) consider the effects of the addition of recycled pelagic sediments, low-temperature altered oceanic crust and the deeper peridotitic parts of the recycled high-temperature altered oceanic crust to the Baffin Island magmas. Although, $\delta^{18}O$ of olivine crystals in N- and E-type lavas allows for a few percent of the former two components being incorporated into the depleted source, subsequent melting of such a source cannot reproduce the Nb-Ta contents and LREE concentrations of the E-type lavas (Kent et al., 2004). Addition of around 10-15% of high-temperature hydrothermally altered oceanic crust can explain the differences in $\delta^{18}O$ between the N- and E-type lavas (Kent et al., 2004). However, such material would be unlikely to be associated with enriched isotope compositions and enriched chemical signatures (Kent et al., 2004).

In summary, it is shown here that the E-type Baffin Island and West Greenland lavas share only some of the geochemical characteristics displayed by the Icelandic lavas. The main similarity is that both the Icelandic lavas and the E-type Baffin Island-West Greenland lavas require the addition of more fertile material to their originally depleted source. There is not enough evidence to conclude whether the same component of subducted slab thought to be available in the Icelandic magma source was also available in the earlier NAIP magma source. However, there is a strong possibility that at least some of the Baffin Island and West Greenland lavas require the presence of recycled material in their source to explain their enrichment relative

to N-MORB, and therefore their similarity to E-MORB. It is possible that the pressure and temperature conditions under which the magmas were produced in the two regions was so different that a simple comparison between the products of magmatism, to ascertain the source of the early and more recent NAIP lavas, is not possible. The continuous trend in incompatible trace element and radiogenic isotope compositions from N- to E-type in Baffin Island and West Greenland has been shown not to result from crustal or lithospheric contamination of depleted magmas. Therefore, the compositional variations must be inherited from the sub-lithospheric mantle source. As shown, the early NAIP lavas sample N-type material not seen in Iceland. The N-type lavas were erupted near-simultaneously with the more enriched lavas to produce inter bedded sequences in Baffin Island and West Greenland suggesting that both depleted and relatively enriched sources were closely spaced in the melting region. A model whereby portions of subducted ocean crust are mixed into the depleted upper mantle can, on the whole, account for the Baffin Island-West Greenland data as long as the depleted N-MORB component was phased out during more recent (Iceland) magmatism and if the source of heat and helium is independent of enrichment. Importantly, one of the most significant differences between the E-type lavas of the early and more recent NAIP is related to their $^{3}He/^{4}He$. Baffin Island and West Greenland lavas display substantially higher $^{3}He/^{4}He$ than Iceland and, as shown, the $^{3}He/^{4}He$ of the N- and E-type lavas is indistinguishable, with both reaching 50 R_a. Any model proposed for the NAIP magmatism from 60 Ma to present must be able to account for this observation.

5.3.7 Timescale for the production of the heterogeneity in the NAIP source

The length of time that the heterogeneity, in this case subducted ocean crust, has been present in the Iceland source can be assessed geochemically. Chauvel and Hémond (2000) and Skovgaard et al. (2001) show that the compositional variations in the Icelandic mantle source are long-lived features, present for over ~2.5 Ga. Thirlwall et al. (2004) recognised that negative $\Delta^{207}Pb$ (low $^{207}Pb/^{204}Pb$ for any given $^{206}Pb/^{204}Pb$) in Iceland correlates with elevated $^{3}He/^{4}He$ (Thirlwall et al., 2004), implying elevated source μ ($^{238}U/^{204}Pb$) since the Palaeozoic (for at least the last

~400 my). It is thought that this could indicate the potential involvement of Palaeozoic basaltic oceanic crust in the North Atlantic mantle (Thirlwall et al., 2004). As shown in Chapter 3, Sm-Nd isochrons indicate that if the Baffin Island-West Greenland magmas initially shared the same depleted source, then the depleted and relatively enriched groups separated from this source, and each other, around 400-800 Ma. Although this is a large time spread, it is in keeping with the potential U enrichment around 400 Ma indicated in the Icelandic source proposed by Thirlwall et al. (2004). Such U enrichment may also help to explain why high $^{3}He/^{4}He$ occurs less commonly in E-type magmas, since they contain more ^{4}He, produced from the radioactive decay of U in their source. Thirlwall et al. (2004) make it clear, however, that this view is inconsistent with models where high $^{3}He/^{4}He$ is generated in low-U/Th upper mantle reservoirs such as that proposed by Foulger and Pearson (2001). Foulger et al. (2005) use this ~400 Ma age to invoke remelting of Iapetus ocean crust in the source of the Icelandic lavas. They propose that remelting of such material could account for the large melt volumes and isotopic composition (Sr, Nd, Os, Pb) of Icelandic lavas without requiring high temperatures (Foulger et al., 2005). However, Iapetus crust itself seems unlikely to have been present in the mantle region at the time. Plate reconstructions (using PLATES project (http://www.ig.utexas.edu/research/projects/plates/)) show Britain to be south of the equator around 400 Ma, when the Iapetus Ocean was closing. For the subducted Iapetus oceanic crust to be involved in North Atlantic magmatism from 60 Ma to the present day requires it to have been transported in the mantle along with the overriding plate from the region in which it was subducted in the southern hemisphere to the northern hemisphere where the magmatism occurred. Therefore, although it seems unlikely that the Iapetus ocean crust was itself involved in North Atlantic magmatism it is possible that some recycled ocean crust from another unidentifiable subduction zone was present in the NAIP mantle source.

5.4 High $^{3}He/^{4}He$ source lithology

The Earth's mantle is generally thought to be heterogeneous. However, understanding the scale and distribution of heterogeneity in the mantle has proven

difficult using both geophysical and geochemical techniques. On the whole the mantle is considered to be dominated by peridotite, but calculating the proportion of more enriched lithologies such as eclogite and pyroxenite within the depleted peridotite has been an important research focus. Gaining a better idea of the source lithology for OIB and the high-$^{3}He/^{4}He$ mantle will help in understanding the evolution and survival of high $^{3}He/^{4}He$ in the Earth. It is thought that peridotite could form a potential reservoir for high $^{3}He/^{4}He$ since it may be able to preserve high $^{3}He/^{238}U$ if it was isolated from the convecting mantle early in Earth history (Hart et al., 1992; Anderson, 1998b; Parman et al., 2005; Heber et al., 2007). However, as shown above, the role of recycled oceanic crust is often invoked in OIB sources, suggesting that some sources must contain a substantial proportion of eclogite from subducted oceanic crust. As noted in the previous section, several authors propose that the NAIP source appears to have experienced a period of enrichment in its past, in agreement with the Sm-Nd study on the Baffin Island-West Greenland picrites in Chapter 3. However, recycled oceanic crust itself is unlikely to be able to preserve high $^{3}He/^{4}He$ because subduction zones are thought to form a barrier to noble gases (Staudacher and Allègre, 1988). Subsequent ^{4}He ingrowth from U and Th decay within subducted material would be expected to lower $^{3}He/^{4}He$ further, unless it is possible for U and Th to be preferentially removed (Jackson et al., 2008). Therefore, the exact contributions of depleted and enriched components to a source may affect the level of helium isotope ratio that can be obtained.

Prytulak and Elliott (2007) show that Ti enrichments in global OIB are too high for OIB to be derived from melting of peridotitic mantle. Instead, small amounts (~1-10%) of more enriched components, such as recycled mafic crust and in some cases sediments and/or metasomatic veins, are required to explain both the Ti enrichments and extreme radiogenic isotope signatures of some OIB. Jackson et al. (2008) extend this modelling to focus on the enrichment of Ti, Ta and Nb (TITAN elements) specifically in relation to high-$^{3}He/^{4}He$ OIB (up to ~30 R_a). TITAN enrichments in high-$^{3}He/^{4}He$ OIB globally are cited as evidence for recycled, refractory eclogite in the OIB source since TITAN elements are strongly partitioned into rutile during the formation of eclogite (Green and Pearson, 1986; Ryerson and Watson, 1987; Foley et

al., 2000). It is suggested that eclogite itself is unlikely to be the source for high $^{3}He/^{4}He$ (Jackson et al., 2008). Instead, it is proposed that eclogite is melted along with the lherzolitic peridotite supplied from the deep part of ancient oceanic lithosphere (Jackson et al., 2008).

Modelling carried out by Jackson et al. (2008) indicates the possibility of producing high-$^{3}He/^{4}He$ OIB with positive TITAN anomalies from reasonable eclogite/peridotite mixtures and melting expected in the Earth's mantle. However, it was noted in the Jackson et al. (2008) study that it is unknown how this modelling would apply to the extremely high $^{3}He/^{4}He$ of the Baffin Island and West Greenland lavas since no trace element data were available for these samples at the time. To obtain such high $^{3}He/^{4}He$ (up to 50 R_a) it was suggested that the Baffin Island-West Greenland magmas require a source of pure peridotite, signifying that such magmas would not display positive TITAN anomalies (Jackson et al., 2008). This is explained by the fact that any eclogite present in the source that contributes to melts would also contribute radiogenic ^{4}He thus lowering the overall $^{3}He/^{4}He$ of the melt. The Baffin Island and West Greenland data of this study, along with data in the thesis of Lass-Evans (2004), provide the perfect test for this hypothesis (these data are found together in Starkey et al. (2009)).

The Baffin Island-West Greenland picrites are plotted together with the hotspot data of Jackson et al. (2008) in $^{3}He/^{4}He$ against Ti/Ti* and Nb/Nb* to investigate whether the samples display a positive TITAN anomaly that might be suggestive of eclogite melting in their source. TITAN anomalies are calculated as follows, where $_N$ denotes normalisation to primitive mantle values: $Ti/Ti^* = Ti_N/(Sm_N \times Tb_N)^{0.5}$, $Ta/Ta^* = Ta_N/(Th_N \times La_N)^{0.5}$ and $Nb/Nb^* = Nb_N/(Th_N \times La_N)^{0.5}$ (Jackson et al., 2008). Positive TITAN anomalies are not found in the Baffin Island-West Greenland picrites (Figure 5.13), as predicted by Jackson et al. (2008). Instead, the Baffin Island-West Greenland samples display very similar Ti/Ti* values, regardless of $^{3}He/^{4}He$, and low Nb/Nb* values compared to OIB but display a wider range in Nb/Nb* at higher $^{3}He/^{4}He$ (Figure 5.13). The lack of TITAN enrichments in the Baffin Island and West Greenland samples indicates that melting occurred in pure peridotite to produce high-

$^{3}He/^{4}He$ magmas with no contribution from an eclogitic source (the repository for TITAN elements and low $^{3}He/^{4}He$). However, it should be noted that a very small proportion of eclogite in the source could be overwhelmed by the more depleted peridotitic component during melting such that no TITAN enrichment is apparent in the lavas (Jackson et al., 2008). The maximum amount of eclogite permitted in the source that when it is melted it does not produce a TITAN anomaly is unconstrained. However, E-type lavas form a significant proportion (~50%) of the Baffin Island-West Greenland samples and therefore presumably require a significant proportion of an enriched component in their source which may cause some problems for the Jackson et al. (2008) model.

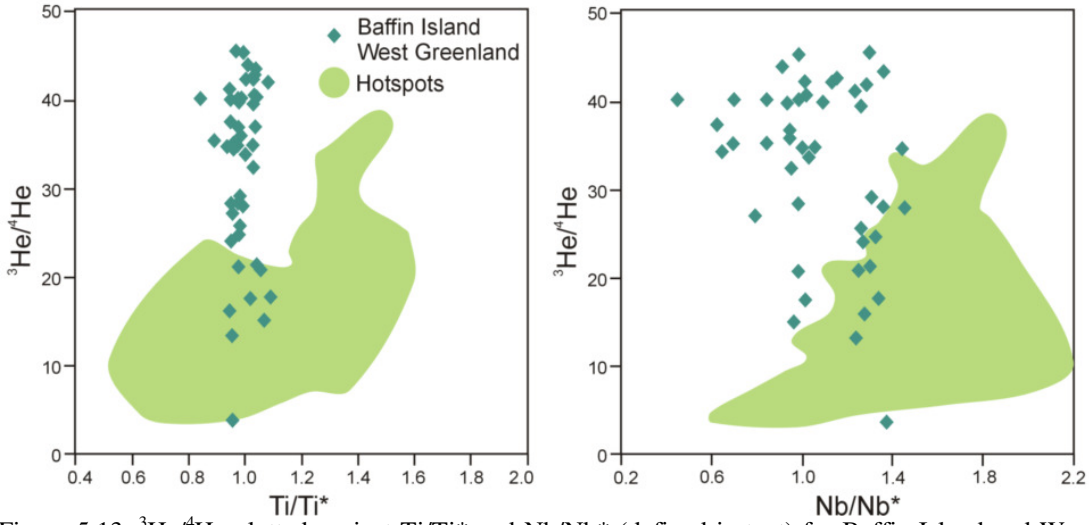

Figure 5.13. $^{3}He/^{4}He$ plotted against Ti/Ti* and Nb/Nb* (defined in text) for Baffin Island and West Greenland samples and hotspots (Jackson et al., 2008). High Ti/Ti* and Nb/Nb* indicates eclogite involvement in melting.

5.4.1 High $^{3}He/^{4}He$ and recycled components

Support for a purely peridotitic source for the extremely high $^{3}He/^{4}He$ picrites of Baffin Island and West Greenland is provided by Os isotopes. $^{187}Os/^{188}Os$ measured on the samples of this study was shown to be similar to chondritic values indicating no involvement of enriched components, such as old recycled crustal material, in the source of the lavas (Dale et al., 2009). However, it is thought that if relatively enriched components are required in the Baffin Island-West Greenland source to account for the wide range in Nd isotopic signatures then their Os isotopic signature

is diluted compared to the contribution from depleted peridotite during melting (Dale et al., 2009). As previously suggested, it is possible that the depleted upper mantle, streaked with relatively more enriched material created from the remnants of subducted slabs, could account for the full range of incompatible trace element and radiogenic isotopic compositions displayed by the Baffin Island and West Greenland picrites. Therefore, the modelling from TITAN elements and Os isotopes does not preclude a streaky mantle model as long as the proportion of relatively enriched components is small. Jackson et al. (2008) suggest that the high-$^{3}He/^{4}He$ peridotitic source has been convectively isolated from the convecting mantle for billions of years in order for it to retain high time-integrated $^{3}He/(U+Th)$. However, the isolation of portions of mantle might be difficult to achieve in a regime of whole-mantle convection unless the lower mantle is much more viscous (by 30 times compared to the upper mantle; van Keken and Ballentine, 1998). Instead, it is suggested here that high-$^{3}He/^{4}He$ helium could be added separately to a dominantly peridotitic source (streaked with eclogite). If helium was added with an associated increase in temperature then the normal convecting upper mantle could represent the source of the early NAIP lavas, with the added heat being responsible for increased melt production in the region. However, a larger proportion of recycled material is required for Icelandic magmatism so this would either need to have been added to the NAIP source very recently (less than 60 Ma) or was always present in the source but not sampled by the early NAIP lavas. An upper mantle source for the NAIP would suggest that a mantle plume may not be a requirement in the region. However, accounting for the longevity and geographical distribution of the NAIP magmatism, along with the high temperatures of the magmas and high $^{3}He/^{4}He$, will be difficult without the involvement of a mantle plume.

5.4.2 Achieving high $^{3}He/^{4}He$ by diffusion

There are several hypotheses that might explain the structure and composition of the NAIP source and these are summarised at the end of this chapter. If the temperature and helium isotope anomalies for the NAIP are disregarded then the NAIP source can be represented by a fairly simple model of normal convecting upper mantle

coupled with the incorporation of variable amounts of recycled material over time. One of the simplest ways for helium and heat to be added to the NAIP source is by diffusion. The idea that helium can diffuse through the Earth was suggested, in an earlier study, to account for the abnormally high $^{3}He/^{4}He$ of the upper mantle (~8 R_a), resulting from diffusion of helium across a mid-mantle thermal boundary above a hot, convectively-isolated primordial noble gas-rich lower mantle (O'Nions and Oxburgh, 1983). It was noted in Chapter 1 that there has been renewed interest in understanding the diffusion and subsequent storage of helium in the Earth in more recent studies (Shuster et al., 2004; Albarède, 2008; Hart et al., 2008). These models rely on the high-$^{3}He/^{4}He$ reservoir being characterised by high helium concentration. Geophysical evidence would seem to preclude a layered mantle model for the Earth that has previously provided the easiest way for a high helium concentration, high-$^{3}He/^{4}He$ reservoir, to be preserved in the lower mantle. This leads to the requirement for a location in the Earth that is protected from the stirring effects of mantle convection so that a store of high-^{3}He material can be preserved through time. The high-$^{3}He/^{4}He$ reservoir is more likely to be represented by high ^{3}He concentrations and low ^{4}He since it is thought that depleted residues of melting formed in the last few billion years would be too low in helium to preserve high $^{3}He/^{4}He$ during subsequent mixing (Porcelli and Elliot, 2008). In addition, storage of depleted residues of mantle melting over time is difficult to achieve in a convecting whole-mantle and it has been shown that it is particularly difficult to retain high helium concentrations in small-scale mantle heterogeneities over time (van Keken and Ballentine, 1999). This precludes the storage of high $^{3}He/^{4}He$ in dispersed blobs in the upper mantle and instead suggests that a much larger reservoir for high $^{3}He/^{4}He$ is required deeper in Earth, away from the upper mantle MORB-source.

In support of the hypothesis of a deep mantle source to account for the helium isotope data, the high temperatures inferred for the lavas of Baffin Island and West Greenland, estimated to be 100-200°C hotter than ambient upper mantle (Herzberg and O'Hara, 2002), also strongly suggest a deep mantle source. It is shown that a high excess temperature at the CMB can be reduced to 200-250°C at the surface due to the non-adiabatic effect of internally heated mantle (Bunge, 2005) and therefore, a

convectively isolated layer at the CMB (Samuel and Farnetani, 2003) or the core itself (Porcelli and Halliday, 2001) could be invoked as possible sources for high ^{3}He in the Earth.

A layer at the CMB (D") enriched in primordial volatiles needs to have retained a high time-integrated ^{3}He/(U+Th). It was shown in Chapter 1 that this layer could be derived from subducted meteoritic material early in Earth history that segregated at the base of the mantle (Tolstikhin and Hofmann, 2005). In this model, small chondrite-like bodies in the solar system, irradiated by early intense solar wind, fell to Earth to rest on basaltic crust. These bodies increased the iron content of the crust making it particularly dense during subduction so that it was able to sink deep into the mantle (Tolstikhin and Hofmann, 2005). However, the loss of helium during subduction may cause some difficulties for this model (Hiyagon, 1994). Alternatively, it has been shown that solid phases from an early crystallising magma ocean might be so dense that they simply sink through the mantle to produce a volatile-rich reservoir (Labrosse et al., 2007). These studies show that there is a potential for a deep mantle helium-rich reservoir but that further experimental studies will be required to understand the processes involved in its formation, storage and preservation.

Alternatively, as outlined in Chapter 1, the outer core could form a reservoir for ^{3}He but it is thought to require exceptionally high initial terrestrial helium concentrations (Sudo et al., 1994). However, more experimental work is required on metal-silicate partitioning in order to better constrain the concentration of helium in the core. Several studies have investigated the potential for helium in mantle plumes being supplied by the core by using Os and W isotopes (Brandon et al. 1999; Schersten et al. 2004; Dale et al., 2009). These studies suggest that if helium is stored in the core and supplied to OIB sources via the outer core then it can only leave the core by diffusion.

5.5 A model for the formation of the North Atlantic Igneous Province

To date, it is unknown whether the mantle exhibits whole or layered mantle convection. Geochemical box models require isolation of the lower mantle to preserve primitive noble gas signatures but geophysical studies (mantle tomography and numerical modelling) support whole-mantle convection. In addition, tomographic evidence for the existence of mantle plumes originating in the lower mantle, particularly for Iceland (Allen et al., 2002), remains equivocal. Therefore, although a mantle plume provides the best explanation for magmatism in the NAIP region, it may not necessarily be required if an explanation can be provided for the excess temperature, high $^{3}He/^{4}He$, large volumes of magma and longevity of magmatism that characterises the region. To date, some models are available that can possibly account for some of the features characteristic of the NAIP (e.g. Anderson, 1995, 1998a,b; Foulger et al., 2005) but there are no models that can account for all of the features characteristic of the NAIP occurring together.

In summary, Baffin Island and West Greenland picrites with low $^{143}Nd/^{144}Nd$ have a helium isotopic range that is indistinguishable from that of the more depleted, high $^{143}Nd/^{144}Nd$, picrites. The Baffin Island and West Greenland picrites extend compositionally into the E-type or 'Icelandic' field based on ΔNb, and therefore have an excess of Nb in their source, indicative of recycled oceanic crust (Fitton et al., 1997). It has been shown that Icelandic lavas require the presence of recycled oceanic crust and lithosphere to account for their incompatible trace element and radiogenic isotope compositions. However, the E-type Baffin Island and West Greenland lavas do not share all of the criteria used to indicate the presence of recycled material in Icelandic lavas. In addition, modelling using TITAN elements and Os isotopes indicates that the extremely high-$^{3}He/^{4}He$ lavas in Baffin Island and West Greenland could be formed by melting of pure peridotite (although a small proportion of eclogite could be permitted in the source; Jackson et al., 2008; Dale et al., 2009). Therefore, it is concluded that the source of the Baffin Island and West Greenland picrites may be no different from that of the convecting upper mantle, except that a separate source is required for the helium isotope and temperature

anomaly that characterise the magmas. The introduction of heat to the NAIP source can, in turn, account for the excess volume of magmatism in the region without the requirement for a substantial proportion of more fertile lithologies in the mantle source.

It is shown in Section 5.4.2 that if the Earth exhibits whole-mantle convection, as would seem more likely from the evidence supplied by recent geophysical studies, then the most likely location for the storage of a reservoir with a high time-integrated $^{3}He/(U+Th)$ is in the deep mantle or core. Irrespective of the ultimate location of a deep high-$^{3}He/^{4}He$ reservoir, the similarity of the isotopic and trace element composition of the Baffin Island-West Greenland picrites to global MORB implies that the whole mantle may have essentially the same composition and degree of heterogeneity as the convecting upper mantle. Whole-mantle convection could be expected to have homogenised the entire mantle over Earth history suggesting that, on a large scale, the mantle may not be particularly heterogeneous (van Keken and Ballentine, 1998). However, small-scale mantle heterogeneities are required to explain the variation in compositions erupted in close proximity on the Earth's surface, particularly along mid-ocean ridges (Mahoney et al., 2002; Fitton, 2007). Small-scale heterogeneities in the mantle could be produced by the injection of oceanic lithosphere into the mantle at subduction zones followed by break-up of the subducted material during convective mixing into the surrounding mantle. Subducted slabs are thought to reach different depths in the mantle depending on their relative size, density and buoyancy (Fukao et al., 2001; Billen, 2008) suggesting that heterogeneities may be present at all depths. It is also possible that some slabs reach all the way to the CMB (van der Hilst et al., 1997; Grand, 2002). The effects of increasing viscosity with depth on mantle mixing are hard to quantify (Bunge et al., 1996) as are the effects of mineral phase changes in the deep mantle and how such minerals are deformed by possible convective forces (Karato, 1996). It is possible that convection is more sluggish at depth (Forte and Mitrovica, 2001), although this would suggest that the deep mantle is not as well stirred as the upper mantle which may result in thermal and compositional stratification of the mantle leading to layered convection.

The Baffin Island and West Greenland picrites, and the NAIP in general, require that the diffusive equilibration of high-$^3He/^4He$ helium and heat occurred after the heterogeneous mantle structure was established. How helium and heat alone could infuse a portion of mantle to produce a high-$^3He/^4He$ source, such as that for an ocean island, while leaving the surrounding mantle with no anomaly is not clear. It is hoped that future experimental studies will be able to help determine the processes by which helium moves in the Earth. Despite this, a model is suggested below for a possible formation of the NAIP source.

The model described here requires that the mantle convects as a single layer and assumes that the mantle, on a large scale, is essentially the same composition throughout (i.e. dominantly depleted N-type material streaked with relatively enriched E-type material). This model is schematically illustrated in Figure 5.14. The high-$^3He/^4He$ source is convectively isolated in either the deep mantle or the core and the model assumes that helium and heat can move together by diffusion. The high-$^3He/^4He$ source is assumed to have a high enough helium concentration such that it can overwhelm any mantle composition, depleted or enriched, with which it is in close proximity or mixes. This model requires that some subducted oceanic lithosphere and crust are transported all the way to the deep mantle to collect at the CMB (D"). The accumulating subducted slabs either mix with the hot high-$^3He/^4He$ convectively isolated material at the CMB, or heat and helium from the core or deep dense layer diffuse into the slabs. At the same time the background lower mantle material, similar in composition to the MORB-source mantle, is also infused with heat and helium. The mixture of hot, high-$^3He/^4He$ subducted slabs becomes thermally unstable and rises through the mantle as a plume, mixing and/or entraining the convecting mantle on the way. The entrained material at the edge of the upwelling plume forms the source of the early NAIP lavas since they are characterised by erupted material with a composition that is no different to that expected for melting of the convecting upper mantle. In addition, a deep mantle source infused with heat from the core can account for the high temperatures and therefore voluminous magmatism of the early NAIP. The source of exclusively recycled oceanic lithosphere for Iceland, with its associated high $^3He/^4He$ and high

temperatures, is provided by the core of the plume. The fact that the temperature and helium isotope anomaly in the NAIP have decreased from 60 Ma to present is in keeping with the diffusion of both heat and helium out of the NAIP source over time. The initial magmatism in the NAIP has the highest $^{3}He/^{4}He$ on Earth which may be because the early stages of magmatism (from the plume head) have, in this locality, been preserved. This is possibly not the case for other moderately high $^{3}He/^{4}He$ regions on Earth.

It is understood that this is a hybrid model using the classic concept of a deep mantle plume but placing it into a modern whole-mantle convection model. It is assumed here that plumes rise through the mantle to counteract the influx of subducted slabs that have been imaged passing through the 670 km transition zone into the lower parts of the mantle. Despite the large number of assumptions that are made here, this model represents a viable suggestion for the NAIP formation based on the data currently available.

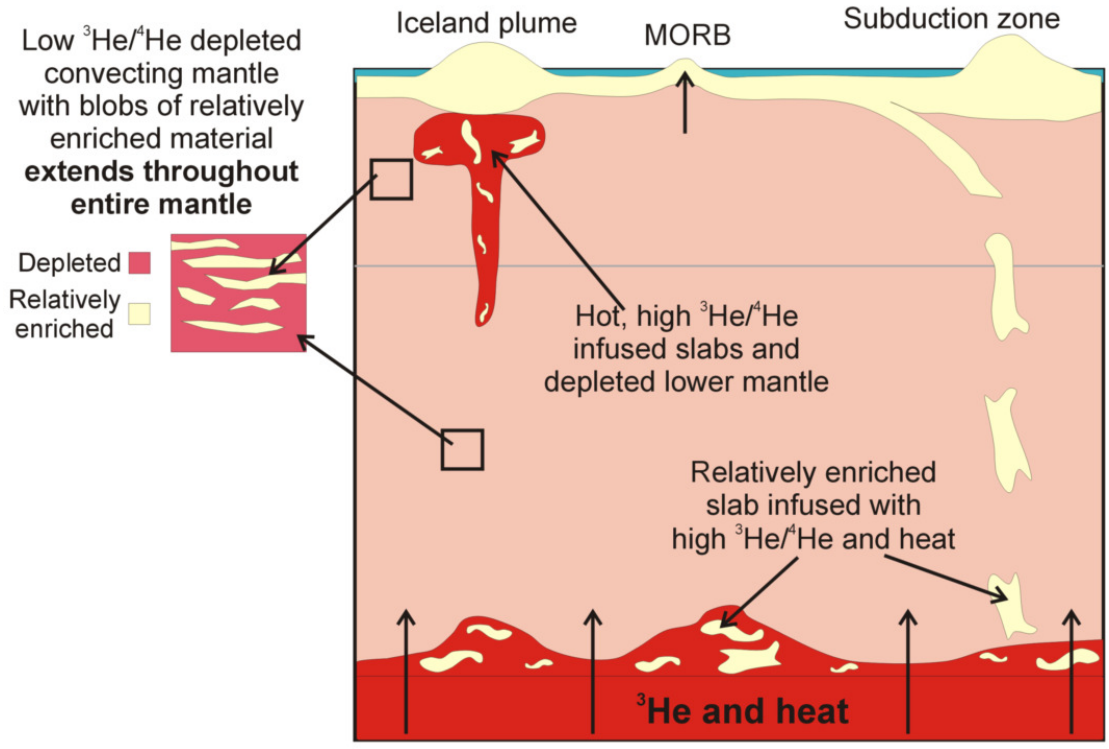

Figure 5.14. Schematic illustration for high $^{3}He/^{4}He$ plume model for the NAIP.

5.6 Suggestions for future work

If this study were to be extended there are a few things that could be investigated:

- Measurement of the trace element concentrations of melt inclusions in a sample (e.g. BI/CS/7 or 400444) that had been identified as crustally contaminated from its whole-rock composition. Such a study could identify the potential timing of crustal contamination and its effects at smaller melt volumes.

- To fully understand the nature of the high-$^{3}He/^{4}He$ reservoir in the Earth will require a multi-disciplinary approach, involving geochemical (experimental and real rock) and geophysical studies. More data and analyses will accelerate the overall understanding of the Earth, particularly with progress in the following areas; 1) improved models for Earth accretion and early storage of volatiles in the mantle and core, 2) increased resolution and accuracy of tomographic images of the deep mantle, 3) improved numerical models for mantle convection, and 4) a better understanding of the partitioning of helium and other elements into the mineral phases relevant to the deep mantle and core.

Conclusions

6 Conclusions

- The Baffin Island and West Greenland picrite lavas are shown to have $^{3}He/^{4}He$ values up to 50 R_a, so establishing this region of the North Atlantic as the highest $^{3}He/^{4}He$ terrestrial magmatic province.

- The Baffin Island and West Greenland picrite lavas display a wide range of major, trace element and lithophile radiogenic isotopic signatures. $(La/Sm)_n$ range from 0.5 to 1.3, $^{87}Sr/^{86}Sr$ range from 0.702883 to 0.711773 and $^{143}Nd/^{144}Nd$ from 0.512712 to 0.513075. Allowing for the effects of crustal contamination, these compositions show a striking similarity to the complete range of compositions produced by lavas at mid-ocean ridges and overlap the range of most northern hemisphere ocean island basalts, including Iceland.

- Highly magnesian olivine crystals (up to Fo_{93}) in the Baffin Island and West Greenland picrites are shown not to have a xenocrystic origin, despite the fact that they probably do not represent true 'phenocrysts' in the petrological sense. These highly magnesian olivine crystals support studies advocating high potential temperatures for the Baffin Island and West Greenland magmas of ~200^{o}C above ambient mantle temperatures.

- High $^{3}He/^{4}He$ in Baffin Island and West Greenland are found in picrite samples with the entire incompatible trace element and radiogenic isotopic range. High $^{3}He/^{4}He$ in the early North Atlantic Igneous Province is not, therefore, confined to a single magma type with a unique trace element and radiogenic isotope composition, whether it be depleted or relatively enriched. Consequently, high $^{3}He/^{4}He$ lavas cannot be distinguished from those with lower $^{3}He/^{4}He$ by any other compositional parameter.

- Crustal contamination modelling in which high-grade Proterozoic crustal basement rocks for the region are mixed with a depleted parent cannot account for the compositional trends displayed by the Baffin Island and West Greenland

picrites. The possibility that the incompatible trace element, Sr and Nd isotope range of the high-$^{3}He/^{4}He$ picrites is due to crustal contamination is ruled out.

- Melt inclusion compositions in olivine crystals in high $^{3}He/^{4}He$ Baffin Island and West Greenland picrites that span a range of whole-rock incompatible trace element and isotopic compositions were measured. Melt inclusion REE profiles are parallel to those of their associated whole-rocks. In addition, there is no evidence for anomalous melt compositions that might have indicated the presence of 'exotic' xenocrystic trapped melts. The melt inclusions therefore support the findings from the whole-rock study that crustal contamination is not responsible for the wide range in whole-rock compositions of the high-$^{3}He/^{4}He$ lavas.

- Melt inclusions provide no evidence for the existence of depleted melts within high-$^{3}He/^{4}He$ relatively enriched whole-rock samples. Melt inclusion compositions therefore rule out the possibility that a small proportion of high-$^{3}He/^{4}He$ depleted melts contributed to the relatively enriched whole-rock high $^{3}He/^{4}He$ samples. The inference is that high $^{3}He/^{4}He$ is a feature of both depleted and relatively enriched mantle sources.

- The compositional range of the Baffin Island and West Greenland picrites at high $^{3}He/^{4}He$ is inconsistent with their derivation from a primordial-helium-rich reservoir that is a residue of ancient mantle depletion. These data strongly suggest that there is no role for a discrete depleted reservoir for high $^{3}He/^{4}He$ in Earth. Furthermore, it is not possible to identify a compositionally unique high $^{3}He/^{4}He$ reservoir, whether it be depleted or enriched.

- There is a range of possible explanations for the evolution of the high-$^{3}He/^{4}He$ reservoir in the Earth. However, the apparent decoupling of helium from incompatible trace elements and lithophile radiogenic isotopes suggests that the most likely model for the production of the high-$^{3}He/^{4}He$ reservoir involves diffusion of primordial helium through the Earth. It is proposed here that

primordial helium diffuses from a deep helium-rich reservoir, located in either the deep mantle or the core, into a reservoir with a composition typical of the convecting upper mantle. If this is the case then helium must have diffused after the development of existing mantle heterogeneities.

- Whatever the ultimate location of the source of high $^{3}He/^{4}He$ in the Earth, it must have a high enough helium concentration to dominate and overwhelm any resultant mixture so that high $^{3}He/^{4}He$ is imposed upon a significant range of mantle compositions with varied $^{3}He/(U+Th)$ histories.

References

Abedini, A. A., Hurwitz, S. and Evans, W. C. (2006). USGS-NoGaDat - a global dataset of noble gas concentrations and their isotopic ratios in volcanic systems. US Geological Survey Digital Series 202.

Albarède, F. (2008). Rogue mantle helium and neon. Science 319, 943-945.

Allègre, C. J., Staudacher, T., Sarda, P. and Kurz, M. (1983). Constraints on evolution of Earths mantle from rare-gas systematics. Nature 303, 762-766.

Allègre, C. J. and Turcotte, D. L. (1986). Implication of a 2-component marble-cake mantle. Nature 323, 123-127.

Allen, R. M., Nolet, G., Morgan, W. J., Vogfjord, K., Bergsson, B. H., Erlendsson, P., Foulger, G. R., Jakobsdottir, S., Julian, B. R., Pritchard, M., Ragnarsson, S. and Stefansson, R. (2002). Imaging the mantle beneath Iceland using integrated seismological techniques. Journal of Geophysical Research 107, 2325.

Anderson, D. L. (1995). Lithosphere, Asthenosphere, and Perisphere. Reviews of Geophysics 33, 125-149.

Anderson, D. L. (1998a). The helium paradoxes. Proceedings of the National Academy of Sciences of the United States of America 95, 4822-4827.

Anderson, D. L. (1998b). A model to explain the various paradoxes associated with mantle noble gas geochemistry. Proceedings of the National Academy of Sciences of the United States of America 95, 9087-9092.

Anderson, D. L. and Schramm, K. A. (2005). Global hotspot maps. In: Foulger, G. R., Natland, J. H., Presnall, D. C. and Anderson, D. L. (eds.) Plates, Plumes and Paradigms: Geological Society of America Special Paper 388, 19-29.

Armienti, P. and Gasperini, D. (2007). Do we really need mantle components to define mantle composition? Journal of Petrology 48, 693-709.

Barling, J. and Goldstein, S. L. (1990). Extreme isotopic variation in Heard-Island lavas and the nature of mantle reservoirs. Nature 348, 59-62.

Batiza, R. (1984). Inverse relationship between Sr isotope diversity and rate of oceanic volcanism has implications for mantle heterogeneity. Nature 309, 440-441.

Beggan, C. and Hamilton, W. (2009). New image processing software for analyzing object size-frequency distributions, geometry, orientation, and spatial distribution. Computers and Geosciences, *in press*.

Bijwaard, H. and Sparkman, W. (1999). Tomographic evidence for a narrow whole mantle plume below Iceland. Earth and Planetary Science Letters 166, 121-126.

Billen, M. I. (2008). Modelling the Dynamics of Subducting Slabs. Annual Review of Earth and Planetary Sciences 36, 325-356.

Blard, P. H. and Farley, K. A. (2008). The influence of radiogenic ^{4}He on cosmogenic ^{3}He determinations in volcanic olivine and pyroxene. Earth and Planetary Science Letters 276, 20-29.

Boyet, M., and Carlson, R. W. (2005). ^{142}Nd evidence for early (>4.53 Ga) global differentiation of the silicate Earth. Science 309, 576-581.

Boyet, M. and Carlson, R. W. (2006). A new geochemical model for the Earth's mantle inferred from ^{146}Sm–^{142}Nd systematics. Earth and Planetary Science Letters 250, 254-268.

Brandon, A. D., Graham, D. W., Waight, T. and Gautason, B. (2007). ^{186}Os and ^{187}Os enrichments and high-^{3}He/^{4}He sources in the Earth's mantle: Evidence from Icelandic picrites. Geochimica et Cosmochimica Acta 71, 4570-4591.

Bunge, H. P. (2005). Low plume excess temperature and high core heat flux inferred from non-adiabatic geotherms in internally heated mantle circulation models. Physics of the Earth and Planetary Interiors 153, 3-10.

Brandon, A. D., Norman, M. D., Walker, R. J. and Morgan, J. W. (1999). ^{186}Os-^{187}Os systematics of Hawaiian picrites. Earth and Planetary Science Letters 174, 25-42.

Bunge, H.-P., Richards, M. A. and Baumgardner, J. R. (1996). Effect of depth-dependent viscosity on the planform of mantle convection. Nature 379, 436-438.

Chauvel, C. and Blichert-Toft, J. (2001). A hafnium isotope and trace element perspective on melting of the depleted mantle. Earth and Planetary Science Letters 190, 137-151.

Chauvel, C. and Hemond, C. (2000). Melting of a complete section of recycled oceanic crust: Trace element and Pb isotopic evidence from Iceland. Geochemistry Geophysics Geosystems 1, doi: 10.1029/1999GC000002.

Cherniak, D. J. (2007). REE diffusion in olivine. EOS Trans, American Geophysical Union 88, MR13C-1397.

Christensen, U. (1995). Effects of phase-transitions on mantle convection. Annual Review of Earth and Planetary Sciences 23, 65-87.

Clarke, D. B. (1970). Tertiary basalts of Baffin Bay: Possible primary magma from the mantle. Contributions to Mineralogy and Petrology 25, 203-224.

Clarke, D. B. and Pedersen, A. K. (1976). Tertiary volcanic province of West Greenland. In: Escher, A. and Watts, W. S. (eds.) Geology of Greenland. Geological Survey of Greenland, Copenhagen., 365-385.

Clarke, D. B. and Upton, B. G. J. (1971). Tertiary basalts of Baffin Island - Field relations and tectonic setting. Canadian Journal of Earth Sciences 8, 248-258.

Clarke, W. B., Beg, M. A. and Craig, H. (1969). Excess ^{3}He in sea: Evidence for terrestrial primordial helium. Earth and Planetary Science Letters 6, 213-220.

Class, C. and Goldstein, S. L. (2005). Evolution of helium isotopes in the Earth's mantle. Nature 436, 1107-1112.

Cottrell, E., Spiegelman, M. and Langmuir, C. H. (2002). Consequences of diffusive reequilibration for the interpretation of melt inclusions. Geochemistry Geophysics Geosystems 3, doi:10.1029/2001GC000205.

Cox, K. G., Bell, J. D. and Pankhurst, R. J. (1979). The interpretation of igneous rocks. Boston, George Allen & Unwin.

Craig, H. and Lupton, J. E. (1976). Primordial neon, helium and hydrogen in oceanic basalts. Earth and Planetary Science Letters 31, 369-385.

Dale, C. W., Pearson, D. G., Starkey, N. A., Stuart, F. M., Ellam, R. M., Larsen, L. M., Fitton, J. G. and Macpherson, C. G. (2009). Osmium isotopes in Baffin Island and West Greenland picrites: Implications for the ^{187}Os/^{188}Os composition of the convecting mantle and the nature of high ^{3}He/^{4}He mantle. Earth and Planetary Science Letters 278, 267-277.

Danyushevsky, L. V., Della-Pasqua, F. N. and Sokolov, S. (2000). Re-equilibration of melt inclusions trapped by magnesian olivine phenocrysts from subduction-related magmas: petrological implications. Contributions to Mineralogy and Petrology 138, 68-83.

Danyushevsky, L. V., Leslie, R. A. J., Crawford, A. J. and Durance, P. (2004). Melt inclusions in primitive olivine phenocrysts: The role of localized reaction processes in the origin of anomalous compositions. Journal of Petrology 45, 2531-2553.

Danyushevsky, L. V., McNeill, A. W. and Sobolev, A. V. (2002a). Experimental and petrological studies of melt inclusions in phenocrysts from mantle-derived magmas: an overview of techniques, advantages and complications. Chemical Geology 183, 5-24.

Danyushevsky, L. V., Sokolov, S. and Falloon, T. J. (2002b). Melt inclusions in olivine phenocrysts: Using diffusive re-equilibration to determine the cooling history of a crystal, with implications for the origin of olivine-phyric volcanic rocks. Journal of Petrology 43, 1651-1671.

Davidson, J. P., Morgan, D. J., Charlier, B. L. A., Harlou, R. and Hora, J. M. (2007). Microsampling and isotopic analysis of igneous rocks: Implications for the study of magmatic systems. Annual Review of Earth and Planetary Sciences 35, 273-311.

DePaolo, D. J. and Manga, M. (2003). Deep origin of hotspots - The mantle plume model. Science 300, 920-921.

Deutsch, E. R., Kristjansson, L. G. and May, B. T. (1971). Remanent magnetism of lower Tertiary lavas on Baffin Island. Canadian Journal of Earth Sciences 8, 1542-1552.

Donaldson, C. H. (1976). Experimental investigation of olivine morphology. Contributions to Mineralogy and Petrology 57, 187-213.

Dupré, B. and Allègre, C. J. (1983). Pb-Sr isotope variation in Indian Ocean basalts and mixing phenomena. Nature 303, 142-146.

Ellam, R. M. and Stuart, F. M. (2004). Coherent He-Nd-Sr isotope trends in high $^{3}He/^{4}He$ basalts: implications for a common reservoir, mantle heterogeneity and convection. Earth and Planetary Science Letters 228, 511-523.

Elliott, T. R., Hawkesworth, C. J. and Gronvold, K. (1991). Dynamic melting of the Iceland plume. Nature 351, 201-206.

Farley, K. A., Natland, J. H. and Craig, H. (1992). Binary mixing of enriched and undegassed (primitive?) mantle components (He, Sr, Nd, Pb) in Samoan Lavas. Earth and Planetary Science Letters 111, 183-199.

Farley, K. A. and Neroda, E. (1998). Noble gases in the Earth's mantle. Annual Review of Earth and Planetary Sciences 26, 189-218.

Fisher, D. E. (1985). Noble-gases from oceanic island basalts do not require an undepleted mantle source. Nature 316, 716-718.

Fitton, J. G. (2007). The OIB paradox, In: Foulger, G.R. and Jurdy, D.M. (Eds.) Plates, Plumes, and Planetary Processes, Geological Society of America Special Paper 430, 387-412.

Fitton, J. G. and Godard, M. (2004). Origin and evolution of magmas on the Ontong Java Plateau. In: Fitton, J. G., Mahoney, J. J., Wallace, P. J. and Saunders, A. D. (eds.) Origin and evolution of the Ontong Java Plateau. Geological Society, London, Special Publication 229, 151-178.

Fitton, J. G., Saunders, A. D., Kempton, P. D. and Hardarson, B. S. (2003). Does depleted mantle form an intrinsic part of the Iceland plume? Geochemistry Geophysics Geosystems 4, doi:10.1029/2002GC000424.

Fitton, J. G., Saunders, A. D., Larsen, L. M., Hardarson, B. S. and Norry, M. J. (1998). Volcanic rocks from the southeast Greenland margin at 63°N: composition, petrogenesis and mantle sources. Proceedings of the Ocean Drilling Program Scientific Results 152, 331-350.

Fitton, J. G., Saunders, A. D., Norry, M. J., Hardarson, B. S. and Taylor, R. N. (1997). Thermal and chemical structure of the Iceland plume. Earth and Planetary Science Letters 153, 197-208.

Foeken, J. P. T., Day, S. and Stuart, F. M. (2009). Cosmogenic ^{3}He exposure dating of the Quaternary basalts from Fogo, Cape Verdes: Implications for rift zone and magmatic reorganisation. Quaternary Geochronology 4, 37-49.

Foley, S. F., Barth, M. G. and Jenner, G. A. (2000). Rutile/melt partition coefficients for trace elements and an assessment of the influence of rutile on the trace element characteristics of subduction zone magmas. Geochimica et Cosmochimica Acta 64, 933-938.

Forte, A. M. and Mitrovica, J. X. (2001). Deep-mantle high-viscosity flow and thermochemical structure inferred from seismic and geodynamic data. Nature 410, 1049-1056.

Foulger, G. R., Natland, J. H. and Anderson, D. L. (2005). A source for Icelandic magmas in remelted Iapetus crust. Journal of Volcanology and Geothermal Research 141, 23-44.

Foulger, G. R. and Pearson, D. G. (2001). Is Iceland underlain by a plume in the lower mantle? Seismology and helium isotopes. Geophysical Journal International 145, F1-F5.

Francis, D. (1985). The Baffin Bay lavas and the value of picrites as analogues of primary magmas. Contributions to Mineralogy and Petrology 89, 144-154.

Fukao, Y., Widiyantoro, S. and Obayashi, M. (2001). Stagnant slabs in the upper and lower mantle transition region. Reviews of Geophysics 39, 291-323

Gaetani, G. A. and Watson, E. B. (2000). Open system behaviour of olivine-hosted melt inclusions. Earth and Planetary Science Letters 183, 27-41.

Gast, P. W., Hedge, C. and Tilton, G. R. (1964). Isotopic composition of lead and strontium from Ascension and Gough Islands. Science 145, 1181-1185.

Gill, R. C. O., Pedersen, A. K. and Larsen, J. G. (1992). Tertiary picrites in West Greenland: melting at the periphery of a plume? In: Storey, B. C., Alabaster, T. and Pankhurst, R. J. (eds.) Magmatism and the Causes of Continental Break-up. Geological Society, London, Special Publication 68, 335-348.

Gonnermann, H. M. and Mukhopadhyay, S. (2007). Non-equilibrium degassing and a primordial source for helium in ocean-island volcanism. Nature 449, 1037-1040.

Govindaraju, K. (1994). 1994 compilation of working values and sample description for 383 geostandards. Geostandards Newsletter 18, 331-331.

Graham, D. W., Larsen, L. M., Hanan, B. B., Storey, M., Pedersen, A. K. and Lupton, J. E. (1998). Helium isotope composition of the early Iceland mantle plume inferred from the Tertiary picrites of West Greenland. Earth and Planetary Science Letters 160, 241-255.

Grand, S. P. (1987). Tomographic inversion for shear velocity beneath the North American plate. Journal of Geophysical Research 92, 14,065-14,090.

Grand, S. P. (2002). Mantle shear-wave tomography and the fate of subducted slabs. Philosophical Transactions of the Royal Society of London. Series A: Mathematical, Physical and Engineering Sciences 360, 2475-2491.

Green, D. H., Falloon, T. J., Eggins, S. M. and Yaxley, G. M. (2001). Primary magmas and mantle temperatures. European Journal of Mineralogy 13, 437-452.

Green, T. H. and Pearson, N. J. (1986). Ti-rich accessory phase saturation in hydrous mafic-felsic compositions at high P,T. Chemical Geology 54, 185-201.

Gurenko, A. A., Hansteen, T. H. and Schmincke, H. U. (1996). Evolution of parental magmas of Miocene shield basalts of Gran Canaria (Canary Islands): Constraints from crystal, melt and fluid inclusions in minerals. Contributions to Mineralogy and Petrology 124, 422-435.

Hald, N. and Pedersen, A. K. (1975). Lithostratigraphy of the early Tertiary volcanic rocks of central West Greenland. Rapport Gronlands Geologiske Undersogelse 69, 17-24.

Hanan, B. B. and Graham, D. W. (1996). Lead and helium isotope evidence from oceanic basalts for a common deep source of mantle plumes. Science 272, 991-995.

Hanan, B. B., Blichert-Toft, J., Kingsley, R. and Schilling, J. G. (2000). Depleted Iceland mantle plume geochemical signature: Artifact of multicomponent mixing? Geochemistry Geophysics Geosystems 1, doi: 10.1029/1999GC000009.

Hanan, B. B. and Schilling, J. G. (1997). The dynamic evolution of the Iceland mantle plume: the lead isotope perspective. Earth and Planetary Science Letters 151, 43-60.

Hards, V. L., Kempton, P. D. and Thompson, R. N. (1995). The heterogeneous Iceland plume: new insights from the alkaline basalts of the Snaefell volcanic centre. Journal of the Geological Society 152, 1003-1009.

Harlou, R., Pearson, D. G., Davidson, J. P., Kamenetsky, V. S. and Yaxley, G. M. (2006). Source variability and crustal contamination of the Baffin Island picrites – coupled Sr isotope and trace element study of individual melt inclusions. Geochimica et Cosmochimica Acta 70, A231.

Hart, S. R., Hauri, E. H., Oschmann, L. A. and Whitehead, J. A. (1992). Mantle plumes and entrainment - isotopic evidence. Science 256, 517-520.

Hart, S. R., Kurz, M. D. and Wang, Z. (2008). Scale length of mantle heterogeneities: Constraints from helium diffusion. Earth and Planetary Science Letters 269, 507-516.

Hauri, E. H. and Hart, S. R. (1993). Re-Os isotope systematics of HIMU and EMII oceanic island basalts from the south-pacific ocean. Earth and Planetary Science Letters 114, 353-371.

Heber, V. S., Brooker, R. A., Kelley, S. P. and Wood, B. J. (2007). Crystal-melt partitioning of noble gases (helium, neon, argon, krypton, and xenon) for olivine and clinopyroxene. Geochimica et Cosmochimica Acta 71, 1041-1061.

Herzberg, C., Asimow, P. D., Arndt, N., Niu, Y. L., Lesher, C. M., Fitton, J. G., Cheadle, M. J. and Saunders, A. D. (2007). Temperatures in ambient mantle and plumes: Constraints from basalts, picrites, and komatiites. Geochemistry Geophysics Geosystems 8, doi: 10.1029/2006GC001390.

Herzberg, C. and O'Hara, M. J. (1998). Phase equilibrium constraints on the origin of basalts, picrites, and komatiites. Earth-Science Reviews 44, 39-79.

Herzberg, C. and O'Hara, M. J. (2002). Plume-associated ultramafic magmas of Phanerozoic age. Journal of Petrology 43, 1857-1883.

Hilton, D. R. and Porcelli, D. (2003). Noble Gases as Mantle Tracers. In: Carlson, R. W. (ed.) Treatise on Geochemistry Elsevier, 277-318.

Hilton, D. R., Thirlwall, M. F., Taylor, R. N., Murton, B. J. and Nichols, A. (2000). Controls on magmatic degassing along the Reykjanes Ridge with implications for the helium paradox. Earth and Planetary Science Letters 183, 43-50.

Hiyagon, H. (1994). Retention of solar helium and neon in IDPS in deep-sea sediment. Science 263, 1257-1259.

Hiyagon, H., Ozima, M., Marty, B., Zashu, S. and Sakai, H. (1992). Noble-gases in submarine glasses from mid-ocean ridges and Loihi Seamount - constraints on the early history of the Earth. Geochimica et Cosmochimica Acta 56, 1301-1316.

Hofmann, A. W. (1988). Chemical differentiation of the Earth: the relationship between mantle, continental-crust, and oceanic-crust. Earth and Planetary Science Letters 90, 297-314.

Hofmann, A. W. (1997). Mantle geochemistry: The message from oceanic volcanism. Nature 385, 219-229.

Hofmann, A. W. and White, W. M. (1982). Mantle plumes from ancient oceanic-crust. Earth and Planetary Science Letters 57, 421-436.

Holm, P. M., Gill, R. C. O., Pedersen, A. K., Larsen, J. G., Hald, N., Nielsen, T. F. D. and Thirlwall, M. F. (1993). The Tertiary picrites of West Greenland: contributions from Icelandic and other sources. Earth and Planetary Science Letters 115, 227-244.

Honda, M., McDougall, I., Patterson, D. B., Doulgeris, A. and Clague, D. A. (1991). Possible solar noble-gas component in Hawaiian basalts. Nature 349, 149-151.

Jackson, G. D. and Taylor, F. C. (1972). Correlation of major Aphebian rock units in Northeastern Canadian Shield. Canadian Journal of Earth Sciences 9, 1650-1669.

Jackson, M. G. and Dasgupta, R. (2008). Compositions of HIMU, EM1, and EM2 from global trends between radiogenic isotopes and major elements in ocean island basalts. Earth and Planetary Science Letters 276, 175-186.

Jackson, M. G. and Hart, S. R. (2006). Strontium isotopes in melt inclusions from Samoan basalts: Implications for heterogeneity in the Samoan plume. Earth and Planetary Science Letters 245, 260-277.

Jackson, M. G., Kurz, M. D., Hart, S. R. and Workman, R. K. (2007). New Samoan lavas from Ofu Island reveal a hemispherically heterogeneous high $^{3}He/^{4}He$ mantle. Earth and Planetary Science Letters 264, 360-374.

Jochum, K. P., Seufert, H. M. and Thirlwall, M. F. (1990). High sensitivity Nb analysis by spark-source mass spectrometry (SSMS) and calibration of XRF Nb and Zr. Chemical Geology 81, 1-16.

Kamenetsky, V. S., Crawford, A. J., Eggins, S. and Muhe, R. (1997). Phenocryst and melt inclusion chemistry of near-axis seamounts, Valu Fa Ridge, Lau Basin: insight into mantle wedge melting and the addition of subduction components. Earth and Planetary Science Letters 151, 205-223.

Kamenetsky, V. S. and Gurenko, A. A. (2007). Cryptic crustal contamination of MORB primitive melts recorded in olivine-hosted glass and mineral inclusions. Contributions to Mineralogy and Petrology 153, 465-481.

Kamenetsky, V. S., Sobolev, A. V., Joron, J. L. and Semet, M. P. (1995). Petrology and geochemistry of Cretaceous ultramafic volcanics from eastern Kamchatka. Journal of Petrology 36, 637-662.

Karato, S. I. (1996). Seismic anisotropy in the deep mantle, boundary layers and the geometry of mantle convection. International Workshop on Geodynamics of the Lithosphere and the Earths Mantle - Seismic Anisotropy as a Record of the Past and Present Dynamic Processes. Trest, Czech Republic, 565-587.

Keller, W. R., Anderson, D. L. and Clayton, R. W. (2000). Resolution of tomographic models of the mantle beneath Iceland. Geophysical Research Letters 27, 3993-3996.

Kellogg, L. H., Hager, B. H. and van der Hilst, R. D. (1999). Compositional stratification in the deep mantle. Science 283, 1881-1884.

Kempton, P. D., Fitton, J. G., Saunders, A. D., Nowell, G. M., Taylor, R. N., Hardarson, B. S. and Pearson, G. (2000). The Iceland plume in space and time: a Sr-Nd-Pb-Hf study of the North Atlantic rifted margin. Earth and Planetary Science Letters 177, 255-271.

Kent, A. J. R. (2008). Melt Inclusions in Basaltic and Related Volcanic Rocks. In: Putirka, K. D. and Tepley, F. J. (eds.) Reviews in Mineralogy and Geochemistry 69, 273-331.

Kent, A. J. R., Baker, J. A. and Wiedenbeck, M. (2002). Contamination and melt aggregation processes in continental flood basalts: constraints from melt inclusions in Oligocene basalts from Yemen. Earth and Planetary Science Letters 202, 577-594.

Kent, A. J. R., Norman, M. D., Hutcheon, I. D. and Stolper, E. M. (1999). Assimilation of seawater-derived components in an oceanic volcano: evidence from matrix glasses and glass inclusions from Loihi seamount, Hawaii. Chemical Geology 156, 299-319.

Kent, A. J. R., Stolper, E. M., Francis, D., Woodhead, J., Frei, R. and Eiler, J. (2004). Mantle heterogeneity during the formation of the North Atlantic Igneous Province: Constraints from trace element and Sr-Nd-Os-O isotope systematics of Baffin Island picrites. Geochemistry Geophysics Geosystems 5, doi:10.1029/2004GC000743.

Kerr, A. C., Saunders, A. D., Tarney, J., Berry, N. H. and Hards, V. L. (1995). Depleted mantle-plume geochemical signatures: No paradox for plume theories. Geology 23, 843-846.

Kress, V. C. and Ghiorso, M. S. (2004). Thermodynamic modelling of post-entrapment crystallization in igneous phases. Journal of Volcanology and Geothermal Research 137, 247-260.

Krishnamurthy, P. and Cox, K. G. (1977). Picrite basalts and related lavas from Deccan Traps of Western India. Contributions to Mineralogy and Petrology 62, 53-75.

Kurz, M. D. (1986). In situ production of terrestrial cosmogenic helium and some applications to geochronology. Geochimica et Cosmochimica Acta 50, 2855-2862

Kurz, M. D. and Geist, D. (1999). Dynamics of the Galapagos hotspot from helium isotope geochemistry. Geochimica et Cosmochimica Acta 63, 4139-4156.

Kurz, M. D. and Kammer, D. P. (1991). Isotopic evolution of Mauna Loa volcano. Earth and Planetary Science Letters 103, 257-269.

Kurz, M. D., Jenkins, W. J. and Hart, S. R. (1982). Helium isotopic systematics of oceanic islands and mantle heterogeneity. Nature 297, 43-47.

Labrosse, S., Hernlund, J. W. and Coltice, N. (2007). A crystallizing dense magma ocean at the base of the Earth's mantle. Nature 450, 866-869.

Larsen, H. C. and Saunders, A. D. (1998). Tectonism and volcanism at the southeast Greenland rifted margin: A record of plume impact and later continental rupture. In: Saunders, A. D., Larsen, H. C. and Wise, S. W. (eds.) Proceedings of the Ocean Drilling Program, Scientific Results 152, 503-533.

Larsen, L. M. and Pedersen, A. K. (2000). Processes in high-mg, high-T magmas: Evidence from olivine, chromite and glass in Palaeogene picrites from West Greenland. Journal of Petrology 41, 1071-1098.

Larsen, L. M. and Pedersen, A. K. (2009). West Greenland was hot – how else can you make 22,000 km^3 of picrites? : http://www.mantleplumes.org.

Larsen, L. M., Pedersen, A. K., Sundvoll, B. and Frei, R. (2003). Alkali picrites formed by melting of old metasomatized lithospheric mantle: Manîtdlat member, Vaigat Formation, Palaeocene of West Greenland. Journal of Petrology 44, 3-38.

Lass-Evans, S. (2004). The anatomy of the ancestral Iceland Plume: a chemical and isotopic study of the Tertiary basalts and picrites from Baffin Island. PhD Thesis. University of Edinburgh.

Lay, T., Williams, Q. and Garnero, E. J. (1998). The core-mantle boundary layer and deep Earth dynamics. Nature 392, 461-468.

Le Bas, M. J. (2000). IUGS reclassification of the high-Mg and picritic volcanic rocks. Journal of Petrology 41, 1467-1470.

Le Maitre, R. W., Bateman, P., Dudek, A., Keller, J., Lameyre Le Bas, M. J., Sabine, P. A., Schmid, R., Sorensen, H., Streckeisen, A., Woolley, A. R. and Zanettin, B. (1989). A classification of igneous rocks and glossary of terms. Blackwell, Oxford.

Lightfoot, P. C., Hawkesworth, C. J., Olshefsky, K., Green, T., Doherty, W. and Keays, R. R. (1997). Geochemistry of Tertiary tholeiites and picrites from Qeqertarssuaq (Disko Island) and Nuussuaq, West Greenland with implications for the mineral potential of comagmatic intrusions. Contributions to Mineralogy and Petrology 128, 139-163.

Lowenstern, J. B. (1994). Chlorine, fluid immiscibility, and degassing in peralkaline magmas from Panterlleria, Italy. American Mineralogist 79, 353-369.

Maclennan, J. (2008). Lead isotope variability in olivine-hosted melt inclusions from Iceland. Geochimica et Cosmochimica Acta 72, 4159-4176.

Maclennan, J., McKenzie, D., Hilton, F., Grönvold, K. and Shimizu, N. (2003). Geochemical variability in a single flow from northern Iceland. Journal of Geophysical Research 108, paper number 2007.

Macpherson, C. G., Hilton, D. R., Day, J. M. D., Lowry, D. and Grönvold, K. (2005). High-$^{3}He/^{4}He$, depleted mantle and low-$\delta^{18}O$, recycled oceanic lithosphere in the source of central Iceland magmatism. Earth and Planetary Science Letters 233, 411-427.

Mahoney, J. J., Graham, D. W., Christie, D. M., Johnson, K. T. M., Hall, L. S. and Vonderhaar, D. L. (2002). Between a Hotspot and a Cold Spot: Isotopic Variation in the Southeast Indian Ridge Asthenosphere, $86^{o}E$-$118^{o}E$. Journal of Petrology 43, 1155-1176.

Mamyrin, B. A., Tolstikhin, I. N, Anufriyev, G. S. and Kamenskiy, I. L. (1969). Anomalous isotopic composition of helium in volcanic gas. Doklady Akademii Nauk SSR 184, 1197-1199.

Marty, B. and Lussiez, P. (1993). Constraints on rare-gas partition coefficients from analysis of olivine glass from a picritic mid-ocean ridge basalt. Chemical Geology 106, 1-7.

Marty, B., Upton, B. G. J. and Ellam, R. M. (1998). Helium isotopes in early Tertiary basalts, northeast Greenland: Evidence for 58 Ma plume activity in the north Atlantic-Iceland volcanic province. Geology 26, 407-410.

Montelli, R., Nolet, G., Masters, G., Dahlen, F. A. and Hung, S.-H. (2003). Finite frequency global P wave tomography. EGS-AGU-EUG Joint Assembly, Abstracts from the meeting held in Nice, France, 6-11 April 2003.

Morgan, J. P. (1999). Isotope topology of individual hotspot basalt arrays: Mixing curves or melt extraction trajectories? Geochemistry Geophysics Geosystems 1, 1003, doi:10.1029/1999GC000004.

Morgan, W. J. (1971). Convection plumes in lower mantle. Nature 230, 42-43.

Neuhoff, P. S., Rogers, K. L., Stannius, L. S., Bird, D. K. and Pedersen, A. K. (2006). Regional very low-grade metamorphism of basaltic lavas, Disko-Nuussuaq region, West Greenland. Lithos 92, 33-54.

Nielsen, R. L., Crum, J., Bourgeois, R., Hascall, K., Forsythe, L. M., Fisk, M. R. and Christie, D. M. (1995). Melt inclusions in high-An plagioclase from the Gorda Ridge: an example of the local diversity of MORB parent magmas. Contributions to Mineralogy and Petrology 122, 34-50.

Nielsen, R. L., Michael, P. J. and Sours-Page, R. (1998). Chemical and physical indicators of compromised melt inclusions. Geochimica et Cosmochimica Acta 62, 831-839.

Norman, M. D., Garcia, M. O., Kamenetsky, V. S. and Nielsen, R. L. (2002). Olivine-hosted melt inclusions in Hawaiian picrites: Equilibration, melting, and plume source characteristics. Chemical Geology 183, 143-168.

Norrish, K. and Hutton, J. T. (1969). An accurate X-ray spectrographic method for the analysis of a wide range of geological samples. Geochimica et Cosmochimica Acta 33, 431–453.

O'Hara, M. J. (1968). Are Ocean Floor Basalts Primary Magma? Nature 220, 683-686.

Olive, V., Ellam, R. M. and Wilson, L. (2001). A protocol for the determination of the rare earth elements at picomole level in rocks by ICP-MS: Results on geological reference materials USGS PCC-1 and DTS-1. Geostandards Newsletter-the Journal of Geostandards and Geoanalysis 25, 219-228.

Onions, R. K. and Oxburgh, E. R. (1983). Heat and helium in the Earth. Nature 306, 429-431.

Parman, S. W. (2007). Helium isotopic evidence for episodic mantle melting and crustal growth. Nature 446, 900-903.

Parman, S. W., Kurz, M. D., Hart, S. R. and Grove, T. L. (2005). Helium solubility in olivine and implications for high $^{3}He/^{4}He$ in ocean island basalts. Nature 437, 1140-1143.

Peate, D. W., Peate Ukstins, I., Behanish, S. and Kent, A. J. R. (2007). Petrogenesis of West Greenland picrites: a melt inclusion perspective. Geological Society of America abstracts with programs, 39, 57 (29-12).

Pedersen, A. K. (1985). Reaction between picrite magma and continental crust: early Tertiary silicic basalts and magnesian andesites from Disko, West Greenland. Bulletin Gronlands Geologiske Undersogelse 152.

Pedersen, A. K., Larsen, L. M., Riisager, P. and Dueholm, K. S. (2002). Rates of volcanic deposition, facies changes and movements in a dynamic basin: the Nuussuaq Basin, West Greenland, around the C27n-C26r transition. In: Jolley, D. W. and Bell, B. R. (eds.) The North Atlantic Igneous Province: stratigraphy, tectonics, volcanic and magmatic processes. Geological Society, London, Special Publication 197, 157-181.

Porcelli, D. and Ballentine, C. J. (2002). Models for the distribution of terrestrial noble gases and evolution of the atmosphere. In: Porcelli, D., Ballentine, C. J. and Wieler, R. (eds.) Reviews in Mineralogy and Geochemistry 47, 411-480.

Porcelli, D. and Elliott, T. (2008). The evolution of He Isotopes in the convecting mantle and the preservation of high $^{3}He/^{4}He$ ratios. Earth and Planetary Science Letters 269, 175-185.

Porcelli, D. and Halliday, A. N. (2001). The core as a possible source of mantle helium. Earth and Planetary Science Letters 192, 45-56.

Porcelli, D. and Pepin, R. O. (2000). Rare gas constraints on early Earth history. In: Canup, R. and Righter, K. (eds.) Origin of the Earth and Moon, University of Arizona Press, Tucson, AZ, 435-458.

Prytulak, J. & Elliott, T. (2007). TiO_2 enrichment in ocean island basalts. Earth and Planetary Science Letters 263, 388-403

Qin, Z. W., Lu, F. Q. and Anderson, A. T. (1992). Diffusive reequilibration of melt and fluid inclusions. American Mineralogist 77, 565-576.

Reynolds, R. C. (1963). Matrix corrections in trace element analysis by x-ray fluorescence: estimation of mass absorption coefficient by compton scattering. American Mineralogist 48, 1133-1143.

Robillard, I., Francis, D. and Ludden, J. N. (1992). The relationship between E-type and N-type magmas in the Baffin Bay lavas. Contributions to Mineralogy and Petrology 112, 230-241.

Roedder, E. (1979). Origin and significance of magmatic inclusions. Bulletin De Mineralogie 102, 487-510.

Roedder, E. (1984). Fluid Inclusions. Reviews in Mineralogy 12, 1-644.

Roedder, P. L. and Emslie, R. F. (1970). Olivine-liquid equilibrium. Contributions to Mineralogy and Petrology 29, 275-289.

Roest, W. R. and Srivastava, S. P. (1989). Sea-floor spreading in the Labrador Sea: a new reconstruction. Geology 17, 1000-1003.

Rudge, J. F. (2008). Finding peaks in geochemical distributions: A re-examination of the helium-continental crust correlation. Earth and Planetary Science Letters 274, 179-188.

Ryerson, F. J. and Watson, E. B. (1987). Rutile saturation in magmas - implications for Ti-Nb-Ta depletion in island-arc basalts. Earth and Planetary Science Letters 86, 225-239.

Saal, A. E., Hart, S. R., Shimizu, N., Hauri, E. H. and Layne, G. D. (1998). Pb isotopic variability in melt inclusions from oceanic island basalts, Polynesia. Science 282, 1481-1484.

Salters, V. J. M. and Stracke, A. (2004). Composition of the depleted mantle. Geochemistry Geophysics Geosystems 5, doi: 10.1029/2003GC000597.

Samuel, H. and Farnetani, C. G. (2003). Thermochemical convection and helium concentrations in mantle plumes. Earth and Planetary Science Letters 207, 39-56.

Saunders, A. D., Fitton, J. G., Norry, M. J. and Kent, R. W. (1997). The North Atlantic Igneous Province. In: Mahoney, J. J. and Coffin, M. F. (eds.) Large Igneous Provinces American Geophysical Union Monograph, 45-93.

Saunders, A. D., Norry, M. J. and Tarney, J. (1988). Origin of MORB and chemically-depleted mantle reservoirs: trace element constraints. In: Menzies, M. A. and Cox, K. G. (eds.) Oceanic and Continental Lithosphere: Similarities and Differences. Journal of Petrology Special Issue, 415-445.

Scarrow, J. H. and Cox, K. G. (1995). Basalts generated by decompressive adiabatic melting of a mantle plume: a case study from the Isle of Skye, NW Scotland. Journal of Petrology 36, 3-22.

Schersten, A., Elliott, T., Hawkesworth, C. and Norman, M. (2004). Tungsten isotope evidence that mantle plumes contain no contribution from the Earth's core. Nature 427, 234-237.

Schmalzl, J., Houseman, G. A. and Hansen, U. (1995). Mixing properties of 3-dimensional (3D) stationary convection. Physics of Fluids 7, 1027-1033.

Shen, Y., Solomon, S. C., Bjarnason, I. T. and Wolfe, C. J. (1998). Seismic evidence for a lower-mantle origin of the Iceland plume. Nature 395, 62-65.

Shimizu, N. (1998). The geochemistry of olivine-hosted melt inclusions in a FAMOUS basalt ALV519-4-1. Physics of the Earth and Planetary Interiors 107, 183-201.

Shuster, D. L., Farley, K. A., Sisterson, J. M. and Burnett, D. S. (2004). Quantifying the diffusion kinetics and spatial distributions of radiogenic ^{4}He in minerals containing proton-induced ^{3}He. Earth and Planetary Science Letters 217, 19-32.

Sinton, C. W., Christie, D. M., Coombs, V. L., Nielsen, R. L. and Fisk, M. R. (1993). Near-primary melt inclusions in anorthite phenocrysts from the Galapagos Platform. Earth and Planetary Science Letters 119, 527-537.

Sinton, J. M. and Detrick, R. S. (1992). Midocean ridge magma chambers. Journal of Geophysical Research 97, 197-216.

Skovgaard, A. C., Storey, M., Baker, J., Blusztajn, J. and Hart, S. R. (2001). Osmium-oxygen isotopic evidence for a recycled and strongly depleted component in the Iceland mantle plume. Earth and Planetary Science Letters 194, 259-275.

Slater, L., McKenzie, D., Grönvold, K. and Shimizu, N. (2001). Melt generation and movement beneath Theistareykir, NE Iceland. Journal of Petrology 42, 321-354.

Smit, Y., Schiano, P. and Faure, F. (2004). Melt inclusions in primitive olivines from Padloping Island, Baffin Bay. American Geophysical Union Fall Meeting abstracts V31C-1446.

Sobolev, A. V. (1996). Melt inclusions as a source of primary petrographic information. Petrology 4, 209-220.

Sobolev, A. V. and Shimizu, N. (1993). Ultra-depleted primary melt included in an olivine from the Mid-Atlantic ridge. Nature 363, 151-154.

Sobolev, A. V. and Chaussidon, M. (1996). H_2O concentrations in primary melts from supra-subduction zones and mid-ocean ridges: Implications for H_2O storage and recycling in the mantle. Earth and Planetary Science Letters 137, 45-55.

Spandler, C., O'Neill, H. S. C. and Kamenetsky, V. S. (2007). Survival times of anomalous melt inclusions from element diffusion in olivine and chromite. Nature 447, 303-306.

Starkey, N. A., Stuart, F. M., Ellam, R. M., Fitton, J. G., Basu, S. and Larsen, L. M. (2009). Helium isotopes in early Iceland plume picrites: Constraints on the composition of high $^{3}He/^{4}He$ mantle. Earth and Planetary Science Letters 277, 91-100.

Staudacher, T. and Allègre, C. J. (1988). Recycling of oceanic crust and sediments: the noble gas subduction barrier. Earth and Planetary Science Letters 89, 173-183.

Storey, M., Duncan, R. A., Pedersen, A. K., Larsen, L. M. and Larsen, H. C. (1998). $^{40}Ar/^{39}Ar$ geochronology of the West Greenland Tertiary volcanic province. Earth and Planetary Science Letters 160, 569-586.

Stuart, F. M., Ellam, R. M., Harrop, P. J., Fitton, J. G. and Bell, B. R. (2000). Constraints on mantle plumes from the helium isotopic composition of basalts from the British Tertiary Igneous Province. Earth and Planetary Science Letters 177, 273-285.

Stuart, F. M., Lass-Evans, S., Fitton, J. G. and Ellam, R. M. (2003). High $^{3}He/^{4}He$ ratios in picritic basalts from Baffin Island and the role of a mixed reservoir in mantle plumes. Nature 424, 57-59.

Su, Y. (2003). Global MORB chemistry compilation at the segment scale. PhD Thesis. Department of Earth and Environmental Sciences, Colombia University.

Sudo, M., Ohtaka, O. and Matsuda, J. (1994). Noble gas partitioning between metal and silicate under high pressures: the case of iron and peridotite. In: Matsuda, J. (ed.)

Noble Gas Geochemistry and Cosmochemistry Terra Scientific Publishing Company, 355-372.

Tackley, P. J. (2000). Mantle convection and plate tectonics: Toward an integrated physical and chemical theory. Science 288, 2002-2007.

Tait, S. (1992). Selective preservation of melt inclusions in igneous phenocrysts. American Mineralogist 77, 146-155.

Taylor, R. N., Thirlwall, M. F., Murton, B. J., Hilton, D. R. and Gee, M. A. M. (1997). Isotopic constraints on the influence of the Icelandic plume. Earth and Planetary Science Letters 148, 1-8.

Theriault, R. J., St-Onge, M. R. and Scott, D. J. (2001). Nd isotopic and geochemical signature of the Paleoproterozoic Trans-Hudson Orogen, southern Baffin Island, Canada: implications for the evolution of eastern Laurentia. Precambrian Research 108, 113-138.

Thirlwall, M. F. (1995). Generation of the Pb isotopic characteristics of the Iceland plume. Journal of the Geological Society 152, 991-996.

Thirlwall, M. F., Gee, M. A. M., Taylor, R. N. and Murton, B. J. (2004). Mantle components in Iceland and adjacent ridges investigated using double-spike Pb isotope ratios. Geochimica et Cosmochimica Acta 68, 361-386.

Tolstikhin, I. and Hofmann, A. W. (2005). Early crust on top of the Earth's core. Physics of the Earth and Planetary Interiors 148, 109-130.

van der Hilst, R. D., Widiyantoro, S. and Engdahl, E. R. (1997). Evidence for deep mantle circulation from global tomography. Nature 386, 578-584.

van Keken, P. E. and Ballentine, C. J. (1998). Whole-mantle versus layered mantle convection and the role of a high-viscosity lower mantle in terrestrial volatile evolution. Earth and Planetary Science Letters 156, 19-32.

van Keken, P. E. and Ballentine, C. J. (1999). Dynamical models of mantle volatile evolution and the role of phase transitions and temperature-dependent rheology. Journal of Geophysical Research 104, 7137-7151.

van Keken, P. E., Hauri, E. H. and Ballentine, C. J. (2002). Mantle mixing: The generation, preservation, and destruction of chemical heterogeneity. Annual Review of Earth and Planetary Sciences 30, 493-525.

Vogt, P. R. and Avery, O. E. (1974). Detailed magnetic surveys in northeast Atlantic and Labrador Sea. Journal of Geophysical Research 79, 363-389.

Wessel, P. and Lyons, S. (1997). Distribution of large Pacific seamounts from Geosat/ERS-1: Implications for the history of intraplate volcanism. Journal of Geophysical Research 102, 22,459-22,475.

Williams, A. J., Stuart, F. M., Day, S. J. and Phillips, W. M. (2005). Using pyroxene microphenocrysts to determine cosmogenic ^{3}He concentrations in old volcanic rocks: an example of landscape development in central Gran Canaria. Quaternary Science Reviews 24, 211-222.

Wolfe, C. J., Bjarnason, I. Th., VanDecar, J. C. and Solomon, S. C. (2002). Assessing the depth of tomographic models of upper mantle structure beneath Iceland. Geophysical Research Letters 29 (2), doi: 10.1029/2001GL013657.

Workman, R. K. and Hart, S. R. (2005). Major and trace element composition of the depleted MORB mantle (DMM). Earth and Planetary Science Letters 231, 53-72.

Yaxley, G. M., Kamenetsky, V. S., Kamenetsky, M., Norman, M. D. and Francis, D. (2004). Origins of compositional heterogeneity in olivine-hosted melt inclusions from the Baffin Island picrites. Contributions to Mineralogy and Petrology 148, 426-442.

Zindler, A. and Hart, S. (1986). Chemical Geodynamics. Annual Review of Earth and Planetary Sciences 14, 493-571.

Appendix

Appendix A: Analytical Methods

A1 Crushing and powdering

Baffin Island samples were available at SUERC as large rock samples weighing over 1kg each. West Greenland samples were received from GEUS as smaller fragments of less than 0.5kg and also as powders (powdered in tungsten-carbide at GEUS). The rock samples from both Baffin Island and West Greenland were washed, dried and coarsely crushed (<2mm) in a jaw crusher at SUERC, East Kilbride (by S. Basu, SUERC) for Baffin Island samples and at the University of Edinburgh for West Greenland samples. Portions of Baffin Island crushed rock were separated and powdered in agate at the University of Edinburgh for XRF, ICP-MS and TIMS analyses. Prior to powdering, portions of crushed rock from Baffin Island and West Greenland samples were separated from the coarsely crushed rock for olivine crystals to be picked from for helium isotope analyses.

A2 X-ray fluorescence (XRF) spectrometry

XRF analyses were carried out in the Grant Institute at the University of Edinburgh. The techniques used are similar to those described by Fitton et al. (1998), with modifications noted by Fitton and Godard (2004).

Major-element concentrations were determined after fusion with a lithium borate flux containing La_2O_3 as a heavy absorber, by a method similar to that developed by Norrish and Hutton (1969). Rock powder was dried at 110°C for at least 1 hour, and a nominal but precisely-weighed 1-g aliquot ignited at 1100°C to determine loss on ignition (LOI). The residue was then mixed with Johnson Matthey Spectroflux™ 105 in a sample:flux ratio of 1:5, based on the *unignited* sample mass, and fused in a muffle furnace in a Pt5%Au crucible. After the initial fusion, the crucible was reweighed and any flux weight loss was made up with extra flux. After a second fusion over a Meker burner, the molten mixture was swirled several times to ensure homogeneity, cast onto a graphite mold, and flattened with an aluminium plunger

into a thin disk. The mold and plunger were maintained at a temperature of 220° C on a hotplate.

Trace-element concentrations were determined on pressed-powder samples. Eight grams of rock powder were mixed thoroughly with eight drops of a 2% aqueous solution of polyvinyl alcohol. The mixture was loaded into a 40-mm diameter aluminium cup in a stainless steel die and compressed against a polished tungsten carbide disc in a hydraulic press at 0.6 tons/cm^2.

The fused and pressed samples were analyzed using a Philips PW 2404 automatic X-ray fluorescence spectrometer with a Rh-anode X-ray tube. Trace-element background positions were placed as close as possible to peaks, and long count times were used at both peak and background positions. Where background count rates were measured on either side of the peak, as in most trace-element determinations, the count time was divided between the two positions. Analytical conditions are given in Fitton et al. (1998) and Fitton and Godard (2004).

Corrections for matrix effects on the intensities of major-element lines were made using theoretical alpha coefficients calculated on-line using the Philips software. The coefficients were calculated to allow for the amount of extra flux replacing volatile components in the sample so that analytical totals should be 100% less the measured LOI. Intensities of the longer wavelength trace-element lines (La, Ce, Nd, Cu, Ni, Co, Cr, V, Ba, and Sc) were corrected for matrix effects using alpha coefficients based on major-element concentrations measured at the same time on the powder samples. Matrix corrections were applied to the intensities of the other trace-element lines by using the count rate from the RhK_a Compton scatter line as an internal standard (Reynolds, 1963). Line-overlap corrections were applied using synthetic standards.

The spectrometer was calibrated against USGS and CRPG geochemical reference standards using the values given by Govindaraju (1994) except that the values of Jochum et al. (1990) were used for Nb and Zr in BCR-1 and BHVO-1. Excellent

calibration lines were obtained using these standards. Analytical precision and accuracy are comparable to the values reported by Fitton et al. (1998) and Fitton and Godard (2004). Four USGS geostandards were analysed along with the Baffin Island and West Greenland samples and the data from these (Table A2) can be used to assess accuracy and precision.

Table A2. Trace element concentrations in international standards measured at the University of Edinburgh by XRF compared with recommended values.

	BHVO-1			BCR-1			BIR-1			DTS-1		
	R	E	1σ	R	E	1σ	R	E	1σ	R	E	1σ
Nb	19.8	19.8	0.05	13.6	13.0	0.07	0.6	0.6	0.14	0	0.1	0.06
Zr	182	175.0	0.10	186	192.3	0.60	15.5	16.2	0.19	0.23	0.3	0.12
Y	27.6	27.3	0.09	38	38.0	0.43	16.0	16.3	0.15	0.04	0.0	0.12
Sr	403	396.4	0.94	330	336.2	1.72	108	107.5	1.16	0.32	0.0	0.12
Rb	11	9.1	0.27	47.2	47.1	1.20	0.25	0.2	0.13	0.058	0.0	0.06
Zn	105	105.3	0.42	129.5	130.4	0.31	71	66.7	0.60	46	46	0.5
Cu	136	132.0	0.54	19	19.7	0.35	126	130.0	0.40	7.1	7	0.2
Ni	121	124.5	0.96	13	15.8	4.25	166	160.3	2.76	2360	2323	2.5
Cr	289	292.5	2.58	16	9.7	6.54	382	385.7	5.19	3990	3821	93
V	317	311.4	1.48	407	403.0	2.20	313	323.3	2.37	11	10	0.7
Ba	139	135.2	3.22	681	681.7	2.88	7	8.2	0.70	1.7	4.3	1.4
Sc	31.8	33.0	0.88	32.6	33.5	0.39	44	42.3	0.51	3.5	2.7	0.4

R. Recommended values from Govindaraju (1994) (except Nb and Zr in BHVO-1 and BCR-1 which are from Jochum et al., 1990).
E. Mean and standard deviation of six measurements carried out in Edinburgh during this study.

A3 Multi-collector Inductively Coupled Plasma Emission Mass Spectrometry

Rare Earth elements (REE), Hf, Ta, Pb, Th and U were determined by ICP-MS at SUERC, East Kilbride. ~0.1g of whole-rock powder was measured accurately into a PFA Teflon screw top beaker. Powders were dissolved using HF/HNO_3-HNO_3-6M HCl acid digestion on a 150ºC hotplate. For the REE, samples were diluted in 5% HNO_3 by a factor of 5000. 10ml of each sample was spiked with 0.1ml (1ppm solution) of In, Re and Ru. For Hf, Ta, Pb, Th and U, samples were diluted in 5% HNO_3 by a factor of 1000. 10ml of each sample was spiked with 0.1ml (1ppm solution) of In, Re and Bi. During the analytical procedure a blank, International Standards and external drift correcting solution were run interspersed with samples to allow for calibration and correction (Table A4). Further details of the analytical procedure can be found in Olive et al. (2001).

Table A3. Trace element precisions for BCR-1.

	Average	1σ	Relative Standard Deviation
La	24.6	0.44	1.79
Ce	53.0	0.99	1.87
Pr	6.7	0.13	1.86
Nd	28.4	0.56	1.98
Sm	6.5	0.15	2.37
Eu	1.9	0.04	2.10
Gd	6.6	0.15	2.28
Tb	1.0	0.02	2.36
Dy	6.3	0.15	2.34
Ho	1.2	0.03	2.51
Er	3.6	0.10	2.68
Tm	0.6	0.01	2.68
Yb	3.3	0.08	2.53
Lu	0.5	0.01	2.88
Hf	5.2	0.20	3.88
Ta	0.8	0.02	2.45
Pb	13.8	0.30	2.16
Th	6.1	0.09	1.49
U	1.8	0.02	1.30

A4 Thermal Ionisation Mass Spectrometry (TIMS)

Strontium and Neodymium isotopic values ($^{87}Sr/^{86}Sr$ and $^{143}Nd/^{144}Nd$) were determined using a VG Sector 54-30 thermal ionisation mass spectrometer at SUERC, East Kilbride. The instrument was operated in dynamic peak-jumping mode measuring Sr^+ and Nd^+ ions. Data were monitored and corrected for minor isobaric interferences (^{87}Rb and ^{144}Sm) and for mass fractionation using the exponential law and assuming the ratios given in Table 3. ~0.1g of whole-rock powder was measured accurately into a PFA Teflon screw top beaker. Powders were dissolved using HF/HNO_3-HNO_3-6M HCl acid digestion on a hotplate at 150°C. Sr and REE were separated using cation exchange chromatography. Dissolved samples were loaded in 2ml of 2.5M HCl onto pre-conditioned cation exchange columns containing Bio-Rad AG50W X8 200-400 mesh resin in 2.5M HCl. The Sr fraction was collected in 2.5M HCl and dried down under hot-lamps with a constant stream of filtered air through Teflon drying hoods. The REE fraction was eluted in 2.5M HCl and collected in 3M HNO_3 and again dried down under hot-lamps. The REE fraction was dissolved in a mixture of acetic acid, methanol and nitric acid and was loaded into anion exchange

columns containing Bio-Rad AG1 X8 200-400 mesh resin. Nd was eluted and dried under hot-lamps.

Sr fractions were dissolved in 1µl 1M H_3PO_4 and loaded onto single Ta filaments. Nd fractions were dissolved in 1µl of H_2O and loaded onto single Ta side filaments of Ta-Re-Ta filaments. The standard analysed for Sr analyses was NBS987 and for Nd analyses was the Johnson and Matthey Nd standard (Table A4).

Table A4. Information on Sr and Nd isotope standards run during analyses of samples in this study

		NBS987 87/86		J&M 143/144
mean		0.7102537		0.511515
stdev		0.0000097		0.000009
%stdev		0.0013687		0.0017
StErr		0.0000016		0.0000029
%StErr		0.0002250		0.0005754
Fractionation control	86/88	0.1194	146/144	0.7219

A5 Helium isotope analyses

Helium isotope ($^3He/^4He$) analyses were carried out at the Noble Gas Laboratory at SUERC, East Kilbride. Olivine phenocrysts were separated from coarsely crushed rock by picking under binocular microscope. Care was taken to pick a representative population of olivine phenocryst sizes from the crushed rock that had been sieved and separated into size fractions (>2mm, 1-2mm, 0.5-1mm, 0.25-0.5mm and <0.25mm) which were washed in tap water to remove dust. Once ~2g of olivine phenocrysts were picked they were ultrasonically cleaned in 20% HNO_3 followed by 1% oxalic acid to digest any adhering basalt, carbonate and clay from the surface of crystals then rinsed in de-ionised water. Following these cleaning steps it was necessary to re-pick the crystals to remove any remaining crystals that showed alteration or adhering basalt. The sample was then cleaned ultrasonically in Analar acetone for 15 minutes.

Approximately 1g of clean olivine phenocrysts were loaded into 25mm diameter stainless steel pots with single layers of phenocrysts separated by 2mm think stainless steel plates. 10 pots were loaded into the multi-sample hydraulic crusher. The crusher was baked at in excess of 100ºC for 24 hours prior to gas extraction. All samples were crushed at between 500 and 2000 psi. Crushing ceased before all crystals were completely powdered in order to prevent release of lattice-stored helium. Gases were exposed to two SAES GP50 getters at 500ºC for 20 minutes to remove active gases then to activated charcoal cooled to 77ºK by liquid nitrogen for 20 minutes to remove heavy rare gases. Williams et al. (2005) provides additional information on this procedure. This crushing procedure does not release in situ cosmogenic helium (e.g. Foeken et al. 2009) or a significant contribution of post-eruptive radiogenic ^{4}He (Stuart et al. 2003). In the case that a small contribution of radiogenic He is released the reported ^{3}He/^{4}He are lower limits of the magmatic value.

Helium isotope ratios were determined in a MAP 215-50 mass spectrometer fitted with an electrostatic analyser. A cold GP50 getter and liquid nitrogen-cooled charcoal were used to minimise the partial pressure of residual gases during analysis. ^{3}He was measured in pulse-counting mode using a Burle Channeltron 4869 electron multiplier. ^{4}He was measured on a Faraday cup. Procedural blanks were measured prior to the first crush analysis of each batch of 10 samples and between samples, especially if a very high helium concentration was measured. This was to assess the potential for increased blank-level due to insufficient pump time between analyses or the potential for 'memory-effect' in the mass spectrometer itself. ^{4}He blanks averaged 2 x 10^{-11} cm^{3} STP and ^{3}He blanks (2.9 x 10^{-16} cm^{3} STP) were less than 4% of the measured ^{3}He.

Helium isotopes and abundances were calculated by peak height comparison to pipettes of 2.9 x 10^{12} atoms of helium from an artificial standard (^{3}He/^{4}He = 5.95 x 10^{-5}, ^{4}He/^{22}Ne > 6000). ^{3}He/^{4}He ratios were normalised to the atmospheric ratio of 1.39 x 10^{-6} (R_a). Standard helium abundance measurements were made regularly,

generally at the end of each day of analyses for calibration. Reproducibility over the period of analyses was less than 1% for ^{3}He and ^{4}He.

Helium isotopes for Baffin Island samples were measured by Dr Sudeshna Basu of SUERC, East Kilbride following the same procedure as outlined here.

A6 Electron Microprobe Facility

Major elements were measured in olivine crystals and olivine-hosted melt inclusions on the Cameca SX100 electron microprobe at the University of Edinburgh during February-March 2007, March 2008 and May 2008. A 1µm beam was used to determine olivine compositions at 15kV and a maximum of 100nA. A 5µm beam was used to determine compositions of small melt inclusions and a 10µm beam was used for larger melt inclusions both at 15kV and a maximum of 60nA. The samples were analysed with well-established standards. For olivine; forsterite, fayalite, wollastonite, rutile and corundum. For melt inclusions; jadeite, forsterite, corundum, wollastonite.

A7 Secondary Ion Mass Spectrometry (SIMS) Ion Microprobe Facility

A one-day feasibility study was undertaken in May 2007 on sample Pad6 prior to submission of a full proposal for ion microprobe time which was awarded during April 2008. REE, Si, K, Ca, Ti, Sr, Y, Zr, Nb and Ba were measured in olivine-hosted melt inclusions using the Cameca ims-4f of the Ion Microprobe facility at the University of Edinburgh. The basaltic glass melt inclusions, which were electron microprobed prior to ion microprobe work, were analysed using a 0- primary beam at ~4 nA with a spot size of 15µm. The image field was 25µm. Secondary ions were measured at 75eV offset. The energy beam was 15eV. Corrections made were BaO on Eu, LREE oxide on Gd and GdO on Yb. Counts were taken at peaks associated with the following masses (brackets indicate elements not necessarily analysed on all samples): (^{26}Mg), ^{30}Si, ^{39}K, ^{42}Ca, ^{47}Ti, Mass 84 correction for FeSi and FeAl, ^{88}Sr, ^{89}Y, ^{90}Zr, ^{93}Nb, Background 130.5, ^{138}Ba, ^{139}La, ^{140}Ce, ^{141}Pr, ^{143}Nd, ^{149}Sm, ^{151}Eu,

^{154}BaO, ^{156}CeO, ^{157}Gd ^{159}Tb, ^{161}Dy, ^{165}Ho, ^{167}Er, (^{169}Tm), ^{174}Yb, ^{175}Lu, ^{232}Th and ^{238}U. Analyses were compared to glass standards SRM-610, BCR-2 and BHVO-1 (Table A7). Overall reproducibility of the three standards measured over the week of analyses is better than 5% for all elements, except U which is ~12%.

Table A7. Trace element concentration and precision for three standards measured over the week of analyses.

	SRM610			BCR2			BHVO			
	Mean	St Dev	Rel. St Dev	Mean	St Dev	Rel. St Dev	Mean	St Dev	Rel. St Dev	Overall Relative St Dev
K	456.48	5.45	1.19	10487.25	72.15	0.69	3065.56	29.33	0.96	0.95
Ca	82118.60	956.22	1.16	45538.25	639.64	1.40	74214.00	692.72	0.93	1.17
Ti	428.79	5.54	1.29	11302.00	207.04	1.83	13839.00	175.20	1.27	1.46
Sr	506.39	6.60	1.30	274.61	4.74	1.72	325.35	5.13	1.58	1.54
Y	409.17	3.36	0.82	27.39	0.67	2.46	20.85	0.46	2.20	1.83
Zr	491.51	5.70	1.16	186.96	3.87	2.07	176.04	2.26	1.28	1.50
Nb	495.76	6.24	1.26	11.82	0.19	1.61	16.90	0.26	1.56	1.48
Ba	496.25	5.05	1.02	577.10	7.14	1.24	113.87	2.88	2.53	1.59
La	505.34	4.40	0.87	22.89	0.39	1.69	14.86	0.39	2.63	1.73
Ce	514.88	6.68	1.30	47.53	0.87	1.83	36.28	0.70	1.92	1.68
Pr	492.07	6.39	1.30	5.97	0.22	3.62	5.02	0.18	3.51	2.81
Nd	523.48	6.50	1.24	28.38	0.73	2.56	25.89	0.69	2.65	2.15
Sm	508.62	6.67	1.31	5.85	0.25	4.21	5.79	0.15	2.66	2.73
Eu	509.45	6.52	1.28	2.72	0.04	1.32	2.00	0.05	2.51	1.70
Gd	498.72	13.15	2.64	7.90	0.40	5.00	6.26	0.37	5.95	4.53
Tb	493.93	6.16	1.25	1.13	0.06	4.92	1.00	0.07	6.58	4.25
Dy	494.37	6.45	1.31	6.85	0.19	2.74	5.70	0.34	6.03	3.36
Ho	492.30	6.67	1.36	1.37	0.05	4.00	0.99	0.02	2.33	2.56
Er	489.30	8.35	1.71	3.53	0.09	2.66	2.54	0.11	4.47	2.95
Tm	477.33	3.05	0.64	0.51	0.01	1.27	0.38	0.02	4.96	2.29
Yb	490.94	7.12	1.45	3.44	0.15	4.41	2.13	0.05	2.53	2.80
Lu	494.40	7.91	1.60	0.57	0.03	5.71	0.32	0.02	6.93	4.75
Th	453.97	10.84	2.39	3.78	0.07	1.95	0.84	0.07	8.37	4.23
U	461.64	9.72	2.10	1.16	0.14	11.81	0.35	0.07	21.14	11.69

Appendix B Petrology

B1 Sample descriptions

Sample	Texture	Phenocryst phases	Olivine morphology	Phenocryst size max (mm)	Volume % crystals
GGU 138345	Porphyritic	Ol	Eu/Sub/An/Lng/Tb	<1	31.88
GGU 264217	Porphyritic, glomeroporphyritic	Ol	Eu/Tb	<0.5	34.73
GGU 332771	Porphyritic	Ol	Eu/Tb/Em/Sk	<0.5	33.22
GGU 332901	Porphyritic	Ol	Eu/Tb	<0.5	29.52
GGU 340740	Porphyritic, glomeroporphyritic	Ol	Eu/Tb/An	<1	29.87
GGU 354754	Porphyritic, glomeroporphyritic	Ol	Eu/Sub/An	<0.25	21.67
GGU 362077	Porphyritic, glomeroporphyritic	Ol	Eu/Sub/An/Sk/Em	<1.5	43.34
GGU 400230	Porphyritic, glomeroporphyritic	Ol	Eu/Sub/An/Tb	<0.75	35.32
GGU 400444	Porphyritic	Ol	Eu/Sub	<0.5	26.94
GGU 400452	Porphyritic	Ol	Eu/Lng/Tb	<0.5	23.71
GGU 400457	Porphyritic, glomeroporphyritic	Ol	Eu/Sub/An	<0.5	22.77
GGU 400485	Porphyritic	Ol	Eu/Sub/Em	<1	36
GGU	Porphyritic,	Ol	Eu/Sub/Tb/	<1.5	28.68

400492	glomeroporphyritic				
GGU 410252	Porphyritic, glomeroporphyritic	Ol	Eu/Sub/Tb	<1.5	26.86
PAD2	Porphyritic	Ol	Eu/Sub/An/Tb	<1	26.48
PAD3	Porphyritic, glomeroporphyritic	Ol	Eu/Sub	<0.5	27.13
PAD4	Porphyritic	Ol	Eu/Sub	<1	24.92
PAD5	Porphyritic, glomeroporphyritic	Ol	Sub/An	<0.5	20.73
PAD6	Porphyritic, glomeroporphyritic	Ol	Eu/Sub/Lng/Sk	<1	26.09
PAD7	Porphyritic	Ol	Sub/An/Tab	<0.5	25.43
PAD8	Porphyritic, glomeroporphyritic	Ol	Eu/Sub/Tab	<1.5	24.46
PAD9	Porphyritic	Ol	Sub/An/Tab	<0.5	44.8
DUR1	Porphyritic	Ol	Sub	<0.25	2.49
DUR3	Porphyritic, glomeroporphyritic	Ol	Eu/Sub/An/Tab	<1	23.03
DUR5	Porphyritic	Ol	Eu/Sub/Tab	<0.5	29.44
DUR6	Porphyritic	Ol	Eu/Sub/Tab/Sk	<0.5	23.16
DUR7	Porphyritic	Ol	Eu/Sub/Tab	<0.5	33.79
DUR8	Porphyritic	Ol	Sub/An	<0.5	21.89
APO1	Porphyritic	Ol	Eu/Sub/Tab	<0.5	39.19
APO3	Porphyritic	Ol	Eu/Sub/Tab	<0.5	30.9
APO4	Porphyritic	Ol	Eu/Sub/Tab	<1	37.25
APO5	Porphyritic	Ol	Eu/Sub/Tab/Lng	<0.5	21.81
APO7	Porphyritic	Ol	Eu/Sub/Tab	<0.5	30.35

B2 Estimation of olivine phenocryst contents

The percentage of olivine phenocrysts in each thin section was estimated using Geological Image Analysis Software (GIAS; Beggan and Hamilton, 2009). This program requires that the image is input in a binary format. Photomicrographs were prepared for each thin section and loaded into a drawing package where the olivine phenocryst outlines were traced. Olivine phenocrysts were in white and the groundmass was in black (Figure B2a,b), providing a binary image. The images were loaded into GIAS for the percentage of olivine to be estimated. GIAS provides a statistical summary stating a percentage for the white regions, reflecting, in this case, the percentage of olivine phenocrysts in the sample.

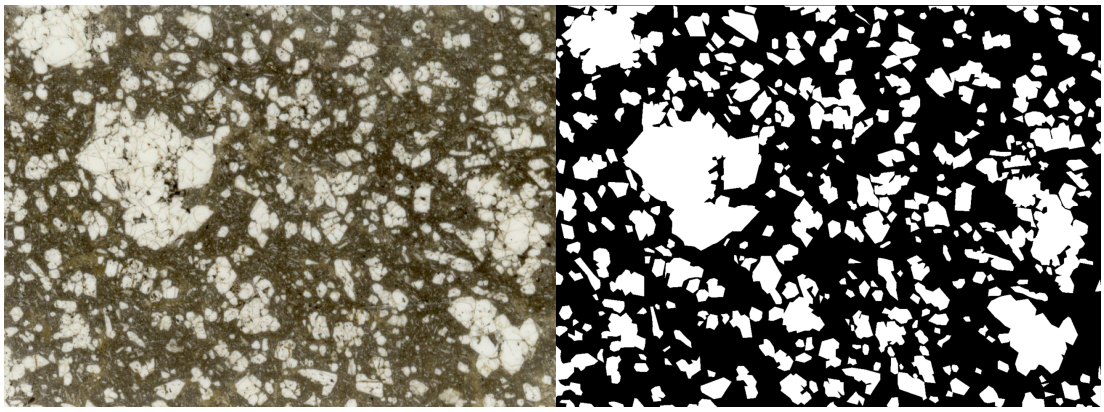

Figure B2. a) Photomicrograph 400230, olivine phenocrysts are white and groundmass is brown/beige. b) CorelDraw image showing traced olivine phenocrysts in 400230 photomicrograph. c) GIAS software showing input image and output percentage of white region (in statistical summary; 35.32%).

Appendix C Sample locations

Table C1: Locations of Baffin Island and West Greenland samples.

Baffin Island		
Sample	**Latitude**	**Longitude**
PAD2	67.18	62.44
PAD3	67.18	62.44
PAD4	67.17	62.44
PAD5	67.17	62.44
PAD6	67.17	62.45
PAD7	67.17	62.45
PAD8	67.15	62.46
PAD9	67.17	62.43
DUR1	67.08	62.25
DUR3	67.08	62.23
DUR5	67.08	62.22
DUR6	67.08	62.22
DUR7	67.09	62.16
DUR8	67.07	62.19
APO1	66.93	61.75
APO3	66.93	61.74
APO4	66.93	61.74
APO5	66.92	61.77
APO7	66.93	61.74

West Greenland		
Sample	**Latitude**	**Longitude**
138345	70.13	53.27
264217	70.38	53.68
332771	70.59	53.98
332901	70.38	53.22
340740	70.33	52.98
354754	70.49	53.29
362077	70.50	53.57
400230	70.59	53.11
400444	70.52	54.21
400452	70.54	54.21
400457	70.52	54.17
400485	70.55	53.66
400492	70.54	54.07
410152	70.67	53.76

Appendix D MORB database

Locations of samples (red dots) from PetDB used in MORB database in Chapter 2 for Nb/Zr plotted against $(La/Sm)_n$.

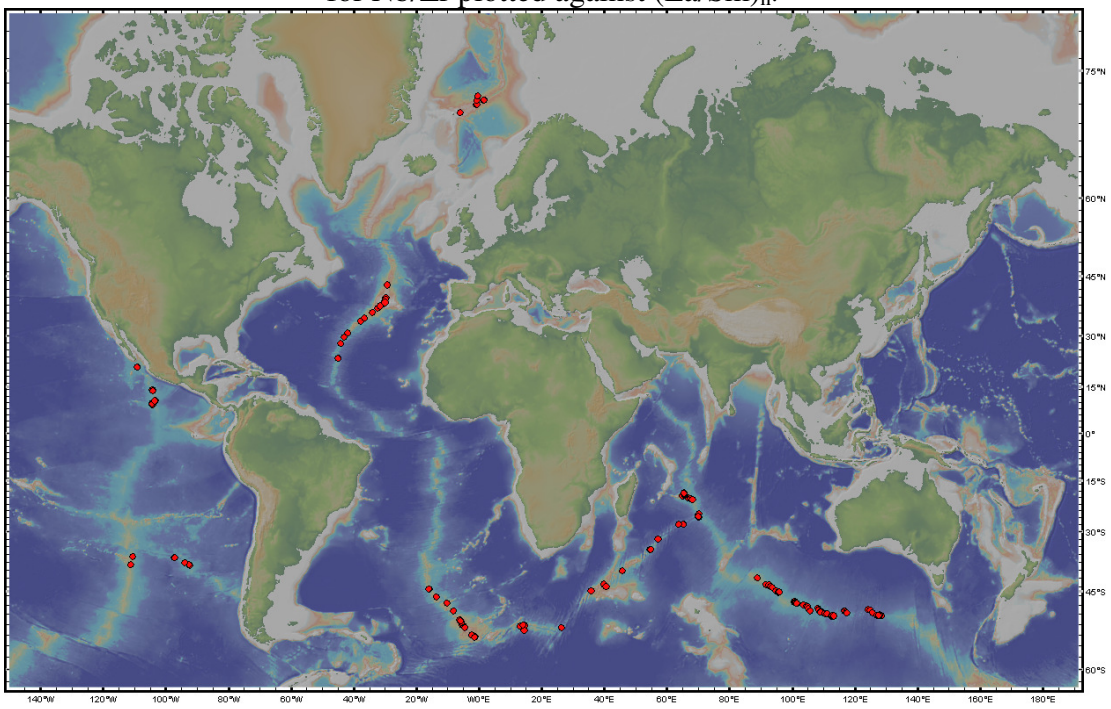

Locations of samples (red dots) from PetDB used in MORB database for $^3He/^4He$ compilation in Chapter 3.

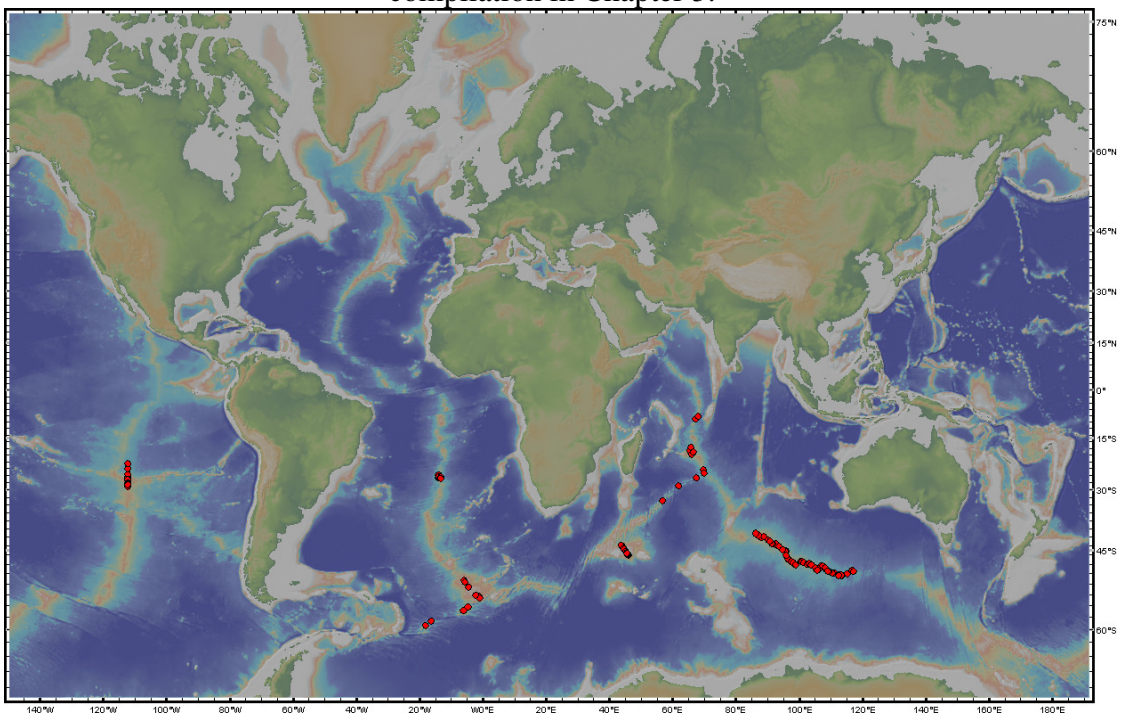

Samples from PetDB (http://www.petdb.org/petdbWeb/index.jsp).
Maps made in GeoMapApp

Appendix E Major elements

Major and trace element abundances (wt%) for Baffin Island and West Greenland samples determined by XRF. Major elements recalculated to 100% on a volatile free basis.

Baffin Island

Sample	SiO_2	$Al2O_3$	FeO	MgO	CaO	Na_2O	K_2O	TiO_2	MnO	P_2O_5	LOI
PAD2	46.54	10.88	10.29	20.42	9.59	1.19	0.03	0.83	0.17	0.07	-0.23
PAD3	45.49	8.56	10.41	26.14	7.67	0.88	0.02	0.59	0.18	0.05	-0.29
PAD4	46.73	11.08	10.31	20.62	9.13	1.07	0.03	0.78	0.18	0.06	0.45
PAD5	47.25	11.84	9.89	18.51	10.22	1.22	0.03	0.80	0.18	0.07	0.06
PAD6	47.68	12.24	10.09	17.20	10.32	1.34	0.04	0.86	0.17	0.07	-0.01
PAD7	47.04	11.57	10.01	18.93	10.08	1.30	0.02	0.80	0.18	0.07	-0.22
PAD8	46.73	11.06	10.37	19.95	9.48	1.29	0.05	0.81	0.18	0.07	-0.38
PAD9	45.12	8.08	9.60	28.28	7.39	0.84	0.03	0.45	0.16	0.04	-0.52
DUR1	49.10	14.74	10.63	9.66	12.62	1.77	0.10	1.09	0.19	0.10	-0.34
DUR3	47.53	12.39	9.78	17.49	10.42	1.39	0.02	0.75	0.17	0.06	-0.28
DUR5	46.12	10.51	9.76	22.60	9.20	1.02	0.03	0.56	0.17	0.05	-0.17
DUR6	48.10	12.62	9.90	16.38	10.58	1.35	0.04	0.78	0.17	0.07	-0.17
DUR7	47.38	12.97	10.05	16.68	10.24	1.06	0.41	0.92	0.18	0.09	3.18
DUR8	45.46	9.92	11.23	22.89	8.30	1.16	0.05	0.73	0.19	0.07	-0.64
APO1	44.96	8.55	10.23	27.68	7.15	0.76	0.02	0.44	0.17	0.04	-0.44
APO3	45.56	9.49	10.71	23.77	8.28	1.08	0.04	0.83	0.17	0.07	-0.36
APO4	46.50	10.46	9.78	22.32	8.94	1.11	0.03	0.64	0.17	0.05	-0.02
APO5	47.27	11.93	10.26	17.54	10.31	1.37	0.05	1.02	0.18	0.08	-0.18
APO7	45.60	8.87	10.32	25.43	7.80	1.00	0.03	0.72	0.17	0.06	-0.29

West Greenland

Sample	SiO_2	Al_2O_3	FeO	MgO	CaO	Na_2O	K_2O	TiO_2	MnO	P_2O_5	LOI
138345	45.22	10.14	10.69	23.29	8.25	1.03	0.23	0.88	0.17	0.08	1.22
264217	45.48	10.50	10.70	21.97	8.96	1.19	0.02	0.93	0.18	0.07	2.49
332771	45.71	10.61	10.87	20.09	10.24	1.16	0.04	1.02	0.18	0.08	0.2
332901	45.05	8.31	12.00	24.60	7.24	1.18	0.16	1.16	0.18	0.12	-0.03
340740	45.07	10.32	10.95	20.84	9.99	1.25	0.06	1.21	0.18	0.14	0.2
354754	45.70	10.74	11.29	20.74	8.95	1.20	0.17	0.94	0.18	0.08	1.86
362077	44.40	9.03	10.96	25.21	8.21	1.15	0.04	0.76	0.18	0.06	2.35
400230	45.12	10.04	11.45	21.77	8.98	1.23	0.08	1.05	0.18	0.09	0.01
400444	46.62	10.40	11.29	20.81	8.18	1.26	0.14	1.03	0.18	0.08	1.02
400452	45.74	10.32	10.67	21.55	9.37	1.14	0.05	0.91	0.19	0.07	2.52
400457	45.35	10.01	11.04	22.65	8.67	1.03	0.07	0.94	0.18	0.07	2.21
400485	44.24	8.29	11.25	27.02	7.36	0.73	0.14	0.73	0.18	0.06	1.54
400492	45.83	10.71	10.73	20.05	10.17	1.17	0.04	1.03	0.18	0.08	0.39
410152	45.36	10.14	11.44	21.06	8.84	1.32	0.27	1.26	0.19	0.12	1.35

Appendix F Trace elements

Selected trace element abundances (ppm) for Baffin Island and West Greenland samples determined by XRF.

Baffin Island

Sample	Nb	Zr	Y	Sr	Rb	Zn
PAD2	1.40	43.05	15.99	86.05	0.47	74.40
PAD3	0.80	29.91	12.88	55.89	0.27	75.47
PAD4	1.10	39.62	15.49	74.31	0.37	75.15
PAD5	1.00	39.92	16.89	80.99	0.47	68.07
PAD6	4.19	49.93	17.60	96.98	0.37	78.69
PAD7	1.10	40.53	16.19	82.10	0.27	68.61
PAD8	1.40	42.85	16.19	87.97	0.00	75.15
PAD9	0.70	22.23	9.67	53.05	0.27	65.49
DUR1	2.90	58.01	22.72	120.57	0.67	71.07
DUR3	0.90	38.91	16.99	75.42	0.16	72.68
DUR5	0.50	27.19	12.38	62.16	0.57	69.68
DUR6	1.00	39.72	17.80	76.43	0.06	74.94
DUR7	5.09	52.35	17.80	224.93	32.58	75.37
DUR8	3.50	41.74	14.08	95.46	0.16	78.48
APO1	0.50	20.72	9.37	46.67	0.16	73.44
APO3	1.50	42.75	14.99	88.18	0.27	76.65
APO4	0.80	31.13	13.78	62.97	0.27	69.89
APO5	1.70	54.58	18.40	119.25	0.37	69.04
APO7	1.20	36.48	13.38	76.43	0.47	82.23

Sample	Cu	Ni	Cr	V	Ba	Sc
PAD2	96.40	868.58	1683.25	242.89	7.53	35.19
PAD3	77.15	1233.65	2324.21	198.71	9.65	31.08
PAD4	80.88	892.42	1671.66	241.09	12.37	35.39
PAD5	86.02	749.03	1519.70	251.28	11.26	38.59
PAD6	97.00	647.10	1465.44	265.98	21.24	40.40
PAD7	94.28	787.63	1531.18	236.59	11.77	35.29
PAD8	93.07	788.72	1983.58	243.19	11.97	35.09
PAD9	54.49	1383.54	2488.45	149.73	1.89	27.28
DUR1	131.65	146.63	419.69	283.07	27.29	45.30
DUR3	102.44	597.86	1507.31	285.57	9.45	39.19
DUR5	74.84	977.60	2145.57	199.51	8.54	35.69
DUR6	103.04	565.76	1337.45	272.88	19.33	38.69
DUR7	82.19	511.99	1232.65	245.59	52.38	35.79
DUR8	75.54	855.88	1866.06	204.90	27.79	29.58
APO1	60.03	1268.71	2679.47	150.93	0.68	25.88
APO3	88.64	1044.18	1890.04	218.80	10.76	30.38
APO4	77.36	977.31	2204.66	209.00	8.94	33.89
APO5	88.03	679.01	1197.53	257.38	19.22	34.89
APO7	91.56	1409.44	2121.14	217.60	5.42	32.28

Appendix F continued

West Greenland

Sample	Nb	Zr	Y	Sr	Rb	Zn
138345	1.60	43.25	15.00	99.70	16.10	79.13
264217	1.30	43.46	16.90	84.10	0.00	77.00
332771	1.91	54.88	17.90	110.80	0.50	78.91
332901	4.72	66.61	15.10	153.80	1.40	91.58
340740	5.02	70.25	17.70	142.90	0.30	93.28
354754	2.21	49.02	16.50	127.40	2.80	79.23
362077	0.90	38.00	14.50	93.70	0.50	78.27
400230	3.21	57.31	17.20	136.20	0.70	86.68
400444	2.61	62.97	18.30	110.10	2.40	81.25
400452	1.10	44.97	15.60	148.70	2.00	78.91
400457	1.20	49.02	16.00	107.50	2.40	73.27
400485	1.00	37.09	12.80	82.40	4.70	80.08
400492	1.50	55.18	18.00	119.80	0.20	78.17
410152	6.12	69.54	17.60	171.40	10.50	84.87

Sample	Cu	Ni	Cr	V	Ba	Sc
138345	92.15	1005.45	1976.78	219.24	16.86	28.60
264217	109.16	948.56	1807.63	234.42	8.24	31.51
332771	103.83	823.84	1560.68	267.00	6.64	33.93
332901	106.75	1098.47	1594.60	235.13	46.50	27.19
340740	116.11	891.96	1556.19	273.74	25.37	31.21
354754	109.77	810.26	1520.46	251.11	24.17	30.41
362077	105.24	1158.72	1885.30	223.06	13.75	32.22
400230	119.13	934.88	1639.75	274.85	23.27	30.11
400444	70.40	768.82	1584.97	246.89	40.69	30.71
400452	110.87	912.73	1653.98	269.92	10.85	37.75
400457	83.69	848.25	1783.66	252.52	41.19	30.71
400485	94.16	1184.21	2156.10	216.12	89.07	27.09
400492	116.11	801.50	1624.88	268.31	10.04	33.22
410152	111.28	846.88	1874.07	248.00	65.53	31.01

Appendix G Rare Earth Elements

Rare earth element abundances (ppm) for Baffin Island and West Greenland samples determined by ICP-MS.

Baffin Island

Sample	La	Ce	Pr	Nd	Sm	Eu	Gd	Tb	Dy	Ho
PAD2	1.874	5.587	0.941	5.127	1.682	0.594	2.149	0.382	2.544	0.530
PAD3	1.129	3.530	0.609	3.465	1.221	0.447	1.686	0.304	2.046	0.433
PAD4	1.620	4.700	0.821	4.466	1.536	0.549	2.054	0.373	2.486	0.517
PAD5	1.589	4.755	0.849	4.671	1.642	0.604	2.262	0.406	2.754	0.572
PAD6	3.385	8.389	1.224	6.037	1.898	0.666	2.452	0.436	2.885	0.605
PAD7	1.675	5.168	0.880	4.815	1.668	0.607	2.237	0.401	2.646	0.561
PAD8	1.917	5.715	0.957	5.041	1.678	0.595	2.196	0.386	2.565	0.530
PAD9	0.914	2.860	0.498	2.728	0.963	0.353	1.312	0.236	1.583	0.333
DUR1	3.148	8.537	1.354	7.074	2.360	0.858	3.147	0.555	3.716	0.775
DUR3	1.381	4.074	0.738	4.197	1.549	0.574	2.181	0.398	2.699	0.577
DUR5	1.165	3.254	0.576	3.232	1.152	0.434	1.659	0.297	2.020	0.427
DUR6	1.681	4.561	0.818	4.532	1.639	0.617	2.262	0.409	2.828	0.595
DUR7	3.925	9.359	1.312	6.331	1.903	0.684	2.426	0.414	2.787	0.576
DUR8	2.966	7.548	1.093	5.422	1.636	0.579	2.034	0.351	2.283	0.470
APO1	0.702	2.317	0.414	2.358	0.871	0.329	1.238	0.222	1.515	0.319
APO3	1.850	5.694	0.958	5.129	1.704	0.606	2.221	0.380	2.510	0.513
APO4	1.079	3.395	0.616	3.493	1.312	0.493	1.803	0.325	2.204	0.463
APO5	2.464	7.424	1.254	6.792	2.219	0.775	2.793	0.478	3.081	0.622
APO7	1.675	5.043	0.853	4.659	1.528	0.552	1.961	0.340	2.249	0.459

Sample	Er	Tm	Yb	Lu	Hf	Ta	Pb	Th	U
PAD2	1.563	0.244	1.473	0.220	1.43	0.13	4.92	0.12	0.04
PAD3	1.301	0.202	1.227	0.187	0.98	0.08	2.74	0.07	0.02
PAD4	1.552	0.243	1.490	0.227	1.20	0.09	24.64	0.09	0.03
PAD5	1.724	0.267	1.651	0.247	1.29	0.09	37.00	0.08	0.04
PAD6	1.792	0.279	1.700	0.262	1.50	0.25	14.00	0.41	0.06
PAD7	1.663	0.258	1.582	0.243	1.17	0.14	5.94	0.10	0.05
PAD8	1.569	0.246	1.492	0.227	1.18	0.28	13.60	0.15	0.11
PAD9	0.972	0.152	0.922	0.142	0.84	0.05	13.80	0.05	0.03
DUR1	2.297	0.359	2.178	0.332	1.83	0.20	14.10	0.26	0.08
DUR3	1.727	0.272	1.654	0.256	1.18	0.07	16.72	0.10	0.03
DUR5	1.351	0.199	1.210	0.183	0.87	0.05	55.11	0.07	0.02
DUR6	1.780	0.277	1.688	0.255	1.13	0.10	1.00	0.11	0.04
DUR7	1.682	0.264	1.591	0.241	1.46	0.36	13.46	0.45	0.14
DUR8	1.401	0.215	1.278	0.196	1.13	0.32	2.57	0.29	0.09
APO1	0.965	0.148	0.900	0.139	0.78	0.05	6.97	0.04	0.02
APO3	1.527	0.234	1.410	0.211	1.54	0.10	5.62	0.11	0.04
APO4	1.382	0.215	1.331	0.203	1.25	0.07	3.03	0.06	0.03
APO5	1.805	0.274	1.625	0.245	1.77	0.13	3.79	0.16	0.05
APO7	1.351	0.209	1.262	0.186	0.97	0.11	6.06	0.10	0.04

Appendix G continued

West Greenland

Sample	La	Ce	Pr	Nd	Sm	Eu	Gd	Tb	Dy	Ho
138345	2.007	5.963	0.994	5.297	1.796	0.649	2.281	0.388	2.524	0.511
264217	1.682	5.462	0.959	5.365	1.910	0.687	2.479	0.433	2.838	0.578
332771	2.356	7.254	1.217	6.544	2.196	0.773	2.748	0.466	3.053	0.614
332901	4.575	12.321	1.837	8.961	2.538	0.853	2.829	0.451	2.735	0.516
340740	4.564	12.185	1.850	9.162	2.653	0.877	3.014	0.503	3.089	0.616
354754	2.386	6.902	1.110	5.904	1.933	0.678	2.450	0.422	2.742	0.557
362077	1.385	4.418	0.770	4.333	1.525	0.538	2.032	0.354	2.369	0.490
400230	2.950	8.448	1.348	7.035	2.254	0.781	2.747	0.456	2.893	0.574
400444	3.982	10.502	1.572	7.854	2.340	0.784	2.822	0.470	2.993	0.606
400452	1.702	5.511	0.968	5.378	1.853	0.655	2.403	0.419	2.694	0.557
400457	1.806	5.757	0.993	5.499	1.874	0.678	2.393	0.417	2.685	0.538
400485	1.435	4.606	0.796	4.448	1.505	0.557	1.919	0.332	2.179	0.450
400492	2.105	6.685	1.141	6.376	2.177	0.764	2.745	0.471	3.047	0.612
410152	5.372	13.781	1.990	9.680	2.678	0.902	3.038	0.496	3.002	0.587

Sample	Er	Tm	Yb	Lu	Hf	Ta	Pb	Th	U
138345	1.497	0.224	1.310	0.196	1.21	0.17	1.39	0.16	0.07
264217	1.656	0.255	1.501	0.226	1.28	0.22	0.79	0.12	0.09
332771	1.759	0.266	1.569	0.232	2.22	0.17	0.79	0.19	0.07
332901	1.438	0.207	1.220	0.177	1.82	0.32	1.07	0.35	0.11
340740	1.709	0.259	1.539	0.223	1.91	0.39	1.68	0.39	0.13
354754	1.585	0.244	1.449	0.210	1.63	0.17	0.65	0.18	0.06
362077	1.407	0.218	1.287	0.193	1.24	0.12	0.81	0.10	0.04
400230	1.637	0.245	1.433	0.213	1.52	0.25	1.08	0.23	0.08
400444	1.730	0.261	1.533	0.230	1.88	0.19	1.45	0.73	0.16
400452	1.602	0.246	1.492	0.221	1.39	0.08	0.79	0.10	0.04
400457	1.537	0.234	1.402	0.203	1.36	0.10	0.61	0.10	0.03
400485	1.282	0.198	1.171	0.179	1.14	0.10	0.99	0.09	0.03
400492	1.771	0.268	1.571	0.238	1.67	0.14	0.70	0.13	0.05
410152	1.652	0.244	1.420	0.213	2.00	0.48	0.86	0.46	0.12

Appendix H Strontium isotopes

Table of $^{87}Sr/^{86}Sr$ data for Baffin Island and West Greenland samples.
'(m)' denotes the measured value
'(60)' denotes the value age corrected to eruption 60Ma.

Baffin Island

Sample	$^{87}Sr/^{86}Sr_{(m)}$	$\%StErr_{(m)}$	2SE	$^{87}Sr/^{86}Sr_{(60)}$	εSr
PAD2	0.703155	0.00140	0.000020	0.703142	-21.1
PAD3	0.703062	0.00130	0.000018	0.703050	-22.4
PAD4	0.703551	0.00120	0.000017	0.703539	-15.5
PAD5	0.703384	0.00120	0.000017	0.703370	-17.9
PAD6	0.703815	0.00120	0.000017	0.703806	-11.7
PAD7	0.703066	0.01670	0.000235	0.703058	-22.3
PAD8	0.703109	0.00110	0.000015	0.703109	-21.6
PAD9	0.703213	0.00140	0.000020	0.703200	-20.3
DUR1	0.703249	0.00180	0.000025	0.703235	-19.8
DUR3	0.703456	0.00120	0.000017	0.703451	-16.7
DUR5	0.703601	0.00140	0.000020	0.703578	-14.9
DUR6	0.706430	0.01200	0.000170	0.706428	25.5
DUR7	0.712131	0.00120	0.000017	0.711773	101.4
DUR8	0.703402	0.00120	0.000017	0.703398	-17.5
APO1	0.702892	0.00120	0.000017	0.702883	-24.8
APO3	0.703250	0.00120	0.000017	0.703243	-19.7
APO4	0.703142	0.00130	0.000018	0.703132	-21.2
APO5	0.703233	0.00140	0.000020	0.703225	-19.9
APO7	0.703161	0.00130	0.000018	0.703146	-21.0

West Greenland

Sample	$^{87}Sr/^{86}Sr_{(m)}$	$\%StErr_{(m)}$	2SE	$^{87}Sr/^{86}Sr_{(60)}$	εSr
138345	0.704050	0.00120	0.000017	0.703652	-13.8
264217	0.703052	0.00190	0.000027	0.703052	-22.4
332771	0.703128	0.00200	0.000028	0.704117	-21.4
332901	0.703483	0.00110	0.000015	0.703461	-16.6
340740	0.703293	0.00140	0.000020	0.703287	-19.0
354754	0.703390	0.00130	0.000018	0.703336	-18.3
362077	0.703055	0.00110	0.000015	0.703042	-22.5
400230	0.703397	0.00170	0.000024	0.703384	-17.6
400444	0.704681	0.00140	0.000020	0.704628	0.0
400452	0.704066	0.00150	0.000021	0.704033	-8.4
400457	0.703336	0.00150	0.000021	0.703281	-19.1
400485	0.703514	0.00150	0.000021	0.703374	-17.8
400492	0.703241	0.00170	0.000024	0.703237	-19.7
410152	0.703620	0.00160	0.000023	0.703469	-16.4

Appendix I Neodymium isotopes

Table of $^{143}Nd/^{144}Nd$ data for Baffin Island and West Greenland samples.
'(m)' denotes the measured value
'(60)' denotes the value age corrected to eruption 60Ma.

Baffin Island

Sample	$^{143}Nd/^{144}Nd_{(m)}$	$\%StErr_{(m)}$	2SE	$^{143}Nd/^{144}Nd_{(60)}$	εNd
PAD2	0.513129	0.000500	0.000005	0.513000	8.57
PAD3	0.513078	0.000012	0.000000	0.512994	8.45
PAD4					
PAD5	0.513070	0.000013	0.000000	0.512987	8.31
PAD6	0.512951	0.000600	0.000006	0.512876	6.15
PAD7					
PAD8	0.513114	0.001500	0.000015	0.513034	9.24
PAD9	0.513114	0.000700	0.000007	0.513031	9.16
DUR1	0.513065	0.000700	0.000007	0.512986	8.29
DUR3					
DUR5	0.513053	0.000700	0.000007	0.512968	7.95
DUR6					
DUR7					
DUR8	0.513047	0.000600	0.000006	0.512975	8.09
APO1					
APO3	0.513109	0.000600	0.000006	0.513030	9.15
APO4					
APO5	0.513121	0.000700	0.000007	0.513043	9.41
APO7	0.513135	0.000600	0.000006	0.513058	9.69

West Greenland

Sample	$^{143}Nd/^{144}Nd_{(m)}$	$\%StErr_{(m)}$	2SE	$^{143}Nd/^{144}Nd_{(60)}$	εNd
138345	0.513089	0.001800	0.000018	0.513008	8.7
264217	0.513154	0.001500	0.000015	0.513069	9.9
332771	0.513120	0.000700	0.000007	0.513040	9.4
332901	0.513019	0.000600	0.000006	0.512952	7.6
340740	0.513026	0.000900	0.000009	0.512957	7.7
354754	0.513016	0.000700	0.000007	0.512938	7.4
362077					
400230	0.512986	0.001000	0.000010	0.512910	6.8
400444	0.512783	0.000800	0.000008	0.512712	3.0
400452	0.513135	0.000700	0.000007	0.513053	9.6
400457	0.513137	0.000700	0.000007	0.513056	9.7
400485	0.513155	0.000600	0.000006	0.513075	10.0
400492	0.513153	0.000600	0.000006	0.513072	10.0
410152	0.512998	0.000600	0.000006	0.512932	7.2

Appendix J Helium isotopes

Table of $^{3}He/^{4}He$ data for Baffin Island and West Greenland samples.
NOTE: Helium isotopes for Baffin Island samples were measured by Dr Sudeshna Basu at SUERC, East Kilbride under the same conditions as the West Greenland samples.

Baffin Island

Sample	$^{3}He/^{4}He$ (R_a)	±	^{4}He ($10^{-9}cm^3$ STP g^{-1})	±
PAD2	38.1	3.0	0.7	0.02
PAD3	31.1	2.7	2.0	0.03
PAD4	44.4	0.1	306.2	3.00
PAD5	40.3	0.4	55.4	0.60
PAD6	45.0	1.0	13.8	0.10
PAD7	43.4	0.3	107.4	1.00
PAD8	48.0	0.8	8.1	0.08
PAD9	43.6	0.6	36.8	0.40
DUR1				
DUR3	38.5	2.0	8.4	0.08
DUR5	40.9	0.6	54.7	0.50
DUR6	29.7	4.5	0.5	0.02
DUR7				
DUR8	49.8	0.7	35.3	0.30
APO1	36.9	2.1	6.6	0.07
APO3	46.2	0.1	60.8	0.60
APO4	38.1	2.0	3.6	0.04
APO5	39.2	0.2	343.8	3.00
APO7	46.2	0.3	227.5	2.00

West Greenland

Sample	$^{3}He/^{4}He$ (R_a)	±	^{4}He ($10^{-9}cm^3$ STP g^{-1})	±
138345	22.7	1.7	4.2	0.05
264217	19.1	6.1	0.3	0.04
332771				
332901	45.8	1.0	17.5	0.20
340740	23.4	0.9	14.3	0.10
354754	46.7	0.7	10.6	0.10
362077	44.0	0.8	20.0	0.20
400230	47.6	1.3	1.3	0.10
400444				
400452	35.4	2.2	3.1	0.04
400457	16.4	2.0	1.0	0.02
400485	40.3	3.2	1.9	0.03
400492				
410152	19.3	1.8	3.7	0.04

Appendix K Olivine crystal compositions

Major element abundances (wt%) for olivine crystals measured by electron microprobe.

Sample	SiO_2	Al_2O_3	FeO	MgO	CaO	TiO_2	MnO	Cr_2O_3	NiO
PAD4 Ol 1	40.619	0.124	7.214	50.993	0.280	0.002	0.126	0.162	0.480
PAD4 Ol 2	39.961	0.089	11.148	47.837	0.314	0.005	0.171	0.089	0.387
PAD4 Ol 3	39.726	0.058	12.044	47.232	0.334	0.003	0.191	0.073	0.339
PAD4 Ol 4	39.503	0.095	12.023	47.426	0.311	0.005	0.181	0.095	0.361
PAD4 Ol 5	39.933	0.058	11.430	47.667	0.334	0.002	0.159	0.062	0.356
PAD4 Ol 6	40.313	0.055	9.572	49.101	0.292	0.001	0.157	0.082	0.426
PAD4 Ol 7	39.671	0.056	12.534	46.818	0.346	0.003	0.191	0.072	0.309
PAD4 Ol 8	39.733	0.053	12.721	46.570	0.336	0.008	0.195	0.054	0.328
PAD4 Ol 9	39.802	0.076	11.841	47.350	0.306	0.003	0.181	0.072	0.369
PAD4 Ol 10	39.492	0.083	12.536	46.946	0.327	0.000	0.192	0.083	0.341
PAD4 Ol 11	39.626	0.065	12.960	46.438	0.328	0.002	0.202	0.058	0.321
PAD4 Ol 12	40.666	0.087	8.237	50.022	0.284	0.003	0.127	0.131	0.444
PAD4 Ol 13	40.008	0.103	12.060	46.879	0.326	0.006	0.193	0.077	0.347
PAD4 Ol 14	39.868	0.088	10.977	48.111	0.322	0.004	0.173	0.104	0.353
PAD4 Ol 15	39.709	0.061	12.414	46.911	0.325	0.003	0.181	0.072	0.324
PAD4 Ol 16	39.559	0.121	12.402	46.963	0.327	0.011	0.192	0.091	0.336
PAD5 Ol 1	39.839	0.074	11.897	47.245	0.318	0.006	0.186	0.068	0.366
PAD5 Ol 2	40.300	0.101	7.767	50.823	0.297	0.006	0.116	0.135	0.455
PAD5 Ol 3	40.647	0.092	7.326	50.958	0.290	0.006	0.105	0.117	0.459
PAD5 Ol 4	39.770	0.085	10.499	48.679	0.331	0.000	0.159	0.085	0.392
PAD5 Ol 5	39.979	0.077	11.894	47.082	0.336	0.008	0.191	0.083	0.350
PAD5 Ol 6	39.944	0.081	12.070	46.968	0.335	0.002	0.186	0.072	0.341
PAD5 Ol 7	39.793	0.048	12.029	47.209	0.333	0.001	0.196	0.063	0.328
PAD5 Ol 8	40.521	0.115	7.647	50.703	0.298	0.005	0.122	0.133	0.456
PAD5 Ol 9	39.575	0.054	12.824	46.640	0.345	0.002	0.202	0.056	0.302
PAD5 Ol 10	40.558	0.112	9.112	49.220	0.279	0.006	0.129	0.146	0.439
PAD5 Ol 11	39.844	0.063	10.595	48.576	0.285	0.004	0.153	0.079	0.402
PAD5 Ol 12	40.152	0.076	10.575	48.244	0.327	0.004	0.174	0.093	0.356
PAD5 Ol 13	39.944	0.102	11.748	47.231	0.329	0.004	0.190	0.096	0.357
PAD5 Ol 14	40.010	0.073	10.965	48.002	0.323	0.001	0.183	0.078	0.364
PAD5 Ol 15	40.090	0.067	11.337	47.580	0.287	0.004	0.189	0.082	0.365
PAD5 Ol 16	40.047	0.088	9.329	49.547	0.274	0.003	0.129	0.133	0.450
PAD6 Ol 1	40.041	0.075	11.901	47.083	0.332	0.004	0.165	0.088	0.311
PAD6 Ol 2	40.224	0.090	12.347	46.441	0.330	0.020	0.193	0.091	0.264
PAD6 Ol 3	39.834	0.091	12.987	46.225	0.338	0.012	0.182	0.073	0.258
PAD6 Ol 4	40.162	0.105	12.557	46.277	0.319	0.014	0.169	0.093	0.304
PAD6 Ol 5	40.653	0.066	12.595	45.780	0.305	0.000	0.196	0.102	0.304
PAD6 Ol 6	40.641	0.060	12.175	46.240	0.291	0.000	0.213	0.080	0.300
PAD6 Ol 7	39.962	0.122	15.500	43.521	0.423	0.009	0.224	0.045	0.195
PAD6 Ol 8	39.984	0.198	12.593	46.306	0.337	0.032	0.149	0.123	0.277
PAD6 Ol 9	40.363	0.099	12.908	45.715	0.333	0.004	0.173	0.099	0.307
PAD6 Ol 10	40.541	0.070	12.649	45.851	0.327	0.016	0.211	0.063	0.273
PAD6 Ol 11	40.202	0.066	12.716	46.185	0.328	0.011	0.163	0.061	0.267
PAD6 Ol 12	40.513	0.074	12.479	45.994	0.332	0.005	0.239	0.058	0.306
PAD6 Ol 13	40.375	0.040	12.415	46.310	0.322	0.000	0.202	0.056	0.280
PAD6 Ol 14	40.214	0.080	12.914	45.880	0.347	0.007	0.195	0.068	0.296
PAD6 Ol 15	40.959	0.073	7.484	50.547	0.296	0.002	0.147	0.126	0.368
PAD6 Ol 16	40.023	0.085	13.119	45.874	0.340	0.025	0.182	0.088	0.264
PAD6 Ol 17	40.882	0.075	8.570	49.514	0.289	0.004	0.149	0.128	0.389
PAD6 Ol 18	40.364	0.069	13.171	45.510	0.346	0.000	0.192	0.039	0.308
PAD6 Ol 19	39.882	0.097	13.666	45.459	0.328	0.009	0.219	0.061	0.280
PAD6 Ol 20	40.673	0.060	11.199	47.172	0.286	0.005	0.169	0.102	0.333
PAD6 Ol 21	40.009	0.042	13.961	45.131	0.366	0.008	0.182	0.062	0.239
PAD6 Ol 22	39.907	0.109	13.606	45.506	0.340	0.005	0.177	0.103	0.247
PAD6 Ol 23	39.982	0.066	11.945	47.085	0.322	0.002	0.185	0.068	0.345
PAD6 Ol 24	39.641	0.071	12.246	47.054	0.329	0.007	0.203	0.095	0.354
PAD6 Ol 25	39.760	0.054	12.202	47.066	0.333	0.002	0.199	0.054	0.329
PAD6 Ol 26	39.490	0.070	12.470	47.058	0.326	0.006	0.188	0.061	0.329
PAD6 Ol 27	39.736	0.047	12.381	46.898	0.337	0.004	0.206	0.074	0.318
PAD6 Ol 28	39.529	0.081	12.945	46.495	0.327	0.008	0.195	0.084	0.336

Sample	SiO_2	Al_2O_3	FeO	MgO	CaO	TiO_2	MnO	Cr_2O_3	NiO
PAD6 Ol 29	39.677	0.055	12.792	46.556	0.350	0.004	0.191	0.050	0.325
PAD6 Ol 30	39.253	0.028	13.163	46.642	0.350	0.000	0.214	0.043	0.308
PAD6 Ol 31	39.765	0.064	12.386	46.839	0.325	0.003	0.194	0.075	0.349
PAD6 Ol 32	39.579	0.119	12.383	46.945	0.324	0.011	0.194	0.097	0.349
PAD6 Ol 33	39.345	0.124	12.297	47.274	0.336	0.011	0.190	0.099	0.326
PAD6 Ol 34	40.247	0.088	9.776	48.891	0.297	0.003	0.146	0.100	0.452
PAD6 Ol 35	39.387	0.072	12.383	47.209	0.344	0.004	0.182	0.071	0.347
PAD6 Ol 36	39.449	0.052	14.725	44.875	0.351	0.007	0.222	0.054	0.264
PAD6 Ol 37	39.277	0.054	14.819	44.921	0.351	0.004	0.253	0.046	0.273
PAD6 Ol 38	39.005	0.090	12.325	47.653	0.339	0.006	0.185	0.070	0.326
PAD6 Ol 39	39.390	0.060	12.705	46.904	0.343	0.003	0.211	0.056	0.327
PAD6 Ol 40	39.637	0.085	12.232	47.110	0.332	0.007	0.188	0.084	0.325
PAD6 Ol 41	39.716	0.053	12.230	47.082	0.330	0.005	0.190	0.057	0.338
PAD6 Ol 42	39.454	0.069	12.676	46.906	0.330	0.007	0.186	0.054	0.317
PAD6 Ol 43	39.838	0.054	11.977	47.199	0.337	0.002	0.193	0.058	0.342
PAD6 Ol 44	39.754	0.057	12.871	46.376	0.324	0.002	0.198	0.078	0.340
PAD6 Ol 45	39.764	0.062	12.382	46.857	0.341	0.006	0.196	0.061	0.331
PAD6 Ol 46	39.678	0.082	12.573	46.724	0.326	0.005	0.192	0.080	0.341
PAD6 Ol 47	39.903	0.042	12.434	46.712	0.333	0.004	0.189	0.045	0.338
PAD6 Ol 48	39.859	0.048	12.193	46.950	0.339	0.002	0.199	0.062	0.348
PAD8 Ol 1	40.913	0.067	8.455	49.741	0.299	0.000	0.112	0.083	0.331
PAD8 Ol 2	38.839	0.032	20.001	40.296	0.253	0.027	0.328	0.018	0.207
PAD8 Ol 3	39.930	0.047	16.397	42.842	0.266	0.000	0.264	0.014	0.240
PAD8 Ol 4	40.118	0.065	12.970	46.098	0.284	0.002	0.172	0.049	0.242
PAD8 Ol 5	39.495	0.033	16.546	43.083	0.287	0.009	0.268	0.040	0.239
PAD8 Ol 6	40.729	0.075	10.146	48.173	0.319	0.000	0.178	0.074	0.306
PAD8 Ol 7	39.041	0.043	19.274	40.850	0.237	0.010	0.293	0.020	0.231
PAD8 Ol 8	39.545	0.048	17.619	41.928	0.271	0.002	0.298	0.040	0.248
PAD8 Ol 9	40.190	0.070	12.957	45.916	0.305	0.009	0.198	0.053	0.302
PAD8 Ol 10	41.093	0.073	8.322	49.643	0.307	0.002	0.123	0.108	0.330
PAD8 Ol 11	40.677	0.065	9.264	49.077	0.300	0.007	0.151	0.104	0.356
PAD8 Ol 12	41.022	0.088	9.052	48.950	0.279	0.000	0.137	0.129	0.343
PAD8 Ol 13	39.476	0.076	16.624	43.047	0.283	0.000	0.242	0.054	0.198
PAD8 Ol 14	40.174	0.070	14.030	44.821	0.292	0.001	0.232	0.077	0.303
PAD8 Ol 15	40.426	0.067	12.721	45.877	0.299	0.006	0.210	0.094	0.299
PAD8 Ol 16	40.996	0.066	9.125	48.985	0.280	0.016	0.114	0.071	0.346
PAD8 Ol 17	39.631	0.079	17.390	42.052	0.272	0.011	0.282	0.055	0.229
PAD8 Ol 18	39.673	0.050	15.280	44.219	0.290	0.002	0.242	0.035	0.209
PAD8 Ol 19	40.382	0.080	11.608	47.016	0.305	0.000	0.188	0.104	0.317
PAD8 Ol 20	41.293	0.073	8.476	49.313	0.292	0.004	0.129	0.078	0.342
PAD8 Ol 21	39.051	0.041	18.746	41.382	0.219	0.022	0.268	0.065	0.206
PAD8 Ol 22	41.032	0.042	9.236	48.848	0.287	0.001	0.147	0.073	0.334
PAD8 Ol 23	39.802	0.079	15.104	44.086	0.287	0.000	0.269	0.099	0.276
PAD8 Ol 24	40.297	0.086	12.229	46.487	0.309	0.002	0.213	0.061	0.316
PAD8 Ol 25	40.897	0.082	8.243	49.927	0.283	0.007	0.105	0.116	0.340
PAD8 Ol 26	40.417	0.072	11.852	46.736	0.287	0.005	0.228	0.085	0.319
PAD8 Ol 27	40.634	0.036	10.649	47.846	0.302	0.000	0.174	0.063	0.296
PAD9 Ol 1	39.948	0.100	9.333	49.596	0.302	0.005	0.157	0.119	0.440
PAD9 Ol 2	39.613	0.061	12.328	47.080	0.297	0.006	0.189	0.063	0.363
PAD9 Ol 3	40.232	0.069	8.923	49.842	0.261	0.008	0.132	0.091	0.443
PAD9 Ol 4	39.238	0.067	14.887	44.890	0.292	0.002	0.247	0.056	0.321
PAD9 Ol 5	39.916	0.088	9.751	49.261	0.286	0.001	0.142	0.118	0.436
PAD9 Ol 6	40.242	0.096	9.020	49.664	0.275	0.009	0.138	0.121	0.434
PAD9 Ol 7	39.865	0.093	10.180	48.901	0.298	0.004	0.155	0.094	0.411
PAD9 Ol 8	40.073	0.094	9.420	49.452	0.276	0.006	0.145	0.105	0.428
PAD9 Ol 9	39.888	0.092	10.237	48.829	0.272	-0.003	0.143	0.114	0.429
PAD9 Ol 10	39.632	0.077	11.777	47.572	0.287	0.005	0.176	0.094	0.379
PAD9 Ol 11	40.121	0.091	9.249	49.528	0.282	0.002	0.162	0.133	0.432
PAD9 Ol 12	39.435	0.090	12.582	46.922	0.296	0.004	0.192	0.110	0.369
PAD9 Ol 13	40.276	0.105	7.747	50.849	0.275	0.001	0.121	0.143	0.483
PAD9 Ol 14	39.122	0.078	14.423	45.426	0.303	0.005	0.212	0.079	0.352
PAD9 Ol 15	38.646	0.049	16.506	43.867	0.321	0.003	0.274	0.040	0.293
DUR3 Ol 1	38.499	0.047	19.197	41.379	0.301	0.000	0.298	0.030	0.248
DUR3 Ol 2	38.923	0.064	16.000	44.115	0.324	0.009	0.247	0.041	0.276
DUR3 Ol 3	39.663	0.045	13.956	45.429	0.329	0.004	0.215	0.047	0.313
DUR3 Ol 4	39.649	0.061	12.023	47.343	0.329	0.005	0.184	0.064	0.343
DUR3 Ol 5	38.250	0.041	20.031	40.788	0.297	0.004	0.303	0.030	0.257
DUR3 Ol 6	38.527	0.148	16.755	43.579	0.322	0.015	0.255	0.111	0.289

Sample	SiO_2	Al_2O_3	FeO	MgO	CaO	TiO_2	MnO	Cr_2O_3	NiO
DUR3 Ol 7	40.120	0.079	11.239	47.599	0.287	0.001	0.178	0.101	0.396
DUR3 Ol 8	39.091	0.043	15.894	44.047	0.319	0.002	0.255	0.050	0.299
DUR3 Ol 9	38.967	0.054	18.739	41.362	0.305	0.000	0.290	0.028	0.254
DUR3 Ol 10	38.828	0.069	17.739	42.438	0.328	0.006	0.286	0.022	0.283
DUR3 Ol 11	40.426	0.099	8.329	50.179	0.277	0.007	0.130	0.141	0.413
DUR3 Ol 12	38.663	0.046	17.786	42.661	0.307	0.002	0.269	0.021	0.246
DUR3 Ol 13	38.618	0.088	18.492	41.904	0.295	0.011	0.300	0.036	0.257
DUR3 Ol 14	39.884	0.063	11.188	47.898	0.299	0.000	0.165	0.100	0.404
DUR3 Ol 15	40.118	0.080	11.319	47.536	0.293	0.008	0.179	0.094	0.371
DUR3 Ol 16	39.602	0.098	11.974	47.376	0.299	0.005	0.178	0.107	0.361
DUR3 Ol 17	39.310	0.098	12.666	46.979	0.302	0.002	0.184	0.107	0.353
DUR3 Ol 18	38.835	0.069	16.017	44.173	0.314	0.000	0.245	0.062	0.285
DUR3 Ol 19	40.040	0.048	12.013	46.975	0.323	0.000	0.199	0.066	0.337
DUR6 Ol 1	39.998	0.084	11.067	47.884	0.332	0.006	0.178	0.093	0.359
DUR6 Ol 2	39.827	0.066	11.197	47.993	0.336	0.001	0.165	0.072	0.343
DUR6 Ol 3	39.870	0.060	12.044	47.093	0.329	0.005	0.200	0.080	0.319
DUR6 Ol 4	39.697	0.095	11.082	48.172	0.302	0.001	0.177	0.105	0.369
DUR6 Ol 5	40.108	0.091	8.956	49.847	0.281	0.004	0.140	0.130	0.444
DUR6 Ol 6	39.776	0.096	11.166	48.008	0.315	0.005	0.183	0.089	0.363
DUR6 Ol 7	39.995	0.049	10.095	48.928	0.332	0.006	0.154	0.073	0.370
DUR6 Ol 8	40.388	0.095	7.266	51.222	0.293	0.000	0.118	0.149	0.470
DUR6 Ol 9	39.985	0.079	10.920	48.045	0.309	0.000	0.167	0.107	0.388
DUR6 Ol 10	40.419	0.091	7.439	51.023	0.286	0.002	0.107	0.170	0.462
DUR6 Ol 11	40.042	0.095	11.095	47.803	0.298	0.003	0.170	0.098	0.394
DUR6 Ol 12	39.607	0.085	12.355	46.997	0.330	0.008	0.196	0.085	0.337
DUR6 Ol 13	39.906	0.057	11.686	47.430	0.334	0.002	0.184	0.060	0.341
DUR6 Ol 14	39.854	0.071	11.529	47.617	0.336	0.011	0.186	0.064	0.333
DUR6 Ol 15	39.839	0.087	11.853	47.258	0.324	0.007	0.193	0.084	0.355
DUR6 Ol 16	39.990	0.054	12.420	46.602	0.328	0.004	0.191	0.077	0.335
DUR6 Ol 17	39.681	0.078	11.814	47.494	0.336	0.003	0.187	0.072	0.335
DUR6 Ol 18	40.061	0.094	10.961	47.917	0.318	0.004	0.178	0.106	0.362
DUR6 Ol 19	40.160	0.084	10.764	48.040	0.319	0.001	0.176	0.092	0.364
DUR8 Ol 1	41.181	0.101	8.889	48.918	0.300	0.011	0.124	0.115	0.360
DUR8 Ol 2	39.510	0.050	16.342	43.276	0.347	0.016	0.223	0.035	0.201
DUR8 Ol 3	39.669	0.092	14.863	44.467	0.305	0.009	0.208	0.106	0.281
DUR8 Ol 4	40.169	0.050	14.359	44.562	0.346	0.002	0.207	0.075	0.231
DUR8 Ol 5	41.409	0.060	8.566	48.981	0.361	0.000	0.154	0.140	0.328
DUR8 Ol 6	40.028	0.048	13.592	45.430	0.352	0.013	0.223	0.061	0.253
DUR8 Ol 7	38.282	0.112	20.700	39.946	0.296	0.014	0.320	0.118	0.212
DUR8 Ol 8	40.163	0.051	14.448	44.467	0.352	0.007	0.208	0.050	0.255
DUR8 Ol 9	38.846	0.040	17.116	43.076	0.349	0.006	0.261	0.057	0.249
DUR8 Ol 10	39.555	0.034	15.260	44.238	0.351	0.006	0.247	0.053	0.257
DUR8 Ol 11	39.154	0.058	14.500	45.371	0.349	0.008	0.218	0.067	0.274
DUR8 Ol 12	39.106	0.042	14.309	45.628	0.349	0.004	0.215	0.058	0.289
DUR8 Ol 13	39.355	0.037	14.641	45.038	0.357	0.003	0.248	0.065	0.257
DUR8 Ol 14	39.050	0.063	15.162	44.839	0.353	0.007	0.234	0.050	0.241
APO1 Ol 1	40.104	0.038	11.940	47.019	0.331	0.000	0.185	0.045	0.337
APO1 Ol 2	40.187	0.057	10.836	47.992	0.317	0.003	0.167	0.072	0.368
APO1 Ol 3	39.651	0.043	13.132	46.235	0.325	0.000	0.216	0.061	0.336
APO1 Ol 4	39.769	0.079	11.805	47.438	0.317	0.004	0.195	0.063	0.330
APO1 Ol 5	39.827	0.076	12.021	47.152	0.331	0.004	0.188	0.068	0.333
APO1 Ol 6	39.625	0.059	12.880	46.497	0.316	0.006	0.195	0.079	0.343
APO1 Ol 7	40.204	0.094	9.768	48.988	0.257	0.004	0.166	0.120	0.399
APO4 Ol 8	39.538	0.114	11.112	48.264	0.292	0.010	0.175	0.120	0.374
APO4 Ol 9	39.969	0.084	10.755	48.228	0.336	0.010	0.166	0.078	0.374
APO4 Ol 10	39.704	0.073	11.619	47.661	0.329	0.010	0.181	0.081	0.341
APO4 Ol 11	39.758	0.054	12.208	47.063	0.323	0.006	0.187	0.053	0.347
APO4 Ol 12	39.685	0.056	11.762	47.592	0.315	0.002	0.163	0.081	0.343
APO4 Ol 13	39.883	0.078	10.916	48.193	0.305	0.002	0.181	0.094	0.349
APO4 Ol 14	39.659	0.079	11.373	47.941	0.299	0.001	0.175	0.096	0.377
APO4 Ol 15	40.032	0.082	11.066	47.884	0.317	0.004	0.193	0.067	0.356
APO4 Ol 16	40.035	0.087	11.417	47.509	0.320	0.004	0.186	0.083	0.358
APO7 Ol 1	40.431	0.093	7.011	51.429	0.279	0.003	0.122	0.167	0.464
APO7 Ol 2	40.598	0.103	8.047	50.261	0.276	0.002	0.118	0.162	0.433
APO7 Ol 3	40.651	0.094	7.542	50.700	0.286	0.003	0.127	0.144	0.453
APO7 Ol 4	40.130	0.110	8.540	50.192	0.277	0.003	0.139	0.148	0.461
APO7 Ol 5	40.526	0.074	7.871	50.539	0.283	0.006	0.134	0.132	0.435

Sample	SiO_2	Al_2O_3	FeO	MgO	CaO	TiO_2	MnO	Cr_2O_3	NiO
APO7 Ol 6	40.346	0.094	9.006	49.569	0.289	0.003	0.133	0.147	0.413
APO7 Ol 7	39.993	0.096	11.427	47.498	0.344	0.018	0.183	0.085	0.357
APO7 Ol 8	39.543	0.055	12.750	46.704	0.344	0.010	0.200	0.064	0.329
APO7 Ol 9	39.747	0.062	12.555	46.708	0.342	0.006	0.193	0.054	0.333
APO7 Ol 10	40.680	0.066	7.067	51.167	0.295	0.005	0.109	0.151	0.460
APO7 Ol 11	40.849	0.077	7.473	50.595	0.283	0.000	0.133	0.133	0.456
APO7 Ol 12	39.160	0.127	14.113	45.674	0.294	0.009	0.199	0.088	0.336
APO7 Ol 13	40.194	0.059	10.538	48.190	0.342	0.009	0.190	0.089	0.390
APO7 Ol 14	40.871	0.080	7.689	50.345	0.277	0.000	0.135	0.139	0.464
APO7 Ol 15	40.590	0.092	7.267	51.024	0.276	0.000	0.120	0.151	0.481
APO7 Ol 16	40.735	0.105	7.132	51.017	0.285	0.002	0.100	0.166	0.458
APO7 Ol 17	40.262	0.044	10.141	48.603	0.345	0.003	0.159	0.069	0.374
APO7 Ol 18	40.912	0.073	7.467	50.534	0.284	0.000	0.114	0.161	0.455
APO7 Ol 19	40.377	0.109	9.141	49.326	0.289	0.004	0.154	0.171	0.430
APO7 Ol 20	39.927	0.056	12.237	46.879	0.318	0.001	0.178	0.074	0.330
APO7 Ol 21	39.972	0.045	10.837	48.209	0.319	0.000	0.158	0.075	0.387
APO7 Ol 22	40.246	0.038	10.323	48.419	0.330	0.000	0.171	0.070	0.401
APO7 Ol 23	40.294	0.053	8.678	50.006	0.279	0.000	0.140	0.102	0.448
APO7 Ol 24	39.189	0.163	14.511	45.106	0.304	0.019	0.215	0.135	0.358
APO7 Ol 25	40.130	0.067	11.526	47.353	0.296	0.003	0.166	0.081	0.379
APO7 Ol 26	39.835	0.060	11.093	48.077	0.326	0.006	0.172	0.066	0.366
138345 Ol 1	41.585	0.112	6.975	50.389	0.283	0.003	0.101	0.141	0.412
138345 Ol 2	38.795	0.033	20.262	39.993	0.285	0.028	0.355	0.009	0.240
138345 Ol 3	39.735	0.044	15.840	43.499	0.322	0.004	0.210	0.059	0.288
138345 Ol 4	40.285	0.038	13.655	45.114	0.304	0.016	0.234	0.055	0.298
138345 Ol 5	38.881	0.081	18.698	41.468	0.289	0.005	0.279	0.052	0.246
138345 Ol 6	41.277	0.102	7.259	50.433	0.260	0.004	0.128	0.116	0.422
138345 Ol 7	37.951	0.039	23.167	38.027	0.277	0.000	0.325	0.030	0.183
138345 Ol 8	39.355	0.034	18.124	41.608	0.305	0.000	0.291	0.044	0.240
138345 Ol 9	39.837	0.051	14.872	44.411	0.321	0.005	0.223	0.013	0.266
138345 Ol 10	38.769	0.057	20.256	40.055	0.323	0.007	0.303	0.030	0.200
138345 Ol 11	39.623	0.031	14.839	44.750	0.306	0.009	0.199	0.039	0.204
138345 Ol 12	39.368	0.035	17.261	42.476	0.309	0.002	0.283	0.026	0.240
138345 Ol 13	39.419	0.053	17.191	42.501	0.312	0.013	0.247	0.049	0.216
138345 Ol 14	39.442	0.070	16.605	43.009	0.316	0.010	0.253	0.059	0.235
138345 Ol 15	40.332	0.049	14.204	44.577	0.328	0.006	0.184	0.027	0.293
138345 Ol 16	40.245	0.053	14.288	44.540	0.339	0.003	0.213	0.053	0.266
138345 Ol 17	39.369	0.043	17.574	42.168	0.306	0.006	0.245	0.061	0.229
138345 Ol 18	39.228	0.074	19.376	40.457	0.309	0.012	0.299	0.033	0.211
138345 Ol 19	39.918	0.067	16.979	42.178	0.312	0.007	0.252	0.052	0.234
138345 Ol 20	41.170	0.047	9.465	48.445	0.278	0.011	0.139	0.113	0.331
138345 Ol 21	38.652	0.043	21.255	39.295	0.283	0.005	0.263	0.004	0.200
138345 Ol 22	39.935	0.071	15.120	43.999	0.320	0.011	0.235	0.071	0.239
138345 Ol 23	39.885	0.105	14.664	44.404	0.290	0.004	0.245	0.119	0.284
138345 Ol 24	39.147	0.037	19.472	40.460	0.312	0.009	0.278	0.041	0.245
138345 Ol 25	39.749	0.065	16.108	43.189	0.326	0.012	0.234	0.066	0.251
138345 Ol 26	40.507	0.040	12.134	46.528	0.319	0.004	0.181	0.042	0.245
138345 Ol 27	39.144	0.036	18.375	41.632	0.317	0.000	0.276	0.021	0.199
138345 Ol 28	41.375	0.115	7.507	50.052	0.270	0.007	0.125	0.141	0.408
138345 Ol 29	38.530	0.036	21.224	39.395	0.298	0.008	0.298	0.024	0.187
138345 Ol 30	40.828	0.100	9.367	48.827	0.271	0.012	0.143	0.115	0.337
264217 Ol 1	40.020	0.063	13.093	45.988	0.302	0.002	0.181	0.063	0.288
264217 Ol 2	40.494	0.082	13.009	45.439	0.337	0.011	0.211	0.078	0.339
264217 Ol 3	40.192	0.051	13.106	45.780	0.347	0.001	0.207	0.048	0.268
264217 Ol 4	39.633	0.060	13.195	46.233	0.329	0.005	0.205	0.067	0.273
264217 Ol 5	62.515	0.108	7.184	29.721	0.085	0.008	0.007	0.106	0.267
264217 Ol 6	40.145	0.077	13.252	45.624	0.330	0.011	0.193	0.090	0.277
264217 Ol 7	40.467	0.071	11.691	46.857	0.329	0.008	0.172	0.073	0.332
264217 Ol 8	40.121	0.081	12.620	46.287	0.328	0.008	0.185	0.075	0.295
264217 Ol 9	40.193	0.053	11.547	47.313	0.320	0.000	0.183	0.077	0.314
264217 Ol 10	41.224	0.063	9.115	48.613	0.317	0.010	0.140	0.110	0.408
264217 Ol 11	40.294	0.086	12.036	46.661	0.314	0.002	0.186	0.089	0.331
264217 Ol 12	40.031	0.053	13.146	45.909	0.351	0.008	0.175	0.061	0.266
264217 Ol 13	40.685	0.064	10.154	48.127	0.338	0.004	0.165	0.076	0.386
264217 Ol 14	40.789	0.048	10.263	47.927	0.348	0.000	0.203	0.079	0.343

Sample	SiO_2	Al_2O_3	FeO	MgO	CaO	TiO_2	MnO	Cr_2O_3	NiO
264217 Ol 15	40.044	0.102	13.149	45.742	0.314	0.004	0.216	0.098	0.331
264217 Ol 16	40.017	0.056	12.580	46.403	0.327	0.008	0.206	0.096	0.308
264217 Ol 17	40.347	0.037	13.373	45.326	0.356	0.007	0.214	0.037	0.304
264217 Ol 18	40.053	0.108	13.237	45.693	0.348	0.024	0.180	0.071	0.287
332901 Ol 1	39.552	0.044	15.096	44.463	0.285	0.013	0.210	0.048	0.289
332901 Ol 2	38.721	0.025	19.865	40.568	0.218	0.015	0.331	0.015	0.240
332901 Ol 3	39.378	0.041	18.817	40.917	0.291	0.013	0.300	0.025	0.217
332901 Ol 5	39.032	0.035	19.593	40.500	0.241	0.017	0.279	0.038	0.266
332901 Ol 6	41.387	0.050	9.086	48.588	0.294	0.015	0.135	0.074	0.371
332901 Ol 7	39.893	0.038	12.717	46.479	0.306	0.009	0.185	0.049	0.324
332901 Ol 8	39.027	0.023	19.597	40.521	0.233	0.013	0.330	0.006	0.251
332901 Ol 9	39.742	0.032	15.756	43.729	0.263	0.003	0.241	0.013	0.221
332901 Ol 10	39.670	0.047	16.511	42.910	0.297	0.000	0.259	0.044	0.263
332901 Ol 11	38.981	0.023	19.680	40.571	0.152	0.037	0.313	0.008	0.235
332901 Ol 12	39.463	0.043	17.428	42.262	0.300	0.005	0.244	0.034	0.221
332901 Ol 13	40.622	0.063	11.674	46.739	0.288	0.013	0.178	0.055	0.368
332901 Ol 14	38.841	0.050	19.007	41.258	0.233	0.014	0.303	0.037	0.257
332901 Ol 15	38.464	0.052	21.111	39.606	0.173	0.010	0.343	0.000	0.241
332901 Ol 16	38.947	0.029	20.423	39.757	0.244	0.011	0.327	0.012	0.249
332901 Ol 17	39.710	0.051	15.316	44.063	0.295	0.007	0.215	0.064	0.279
332901 Ol 18	39.430	0.037	15.942	43.744	0.303	0.009	0.237	0.029	0.269
332901 Ol 19	39.852	0.042	14.207	45.033	0.281	0.007	0.193	0.050	0.337
332901 Ol 20	39.208	0.028	18.519	41.351	0.288	0.006	0.308	0.025	0.267
332901 Ol 21	38.684	0.037	21.604	38.888	0.217	0.010	0.346	0.003	0.211
332901 Ol 22	40.171	0.026	14.147	44.854	0.255	0.015	0.213	0.028	0.291
332901 Ol 23	38.654	0.041	21.222	39.324	0.193	0.016	0.337	0.020	0.194
332901 Ol 24	38.758	0.029	20.461	39.947	0.227	0.000	0.342	0.011	0.226
332901 Ol 25	40.128	0.061	14.178	44.796	0.282	0.011	0.181	0.054	0.309
332901 Ol 26	38.582	0.031	21.062	39.533	0.212	0.008	0.339	0.007	0.227
340740 Ol 1	40.293	0.089	12.345	46.343	0.308	0.009	0.180	0.083	0.350
340740 Ol 2	40.865	0.083	9.647	48.478	0.280	0.007	0.136	0.135	0.370
340740 Ol 3	40.138	0.053	12.906	46.011	0.335	0.009	0.197	0.049	0.302
340740 Ol 4	40.261	0.069	13.295	45.474	0.337	0.008	0.195	0.064	0.296
340740 Ol 5	40.155	0.043	13.607	45.320	0.351	0.018	0.229	0.046	0.232
340740 Ol 6	40.615	0.067	11.922	46.474	0.304	0.000	0.180	0.049	0.390
340740 Ol 7	40.373	0.071	11.841	46.790	0.296	0.016	0.190	0.084	0.339
340740 Ol 8	40.521	0.065	12.340	46.130	0.324	0.022	0.198	0.105	0.296
340740 Ol 9	40.994	0.086	10.346	47.680	0.285	0.000	0.166	0.094	0.350
340740 Ol 10	41.014	0.080	9.108	48.821	0.270	0.009	0.148	0.142	0.408
340740 Ol 11	41.254	0.110	7.636	49.971	0.288	0.009	0.117	0.161	0.455
340740 Ol 12	39.901	0.060	12.915	46.291	0.333	0.000	0.176	0.066	0.259
340740 Ol 13	41.133	0.096	8.615	49.222	0.261	0.012	0.147	0.125	0.387
340740 Ol 14	40.411	0.073	12.413	46.172	0.331	0.010	0.183	0.099	0.308
340740 Ol 15	40.256	0.092	12.445	46.289	0.307	0.004	0.205	0.089	0.314
340740 Ol 16	41.036	0.053	9.748	48.288	0.284	0.013	0.141	0.052	0.384
340740 Ol 17	40.334	0.059	12.994	45.743	0.318	0.000	0.172	0.053	0.327
340740 Ol 18	40.221	0.072	12.999	45.777	0.360	0.012	0.206	0.060	0.293
340740 Ol 19	40.005	0.080	11.971	47.023	0.330	0.009	0.192	0.079	0.313
354754 Ol 1	39.382	0.067	17.760	41.903	0.293	0.002	0.298	0.060	0.235
354754 Ol 2	40.351	0.074	13.352	45.304	0.328	0.008	0.196	0.074	0.313
354754 Ol 3	40.735	0.044	10.880	47.454	0.308	0.000	0.160	0.070	0.349
354754 Ol 4	38.975	0.049	20.699	39.394	0.326	0.014	0.322	0.022	0.200
340740 Ol 5	40.155	0.043	13.607	45.320	0.351	0.018	0.229	0.046	0.232
340740 Ol 6	40.615	0.067	11.922	46.474	0.304	0.000	0.180	0.049	0.390
340740 Ol 7	40.373	0.071	11.841	46.790	0.296	0.016	0.190	0.084	0.339
340740 Ol 8	40.521	0.065	12.340	46.130	0.324	0.022	0.198	0.105	0.296
340740 Ol 9	40.994	0.086	10.346	47.680	0.285	0.000	0.166	0.094	0.350
340740 Ol 10	41.014	0.080	9.108	48.821	0.270	0.009	0.148	0.142	0.408
340740 Ol 11	41.254	0.110	7.636	49.971	0.288	0.009	0.117	0.161	0.455
340740 Ol 12	39.901	0.060	12.915	46.291	0.333	0.000	0.176	0.066	0.259
340740 Ol 13	41.133	0.096	8.615	49.222	0.261	0.012	0.147	0.125	0.387
340740 Ol 14	40.411	0.073	12.413	46.172	0.331	0.010	0.183	0.099	0.308
340740 Ol 15	40.256	0.092	12.445	46.289	0.307	0.004	0.205	0.089	0.314
340740 Ol 16	41.036	0.053	9.748	48.288	0.284	0.013	0.141	0.052	0.384
340740 Ol 17	40.334	0.059	12.994	45.743	0.318	0.000	0.172	0.053	0.327
340740 Ol 18	40.221	0.072	12.999	45.777	0.360	0.012	0.206	0.060	0.293
340740 Ol 19	40.005	0.080	11.971	47.023	0.330	0.009	0.192	0.079	0.313
354754 Ol 1	39.382	0.067	17.760	41.903	0.293	0.002	0.298	0.060	0.235

Sample	SiO_2	Al_2O_3	FeO	MgO	CaO	TiO_2	MnO	Cr_2O_3	NiO
354754 Ol 2	40.351	0.074	13.352	45.304	0.328	0.008	0.196	0.074	0.313
354754 Ol 3	40.735	0.044	10.880	47.454	0.308	0.000	0.160	0.070	0.349
354754 Ol 4	38.975	0.049	20.699	39.394	0.326	0.014	0.322	0.022	0.200
354754 Ol 5	40.134	0.035	14.290	44.645	0.339	0.016	0.210	0.032	0.299
354754 Ol 6	40.002	0.046	14.707	44.301	0.357	0.009	0.233	0.037	0.307
354754 Ol 7	39.630	0.043	16.979	42.428	0.315	0.012	0.273	0.048	0.270
354754 Ol 8	40.370	0.081	13.289	45.346	0.328	0.012	0.196	0.074	0.304
354754 Ol 9	39.129	0.035	20.119	39.878	0.281	0.020	0.320	0.024	0.194
354754 Ol 10	39.470	0.070	17.107	42.421	0.316	0.016	0.269	0.075	0.256
354754 Ol 11	39.602	0.048	16.578	42.854	0.323	0.010	0.275	0.046	0.264
354754 Ol 12	40.040	0.067	14.789	44.160	0.302	0.014	0.238	0.060	0.329
354754 Ol 13	39.911	0.041	14.512	44.680	0.285	0.016	0.229	0.038	0.289
354754 Ol 14	40.124	0.050	14.706	44.266	0.340	0.005	0.216	0.052	0.242
354754 Ol 15	40.648	0.074	13.087	45.334	0.240	0.008	0.209	0.075	0.325
354754 Ol 16	39.237	0.054	18.960	40.866	0.314	0.011	0.313	0.033	0.213
354754 Ol 17	40.278	0.047	13.736	45.094	0.306	0.011	0.208	0.015	0.305
354754 Ol 18	38.608	0.069	21.745	38.657	0.250	0.029	0.379	0.022	0.241
362077 Ol 1	41.350	0.106	8.245	49.392	0.275	0.000	0.097	0.141	0.395
362077 Ol 2	40.416	0.072	13.253	45.320	0.348	0.002	0.205	0.063	0.321
362077 Ol 3	41.349	0.131	7.626	49.863	0.274	0.012	0.122	0.193	0.429
362077 Ol 4	40.613	0.047	13.180	45.262	0.339	0.005	0.181	0.082	0.293
362077 Ol 5	41.637	0.116	7.385	49.811	0.273	0.008	0.135	0.181	0.454
362077 Ol 6	40.388	0.090	13.334	45.250	0.351	0.019	0.226	0.062	0.281
362077 Ol 7	41.175	0.075	8.518	49.270	0.302	0.008	0.119	0.150	0.383
362077 Ol 8	41.195	0.129	10.216	47.504	0.292	0.014	0.146	0.117	0.387
362077 Ol 9	40.490	0.044	13.605	44.918	0.353	0.016	0.202	0.061	0.311
362077 Ol 10	40.151	0.057	13.739	45.170	0.354	0.004	0.187	0.070	0.267
362077 Ol 11	40.209	0.054	13.672	45.125	0.358	0.009	0.225	0.050	0.299
362077 Ol 12	40.023	0.059	13.470	45.537	0.354	0.016	0.213	0.058	0.270
362077 Ol 13	40.294	0.048	13.820	44.990	0.346	0.002	0.210	0.014	0.276
362077 Ol 14	40.416	0.037	13.714	44.935	0.345	0.000	0.203	0.052	0.299
362077 Ol 15	40.077	0.086	13.714	45.218	0.364	0.010	0.181	0.069	0.281
362077 Ol 16	40.382	0.080	13.432	45.191	0.379	0.005	0.219	0.044	0.268
362077 Ol 17	40.310	0.051	13.309	45.424	0.366	0.005	0.195	0.049	0.290
362077 Ol 18	39.914	0.098	13.666	45.395	0.343	0.012	0.198	0.061	0.313
362077 Ol 19	40.168	0.071	13.610	45.195	0.349	0.010	0.222	0.075	0.301
362077 Ol 20	40.240	0.057	13.723	45.041	0.350	0.014	0.236	0.047	0.291
362077 Ol 21	40.118	0.099	13.721	45.065	0.355	0.015	0.266	0.086	0.275
362077 Ol 22	40.710	0.114	7.207	50.906	0.284	0.003	0.124	0.177	0.475
362077 Ol 23	39.596	0.045	13.252	46.139	0.354	0.003	0.208	0.053	0.348
362077 Ol 24	39.429	0.047	13.207	46.407	0.354	0.004	0.191	0.041	0.320
362077 Ol 25	38.576	0.125	7.424	52.876	0.272	0.006	0.122	0.166	0.434
362077 Ol 26	40.710	0.114	7.207	50.906	0.284	0.003	0.124	0.177	0.475
362077 Ol 27	39.596	0.045	13.252	46.139	0.354	0.003	0.208	0.053	0.348
362077 Ol 28	39.429	0.047	13.207	46.407	0.354	0.004	0.191	0.041	0.320
400230 Ol 1	40.231	0.039	14.070	44.754	0.338	0.000	0.222	0.065	0.281
400230 Ol 2	40.762	0.110	10.690	47.535	0.262	0.002	0.136	0.136	0.367
400230 Ol 3	38.900	0.034	21.226	38.900	0.398	0.031	0.331	0.008	0.171
400230 Ol 4	40.246	0.058	14.367	44.442	0.335	0.009	0.213	0.063	0.267
400230 Ol 5	40.241	0.069	14.575	44.187	0.344	0.016	0.223	0.038	0.307
400230 Ol 6	40.298	0.056	13.470	45.281	0.333	0.005	0.190	0.040	0.328
400230 Ol 7	40.302	0.081	13.444	45.280	0.307	0.008	0.172	0.067	0.338
400230 Ol 8	40.242	0.090	14.516	44.179	0.339	0.008	0.223	0.084	0.320
400230 Ol 9	40.128	0.075	14.559	44.302	0.347	0.019	0.200	0.074	0.297
400230 Ol 10	40.417	0.090	12.576	46.043	0.276	0.002	0.132	0.099	0.366
400230 Ol 11	39.323	0.038	19.908	39.792	0.388	0.025	0.331	0.004	0.191
400230 Ol 12	41.330	0.106	9.132	48.434	0.294	0.011	0.155	0.100	0.438
400230 Ol 13	39.828	0.034	16.921	42.241	0.384	0.020	0.273	0.041	0.257
400230 Ol 14	39.903	0.042	14.810	44.289	0.363	0.013	0.253	0.048	0.280
400230 Ol 15	40.123	0.055	13.935	44.978	0.352	0.015	0.217	0.061	0.264
400230 Ol 16	39.868	0.032	15.198	44.032	0.361	0.020	0.205	0.022	0.262
400230 Ol 17	41.438	0.107	7.799	49.695	0.275	0.001	0.099	0.146	0.441
400230 Ol 18	39.566	0.045	16.953	42.494	0.376	0.019	0.254	0.034	0.259
400230 Ol 19	40.431	0.055	13.683	44.934	0.311	0.010	0.215	0.044	0.318
400230 Ol 20	40.412	0.073	13.590	45.068	0.293	0.011	0.161	0.098	0.295
400230 Ol 21	40.807	0.094	10.208	48.017	0.260	0.000	0.128	0.107	0.380
400230 Ol 22	39.708	0.035	17.254	42.101	0.368	0.014	0.250	0.039	0.232
400230 Ol 23	40.030	0.072	14.423	44.562	0.352	0.010	0.211	0.057	0.282

Sample	SiO_2	Al_2O_3	FeO	MgO	CaO	TiO_2	MnO	Cr_2O_3	NiO
400230 Ol 24	40.174	0.046	14.122	44.756	0.361	0.004	0.203	0.072	0.263
400452 Ol 1	39.864	0.065	12.513	46.732	0.324	0.007	0.175	0.054	0.267
400452 Ol 2	40.452	0.053	12.351	46.203	0.345	0.015	0.199	0.074	0.308
400452 Ol 3	40.662	0.087	12.356	45.980	0.332	0.003	0.190	0.090	0.300
400452 Ol 4	40.364	0.069	12.040	46.579	0.339	0.009	0.226	0.061	0.313
400452 Ol 5	40.336	0.095	13.117	45.531	0.328	0.008	0.199	0.076	0.311
400452 Ol 6	39.881	0.055	12.446	46.726	0.334	0.002	0.186	0.068	0.302
400452 Ol 7	40.646	0.056	12.062	46.294	0.330	0.009	0.192	0.071	0.341
400452 Ol 8	40.333	0.058	12.470	46.258	0.335	0.003	0.191	0.060	0.292
400452 Ol 9	40.051	0.044	12.528	46.507	0.337	0.004	0.205	0.050	0.273
400452 Ol 10	39.975	0.066	12.721	46.301	0.348	0.008	0.202	0.097	0.282
400452 Ol 11	40.175	0.084	13.122	45.708	0.334	0.018	0.211	0.074	0.274
400452 Ol 12	40.177	0.048	12.076	46.811	0.333	0.000	0.174	0.041	0.340
400452 Ol 13	40.283	0.107	12.148	46.465	0.345	0.015	0.191	0.106	0.338
400452 Ol 14	39.972	0.085	12.465	46.606	0.322	0.011	0.166	0.093	0.281
400452 Ol 15	40.084	0.079	12.331	46.614	0.322	0.001	0.194	0.087	0.289
400452 Ol 16	39.982	0.054	13.645	45.392	0.377	0.015	0.223	0.052	0.259
400452 Ol 17	39.743	0.079	12.978	46.302	0.348	0.015	0.173	0.080	0.282
400452 Ol 18	40.577	0.066	12.589	45.849	0.349	0.013	0.199	0.064	0.295
400452 Ol 19	39.996	0.051	11.961	47.062	0.341	0.000	0.182	0.056	0.351
400452 Ol 20	39.800	0.051	13.245	45.964	0.359	0.002	0.207	0.068	0.303
400452 Ol 21	40.210	0.052	12.071	46.717	0.340	0.003	0.196	0.057	0.354
400452 Ol 22	39.591	0.047	12.984	46.420	0.334	0.000	0.207	0.057	0.360
400452 Ol 23	39.862	0.079	11.924	47.184	0.337	0.006	0.188	0.085	0.337
400452 Ol 24	39.865	0.102	12.252	46.821	0.308	0.008	0.185	0.093	0.366
400452 Ol 25	39.996	0.051	11.961	47.062	0.341	0.000	0.182	0.056	0.351
400452 Ol 26	39.918	0.045	11.977	47.118	0.335	0.000	0.179	0.066	0.363
400452 Ol 27	39.800	0.051	13.245	45.964	0.359	0.002	0.207	0.068	0.303
400452 Ol 28	40.210	0.052	12.071	46.717	0.340	0.003	0.196	0.057	0.354
400452 Ol 29	39.591	0.047	12.984	46.420	0.334	0.000	0.207	0.057	0.360
400452 Ol 30	39.862	0.079	11.924	47.184	0.337	0.006	0.188	0.085	0.337
400452 Ol 31	39.865	0.102	12.252	46.821	0.308	0.008	0.185	0.093	0.366
400457 Ol 1	40.216	0.043	13.281	45.537	0.339	0.000	0.253	0.052	0.279
400457 Ol 2	39.963	0.041	14.275	44.895	0.345	0.008	0.193	0.045	0.237
400457 Ol 3	39.975	0.065	13.407	45.663	0.328	0.004	0.231	0.064	0.264
400457 Ol 4	40.386	0.052	13.399	45.263	0.337	0.004	0.200	0.045	0.314
400457 Ol 5	40.433	0.047	13.823	44.807	0.341	0.008	0.213	0.031	0.298
400457 Ol 6	39.823	0.084	13.643	45.541	0.330	0.019	0.227	0.062	0.272
400457 Ol 7	40.178	0.090	13.451	45.404	0.328	0.021	0.195	0.055	0.277
400457 Ol 8	40.231	0.045	13.378	45.511	0.339	0.010	0.173	0.025	0.288
400457 Ol 9	39.893	0.034	13.397	45.786	0.336	0.009	0.214	0.057	0.273
400457 Ol 10	40.090	0.050	13.310	45.670	0.337	0.022	0.191	0.051	0.279
400457 Ol 11	40.358	0.053	13.345	45.375	0.342	0.000	0.193	0.048	0.286
400457 Ol 12	40.139	0.073	13.294	45.548	0.350	0.020	0.223	0.073	0.280
400457 Ol 13	40.362	0.053	13.435	45.287	0.338	0.001	0.200	0.027	0.297
400457 Ol 14	40.356	0.047	13.468	45.238	0.327	0.015	0.195	0.038	0.315
400457 Ol 15	40.067	0.044	13.547	45.480	0.331	0.001	0.200	0.056	0.273
400457 Ol 16	40.257	0.044	13.426	45.398	0.338	0.001	0.210	0.035	0.290
400457 Ol 17	40.097	0.046	13.640	45.373	0.328	0.004	0.205	0.046	0.263
400457 Ol 18	40.193	0.057	13.046	45.798	0.341	0.005	0.227	0.038	0.295
400457 Ol 19	40.352	0.052	13.055	45.698	0.328	0.002	0.167	0.037	0.310
400457 Ol 20	40.432	0.073	12.973	45.617	0.343	0.010	0.216	0.050	0.285
400457 Ol 21	40.605	0.106	11.689	46.637	0.292	0.009	0.212	0.093	0.357
400457 Ol 22	40.353	0.033	13.052	45.677	0.333	0.004	0.183	0.077	0.289
400457 Ol 23	40.354	0.061	13.000	45.672	0.341	0.007	0.235	0.051	0.280
400457 Ol 24	40.196	0.053	12.975	45.896	0.330	0.000	0.202	0.055	0.294
400457 Ol 25	40.475	0.045	13.457	45.139	0.360	0.007	0.216	0.026	0.277
400457 Ol 26	40.485	0.044	12.903	45.672	0.346	0.013	0.204	0.054	0.279
400457 Ol 27	40.622	0.052	12.867	45.572	0.339	0.008	0.216	0.031	0.293
400457 Ol 28	40.252	0.051	13.431	45.382	0.325	0.004	0.199	0.060	0.296
400457 Ol 29	40.334	0.065	12.947	45.729	0.308	0.007	0.206	0.076	0.329
400457 Ol 30	40.347	0.060	13.346	45.326	0.341	0.011	0.211	0.033	0.325
400457 Ol 31	40.390	0.090	13.085	45.534	0.337	0.021	0.193	0.051	0.300
400457 Ol 32	40.306	0.051	13.219	45.493	0.344	0.013	0.208	0.056	0.311
400457 Ol 33	40.090	0.042	13.149	45.849	0.346	0.010	0.184	0.039	0.292
410152 Ol 1	40.504	0.047	12.680	45.845	0.338	0.007	0.205	0.036	0.339
410152 Ol 2	40.575	0.040	12.232	46.254	0.333	0.011	0.200	0.067	0.289
410152 Ol 3	38.669	0.047	21.228	39.159	0.299	0.010	0.350	0.027	0.210

Sample	SiO_2	Al_2O_3	FeO	MgO	CaO	TiO_2	MnO	Cr_2O_3	NiO
410152 Ol 4	40.508	0.062	13.152	45.298	0.321	0.008	0.235	0.073	0.343
410152 Ol 5	39.442	0.025	17.489	42.095	0.358	0.012	0.297	0.038	0.245
410152 Ol 6	40.530	0.036	13.719	44.870	0.299	0.012	0.209	0.033	0.293
410152 Ol 7	40.347	0.056	13.559	45.127	0.344	0.007	0.197	0.050	0.313
410152 Ol 8	38.379	0.021	23.744	36.985	0.270	0.022	0.354	0.025	0.199
410152 Ol 9	38.982	0.070	18.953	41.129	0.308	0.006	0.293	0.053	0.206
410152 Ol 10	39.886	0.052	15.119	43.982	0.354	0.002	0.252	0.047	0.306
410152 Ol 11	40.455	0.046	13.314	45.296	0.325	0.012	0.179	0.061	0.312
410152 Ol 12	40.298	0.057	13.447	45.362	0.298	0.000	0.186	0.064	0.289
410152 Ol 13	39.193	0.022	19.692	40.254	0.314	0.011	0.292	0.009	0.213
410152 Ol 14	40.174	0.063	13.005	45.882	0.297	0.014	0.195	0.083	0.286
410152 Ol 15	40.297	0.036	13.568	45.185	0.353	0.013	0.178	0.054	0.316

Appendix L Melt inclusion major element compositions

Sample	SiO_2	Al_2O_3	FeO	MgO	CaO	Na_2O	K_2O	TiO_2	MnO	P_2O_5	Host Ol Fo%
PAD6 MI 1	51.76	17.73	7.18	3.27	15.88	2.17	0.21	1.43	0.16	0.21	86.4
PAD6 MI 3a	51.62	17.68	7.37	3.37	15.83	2.33	0.22	1.13	0.25	0.21	
PAD6 MI 3b	52.62	18.17	5.83	2.85	16.33	2.19	0.24	1.31	0.20	0.25	88.3
PAD6 MI 3c	52.12	18.58	5.59	3.08	16.50	2.05	0.20	1.46	0.19	0.22	88.9
PAD6 MI 4a	52.38	17.37	7.32	4.08	14.88	2.09	0.30	1.13	0.22	0.22	87.5
PAD6 MI 5a	51.60	18.21	7.33	3.00	15.86	2.24	0.18	1.28	0.11	0.19	86.8
PAD6 MI 5b	51.19	18.77	7.04	2.70	16.45	2.23	0.16	1.08	0.19	0.21	87.7
PAD6 MI 5c	52.23	18.52	6.26	2.45	16.51	2.36	0.16	1.12	0.19	0.19	87.0
PAD6 MI 5d	52.90	18.06	6.34	2.77	15.92	2.25	0.13	1.19	0.20	0.23	85.4
PAD6 MI 6a	53.08	17.61	6.62	3.60	15.47	2.16	0.10	0.92	0.25	0.19	87.6
PAD6 MI 6b	54.64	17.03	5.93	3.28	15.20	2.45	0.06	1.07	0.20	0.14	88.5
PAD6 MI 6c	52.32	18.19	6.51	2.93	16.02	2.28	0.21	1.23	0.17	0.16	86.7
PAD6 MI 7	51.96	18.42	6.41	3.15	15.63	2.28	0.19	1.45	0.32	0.19	86.6
PAD6 MI 8a	52.10	18.95	5.27	3.41	16.24	2.26	0.22	1.28	0.05	0.22	88.8
PAD6 MI 8b	52.20	18.08	6.49	3.71	15.66	2.03	0.21	1.15	0.26	0.20	88.8
PAD6 MI 9	51.69	18.07	7.07	3.29	15.93	2.26	0.23	1.26	0.00	0.19	87.6
PAD6 MI 10a	52.07	16.95	7.66	3.60	15.66	2.12	0.23	1.28	0.24	0.19	87.4
PAD6 MI 10b	51.76	17.73	7.41	3.10	15.88	2.30	0.21	1.23	0.18	0.21	87.4
PAD6 MI 11a	54.41	17.22	6.32	3.85	14.63	2.27	0.23	0.70	0.17	0.20	87.8
PAD6 MI 11b	51.56	17.35	7.41	3.75	15.61	2.39	0.22	1.28	0.23	0.20	87.5
PAD6 MI 12a	51.80	17.94	7.31	3.34	15.65	2.18	0.21	1.15	0.22	0.19	86.9
PAD6 MI 12b	52.93	17.84	6.20	2.98	15.87	2.45	0.17	1.28	0.10	0.17	87.3
PAD6 MI 12c	52.26	17.94	7.59	2.93	15.17	2.43	0.28	1.20	0.00	0.21	87.2
PAD6 MI 12d	51.32	18.16	7.45	3.28	15.75	2.24	0.21	1.26	0.12	0.21	86.9
PAD6 MI 12e	52.60	17.70	7.17	3.10	15.36	2.41	0.21	1.14	0.10	0.20	87.2
PAD6 MI 12f	51.81	18.21	7.27	3.15	15.48	2.34	0.23	1.26	0.00	0.24	87.1
PAD6 MI 12g	52.46	17.88	6.99	2.92	15.63	2.20	0.20	1.26	0.25	0.21	87.1
PAD6 MI 13	51.66	18.19	6.71	3.19	16.07	2.44	0.17	1.18	0.13	0.26	87.3
PAD6 MI 14	52.48	16.40	7.78	3.42	15.93	2.21	0.21	1.34	0.04	0.19	87.0
PAD6 MI 15a	51.78	17.68	7.79	3.19	15.46	2.22	0.20	1.37	0.10	0.21	86.4
PAD6 MI 15b	53.08	17.69	6.24	2.91	15.97	2.33	0.17	1.18	0.25	0.19	86.6
PAD6 MI 15c	52.22	17.35	7.32	3.10	15.78	2.46	0.17	1.20	0.23	0.18	86.6
PAD6 MI 16	52.10	18.10	5.84	3.13	16.88	2.11	0.20	1.28	0.13	0.23	87.2
PAD6 MI 17	52.15	17.73	6.91	3.20	16.27	2.16	0.10	1.15	0.16	0.18	88.0
PAD6 MI 18	52.30	18.21	6.87	2.55	15.82	2.30	0.22	1.34	0.16	0.24	86.4
PAD6 MI 19	51.08	16.70	8.60	4.64	15.37	1.98	0.19	1.10	0.18	0.18	86.1
PAD6 MI 20	51.77	17.32	7.47	3.30	16.21	2.15	0.18	1.21	0.14	0.25	87.0
PAD6 MI 21	51.61	17.98	7.25	3.32	15.99	2.03	0.21	1.25	0.14	0.21	87.0
PAD6 MI 22	52.35	17.29	7.40	3.42	15.82	2.23	0.22	1.09	0.00	0.17	86.6
PAD6 MI 23	51.73	17.10	8.26	3.17	15.58	2.33	0.17	1.31	0.16	0.19	86.9
PAD6 MI 24	51.86	16.93	7.81	3.83	15.82	2.14	0.21	1.09	0.14	0.16	86.9
PAD6 MI 25a	52.36	18.00	4.84	5.15	15.89	1.98	0.17	1.10	0.11	0.40	92.3
PAD6 MI 25b	52.36	18.00	4.84	5.15	15.89	1.98	0.17	1.10	0.11	0.40	92.3
PAD6 MI 26	51.01	18.32	7.09	3.62	15.97	2.03	0.15	1.30	0.14	0.35	87.0
PAD6 MI 27	51.35	16.74	8.11	3.27	16.03	2.35	0.17	1.44	0.17	0.37	85.9
PAD6 MI 28	50.71	17.57	8.08	3.70	15.77	2.18	0.18	1.27	0.17	0.36	85.9
PAD6 MI 29	53.71	16.70	6.11	4.60	15.26	2.02	0.20	0.93	0.11	0.36	88.9
PAD6 MI 30	54.08	16.49	6.98	4.09	14.57	2.19	0.17	0.92	0.12	0.39	87.1
PAD6 MI 31	51.01	17.26	7.79	4.81	15.10	2.10	0.17	1.26	0.15	0.36	86.8
PAD6 MI 32	51.18	17.70	7.81	3.45	15.99	1.89	0.15	1.31	0.15	0.37	85.4
PAD6 MI 33	50.49	17.55	8.32	4.27	15.50	2.07	0.13	1.17	0.16	0.34	86.3
PAD6 MI 34	50.54	17.27	8.41	4.24	15.65	1.95	0.13	1.30	0.15	0.35	86.0

Sample	SiO_2	Al_2O_3	FeO	MgO	CaO	Na_2O	K_2O	TiO_2	MnO	P_2O_5	Host Ol Fo%
PAD6 MI 35	50.94	17.61	7.91	3.55	15.73	2.26	0.17	1.30	0.16	0.36	86.3
PAD6 MI 36	51.33	17.64	7.55	3.47	15.79	2.13	0.18	1.37	0.17	0.38	86.6
PAD6 MI 37	51.06	18.12	7.34	3.49	15.94	2.06	0.17	1.30	0.15	0.37	86.5
PAD6 MI 38	51.85	18.57	6.83	2.80	15.67	2.26	0.18	1.31	0.13	0.38	85.8
PAD6 MI 39	50.77	17.09	8.32	4.25	15.38	2.23	0.16	1.30	0.16	0.35	86.1
PAD6 MI 40a	50.49	17.37	8.43	4.19	15.39	2.15	0.18	1.31	0.15	0.34	87.1
PAD6 MI 40b	50.49	17.37	8.43	4.19	15.39	2.15	0.18	1.31	0.15	0.34	87.1
PAD6 MI 41a	50.85	18.12	7.41	3.58	15.84	2.13	0.18	1.32	0.15	0.40	86.9
PAD6 MI 41b	51.05	17.61	7.78	3.94	15.52	2.10	0.17	1.31	0.16	0.36	86.9
PAD6 MI 42	50.85	17.92	7.58	3.62	15.79	2.28	0.18	1.29	0.14	0.36	86.8
PAD6 MI 43	51.57	18.06	7.09	3.54	15.46	2.26	0.19	1.31	0.15	0.39	86.4
PAD6 MI 44	51.38	17.87	7.30	3.54	15.65	2.26	0.18	1.33	0.15	0.34	86.7
PAD6 MI 45	50.63	17.46	8.49	3.96	15.41	2.09	0.15	1.30	0.15	0.35	86.1
PAD6 MI 46	51.30	18.08	7.79	3.22	15.38	2.22	0.19	1.29	0.15	0.38	86.3
PAD6 MI 47	51.24	17.47	8.06	3.51	15.45	2.24	0.18	1.30	0.15	0.39	86.3
PAD6 MI 48a	50.40	18.42	7.61	3.87	15.52	2.19	0.19	1.31	0.15	0.35	86.6
PAD6 MI 49	48.23	24.70	5.75	2.79	14.43	2.22	0.22	1.21	0.13	0.32	87.1
PAD6 MI 52	53.59	17.19	5.65	3.98	15.99	2.07	0.07	1.02	0.12	0.30	89.9
PAD6 MI 53	51.20	17.56	7.89	3.44	15.79	2.30	0.08	1.26	0.15	0.33	87.2
PAD6 MI 54	50.39	17.79	8.31	3.99	15.48	2.21	0.13	1.23	0.15	0.32	87.3
PAD6 MI 55	51.04	17.93	7.56	3.66	15.51	2.33	0.19	1.26	0.15	0.36	87.5
PAD6 MI 58	50.94	18.89	6.63	3.27	16.15	2.16	0.17	1.30	0.14	0.36	86.9
PAD6 MI 60b	51.61	18.68	6.03	3.02	16.34	2.40	0.19	1.24	0.12	0.37	87.3
PAD6 MI 61	51.85	17.80	7.07	2.94	16.05	2.27	0.21	1.33	0.13	0.35	87.3
PAD6 MI 62	51.03	19.06	6.04	3.97	15.29	2.60	0.25	1.30	0.11	0.34	87.1
DUR8 MI 1	52.39	17.36	4.76	5.18	15.77	2.53	0.23	1.55	0.00	0.23	84.2
DUR8 MI 2	55.39	18.94	2.94	1.51	15.93	3.42	0.16	1.07	0.00	0.65	85.3
DUR8 MI 3	53.99	18.92	3.68	1.30	16.94	2.76	0.28	1.68	0.23	0.22	80.9
DUR8 MI 4	54.52	18.54	4.13	1.48	16.54	2.74	0.20	1.62	0.04	0.20	83.6
DUR8 MI 5	53.85	19.61	3.63	1.45	16.44	2.85	0.21	1.65	0.00	0.31	84.8
DUR8 MI 6	54.41	19.58	3.32	1.37	16.89	2.92	0.11	1.23	0.00	0.19	84.5
DUR8 MI 7a	53.39	19.21	3.99	1.42	16.97	2.76	0.25	1.64	0.13	0.23	81.3
DUR8 MI 7b	54.25	19.72	2.95	1.36	16.78	2.74	0.21	1.68	0.05	0.26	81.3
DUR8 MI 8a	53.41	20.22	3.29	1.50	17.02	2.47	0.17	1.45	0.08	0.40	84.6
DUR8 MI 8b	53.41	20.22	3.29	1.50	17.02	2.47	0.17	1.45	0.08	0.40	84.6
DUR8 MI 9	53.85	19.89	3.09	1.73	16.85	2.58	0.17	1.32	0.07	0.44	84.9
DUR8 MI 10	54.40	18.97	3.62	1.39	16.40	2.70	0.30	1.74	0.06	0.42	82.8
DUR8 MI 11	53.13	18.59	3.40	2.50	17.03	2.87	0.27	1.71	0.10	0.40	84.6
BI/DI/27 MI 1	53.80	20.03	3.18	1.24	17.57	2.68	0.12	1.07	0.14	0.17	81.8
BI/DI/27 MI 2	56.89	20.34	1.69	1.26	15.85	2.86	0.07	0.68	0.18	0.19	88.5
BI/DI/27 MI 3	53.97	19.69	2.99	1.20	17.70	2.72	0.09	1.28	0.13	0.22	82.4
BI/DI/27 MI 4	54.25	20.72	2.27	1.45	17.25	2.65	0.08	1.09	0.07	0.17	85.6
BI/DI/27 MI 5	54.43	20.33	2.62	1.30	17.11	2.88	0.07	1.06	0.00	0.20	87.5
BI/DI/27 MI 6	53.64	19.96	3.20	1.41	17.41	2.70	0.07	1.28	0.16	0.16	84.0
138345 MI 1	56.89	18.82	2.74	0.66	14.34	3.76	0.27	2.01	0.29	0.22	82.7
138345 MI 2	54.31	18.88	3.04	1.19	17.09	2.91	0.26	2.01	0.03	0.28	83.4
138345 MI 3	53.90	19.75	3.10	1.25	17.31	2.92	0.12	1.31	0.14	0.19	84.8
138345 MI 4	54.57	20.10	2.13	1.13	16.57	3.30	0.24	1.70	0.00	0.26	87.1
340740 MI 1	52.00	18.66	5.96	2.69	15.36	2.89	0.22	1.90	0.00	0.31	88.7
340740 MI 2	50.62	17.23	7.12	4.08	15.29	2.74	0.28	2.26	0.07	0.31	89.2
340740 MI 3	52.63	18.76	5.93	2.77	13.90	3.15	0.31	2.12	0.08	0.33	89.2
340740 MI 4	52.64	17.93	6.06	2.79	14.63	3.17	0.34	1.98	0.10	0.37	88.5
340740 MI 5	51.48	17.07	7.78	3.14	15.20	2.23	0.29	2.26	0.18	0.37	87.3
340740 MI 6	51.49	17.61	7.07	3.22	14.74	2.83	0.28	2.23	0.19	0.35	87.6

Sample	SiO_2	Al_2O_3	FeO	MgO	CaO	Na_2O	K_2O	TiO_2	MnO	P_2O_5	Host Ol Fo%
340740 MI 7	51.00	17.69	7.61	2.43	15.99	2.78	0.33	1.79	0.12	0.26	87.0
340740 MI 8	50.87	17.77	7.66	2.96	15.09	2.55	0.26	2.39	0.09	0.34	88.3
340740 MI 9	50.37	17.71	7.87	2.92	15.35	2.79	0.28	2.14	0.22	0.35	86.5
340740 MI 10a	49.89	16.48	8.34	3.89	15.05	2.81	0.97	2.20	0.00	0.36	88.4
340740 MI 10b	51.18	16.82	6.97	3.28	15.43	3.00	0.48	2.30	0.20	0.33	88.4
354754 MI 1	53.33	20.23	2.35	1.12	17.13	3.38	0.19	1.93	0.12	0.22	84.5
354754 MI 2	53.48	20.18	2.69	1.00	16.97	3.22	0.18	1.84	0.25	0.21	82.4
362077 MI 1	52.92	18.34	5.42	3.08	15.45	2.75	0.11	1.54	0.05	0.34	91.4
362077 MI 2	52.08	17.28	5.53	5.18	15.98	2.16	0.13	1.35	0.12	0.20	91.4
362077 MI 3	55.50	17.14	4.78	2.65	15.69	2.65	0.08	1.23	0.00	0.27	89.9
362077 MI 4a	53.86	19.72	3.96	2.14	14.96	3.26	0.17	1.52	0.16	0.25	90.1
362077 MI 4b	54.93	18.08	4.22	2.72	15.65	2.66	0.08	1.49	0.00	0.18	90.8
362077 MI 4c	53.17	18.16	4.95	2.77	15.75	2.90	0.16	1.73	0.14	0.27	90.8
362077 MI 5a	54.55	17.97	4.58	2.87	15.74	2.66	0.09	1.38	0.00	0.17	91.1
362077 MI 5b	53.63	18.12	4.67	2.92	15.94	2.38	0.17	1.71	0.22	0.25	91.1
362077 MI 6a	52.22	18.57	6.74	2.25	15.61	2.62	0.14	1.43	0.21	0.22	86.5
362077 MI 6b	53.45	17.83	5.91	2.68	14.99	2.92	0.13	1.45	0.23	0.39	88.7
362077 MI 6c	54.37	18.43	4.17	3.84	12.81	3.32	1.01	1.36	0.00	0.69	88.3
362077 MI 6d	55.70	17.87	5.00	2.37	13.61	3.08	0.51	1.30	0.09	0.46	88.0
362077 MI 6e	53.44	17.32	6.12	3.34	15.00	2.75	0.12	1.65	0.05	0.21	88.9
362077 MI 6f	54.27	17.51	5.34	2.75	14.06	3.34	0.59	1.52	0.01	0.61	89.5
362077 MI 6g	54.75	18.75	4.51	2.31	13.05	3.20	1.16	1.90	0.12	0.25	88.7
362077 MI 7	52.12	17.64	7.86	2.63	15.67	2.50	0.08	1.29	0.02	0.19	86.3
362077 MI 8	54.05	17.08	5.85	3.03	15.56	2.75	0.18	1.22	0.05	0.24	88.6
362077 MI 9	51.83	16.75	7.78	3.28	15.88	2.57	0.21	1.40	0.08	0.22	86.1
362077 MI 10	50.96	18.44	5.43	4.99	15.88	2.20	0.11	1.52	0.09	0.37	92.7
362077 MI 11	50.03	17.18	8.80	3.89	15.81	2.14	0.11	1.58	0.15	0.32	86.1
362077 MI 12	52.81	17.64	6.56	3.06	14.93	2.67	0.12	1.71	0.13	0.36	88.5
362077 MI 13	48.29	19.95	9.01	2.93	15.69	2.04	0.10	1.51	0.16	0.32	86.2
400230 MI 1a	52.20	17.70	6.35	2.63	15.85	2.97	0.24	1.86	0.03	0.17	88.4
400230 MI 1b	51.54	17.69	6.51	2.62	16.17	3.01	0.22	1.87	0.09	0.27	88.4
400230 MI 1c	52.76	17.73	5.31	2.14	16.06	3.13	0.32	2.18	0.01	0.35	87.8
400230 MI 2	56.35	20.24	5.15	2.62	8.91	4.86	0.40	1.02	0.15	0.29	84.7
400230 MI 3a	55.06	17.59	5.37	2.23	14.77	3.12	0.18	1.32	0.15	0.19	86.3
400230 MI 3b	53.05	15.95	6.00	4.47	16.20	2.57	0.22	1.18	0.10	0.26	86.0
400230 MI 4	53.90	17.29	6.60	1.96	14.98	3.42	0.22	1.14	0.13	0.37	84.7
400452 MI 1a	51.26	17.01	8.08	3.90	15.46	2.16	0.11	1.65	0.19	0.19	87.1
400452 MI 1b	50.42	17.53	8.70	3.57	15.52	2.27	0.15	1.51	0.12	0.21	87.1
400452 MI 2	50.36	17.88	8.32	3.49	15.29	2.34	0.13	1.79	0.20	0.21	87.2
400452 MI 3	50.81	17.16	8.60	3.66	15.49	2.18	0.12	1.74	0.04	0.19	87.1
400452 MI 4	50.20	17.31	8.50	4.07	15.60	2.36	0.12	1.53	0.15	0.17	87.2
400452 MI 5	50.46	17.48	8.41	3.80	15.31	2.52	0.13	1.40	0.32	0.17	87.0
400452 MI 6	53.59	17.70	6.20	4.08	14.48	2.64	0.05	0.94	0.18	0.15	87.6
400452 MI 7	50.53	17.45	8.05	3.64	15.60	2.42	0.11	1.56	0.44	0.20	86.6
400452 MI 8	52.63	16.54	7.64	3.23	13.91	2.94	0.15	2.61	0.07	0.28	86.8
400452 MI 9	50.03	14.54	9.67	5.71	15.61	2.05	0.07	1.86	0.29	0.19	86.2
400452 MI 10a	50.48	16.47	8.96	4.53	15.58	2.20	0.15	1.37	0.10	0.18	86.9
400452 MI 10b	51.22	17.01	7.98	4.45	14.73	2.45	0.14	1.62	0.19	0.20	86.9
400452 MI 11a	50.99	17.52	8.03	3.64	15.36	2.42	0.10	1.58	0.13	0.23	87.2
400452 MI 11b	51.16	17.84	7.66	3.01	15.72	2.42	0.10	1.71	0.17	0.22	
400452 MI 11c	50.93	16.97	8.68	3.80	15.45	2.28	0.10	1.50	0.10	0.20	
400452 MI 11d	50.53	17.74	8.39	3.57	15.72	2.15	0.10	1.53	0.03	0.25	87.8
400452 MI 11e	50.92	16.87	8.40	4.14	15.67	2.12	0.07	1.47	0.16	0.17	87.8
400452 MI 12a	50.36	17.86	7.24	3.24	16.17	2.23	0.37	1.91	0.10	0.51	88.0

Sample	SiO_2	Al_2O_3	FeO	MgO	CaO	Na_2O	K_2O	TiO_2	MnO	P_2O_5	Host Ol Fo%
400452 MI 12b	50.72	17.30	7.54	4.17	15.95	2.09	0.24	1.65	0.04	0.31	88.0
400452 MI 13	50.30	16.56	9.32	4.42	15.52	2.08	0.07	1.41	0.13	0.18	87.1
400452 MI 14	50.91	17.15	7.85	4.31	15.60	2.23	0.15	1.63	0.00	0.17	87.3
400452 MI 15	50.56	16.27	8.35	5.22	15.51	1.97	0.09	1.54	0.33	0.15	87.4
400452 MI 16a	51.44	17.67	8.07	3.64	15.07	2.35	0.09	1.37	0.10	0.19	
400452 MI 16b	50.88	17.03	8.93	3.78	15.15	2.47	0.10	1.22	0.14	0.30	
400452 MI 17	49.45	15.47	10.36	5.26	15.24	2.06	0.10	1.56	0.17	0.33	86.1
400452 MI 18	50.33	15.47	9.24	5.21	15.32	2.04	0.10	1.77	0.18	0.34	86.4
400452 MI 19	47.31	16.67	9.24	8.62	14.44	1.80	0.08	1.40	0.15	0.30	87.6
400452 MI 20	50.63	15.40	9.42	6.43	14.19	2.04	0.09	1.35	0.16	0.30	87.2
400452 MI 21	50.05	17.02	9.23	4.15	15.33	2.07	0.10	1.55	0.17	0.34	86.0
400452 MI 22	49.79	16.27	9.53	5.19	14.88	1.98	0.31	1.57	0.16	0.31	87.0
400452 MI 23a	51.04	15.05	8.88	7.25	14.20	1.99	0.06	1.10	0.27	0.15	87.6
400452 MI 23b	51.04	15.05	8.88	7.25	14.20	1.99	0.06	1.10	0.27	0.15	87.6
400452 MI 25a	47.31	16.67	9.24	8.62	14.44	1.80	0.08	1.40	0.15	0.30	87.2
400452 MI 25b	47.31	16.67	9.24	8.62	14.44	1.80	0.08	1.40	0.15	0.30	87.2
400452 MI 27	50.03	14.54	9.67	5.71	15.61	2.05	0.07	1.86	0.29	0.19	85.3
400452 MI 28	50.87	15.81	8.96	4.58	15.21	2.18	0.11	1.80	0.16	0.33	87.3
400452 MI 29	49.88	17.14	8.62	4.80	15.66	1.74	0.10	1.58	0.14	0.35	87.4
400452 MI 30	53.09	20.72	2.68	1.28	17.10	2.78	0.10	1.87	0.15	0.23	86.9
400452 MI 31	54.30	18.56	3.24	1.55	17.32	2.78	0.19	1.83	0.02	0.20	86.7
400452 MI 32	54.26	19.71	2.69	1.42	17.05	2.75	0.16	1.69	0.06	0.20	86.8

Appendix M Melt inclusion incompatible trace element compositions

Sample	Ba	Th	U	Nb	La	Ce	Pr	Sr	Nd	Sm	Zr
PAD6 MI 1	53.18			5.67	5.43	11.96	1.77	119.28	8.90	2.45	
PAD6 MI 3b	52.31			5.33	5.03	10.86	1.44	104.06	7.51	2.15	
PAD6 MI 3c	55.56			5.80	5.47	12.19	1.68	114.86	8.10	2.57	
PAD6 MI 12a	50.46			5.06	4.82	10.98	1.51	107.70	8.70	2.40	
PAD6 MI 12c	45.42			4.58	4.56	10.14	1.38	91.91	7.08	2.13	
PAD6 MI 12e	44.40			4.76	3.89	8.71	1.29	94.52	6.92	1.74	
PAD6 MI 12f	55.41			5.74	5.61	12.21	1.66	116.63	9.34	2.93	
PAD6 MI 12g	44.63			4.54	4.58	10.13	1.41	98.01	7.89	2.02	
PAD6 MI 13	45.34			4.52	4.72	10.87	1.48	109.24	8.59	2.34	
PAD6 MI 14	56.32			5.64	5.70	13.20	1.79	121.92	10.84	2.99	
PAD6 MI 15a	48.92			4.92	5.14	11.88	1.67	119.58	8.65	2.73	
PAD6 MI 15b	42.14			4.54	4.25	13.44	1.22	89.51	7.40	2.29	
PAD6 MI 15c	42.25			4.61	4.22	10.00	1.49	98.93	8.92	1.98	
PAD6 MI 25a	41.48	0.29	0.09	3.55	3.99	8.66	1.17	102.61	6.37	2.04	50.41
PAD6 MI 25b	42.13	0.31	0.13	4.00	4.02	8.96	1.17	101.63	6.05	2.10	50.86
PAD6 MI 26	81.09	0.31	0.09	4.58	4.46	10.68	1.60	120.52	8.52	2.66	89.25
PAD6 MI 27	49.92	0.47	0.11	5.36	5.24	12.61	1.71	118.00	9.56	2.78	72.48
PAD6 MI 28	59.57	0.49	0.18	5.98	5.64	13.30	1.72	127.82	10.09	2.87	68.86
PAD6 MI 29	61.88	0.50	0.11	6.45	5.62	11.43	1.54	108.04	6.81	2.02	54.77
PAD6 MI 30	53.44	0.49	0.10	5.51	4.62	9.98	1.29	103.12	6.65	2.06	56.33
PAD6 MI 31	56.41	0.47	0.15	5.68	5.92	12.25	1.77	120.49	9.46	2.98	67.17
PAD6 MI 32	48.97	0.45	0.08	5.63	5.22	12.51	1.80	124.36	9.77	2.55	67.06
PAD6 MI 33	37.04	0.30	0.12	3.78	3.95	9.61	1.40	104.48	7.27	2.14	58.74
PAD6 MI 34	45.88	0.42	0.14	4.63	5.40	11.53	1.72	123.01	9.55	3.05	69.46
PAD6 MI 35	56.25	0.46	0.14	6.05	5.72	12.61	1.86	122.12	9.79	2.75	67.07
PAD6 MI 36	68.22	0.00	0.00	6.91	6.45	14.80	2.02	131.19	10.96	3.19	71.60
PAD6 MI 37	53.45	0.47	0.14	5.70	5.49	12.96	1.83	121.69	9.32	3.11	65.69
PAD6 MI 38	55.94	0.44	0.21	5.61	5.31	11.79	1.83	124.32	9.16	2.75	66.94
PAD6 MI 39	50.64	0.54	0.11	5.25	5.28	12.69	1.80	122.64	9.89	2.85	69.15
PAD6 MI 40a	61.94	0.46	0.20	6.10	6.12	13.86	2.06	129.28	10.24	2.81	68.69
PAD6 MI 40b	62.16	0.56	0.14	6.13	6.00	14.34	1.86	128.93	9.64	2.98	68.87
PAD6 MI 41a	60.06	0.50	0.19	6.27	6.13	13.91	2.06	127.89	9.98	2.98	69.37
PAD6 MI 41b	58.95	0.52	0.14	6.01	5.85	12.91	1.70	123.52	10.11	3.04	68.21
PAD6 MI 42	55.67	0.59	0.19	5.74	5.50	12.08	1.84	122.48	9.38	2.81	68.55
PAD6 MI 43	58.20	0.61	0.11	5.52	5.96	12.39	1.76	122.43	10.15	2.51	68.47
PAD6 MI 44	58.54	0.45	0.16	6.08	5.63	12.66	1.95	123.84	10.26	2.61	68.22
PAD6 MI 45	51.42	0.44	0.17	5.18	5.61	12.19	1.72	123.99	9.90	2.65	67.08
PAD6 MI 46	56.37	0.55	0.14	5.90	5.46	12.33	1.76	122.77	9.45	2.40	67.00
PAD6 MI 47	58.31	0.55	0.11	6.00	5.46	13.09	1.80	125.53	9.74	2.77	69.66
PAD6 MI 48a	50.29	0.45	0.09	5.23	5.30	12.45	1.80	125.73	9.81	2.81	71.22
PAD6 MI 48b	73.54	0.62	0.15	7.53	6.87	15.41	2.06	138.57	10.69	3.03	75.82
PAD6 MI 49	63.13	0.48	0.11	6.20	6.34	13.02	1.90	126.77	10.15	2.79	67.51
PAD6 MI 50	58.59	0.50	0.14	6.22	5.78	12.69	1.78	121.77	9.96	2.75	69.01
PAD6 MI 51	64.03	0.55	0.14	6.67	5.48	13.47	1.89	130.17	9.69	2.83	71.58
PAD6 MI 54	32.52	0.22	0.05	3.46	3.78	10.29	1.56	119.94	8.57	2.74	68.23
PAD6 MI 55	54.41	0.49	0.12	5.71	5.30	12.45	1.73	120.55	10.14	2.74	67.60
PAD6 MI 56a	47.37	0.46	0.13	5.02	5.08	11.93	1.85	123.46	10.45	3.08	67.22
PAD6 MI 56b	47.01	0.41	0.17	5.01	4.73	11.61	1.67	120.58	8.75	2.64	68.21
PAD6 MI 57	46.33	0.46	0.06	4.94	5.01	11.77	1.61	121.67	8.76	2.76	65.12
PAD6 MI 58	41.44	0.47	0.09	4.50	4.61	10.88	1.64	116.61	8.91	2.70	64.32
PAD6 MI 59	55.21	0.45	0.10	5.89	5.12	12.16	1.60	121.61	9.07	2.74	67.16
PAD6 MI 60a	62.74	0.56	0.10	6.46	5.59	12.94	1.88	125.89	9.64	2.88	69.45
PAD6 MI 61	59.05	0.56	0.16	6.25	5.67	13.34	1.82	128.65	10.44	2.90	70.45

Sample	Ba	Th	U	Nb	La	Ce	Pr	Sr	Nd	Sm	Zr
PAD6 MI 62	53.69	0.46	0.07	5.70	5.56	12.48	1.86	125.72	9.80	2.93	69.62
PAD6 MI 63	58.91	0.55	0.14	6.16	5.60	13.89	1.81	124.95	8.56	2.29	69.00
PAD6 MI 64	43.99	0.28	0.13	3.93	4.45	10.30	1.60	118.10	8.58	2.92	60.53
PAD6 MI 65a	63.46	0.54	0.14	6.61	5.50	12.83	1.78	130.03	9.39	2.64	72.80
PAD6 MI 65b	62.03	0.43	0.11	6.86	6.07	12.33	1.80	128.63	9.40	2.92	71.43
DUR8 MI 8a	35.04	0.39	0.11	4.59	4.35	11.76	1.61	127.93	8.83	2.99	71.06
DUR8 MI 8b	35.06	0.28	0.12	4.35	4.40	11.06	1.60	124.87	8.58	2.59	69.30
DUR8 MI 9	36.32	0.27	0.12	4.71	3.77	7.93	1.38	98.73	8.00	2.85	52.23
DUR8 MI 10	60.90	0.48	0.12	6.82	5.85	14.66	1.89	141.59	11.03	3.28	84.27
DUR8 MI 11	59.25	0.42	0.18	7.14	6.69	15.49	2.26	158.64	11.37	3.12	86.54
DUR8 MI 12	59.96	0.35	0.14	6.76	6.03	14.43	1.98	154.91	11.13	3.05	78.78
DUR8 MI 13	52.91	0.49	0.14	6.16	5.67	13.88	1.94	153.26	10.63	3.12	82.03
DUR8 MI 14	39.09	0.25	0.08	5.22	5.31	13.02	1.97	153.07	10.98	3.00	82.83
DUR8 MI 15	59.02	0.33	0.16	6.93	6.07	14.35	2.19	151.71	12.06	3.26	83.37
DUR8 MI 16	50.63	0.30	0.11	5.71	5.44	12.84	1.82	149.64	10.68	2.85	76.28
DUR8 MI 17	57.62	0.54	0.15	6.66	6.26	14.80	1.92	155.79	11.42	3.25	82.96
DUR8 MI 18	62.91	0.54	0.17	7.40	6.65	15.99	2.32	165.99	11.81	3.59	91.71
362077 MI 10	19.31	0.23	0.06	2.16	3.07	8.88	1.55	124.07	10.10	3.36	73.27
362077 MI 11	13.37	0.24	0.10	2.06	3.09	9.52	1.62	130.44	9.67	3.22	76.25
362077 MI 12	13.98	0.20	0.04	2.01	3.10	10.04	1.85	135.08	13.36	5.13	99.15
362077 MI 13	13.22	0.17	0.08	1.97	3.00	9.22	1.77	127.82	11.08	3.46	75.97
400452 MI 21	11.69	0.16	0.03	1.87	3.04	9.77	1.68	133.50	10.65	3.59	78.04
400452 MI 22	11.44	0.11	0.06	1.94	3.16	10.22	1.74	139.18	10.98	3.81	81.75
400452 MI 23a	11.24	0.12	0.04	1.70	2.73	8.63	1.51	123.34	9.44	3.09	71.91
400452 MI 23b	11.12	0.11	0.03	1.78	2.92	8.25	1.52	121.94	9.05	2.99	69.38
400452 MI 24	11.19	0.17	0.04	1.82	3.07	9.89	1.84	138.00	10.39	3.47	77.30
400452 MI 25a	11.30	0.08	0.06	1.71	2.91	9.89	1.63	133.06	9.73	3.35	77.53
400452 MI 25b	10.85	0.13	0.06	1.66	2.66	9.55	1.65	132.50	10.31	3.28	76.74
400452 MI 26	12.89	0.16	0.06	1.96	3.44	10.37	1.62	140.83	10.21	3.51	81.91
400452 MI 27	12.34	0.11	0.04	1.97	3.63	10.83	1.85	130.96	11.23	4.17	87.66
400452 MI 28	11.43	0.04	0.05	1.89	2.95	9.34	1.67	136.72	9.88	3.34	78.02
400452 MI 29	12.02	0.10	0.01	1.91	3.08	10.11	1.71	134.66	10.74	3.67	79.35

Sample	Eu	Ti	Gd	Tb	Dy	Y	Ho	Er	Tm	Yb	Lu
PAD6 MI 1	0.92	5745	3.13			23.99				2.77	
PAD6 MI 3b	0.77	4879	2.83			20.43				2.10	
PAD6 MI 3c	0.83	5555	3.18			24.79				2.75	
PAD6 MI 12a	0.86	4772	2.94			20.57				2.18	
PAD6 MI 12c	0.74	3839	2.40			17.40				2.03	
PAD6 MI 12e	0.68	4478	2.42			16.81				1.95	
PAD6 MI 12f	0.97	5374	3.41			22.22				2.25	
PAD6 MI 12g	0.70	4935	2.50			19.65				2.20	
PAD6 MI 13	0.93	5113	3.51			23.00				2.46	
PAD6 MI 14	1.06	6644	4.18			26.63				2.82	
PAD6 MI 15a	1.01	6019	3.76			23.72				2.87	
PAD6 MI 15b	0.79	4733	2.85			18.51				1.95	
PAD6 MI 15c	0.85	4794	2.86			21.03				2.42	
PAD6 MI 25a	0.77	4942	2.70	0.56	3.81	23.19	0.83	2.50	0.36	2.46	0.36
PAD6 MI 25b	0.82	4959	3.04	0.56	4.26	23.22	0.83	2.50	0.40	2.38	0.35
PAD6 MI 26	0.87	6077	3.74	0.62	3.86	22.82	0.83	2.60	0.35	2.56	0.35
PAD6 MI 27	1.02	6439	3.35	0.71	4.40	25.34	0.82	2.64	0.39	2.60	0.40
PAD6 MI 28	1.07	5979	3.65	0.70	4.36	24.38	0.88	2.83	0.44	2.49	0.39
PAD6 MI 29	0.75	4012	2.59	0.56	3.97	20.87	0.72	2.17	0.31	2.02	0.29
PAD6 MI 30	0.84	4021	2.76	0.57	3.79	21.27	0.79	2.08	0.30	2.15	0.26
PAD6 MI 31	1.06	5905	3.19	0.66	4.27	23.97	0.85	2.57	0.35	2.39	0.40
PAD6 MI 32	1.06	6062	3.27	0.66	4.27	24.26	0.91	2.67	0.43	2.71	0.33
PAD6 MI 33	1.05	5578	3.13	0.64	4.32	23.42	0.85	2.44	0.38	2.50	0.42
PAD6 MI 34	1.03	6150	3.88	0.67	4.57	25.22	0.95	2.77	0.43	2.75	0.39
PAD6 MI 35	0.93	5922	3.28	0.65	4.16	23.99	0.87	2.43	0.38	2.46	0.32
PAD6 MI 36	1.06	6299	4.32	0.64	4.18	24.97	0.92	2.79	0.41	2.88	0.42
PAD6 MI 37	0.96	6091	3.53	0.72	4.28	24.03	0.85	2.81	0.44	2.48	0.41
PAD6 MI 38	1.03	5890	3.21	0.72	3.87	23.30	0.93	2.52	0.42	2.58	0.38
PAD6 MI 39	1.00	6110	3.05	0.69	4.21	24.90	0.94	2.92	0.39	2.67	0.36
PAD6 MI 40a	0.97	6127	3.65	0.72	4.60	23.85	0.95	2.66	0.43	2.77	0.38
PAD6 MI 40b	1.00	6092	3.49	0.70	4.95	24.05	0.97	2.38	0.46	2.44	0.35
PAD6 MI 41a	1.02	6214	3.83	0.65	4.38	25.00	0.78	2.74	0.41	2.50	0.37
PAD6 MI 41b	0.89	6121	3.37	0.60	4.15	24.62	0.96	2.59	0.38	2.65	0.41
PAD6 MI 42	1.04	5985	3.49	0.69	4.33	24.18	0.87	2.51	0.40	2.44	0.34
PAD6 MI 43	1.02	6003	3.30	0.62	4.37	23.86	0.86	2.29	0.35	2.41	0.45
PAD6 MI 44	0.98	6011	3.18	0.62	4.26	23.85	0.85	2.56	0.38	2.54	0.34
PAD6 MI 45	0.93	6105	3.54	0.66	4.01	24.09	0.86	2.68	0.43	2.61	0.43
PAD6 MI 46	1.01	6081	3.23	0.60	4.03	23.40	0.88	2.65	0.34	2.48	0.36
PAD6 MI 47	0.90	6070	3.67	0.67	4.29	24.27	0.92	2.39	0.36	2.38	0.41
PAD6 MI 48a	1.08	6313	3.86	0.65	4.72	24.10	0.93	2.68		2.61	0.38
PAD6 MI 48b	1.04	6399	3.65	0.70	4.42	24.43	0.89	2.86		2.52	0.37
PAD6 MI 49	1.08	6028	3.64	0.64	4.30	24.45	0.92	2.64		2.49	0.38
PAD6 MI 50	0.94	6069	3.29	0.62	4.18	24.54	0.92	2.41		2.59	0.39
PAD6 MI 51	1.12	6022	3.64	0.68	4.73	25.20	0.97	2.81		2.68	0.47
PAD6 MI 54	1.08	6061	3.16	0.63	4.79	24.23	0.93	2.74		2.60	0.41
PAD6 MI 55	0.99	5988	3.20	0.61	4.39	24.52	0.90	2.55		2.71	0.41
PAD6 MI 56a	1.11	6038	2.90	0.59	4.63	24.38	0.85	2.80		2.70	0.43
PAD6 MI 56b	1.04	6195	3.56	0.62	4.48	23.78	0.93	2.52		2.48	0.40
PAD6 MI 57	0.94	5933	3.43	0.68	4.40	23.76	0.89	2.54		2.69	0.42
PAD6 MI 58	0.93	5813	3.48	0.65	4.43	23.02	0.91	2.50		2.50	0.38
PAD6 MI 59	0.93	5882	3.47	0.67	4.00	23.60	0.82	2.70		2.53	0.41
PAD6 MI 60a	0.96	6051	3.25	0.57	4.14	23.87	0.89	2.53		2.17	0.39
PAD6 MI 61	1.01	6402	3.85	0.65	4.53	25.53	0.95	2.59		2.59	0.41

Sample	Eu	Ti	Gd	Tb	Dy	Y	Ho	Er	Tm	Yb	Lu
PAD6 MI 62	1.07	6110	3.33	0.73	4.33	25.45	0.93	2.60		2.63	0.37
PAD6 MI 63	0.92	6151	2.83	0.66	4.31	23.69	0.83	2.57		2.67	0.39
PAD6 MI 64	0.92	5817	2.93	0.65	3.56	25.27	0.87	2.56		2.38	0.39
PAD6 MI 65a	1.04	6007	3.20	0.64	4.07	24.05	0.90	2.29		2.26	0.35
PAD6 MI 65b	1.03	6172	3.03	0.70	4.67	23.69	1.00	2.81		2.62	0.43
DUR8 MI 8a	1.10	6518	3.34	0.68	4.27	24.67	0.93	2.64	0.40	2.56	0.41
DUR8 MI 8b	0.95	6445	3.21	0.65	4.52	24.22	0.93	2.58	0.43	2.48	0.38
DUR8 MI 9	1.02	5845	2.96	0.64	4.28	23.97	0.92	2.80	0.38	2.38	0.40
DUR8 MI 10	1.01	6959	3.78	0.71	4.43	24.04	0.90	2.54	0.37	2.45	0.32
DUR8 MI 11	1.15	7666	3.81	0.83	4.76	27.34	0.99	2.75		2.92	0.43
DUR8 MI 12	1.10	7245	3.73	0.71	5.14	26.77	1.01	3.00		2.78	0.38
DUR8 MI 13	1.06	7347	3.53	0.68	4.74	26.35	0.98	2.91		2.76	0.42
DUR8 MI 14	1.08	6673	4.36	0.73	4.79	25.98	0.92	2.83		2.63	0.42
DUR8 MI 15	1.04	7451	3.92	0.77	5.17	26.63	0.99	3.13		2.54	0.42
DUR8 MI 16	1.03	7219	3.49	0.69	4.54	25.66	0.88	2.60		2.46	0.38
DUR8 MI 17	0.99	7320	3.75	0.74	5.09	25.70	0.95	2.73		2.65	0.37
DUR8 MI 18	1.23	8041	4.42	0.85	6.04	28.52	1.17	3.81		3.52	0.54
362077 MI 10	1.32	7287	4.12	0.80	5.28	27.92	1.06	3.06	0.48	2.99	0.37
362077 MI 11	1.27	7775	4.44	0.85	5.46	29.26	1.03	3.28	0.50	2.98	0.37
362077 MI 12	1.66	7714	7.66	1.57	10.96	55.20	2.08	5.79	0.79	4.91	0.74
362077 MI 13	1.35	7741	4.55	0.81	5.62	29.14	1.07	3.13	0.46	3.04	0.46
400452 MI 21	1.28	7432	3.89	0.79	5.02	26.59	1.07	2.93		2.77	0.41
400452 MI 22	1.35	7917	4.57	0.89	5.56	28.75	1.16	3.09		2.95	0.43
400452 MI 23a	1.30	6716	3.61	0.73	4.80	25.07	0.89	2.50		2.32	0.36
400452 MI 23b	1.03	6658	3.04	0.72	4.86	24.19	0.84	2.51		2.44	0.35
400452 MI 24	1.43	7763	4.01	0.85	5.04	28.13	1.08	2.96		2.99	0.45
400452 MI 25a	1.40	7624	3.98	0.73	5.53	27.47	1.06	2.90		2.62	0.42
400452 MI 25b	1.30	7592	3.99	0.72	4.77	27.35	0.94	2.72		2.65	0.38
400452 MI 26	1.31	8084	4.54	0.93	5.39	29.64	1.15	2.87		2.91	0.41
400452 MI 27	1.32	8670	4.07	0.82	6.10	31.65	1.15	3.45		3.11	0.47
400452 MI 28	1.19	7664	4.17	0.78	5.11	27.80	1.03	2.91		2.79	0.42
400452 MI 29	1.32	7921	4.04	0.82	4.98	28.02	1.09	3.02		2.77	0.38